# Optical measurement and signal evaluation relating to particulate properties during purification of biological suspensions

Ian Leslie John Holwill
Submitted for PhD examination in Biochemical Engineering
University College, London

For Maria.

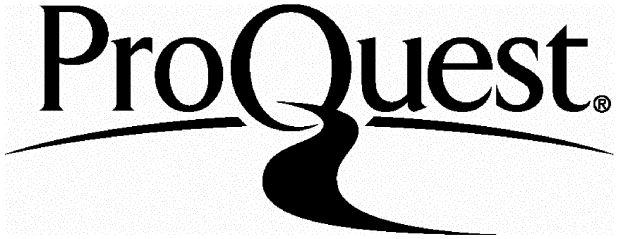

**Acknowledgements**

I gratefully acknowledge the Science and Engineering Research Council for the funding of this project and the following for their help in accomplishing and preparing this thesis: Professor M. Hoare, Professor G. Parry, Mr J. Molloy, Dr. M. Holwill, Dr. N. Goddard, Stephen Chard, Mark Bulmer, Phil Milburn, Gareth Davies and Maria.

## Abstract

The variable nature of conditions in downstream processing operations in biotechnological and other areas necessitates the on-line monitoring of process variables for rapid analysis and possibly subsequent control to optimise yield in a multi-stage purification process. Optical measurement of such parameters offers a fast and non-invasive method to interrogate the process with the added advantage of the possibility to construct a robust, miniaturised measurement system using modern optical components. The problems encountered are turbulent and turbid conditions which are usually unsuitable for light scattering measurements. Also access to the process stream is often not simple and a method of automatic sampling must be employed.

This thesis describes the application of dynamic light scattering to downstream processing operations and particularly to the measurement of virus-like particles and separation from their yeast host. The construction of a miniaturised dynamic light scattering system is also described.

Several data analysis methods are assessed with a view to using them in a rapid analysis configuration. Most of the methods require moderate processing power but consideration is given to extensions to the standard techniques to apply them in a parallel processing environment which today is on the increase. The improvement of the convergence of such routines is discussed with the addition of prior information.

A particular area of interest is the rapid sample preparation required before analysis by light scattering to improve the data quality. Large particulate material is usually not tolerated well in this method of measurement and should be removed.

A technique is described and tested which facilitates rapid in-situ sample preparation and optical analysis. Otherwise sample preparation is carried out prior to analysis.

As well as a dynamic light scattering study, an overview of optical measurement by other means in yeast-based systems is discussed with a view to optimising the system configuration.

**Table of contents**

Table of contents
List of figures
List of tables
Nomenclature
Abbreviations

Chapter 1 - Introduction
1.0 Downstream Processing
1.01 Biochemical engineering challenges
1.02 Requirements for optical measurement of process parameters
1.03 Unit operations
1.031 Flocculation
1.032 Centrifugation
1.033 Precipitation
1.034 Two aqueous phase
1.035 Homogenisation
1.036 Chromatography
1.1 Particle Analysis
1.11 Properties of biological particles and suspensions
1.111 Contents of the cell
1.1111 Procaryotic cell content
1.1112 Eucaryotic cell contents
1.112 Products: size and shape
1.1121 Virus-like particles
1.113 Optical methods and particle properties
1.1131 Size
1.1132 Refractive index
1.1133 Conformation and shape
1.1134 Molecular weight
1.1135 Diffusion coefficient
1.114 Optical methods and suspension properties

1.1141 Distribution of weight or size

1.1142 Concentration

1.1143 Refractive index

1.2 Light Scattering

1.21 Properties of light - the scattered field

1.22 Light scattering theories

1.221 Mie theory

1.222 Approximations and extensions to Mie theory

1.2221 Rayleigh scattering

1.2222 Rayleigh-Gans theory

1.2223 Geometrical optics

1.2224 Other approximations

1.223 Non-spherical scatterers

1.3 Dynamic light scattering

1.31 Correlation theory for dynamic light scattering

1.311 The form of the scattered light

1.312 Autocorrelation function estimators

1.32 PCS versus classical interferometry

1.33 Averaging schemes

1.34 Limitations of dynamic light scattering for particles in suspension

1.341 Gaussian approximation

1.342 Non-interacting particles

1.343 Single and multiple scattering

1.3431 Optical densities of concentrated suspensions

1.344 Polydispersity

1.4 Interpretation of results

1.41 Ill-conditioned problems

1.42 Accuracy and errors

1.421 Considerations on required data accuracy

1.43 Software analysis methods

1.431 Assumed size distribution shapes

1.4311 Cumulants Method

1.4312 Analytical expressions for distribution fitting

1.432 Model free algorithms

1.4321 Eigenfunction expansion

1.4322 Histogram method

1.4323 Sub-distribution method

1.4324 Non-negatively constrained least squares(NNLS)

1.4325 S-exponential sum method

1.4326 Regularised inversion/Constrained regularisation

1.433 Other methods

1.4331 Maximum entropy method (MEM)

1.4332 Fourier Inversion

1.4333 Linear programming

1.434 Choosing methods for on-line analysis

Chapter 2 - Equipment design and construction

2.0 Measurement light scattering

2.01 Lasers and their properties

2.02 Detectors

2.021 Coherence area

2.1 Signal processing

2.11 Clipping and scaling

2.12 Dedicated correlators

2.13 Computer correlation

2.2 Miniaturisation

2.21 Semiconductor lasers

2.22 Photodiodes

2.23 Passive optical components

2.24 Computers

2.25 DLS system for on-line analysis

Chapter 3 - Materials and methods

3.1 Homogenate preparation

3.2 Virus-like particle preparation

3.21 Gel filtration

3.22 Protein assay

3.3 Malvern system 4700c

3.4 Computer software

Chapter 4 - Characterisation of yeast homogenate

4.1 Wavelength scans of yeast homogenate

4.11 Wavelength scans of whole yeast and yeast homogenate

4.12 Spectrophotometric difference assay in clarified homogenate

4.13 Wavelength scan of aged yeast homogenate

4.2 Dynamic light scattering analysis of yeast homogenate

Chapter 5 - Computer simulation and analysis

5.1 Computer simulation of size distributions

5.2 Simulations of correlograms

5.3 Initial assessment of performance algorithms

5.31 Histogram method

5.32 Trapezoidal method

5.33 Expoential sampling method

5.34 Expoentially spaced histogram method

5.35 Non-negatively constrained least squares method

5.36 Regularised iterative method

5.4 Performance of algorithms in noisy conditions

5.41 Expoential sampling

5.42 Expoentially spaced histogram

5.43 Histogram method

5.44 Regularised inversion

5.5 Discussion

5.6 Implimentation of histogram method

5.7 Implimentation of the regularised iterative algorithm in parallel processing

5.8 Considerations for product monitoring

5.9 Summary

Chapter 6 - Analysis of light scattering from experimental data

6.1 Analysis of virus-like particles by dynamic light scattering.

6.2 Latex standards

6.21 The cumulants method

6.22 Histogram method applied to latex spheres

6.23 Performance of the histogram method to homogenate and latex mixtures

6.3 The difference method

6.31 The difference method with homogenate and latex mixtures

6.32 Difference method for clarified homogenate and VLP mixtures

6.33 Difference method for unclarrified homogenate and VLP mixtures

6.4 Run to run variation of correlograms

6.5 Conclusion

Chapter 7 - Internodal light scattering

7.1 Ultrasonic separation of biological particles

7.2 Light scattered from internodal regions

7.21 Applications to bioprocess analysis

7.22 Design of the ultrasonic cell

7.3 Internodal light scattering on latex mixtures

7.31 39nm and 4000nm latex

7.32 2um and 39nm latex

7.33 15um and 85nm latex

7.34 1.4um and 85nm latex

7.4 ILS analysis of yeast homogenate

7.5 Summary

Chapter 8 - Future directions

8.1. Optical measurement of virus-like particles

8.2. Analysis of size distribution

8.3. Internodal light scattering

Bibliography

**List of figures**

1.1. Settling properties for some biological particles.
1.2. Theoretical and experimental grade efficiency curves for latex spheres and protein precipitate.
1.3. Simulated recovery of prochymosin inclusion bodies in an industrial disc stack centrifuge (Mannweiler et al 1989).
1.4. Precipitation profiles for a variety of enzymes.
1.5. Schematic of salt-dextran two aqueous phase system with recycling of the phases (Kula, 1990).
1.6. Optical monitoring of a homogenisation process(Carr et al 1988).
1.7a. Chart showing relative amount of light scattered from different sized particles at three angles using Mie theory.
1.7b. Graph of relative amount of scattered intensity as a function of angle for three particle sizes using Mie theory.
1.8. A plot of scattered intensity as a function of radius for the Rayleigh-Gans approximation.
1.9. Detail of geometrical optics approximation
1.10. Schematic plot of the range of validity of various approximations.
1.11. Plot of disymmetry ratio measured as the ratio of scattered intensity at 45 degrees to that at 135 degrees.
1.12. Schematic of the dynamic light scattering experiment
1.12a. First order autocorrelation function according to equation 1.26a.
1.13. Spectrum of scattered light scattered from a monodisperse suspension of diffusing spheres of 80nm diameter at 25 degrees C.
1.14. Plot to show the critical concentration at which DLS measurements are reportedly affected by multiple scattering processes (Van de Meeren 1988).
1.15. Variation of the direct (coherent) and total scattered (incoherent and coherent contributions to the optical density signal of 94nm latex spheres (Konak et al).
1.16. Schematic solution to ill conditioned problems.

2.1. Diagram of the optical head for the miniaturised DLS system.

2.2. Diagram of modular laser focusing optics.
2.3a. Exploded view and plan of scattered light detection probe.
2.3b. Geometry of GRIN lens and fibre optic cable.
2.4. RCA photon counting module.

4.1. Chart showing wavelength scans of whole yeast and clarified and unclarified yeast homogenate.
4.2. Expanded region of wavelength scan of clarified yeast homogenate showing the increase in absorbance in the 400nm region.
4.3. Chart showing the derivative spectrum of clarified yeast homogenate.
4.4. Plot of derivative spectrum of 150nm latex spheres at approximately 0.005% v/v (c.= 5mg/ml).
4.5. Chart to show the difference between VLP homogenate and homogenate without VLP's present across the wavelength range 350nm - 500nm.
4.6. Chart showing a wavelngth scan of aged yeast homogenate.
4.6. a.b.c. Size distribution of clarified yeast homogenate by DLS using Malvern software.
4.7. Chart showing an apparently positive correlation between experimental time and chi-squared fit value for the Malvern 4700 analyser.

5.1a. Performance of weighted and unweighted histogram fits to a monomodal distribution.
5.1b. Performance of the histogram method to reconstruct a bimodal distribution.
5.2a. Trapezoidal fit to monomodal distribution.
5.2b. Performance of trapezoidal fit to a bimodal distribution.
5.3a. Performance of the expoential sampling method to fit a monomodal distribution.
5.3b. Performance of the expoential sampling algorithm to reconstruct a bimodal distribution.
5.4a. Performance of the expoentially spaced histogram method to a monomodal distribution.
5.4b. Performance of the expoentially spaced histogram method to reconstruct a bimodal distribution.
5.5a. Performance of non-negatively constrained least squares analysis method to a monomodal distribution.
5.5b. Performance of non-negatively constrained least squares analysis to a bimodal

distribution.
5.6a. Performance of regularised iterative algorithm to a monomodal distribution.
5.6b. Performance of the regularised iterative procedure to reconstruct a bimodal distribution.
5.7a. Performance of expoential sampling method in the presence of 0.04% noise in the data.
5.7b. Performance of expoential sampling method in the presence of 0.09% noise.
5.8a. Performance of the expoentially spaced histogram method in the inversion of a bimodal distribution from noisy data.
5.8b. Performance of the histogram method in the inversion of noisy data.
5.9a. Performance of regularised iterative algorithm with 0.04% noise added to the data for a monomodal distribution and for the different values of regularising parameter.
5.9b. Performance of the regularised iterative algorithm with 0.09% noise added to the data.
5.10. Chart constructed from a simulated size distribution to demonstrate the percentage of intensity scattered product to be detected.
5.11. Plot of the difference between a correlogram due to a distribution of homogenate and one due to a product particle of 80nm diameter in homogenate.

6.1a. Inversion of latex sphere correlogram data for 480 and 1030nm standards.
6.1b. Inversion of 39nm and 85nm latex standard correlogram data.
6.2. Graph showing histogram method inversions of correlogram data from mixtures of 85nm latex spheres and clarified homogenate.
6.3a. Graph to show the difference between homogenate and mixtures of homogenate and latex correlograms.
6.3b. Graph showing the difference method applied to the different mixtures of VLP and clarified homogenate suspensions.
6.3c. Graph showing difference methods applied to VLP and unclarified homogenate suspensions.
6.4. Graph showing the difference method applied to three different batches of VLP elution.
6.5a. Graph plotting the fractional standard deviation across channels for 39nm latex sphere data.

6.5b. Chart plotting the fractional standard deviation for 85nm particles and for different experimental times.
6.5c. Chart plotting the fractional standard deviation across correlogram channels for 220nm latex spheres.
6.5d. Chart showing fractional standard deviation across the correlogram channels for 480nm latex particles at different experimental times.
6.5e. Chart plotting fractional standard deviation in correlogram across the channels.

7.1. Schematic of laser beam passing through the internodal space in an ultrasonically separated suspension.
7.2. Particle size analysis of a mixture of 4 micron and 39nm latex spheres.
7.3. Internodal and nodal analyses of a mixture of 2000nm and 39nm latex spheres.
7.4. Internodal analysis (solid line) and normal DLS analysis of a mixture of 85nm and a small quantity of 15000nm latex spheres.
7.5. Chart to show internodal analysis of a suspension of 1.4 micron and 85nm latex spheres.

**List of tables**

1.1. Examples of commercial products and processes (from Dunnill 1988).
1.2. Processing profile for an antibiotic product (from Bioseparations).
1.3. Contents of the eucaryotic cell (from Steer 1982).
1.4. Size and structure of some biological materials.

2.1 Comparison of some of the correlators in the literature.

5.1 Decay constants, radius and diameter equivalents.
5.2 Simulated size distribution details.

6.1. DLS measurement of virus-like particles diameter showing intensity and number of averages for 10 measurements.
6.2. Cumulants method analysis data

**Nomenclature**

Chapter 1

1.1

E = fraction of the desired product remaining soluble

P = fraction of the total protein

$E_1$ = first cut

$E_2$ = second cut

Rm = maximum amount of soluble protein released

R = amount of protein released

N = number of passes through the homogeniser

K = a rate constant

$\alpha$ = absorption coefficient

$m_i$ = imaginary part of refractive index

$\lambda$ = light wave inside particle

$I_o$ = incident light intensity

I = light intensity at distance x

$M_W$ = molecular weight

x = distance into particle

N = number of molecules in suspension

$\Theta$ = scattering angle

Rg = radius of gyration

$R_\Theta$ = ratio of light to angle to that unscattered at zero angle - the Rayleigh ratio

$P(\Theta)$ = form factor describing the variation of scattering intensity from the particle at different angles

g = a constant factor

D = diffusion coefficient

k = Boltzmann's constant

$\eta$ = viscosity of the fluid\suspension viscosity

$R_H$ = hydrodynamic radius of the particle, for spheres

K = Mark-Houwink parameter calculated from the suspending fluid viscosity

$M_W$ = radius of biological particles

c = coefficient of drag

$c = 6\pi\varepsilon R_H$= coefficient of drag for spheres

T = the fluid temperature in kelvin

$c = \Sigma_i ci$ = total concentration

<M> = average molecular weight

N = number concentration

$C^{ext}$ = extinction coefficient

$Q_{ext}$ = extinction efficiency

A = cross sectional area of particle

m = relative refractive index (of the particle to the medium)

r = particle radius

$Re[S_1(O)]$ = real part of forward scattered light amplitude factor

I = total intensity of the wave

Q = polarisation at 0 or 90 degrees to the scattering plane

U = polarisation at +/- 45 degrees to the scattering plane

V = left or right circular polarisation

I,Q,U,V, = Stokes parameters

1.2

$E_i$ = parallel and perpendicular component of the incident light amplitude

$E_s$ = the scattered amplitude

S = interaction of the light with the scattering medium

k = the scattering vector

dV = a volume element

$\delta$ = phase difference of light scattered from a volume element dV with reference to a common point

$\varepsilon$ = ratio of incident to finally transmitted light

$\theta$ =} = angles (shown in fig. 1.9)

$\tau$ =}

$\sigma$ = term describing the phase shift of a particular ray passing through the sphere

$\alpha$= size parameter

$Q_{sca}$ = scattering efficiency per particle

$r_m$ = centre of mass of particle

r = position of volume element dV

1.3

f = frequency of the illuminating radiation

$\lambda$ = wavelength

t = time

$\phi$ = the instantaneous phase relative to a fixed point

i = the particle

$a_i(t)$ = scattering amplitude of particle i

T = measurement time

$\tau$ = correlation delay time

$\Gamma$ = autocorrelation decay constant

1.4

A = fraction of size distribution

$G(\Gamma)$ = decay constant distribution

$\Gamma_1$ = decay constant

$N_{ch}$ = number of correlator channels

$\Delta\Gamma$ = separation in diffusion constants

w = distribution sampling frequency

$g(\tau)$ = first order correlation function

$\gamma$ = decay constant

$k_n$ = parameters of cumulants method

b = data vector

K = Laplace kernal vector

G = exact solution vector

$\beta$ = convergence parameter

Chapter 2

n = number photon counts

K = clipping level

j = correlation channel

$\tau$ = fundamental sample time

$\delta$ = a dilation factor

$K_1$ = the random clipping level

Chapter 4

n = wave exponent

$Y(\lambda)$ = turbidity spectrum of clarrified yeast homogenate

$P(\lambda)$ = product

Chapter 5

$N_P$ = number of parameters

i = the ith data or fit point

Chapter 7

$\kappa$ = phase constant

E = mean energy density of the standing wave

a = particle radius

x = time averaged position of the particle from the node

F = correction factor which accounts for the compressibility of the particle and the different impedences of the particle and fluid

$\Lambda$ = sound wavelength

$\rho$ = density

c = sound velocity

$\sigma$ = relative velocity

**Abbreviations**

DLS - dynamic light scattering

FIA - flow injection analysis

HIV - human immunodeficiency virus

MEM - maximum entropy method (of data analysis)

NNLS - non-negatively constrained least squares.

OD - optical density

PCS - photon correlation spectroscopy

SVD - singular value decomposition

TTL - transistor transistor logic (computer signal standards)

VLP - virus-like particle

## 1.0 Downstream processing

### 1.01 Biochemical engineering challenges

Downstream processing currently offers a major challenge to industry with the advent of rapid developments in biotechnology during the past decade. Recent achievements include the approval and manufacture of human insulin, human growth hormone and alpha-interferon. There is a great number of other examples of biochemical products

| |
|---|
| Fructose enriched glucose by an immobilised enzyme method |
| 6-aminopenicillanic acid from benzylpenicillin by an immobilised enzyme method |
| Fungal food protein ingredient |
| Diagnostic agents based on monoclonal antibodies |
| Human insulin and growth hormone factor by rDNA methods |
| Tissue plasminogen activator |
| Hepatitis B vaccine by rDNA methods |
| Glucose biosensors |
| Cloned palm plants |
| Shikonin pigment by plant tissue culture |

Table 1.1 Examples of commercial products and processes (from Dunnill 1988)

examples of which can be seen in table 1.1. These derive not only from fermentation processes but also from animal and plant tissue culture.

Before reaching the manufacturing stage engineers are guided by the results of considerable research to the efficient design of a particular process. The downstream part of the biochemical process chain is often the most costly and more involved in the case of fermentation processes.

Before describing some of the operations it will be useful to briefly state some of the problems facing the engineer specifically in the area of downstream processing of fermented products.

It is often the case that the desired product is produced intracellularly rather than being excreted into the broth. To free the desired proteins for isolation the cells must be

disrupted. This releases debris in the form of cell wall fragments and contaminants from the contents of the cell. This can affect the rheological properties of the process stream as well as making isolation of the product of interest more difficult due to the large range of additional species of particle introduced to the stream.

The challenge to the biochemical engineer is to recover the desired protein in an active or native form from the crude cell homogenate. All process streams have low product starting concentrations, as indicated in table 1.2 so there is the common problem of producing a pure end product from such a dilute initial suspension. During processing the protein will be susceptible to time-dependent degradative reactions such as protease attack or thermal denaturation and hence it is essential to go from one stable state, often in the fermenter, to another stable state, often in a partially purified low volume form, as quickly as possible.

| Processing stage | % concentration | concentration (g/l) |
|---|---|---|
| Broth harvest | 0.1 - 1 | 0.1 - 5 |
| Removal of insolubles | 0.2 - 2 | 1 - 5 |
| Isolation | 1 - 10 | 5 - 50 |
| Purification | 50 - 80 | 50 - 200 |
| Polishing | 90 - 100 | 50 - 200 |

Table 1.2: Processing profile for an antibiotic product (from Bioseparations)

It has been shown that the protein products can survive the high shear stresses encountered in rapid continuous processing in pumps and filters provided the presence of gas-liquid interfaces and other such hostile environments are avoided (Hetherington et al 1971, Hoare et al 1982). Hence low residence time continuous processing is possible, but necessitates a large number of purification steps all of which require a compromise between yield and purification factor. To maintain a reasonable overall yield it is essential that a high yield is achieved at each processing step.

While it is possible theoretically to develop and achieve this, in practice the variation in

fermenter broth and process streams early in the purification sequence leads to unpredictable changes in the performance of downstream operations. This highlights the need for on-line analysis where rapid assessment of process variables having a direct (ie. product concentration or particle size) rather than an induced (ie. pH or temperature) bearing on process performance can be made.

In the pharmaceutical industries very high final purities are required as the products are often injectables. On-line analysis here of either product or contaminants could be a quality control monitor as well as an active control element.

The appearance of recombinant proteins in biotechnology and the associated regulatory requirements for handling such materials has heightened the awareness for safety and much effort is spent considering containment of such products. Ideally a sealed system from fermentation to final product is required but realistically samples must be taken and analysed. The alternative is sealed on-line or direct in-line analysis.

The downstream operations described in §1.2 are some of those deemed suitable for light scattering application. Removal of insoluble debris is the initial stage. Pretreatment includes flocculation and cell disruption. The second stage involves preliminary fractionation to remove gross contaminants and prepare the process stream for the next stage. The third stage is purification, an enhanced or repeated isolation stage and finally the product is concentrated by drying, crystallisation or membrane separation. Operations from the various stages are covered in the following sections. In all cases the application of on-line analysis of particulate and soluble components will be discussed. Main emphasis will be placed on the application of dynamic light scattering (DLS) with claimed sensitivity to particle size less than 3 microns down to about 3nm depending on the system configuration. The experimental and theoretical details of DLS are described in §1.3.

### 1.02 Requirements for optical measurement of process parameters

Desirable qualities for an instrument to control or monitor downstream operations are that it be fast in response, non-intrusive, able to provide on-line information and physically

compact. A probe using a light beam has the advantage of offering the first three qualities and advances in semiconductor technology has allowed the last. (This is described in more detail in §2.3). The speed of response required depends on the process of interest and must be such that the system reacts in a shorter time than that in which the process variable of interest will change detectably. In a centrifugation process for instance where one might measure the input and output properties of the stream, the measurement must be faster than the throughput time if a controlled system is to be implemented. The speed of an optical instrument depends on the post-detection processing, since the scattering and detection of a light beam are instantaneous in terms of process time. The analysis time of the raw data depends very much on the nature of the sample, the amount of information required and the accuracy of the data. These will all be compromising factors in the system.

The statement that optical techniques are non-intrusive needs to be qualified. Studies of laser damage in biological systems have been carried out (Fine et al 1964) where cell structure and protein activity were affected. However, the laser power needed for these results is much higher than required for normal analysis of process streams. There are several different ways in which scattered light fields can be processed and are highlighted in §1.21. The one of particular interest in this study is that of dynamic light scattering, the theory behind which can be found in §1.3. In the unit operations described in the following sections this technique will be considered in terms of the part that it might play in a monitoring or control situation . Other optical and non-optical techniques already put to use for process monitoring will also be described.

It is worth mentioning here two closely related form of optical sensor. Light scattering techniques, where the measurement volume is defined outside the physical construction and therefore can be described as extrinsic sensors are one form. DLS is a member of this group. The other form which is often included in the broad family of optical sensors is the optical biosensor, where part of the instrument is in contact with the process stream and can be described as an intrinsic sensor. In this study only the extrinsic sensor is considered. In two papers a review of the application and development of optical and non-optical biosensors is given. (Luong et al 1988,1990).

The sample preparation for optical sensors, either in the form of dilution or addition of reagent, prior to measurement is usually required and should also be considered in terms of non-intrusiveness. Dilution brings the sample into the range of the light detector response or of the theoretical approximation while the addition of reagent induces a physical change to the product to sensitise the measurement. Only if the addition of such substances be avoided can the technique be truly non-invasive.

The application of optical sensors in biochemical engineering, with particular reference to laser light scattering, has been discussed in several papers. A review of the potential of laser light scattering and optical fibre sensors in biotechnology covering a wide range of possible applications is the topic of one paper (Brown 1985). On-line analysis of proteins using optical techniques is discussed in another paper (Brown 1987). The key areas of application under the headings bioreactor control, product isolation and product purification have been considered (Carr et al 1986) where the difficulty of operating in turbulent conditions in the fermenter and downstream is identified. This suggests that optical methods will normally be applied to samples taken from the processes rather than directly to the process streams unless non-turbulent areas can be identified. Some approaches to downstream process monitoring including some optical methods, particularly dynamic light scattering, have been described (Clarke et al 1987). They consider applications to cell disruption and protein purification monitoring. This is discussed further in the following sections.

## 1.03 Unit operations

### 1.031 Flocculation

The first four paragraphs in this section refer principally to a paper by Sikora and Stratton 1981 and its related references.

To aid the removal from the process stream of cell wall fragments, nucleic acids, lipids and unwanted protein material it is useful to flocculate the debris thereby creating aggregates which can be separated more efficiently by centrifugation. The addition of polymers or metal ions causes such aggregation by polymer bridging or enhancement of Van der Waals forces between cell particulates. The main variable is the nature of the flocculating agent, where the unravelling of the polymer in solution can take a considerable time and where it is difficult to quantify the polymer molecular weight or charge distributions. These all have a bearing on the specificity of the flocculation and the size and recoverability of the flocs.

The properties of the flocculated particles are of the utmost importance to the optimum performance of the process. Their shear sensitivity, porosity, size and concentration determine the degree of break-up in the feed zone of the centrifuge, the extent of dewatering, the degree of flocculation and rheological properties of the suspension.

The measurement of the parameters usually involves time consuming off-line analyses. For example shear moduli can be measured by rheometry while size and porosity have been estimated by electrical sensing zone analysis. A large amount of potential methods for estimating the extent of aggregation have been highlighted.

The relationship between measured quantities and the process performance characteristics, when established, can provide a useful model for optimisation of flocculation and the subsequent centrifugation process. Relationships based on measures of size, solids fraction, modulus and viscosity have been described an it has been demonstrated that two of the most important properties in terms of subsequent dewatering and clarification are particle

size and solids volume fraction.

For a control situation the acquisition of on-line data is required. Steps towards this have been taken. These invariably use optical techniques (Ditter et al 1982, Eisenlauer and Horn 1984) using the inherent advantages of speed and convenience. The methods give information about the concentration and state of aggregation from which might be derived the details of the floc properties. In one case (Gregory 1987) turbidity fluctuations are measured and allow the calculation of an optimum dosage of polyethyleneimine for the flocculation of a bentonite suspension. The dosage could be rapidly adjusted on a step change in pH of the stream to the new value for the optimum dose.

Application of DLS to flocculation is limited. The flocs tend to grow beyond the upper size limit measurable by the technique. Indeed time of transit techniques (Preikschat 1987) or light diffraction (Brown and Felton 1985) are a better choice in this situation. The DLS technique has been used to monitor the size distribution and concentration of flocculating latex suspensions in real time (Cummins et al 1974) and in polymerisation reactions in biological systems over the time scale of minutes (Cummins et al 1976).

The centrifugation process that follows flocculation needs to be considered as part of the control loop. The supernatant from the centrifuge could be monitored to assess the size distribution and concentration which would be affected by the flocculating conditions before entry. In this situation DLS will be more applicable and is described in the following section.

**1.032 Centrifugation**

Centrifugation is a widely used method for solid-liquid separation fulfilling the requirements of low residence time continuous processing mentioned in §1.01.. This is made possible by the specific design of centrifuge process equipment for this purpose. It is often a more desirable separation technique over filtration and microfiltration where soluble products are concerned due to the product loss problems using these techniques (eg. due to surface binding) and also because of less reliable operation (due to product interaction with the separating surface).

Important properties of the suspension in this case are the size distribution, concentration, viscosity and dewaterability. The settling properties of the biological particles are shown in fig 1.1. In this graph top right to bottom left represents a direction of increasing difficulty of separation by centrifugation. Thus yeast debris represents a particular problem in this operation.

A good measure of centrifuge performance is the grade efficiency curve, an example of which is given in fig 1.2. Here the recovery efficiency is plotted against particle size. The theoretical limit is included for comparison which is based on Stokes law for a spherical particle travelling through a liquid. Complicated flow patterns in the centrifuge and non-sphericity of the particles explain the deviation of real data from this ideal curve.

An important consideration is the effect of feed-zone break-up of particles or aggregates which hinders the efficient removal of debris or precipitates. At the entrance to the centrifuge particles experience high shear which can cause breakage to produce material of smaller size which is more difficult to sediment. This is shown in the grade efficiency curve in fig 1.2. A latex particle standard (ie. shear resistant) curve allows comparison. In the region $d_1/d_c = 1.5$ the precipitate recovery curve appears above the ideal curve. This can be explained by the larger particles being broken and hence disappearing from the population at that diameter and apparently increasing the recovery efficiency of the larger particles, where in reality this is an indication of mass conservation of total solids.

To counter such breakage, conditioning by either mixing, exposure to low frequency acoustic radiation has been shown to produce more robust aggregates. (Hoare et al 1987).

Using data from scaled down laboratory experiments, predictions can be made for the recovery performance of centrifuges at pilot plant scale. Fig 1.3 shows data (Mannweiler et al 1989) which predicts an optimum flow rate of 200 $Lh^{-1}$ providing 95% recovery of protein inclusion bodies with 75% removal of debris. This is backed up by pilot plant scale results (Olbrich et al 1988).

Centrifugation is one of the more promising areas for DLS application particularly if the supernatant is to be observed. Here smaller sizes are present at relatively low

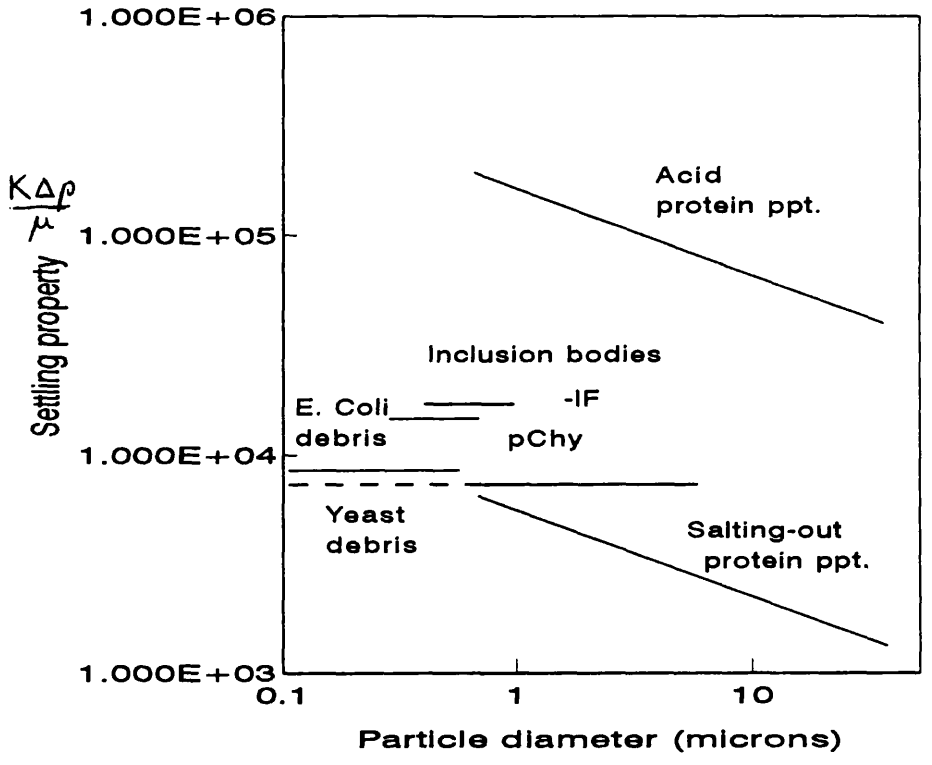


Fig 1.1: Settling properties for some biological particles. K=shape factor, $\mu$ =suspension viscosity, $\Delta\rho$ = density difference.

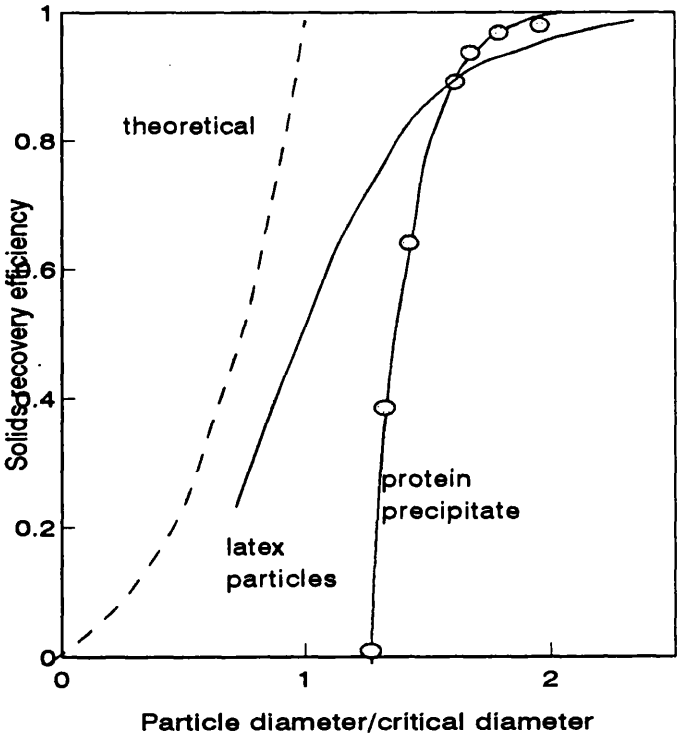


Fig 1.2: Theoretical and experimental grade efficiency curves for latex spheres and protein precipitate. The critical diameter is a theoretical separation limit based on centrifuge geometry and Stokes law..

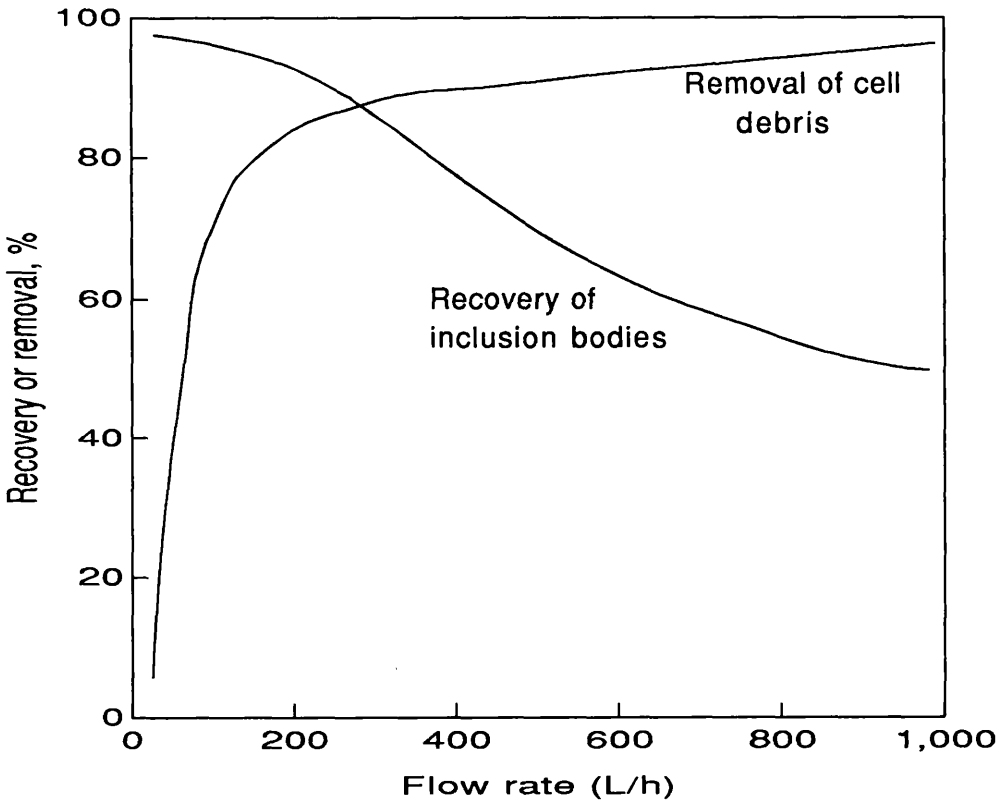


Fig 1.3: Simulated recovery of prochymosin inclusion bodies in an industrial disc stack centrifuge. (Mannweiler et al 1989).

concentration. Protein product concentration might be monitored by an on-line optical method. In the situation where product and debris are of different size, size distribution and total concentration could give a measure of relative debris and product concentration. At the input a more challenging situation occurs with a broader distribution and greater concentration. Methods of measurement here are considered in §1.031.

If the size distribution and concentration were known at the input and output then real time grade efficiency curves could be constructed and parameters such as upstream processing conditions adjusted to optimise this measure. A monitor of the supernatant alone would still give valuable information. The size distribution of unsedimented debris could give clues to the optimisation of the centrifuge operating parameters given models constructed from previous experiments. One would expect different shaped distributions relating to unsheared and sheared feed at different flow rates. It might even be possible to gauge the process performance by measuring the average size only. The debris size information will also be important when considering post-centrifugation operations.

In centrifugation on-line monitoring is a developmental tool to optimise conditions for a particular process.

### 1.033 Precipitation

Precipitation of proteins is often chosen above other separation processes, for example filtration, as a more reliable operation when dealing with process streams with a wide range of soluble components. The principle is based upon the balance of chemical potentials of the individual constituents of the system. A protein in solution can be precipitated by adding for example a salt. The concentration of the salt is critical in determining the fraction of precipitation of the protein.

In downstream processing it is often the case that the product will be in solution with a number of other proteins and the requirement is to separate the desired enzyme from the total protein. For these situations the different properties of particular enzymes are exploited by using the varying precipitation points at different concentrations. An

illustration of this is given in fig 1.4.

As noted earlier for achievement and maintenance of a high overall process yield a high step yield is required . An indication of this can be given by the fractionation diagram as shown in fig 1.4. Here the relative fraction of the desired product remaining soluble, E, is plotted against the fraction of total protein, P, left in solution. The precipitation process can then be performed as a two cut process where the first cut $E_1$ leaves a substantial fraction of the product still in solution and the second cut precipitates the product with a yield $E_2$ - $E_1$ and a purification factor dependent on the gradient between the two cut points:

$$\frac{E_2-E_1}{P_2-P_1} \qquad (1,1)$$

Conditions in the process stream tend to be erratic for example varying amounts of cell debris left after a cleaning stage can affect the precipitation characteristics, and repeatability in terms of retrospective analysis proves to be difficult. On-line monitoring of the precipitation process has been developed using flow injection analysis to measure the percentage of protein in solution (Kula et al 19 , Niktari et al 1990). Using this and a model for the salt concentration as a function of soluble product fraction a controlled precipitation process can be envisaged.

The role of DLS in this process is in the latter stage either before or after the centrifugation process for separation of the precipitated material and also where the product can be measured by size. The weight distribution of the precipitate could be useful complementary data for the FIA modelling where the amount of dissolved protein could be compared with the precipitated volume. As described in §1.032 recovery can be monitored by size distribution and concentration in and out of the centrifuge. In this case the conditions are more desirable as the input stream does not contain a large concentration of debris. However precipitates can reach sizes of up to 20μm, well beyond the range applicable to DLS.

There is also often a need to ensure solution stability during eg. buffer exchange or

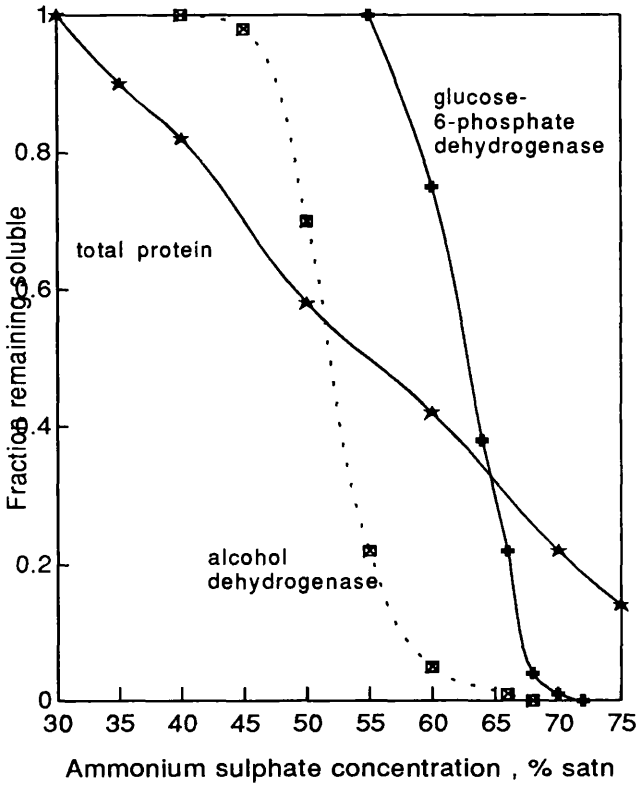


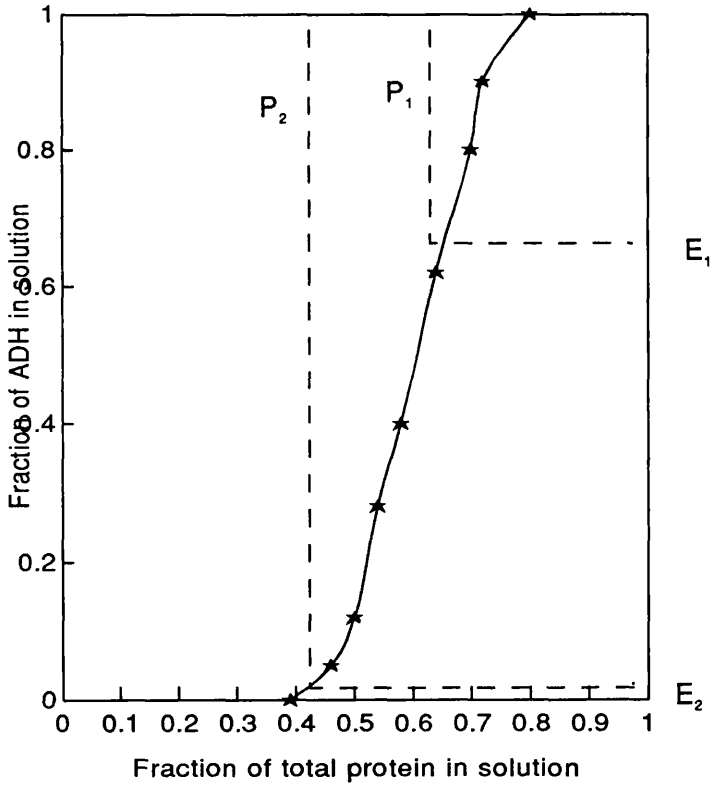


Fig 1.4: Top figure shows precipitation profiles for selected enzymes. Bottom figure shows a fractionation diagram of ADH versus total protein in solution.

concentration by membrane or thermal techniques. DLS may be used to identify the onset of precipitation as an indication of instability before visible to the human eye.

### 1.034 Two aqueous phase separation

This operation consists of a mixture of two aqueous solutions of hydrophillic polymers. If critical concentrations are exceeded then two separate phases of each will form in the mixture. A solution containing the desired product and a complex mixture of debris and other proteins forms one phase. The other polymer solution is added to form the secondary phase. The product is partitioned across the phases until the concentration in the two phases is balanced. The product phase is then either recycled or the process moves on to another purification step. The geometry of the process can take either a batch or a continuous form. In the batch case solvent is bubbled through the product phase increasing the reaction cross section and the bubbles are allowed to disperse before separating the phases. In the continuous process two streams, one of each phase, flow relative to one another to facilitate continuous extraction.

The partition of the product between phases is a function of a wide range of variables. This is made worse by the need to recycle one of the phases (PEG in the case of PEG salt, Dextran in the case of Dextran PEG) with consequent recycling of impurities. Salt pollution is less problematic in two polymer phase systems and other hydrophillic polymers have been applied to the process. Problems encountered are higher phase concentrations or one-sided partition coefficients which would restrict the separating power. Separation of cell debris from any polymer for recycling seems difficult. A diagram of the PEG-salt process is shown in fig 1.5.

Engineering problems also occur with the large viscosity differences of the phases and adaption of conventional solvent extraction equipment for multistage extraction is necessary to cope with this.

Assessment of the economic viability of a scaled-up process shows cost effective operation for large scale processes with 90-95% recycling of the phase forming chemicals and for medium scale, use of a biodegradable phase such as citrate allows cheaper

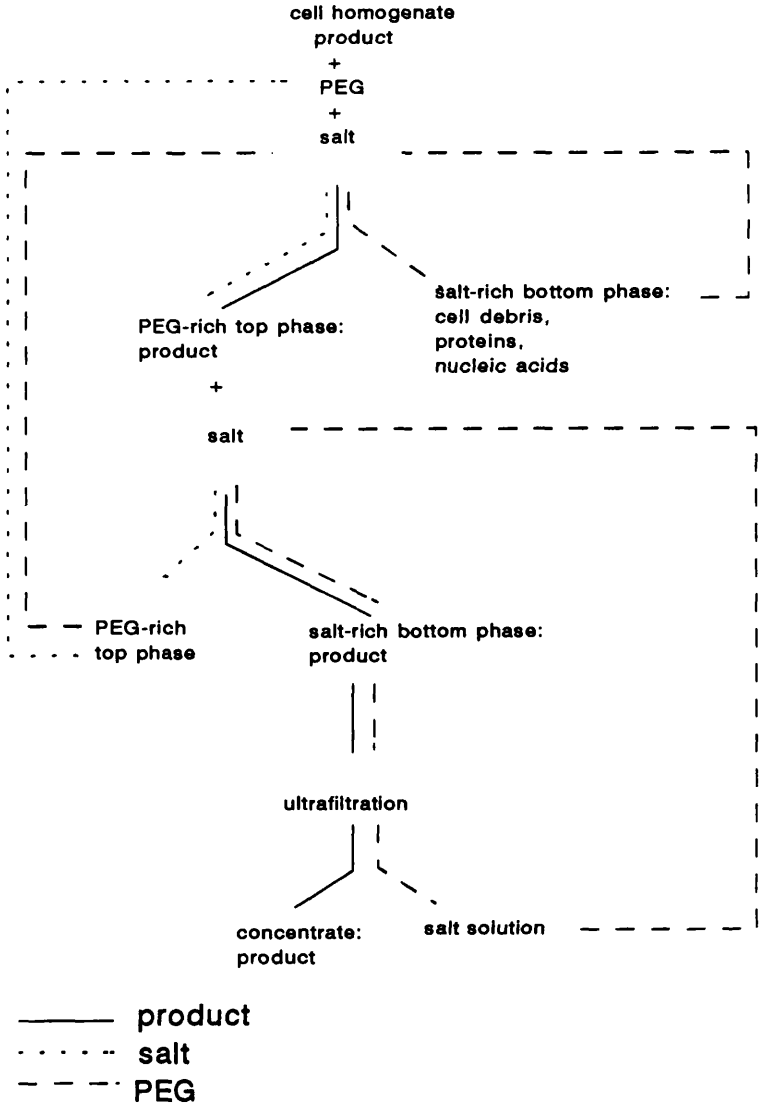


Fig 1.5: Schematic of salt-dextran two aqueous phase system with recycling of the phases (Kula 1990).

discharge to waste (Kula 1990).

On-line monitoring of the product would appear to be necessary to give the basis for control (Papamichael et al 1987), this may be in the form of assessment of the recycling performance of the phases by detecting contaminants or by a measure of product purity. Multiple passes could then be performed in process development stages and the limits of the purification scheme assessed.

DLS could be applicable here as a measure of purity of the product in the top phase with a knowledge of the required size ranges desired to be present. The success of recycling of the salt or polymer phases could also be monitored as the contaminants are likely to be small particulates. Rather than a blind recycling process, optimisation might be achieved by monitoring the recycling success and returning the phase to the process when a certain level of cleanliness is reached. The use of DLS might assume particular importance where the two aqueous phase system is concerned with the recovery of a particulate product, eg. vaccine particles, a common use of two phase separation (Albertsson 1960,1977).

**1.035 Homogenisation**

Often the desired fermented product is contained within a host cell and in order to release it for recovery the cell must be disrupted in some way. The most popular method of doing this is by passing the cell suspension at high pressure through a small orifice onto an impact surface. In doing this a considerable amount of heating can result and to avoid thermal degradation the homogenate is cooled before being passed onto the next process or back for further homogenisation.

The amount of cell breakage governs the protein release. To ensure optimum conditions the cells must be homogenised to the point where there is a maximum amount of product released without degradation due to the heat caused in the process. Hence it is necessary to follow product release and cell breakage in the homogenisation process.

The amount of disruption effected depends upon the pressure, temperature and pH of the

suspension. It is also dependent on the number of passes through he homogeniser. At constant pH and temperature it has been shown that the rate of released protein can be calculated from the following equation:

$$\log\left(\frac{R_m}{R_m - R}\right) = KN \qquad (1,2)$$

$R_m$ and R are the maximum amount of soluble protein released and the amount of protein released respectively. N is the number of passes through the homogeniser and K a rate constant. The process is not only dependent on the stream variables but also on the individual particle characteristics such as cell wall strength. This will depend upon the type of host used. The conditions of growth tend to affect the characteristics and so the process is dependent on other upstream processes. An on-line measurement is therefore useful for control of protein release as ensuring repeated identical fermentation conditions becomes difficult.

The sort of measurements required to assess the performance are an assay to measure the released protein and some measure of cell breakage by the size distribution. The extent of cell breakage will be related to the performance of the subsequent separation stages for removal of cell debris. This is especially important for a particle clarification process; for example for the recovery of large inclusion bodies attention to the cell debris will be important while for the recovery of vaccine or virus-like particles, the less the extent of cell debris attrition the better.

Measurements of the size distribution using the electrical sensing zone technique show bimodal distributions at around 405-494nm and 150nm-229nm after some centrifugation. It has also been shown that the released protein is related to the debris size distribution (Keshavarz-Moore 1987).

The role of DLS in this unit operation then would be to make a measure of the size distribution of the raw homogenate and if a model of protein release with distribution can be built up this could be used to estimate the product concentration. It has already been applied to a certain extent in monitoring the disruption process due to sonication (Clarke

et al 1987). Here the mean size and polydispersity were measured using DLS. The also measured optical density at 600nm and absorbance at 280nm. The results are shown in fig 1.6. If the mean size is sufficient the technique of diffuse light scattering may be useful (Thomas 1989, Auweter and Horn 1985).

Other considerations next to maximum protein release at the homogenisation step must be the further downstream processing steps where small debris size might cause problems. Although this implies a greater release of protein, separation by centrifugation is made easier with debris particles much larger than the desired product.

Problems encountered here for DLS are the concentration and size range of the debris. Typically the homogenate is high in concentration which makes dilution essential prior to measurement. The size range difficulty is the recurring problem of the larger particles masking the smaller ones due to their greater scattering efficiency. This might be overcome by the multiangle measurement technique as described in §1.3 or by the more direct method of physically dividing the size distribution before analysis. This might be effected by a microcentrifuge as used in the on-line apparatus for protein precipitation monitoring described in §1.033 or by miniature ultrasonic separation equipment which is described in chapter 7.

An alternative might be to use a different light scattering method to measure the size distribution. The time of transit technique uses a focused laser beam scanned across the suspension and the reflected light detected. This reputedly works at up to 30% w/w concentration (Preikschat 1987) but has the disadvantage of becoming inaccurate due to diffraction effects when the particle size is of the order of the wavelength (about 500nm in the referenced system). The only convenient technique for measuring size on-line below this size is DLS.

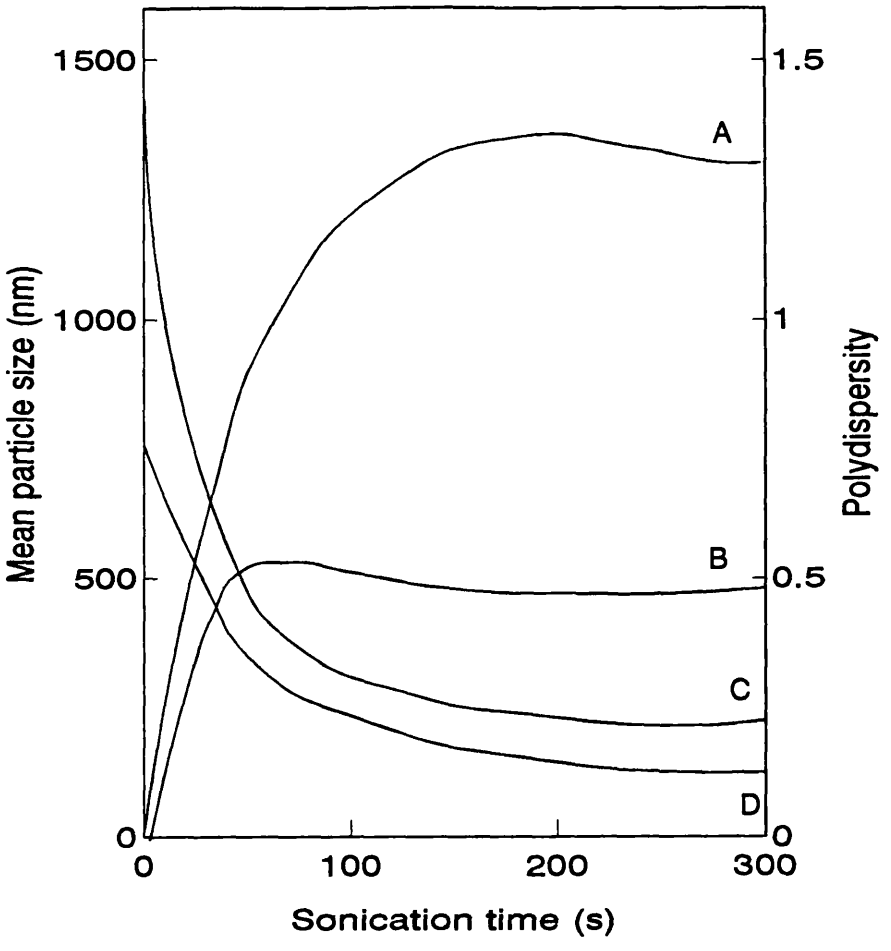


A: Protein absorbance 280nm.
B: Size distribution width (polydispersity)
C: Mean particle size.
D: Optical density at 600nm.

Fig 1.6: Optical monitoring of a homogenisation process. Dynamic light scattering has been used to measure the mean particle size and sample polydispersity (Carr et al 1988).

### 1.036 Chromatography

Since chromatography is a long way down the operations chain a reasonably clean process stream is encountered and the conditions become much easier for low noise data from light scattering experiments. Since the technique is one of a fractionation the problems of large polydispersity are implicitly overcome. It has been shown (Carr et al 1988) that DLS combined with a turbidity measurement can be accomplished with the same light source and detector. The turbidity follows the more normally implemented 280nm absorbance line closely.

The problems encountered for DLS here are that the high dilution of the process leads to low concentration of the product in analytical separations. The lower concentration limit of the technique depends upon the experimental system and is discussed in the theoretical section §2.0. However at process scale where UV detectors are often off scale the scattered light signal can still be used as a reliable measure of relative concentration.

Such a system has been used to aid product detection in chromatographic processes (Claes et al. 1990). This can be useful for peak-splitting procedures in a variable process where separation of the product based on properties other than size might depend upon process conditions. The additional information of size at detection after the column would help to place the product against other impurities.

## 1.1 Particle analysis

### 1.11 Properties of biological particles and suspensions.

Some of the properties of process streams relevant to assessment and control of an operation have been highlighted in previous sections. This study is specifically concerned with individual particle properties such as size and shape and also similar collective properties - size distributions, suspension refractive index, extinction efficiencies and other quantities which are of direct concern in light scattering. Rheological characteristics which might be inferred by optical measurements are also of interest. This section covers those properties pertaining to light scattering experiments in two sections: properties of individual particles and properties of suspensions. Initially a description of the diversity of particles likely to be encountered in a biochemical process plant is described.

#### 1.111 Contents of the cell

At any point along the process chain product or debris from cells will be present. Intracellularly produced proteins are commonly released by cell breakage allowing all the cell contents including cell wall fragments to contaminate the stream. Their size and relative number determines how much of the scattered light signal will be due to these cell components. A detailed description of how the intensity of the scattered light depends on particle size is given in §1.21. The position of the unit operation in the process chain dictates the relative amount and state of the product.

##### 1.1111 Procaryotic cell contents

A common host cell for protein production is Escherichia coli. In common with other procaryotes is has very few contents but being a swimming form has a flagella for locomotion. On disruption the most prolific and sizable component will be the cell wall debris which will be accompanied by small amounts of DNA and flagella.

### 1.1112 Eucaryotic cell contents

A eucaryotic cell contains more organelles than procaryotes. For example yeasts used for expressing the virus like particles described in §1.1121 contain many more organelles. These are listed in table 1.3. All of these are released on disruption with the potential to scatter light and complicate the measurement. It has been shown (Keshavarz-Moore et al 1987) that the cell debris produces a bimodal size distribution peaking at about 200nm and 450nm suggesting that many of the organelles as well as the cell wall have been damaged. The technique for measurement used here is insensitive to the smaller organelles which would nevertheless be a problem in scattering light if they were present in sufficient number. These smaller organelles must be remembered when interpreting scattering from smaller product particles.

| organelle | size | number/cell |
|---|---|---|
| mitochondria & plasmids | 3μm-10μm | several hundred |
| dictosomes | 0.5μm-1μm | thousand |
| secretory vesicles | 0.1μm-0.5μm | $10^4$ |
| ribosomes | 18nm-20nm | $10^7$ |

Table 1.3: Contents of the eucaryotic cell (from Steer 1982)

### 1.112 Products: Size and shape

Products vary widely in form. §1.2 gives details of how light is scattered from different size and shapes of particle. Table 1.4 lists a few products of interest and their shapes to demonstrate the diversity of material encountered. Of particular interest in this thesis is the protein particle which is described in the following section.

| Product | Shape/conformation | Size or molecular weight |
|---|---|---|
| protein precipitate | irregular, variable density | up to 40μm |
| inclusion bodies | irregular folded chains,low density | ≈0.5μm |
| food proteins | fibrous or globular structure | 20 - 200KDa |
| protein particles | spherical | 50 - 100KDa |

Table 1.4: Size and structure of some biological materials.

### 1.1121 Virus-like particles

It has been shown that yeast may be engineered to encode a set of proteins that are assembled into virus-like particles (VLP) (Mellor et al 1985, Garfunkel et al 1985). These particles may be observed by electron microscopy to have a diameter of about 60nm and appear to be spherical. In addition it has been found (Adams et al 1987) that such VLP's may be constructed using fusion proteins comprising part human immunodeficiency virus (HIV) protein. Such particles provide a means of preparing HIV antigens for a variety of immunological purposes eg. vaccines.

Key features of the technology are the ease of construction of the VLP's and the alternative it offers to using a live derivative of the disease producing organisms to produce vaccines. Small scale purification of the particles is relatively easy however in order to produce large quantities of purified particle biochemical engineering design is required as was discussed in §1.0. The detection of such particles by light scattering at various stages of the downstream process is part of this thesis. The ability to follow the product through the downstream process would allow process optimisation and possibly control.

### 1.113 Optical methods and particle properties

#### 1.1131 Size

There are several different definitions of size depending upon the measurement technique used. A good summary of these is compiled (Hunt 1988). Since DLS theory has as its basis the Brownian movement of particles through a medium the measure is the equivalent sphere diameter or Stokes diameter. (The raw calculation actually gives the diffusion coefficient from which the diameter is derived). Care must be taken when comparing particle size obtained by DLS with that measured by different techniques.

#### 1.1132 Refractive index

The refractive index of the particle describes the interaction of the incident light energy with the particle. The refractive index is also important for the scattering process. It is usual to specify the relative refractive index $m = n_p/n_m$. Here m is the relative refractive index defined as the particle refractive index divided by the medium refractive index. Refractive index is a complex quantity $m = m_r + im_i$. The real part ($m_r$) corresponds to the common concept of refractive index i.e. the ratio of the velocity of light in the particle to that in the medium. The imaginary part ($m_i$) corresponds to an absorption factor and appears in the absorption coefficient for the particle. Equation 1.3 defines the absorption coefficient and its relation to the imaginary part of the refractive index.

$$\frac{I}{I_0} = e^{-\alpha x}$$

$$\alpha = \frac{2\pi m_1 x}{\lambda} \qquad \textbf{(1.3)}$$

$\alpha$ *=absorption coefficient* **(1.3a)**
$m_i$ *=imaginary part of refractive index*
$\lambda$ *=light wavelength inside particle*
$I_0$ *=incident light intensity*
$I$ *=light intensity at distance x*
$x$ *=distance into particle*

The refractive index appears in most particle sizing calculations and in absorbance measurements with certain restrictions on its magnitude and range (see §1.222). In some cases e.g. Fraunhofer diffraction (Van der Hulst 1957) the refractive index does not appear but this puts tight restrictions on the type of applicable real particles that can be represented in this approximation. It has been shown (Glatter and Hofer 1987) that knowledge of the refractive index is important in multiple angle light scattering experiments otherwise serious errors can occur. In their example overestimation of the refractive index led to negative portions and undersizing of the true distribution whereas underestimation led to a multimodal solution with 4 peaks instead of the two in the true solution.

The need to know the refractive index of biological particles in order to size them has been recognised as a difficult problem for some time (eg Shchegolev and Klenin 1970). It can be a very difficult property to measure especially for sub-microscopic particles. DLS partially overcomes this problem as the calculation of diffusion coefficient does not involve the refractive index. However when calculating the relative intensity scattered by the components in the range of diffusion coefficients measured the refractive index of individual particles is often assumed to be the same. This is reasonable for particles of similar species but for particles of different species will vary. The variation of refractive index is a manifestation of polydispersity described in §1.344. The measurement of refractive index for particles and suspensions is discussed in §1.1142.

### 1.1133 Conformation and shape

The conformation or shape of a particle or macromolecule influences the scattering diagram as described in §1.2. Particularly to be noted is the case of loosely formed structures such as some polymers which may flex and in so doing introduce motion superimposed on the translational motion of the whole structure which will be detected as intensity fluctuations in the DLS measurement.

For non-spherical particles rotational diffusion is important as the scattered light fluctuates through the different orientations of the particle. This applies to particles with a size of the order of and above the wavelength of the illuminating radiation ie. $\approx 0.5\mu m$.

Dependent on particle structure in the DLS measurement there are three modes of movement affecting the signal: translational, vibrational and rotational. In the static light scattering case where the scattered intensity is integrated over much time's longer than the vibration and rotation periods, the motion serves to smooth out certain scattering functions of irregular particles. (see §1.223).

### 1.1134 Molecular weight

For molecules smaller than wavelength of the radiation, following Rayleigh theory, which states that for small molecules the scattered intensity is proportional to the square of the volume of the scatterers, the intensity should also be proportional to the square of the molecular weight $M_w$. Assuming single particle scattering the total scattered light will then be proportional to $NM_w^2$ where N is the number of molecules in the suspension.

The measurement of molecular weight for molecules larger than the wavelength of the radiation in the Rayleigh-Gans region (§1.2222) can be performed by extrapolating multi-angle intensity measurements to zero scattering angle and concentration. Equation 1.4 demonstrates this.

$$\frac{Kc}{R_\theta}=\frac{1}{M}P(\theta)[1+\frac{16\pi^2}{3\lambda^2}R_g^2\sin^2(\frac{\theta}{2})]=\frac{1}{M}P(\theta)+2Bc \qquad (1.4)$$

Here $\Theta$ is the scattering angle, Rg is the radius of gyration (§1.223), $R_\Theta$ is the ratio of light angle $\Theta$ to that unscattered at zero angle and is termed the Rayleigh ratio. $P(\Theta)$ is a form factor describing the variation of scattering intensity from the particle at different angles.

If a plot of $Kc/R_\Theta$ versus $\sin^2(\Theta/2)$ or c is made 1/M becomes the intercept of the graph. In addition the gradients give the radius if gyration and the first virial coefficient. The whole process can be performed by constructing a Zimm plot of $Kc/R_\Theta$ versus $\sin^2(\Theta/2)$ + gc where g isa constant factor (Zimm 1948).

In DLS the calculated property is the diffusion coefficient and estimates of the $M_w$ can be made with the knowledge of the shape of the scatterers. The expression is:

$$M_w=KD^a \qquad (1.5)$$

$$D=\frac{k_B}{6\pi\eta R_H} \qquad (1.6)$$

***where:***

***D=diffusion coefficient***
***$k_B$=Boltzmann's constant***
***$\eta$=viscosity of the fluid***
***$R_H$=hydrodynamic radius of the particle***

where a = 1 for rigid coils
a = 2 for random coils
a = 3 for spheres

K is the Mark-Houwink parameter calculated from the suspending fluid viscosity.
Similar expressions relating the radius of biological particles to $M_w$ can be found (Parker

and Dalgleish 1977).

eg. globular proteins $M_w = 1.88R^3$
casein micelles $M_w = 0.84R^3$

### 1.1135 Diffusion coefficient

The calculation of size from a DLS measurement is made from the diffusion coefficient calculated from the raw data. The mechanism of Brownian motion can be described as motion initiated by the molecular bombardment of particles in aqueous suspension followed by retardation due to the viscous drag on the particle by the fluid. The energy of the bombarding molecules is proportional to the product $k_BT$ where $k_B$ is Boltzmanns constant and T is the fluid temperature in Kelvin. The coefficient of drag, c, depends upon the particle shape and for a sphere $c = 6\pi\eta R_H$ . The diffusion constant is defined as:

$$D = \frac{k_B T}{c} \qquad (1.7)$$

This equation is known as the Einstein-Stokes equation from which an estimate of particle size can be calculated having measured the diffusion coefficient from the exponentially decaying autocorrelation function described in §1.3. As an example for T = 293 K and a sphere of radius 0.1μm, $D \approx 4.2 \times 10^{-12}$ $m^2s^{-1}$.

### 1.114 Optical methods and suspension properties .

The optical properties of suspensions are determined by the optical properties of their constituent particles. However the relationship between the two is often not straightforward. Some of the important aspects of the relationship are described in this section.

### 1.1141 Distribution of size or weight

Many discussions involving particle suspensions assume a perfectly monodisperse systems whereas any real system will contain a certain degree of polydispersity. This polydispersity need not only be in the form of a size distribution but any other particulate or molecular property e.g. refractive index or shape (see §1.344).

Referring to §1.1134 and simplifying equation 1.4 for the molecular weight by approximating to small concentration and scattering angle we have:

$$R_\theta = KcM \tag{1.8}$$

If there is a distribution of molecular weights of varying mass concentration $c_i$ then the formula becomes a sum of each independent species (this is valid only at low c): Equation 1.8 can be transformed into:

$$R_\theta = K\sum_i c_i M_i \tag{1.8a}$$

$$\textit{where total concentration } c = \sum_i c_i$$

$$R_\theta = Kc\langle M\rangle \tag{1.8b}$$

$$\langle M\rangle = \frac{\sum_i c_i M_i}{\sum_i c_i} \tag{1.8c}$$

<M> is the weight average molecular weight. This concept of average over a quantity other than the commonly-used number arises frequently in light scattering. In DLS this comes in the form of the intensity average which is described fully in §1.33.

### 1.1142 Concentration

The concentration of a particulate suspension is a determining parameter in both process control and light scattering. To ascertain the size distribution and concentration on-line in a process is a difficult aim to achieve. In light scattering approximations are usually made assuming small concentrations of scatterers whereas processing theory covers a wide range of concentrations. It is therefore necessary to adapt the light scattering theory or adjust the concentration prior to measurement. The measurement of suspension concentration is usually facilitated by way of turbidity measurement using the relation:

$$I=I_0\exp^{-\alpha x}$$

$I$ = *transmitted intensity*
$I_0$ = *incident intensity*
$x$ = *pathlength through sample* (1.9)

$$\alpha=NC_{ext}=NAQ_{ext} \qquad (1.9a)$$

$N$=*number concentration*
$C_{ext}$=*extinction coefficient*
$Q_{ext}$=*extinction efficiency*
$A$=*cross sectional area of particle*

This relation (the Beer-Lambert law) only for small concentrations - up to optical densities of approximately 3 (dependent on particle size). Corrections can be made at higher concentrations for particular systems by calibration however sensitivity in this region is lower. On-line systems with diluters (Lee and Lim 1979) or shortened path lengths (Lee 1981) have been used with success . However problems arise again in the case of polydispersity. The formula can be extended to this case:

$$-\ln\frac{I}{I_0}=\sum_i N_i C_{ext_i} \qquad (1.10)$$

In this equation $C_{ext} = C_{ext}(m,r)$ where m = relative refractive index and r = particle radius. Thus in order to make an accurate measure of concentration the size distribution and refractive indices of the different particles must be known. The problem is simplified if the refractive indices are equivalent and then in principle a measure can be made if the $C_{ext}(r)$ function is known, i.e. m is known or constructed experimentally.

Further aspects of concentration related to the interpretation of DLS data are presented in §.1.3431

**1.1143 Refractive index**

At the end of §1.1132 it was highlighted that the relationship between refractive index of the suspension and the individual components are not always simple. In the same sense the refractive index of a particle in suspension is not necessarily the same as that of the bulk material. This implies that if the of refractive index is to be measured it must be done with the particle in suspension.
It has been shown (Nakagaki and Heller 1956) that the relationship between the particle and suspension refractive index can be represented by:

$$m' = 1 + \frac{3}{2}\frac{Re[S_1(0)]}{\alpha^3} \qquad (1.11)$$

$$\alpha = \frac{2\pi r n_m}{\lambda_0} \qquad (1.11a)$$

Where Re[S(0)] is the real part of the forward scattered light amplitude factor.
A graphical method was proposed for measuring the refractive index of spherical particles of known size. Later a proposed method to determine the size and refractive index of a suspension (for moderately polydisperse systems) by a turbidimetric method was described (Shchegolev and Klenin 1970). Measurement of the differential turbidity spectrum and the

specific turbidity together with knowledge of the density of the particles allows the data to be fitted to a theoretical model using Mie theory with $\alpha$ the size parameter and m, the relative refractive index, as parameters. In a study of latex particle suspensions using this approach it was found that $\alpha$ and m could be determined to within 4%.

## 1.21 Properties of light - The scattered field

This study is concerned with light of moderate intensity scattered from biological suspensions and as such will be concerned with elastic light scattering. That is, the biological particle that the light interacts with responds linearly to the radiation and the scattered wavelength is the same as the incident wavelength. This describes effects such as the scattering processes to be described below and polarisation effects such as optical rotary dispersion and circular dichroism (Maestre and Tinoco 1967) used to classify certain types of molecules. These are linear processes in contrast to the non-linear optical processes such as Raman spectroscopy used for the measurement of vibrational modes of molecules.

Visible light is generally taken to be the part of the electromagnetic spectrum between 400nm at the blue end and 740nm at the red end. A light wave can be completely characterised by its polarisation, frequency, amplitude and phase. In general all of these are modified in a scattering process.

In scattering theory a light wave is often described in terms of the Stokes parameters. These are usually represented by the letters I, Q, U and V which are defined below. I is the total intensity of the wave and the others having the same units are dependent on the polarisation. When the wave comes across a particle these parameters are modified. This can be described by a scattering matrix which will describe the scattering process. This has 16 elements not all of which are independent and can be multiplied by the incoming Stokes parameters to give the scattered Stokes parameters. For a collection of particles the resultant Stokes parameter is a summation of the individual Stokes parameters.

In theory information is available from all the matrix elements (Bickel et al 1976) which can give information on almost all particle properties, but most studies are limited to the first matrix element which describes the scattered intensity. Thus sometimes only the scattered intensity is represented and the polarisation effects are not explicitly formulated. It should be noted that the polarisation of the incident light can affect the scattered intensity. Particularly it should be noted that laser light is nearly vertically polarised which must be considered when modelling the scattered light.

Also to be considered in the laser modelling process is the distribution of energy across the beam. Most often formulae are found to represent an incident plane wave whereas laser light has a gaussian profile. However, it has been shown (Ross et al 1978) that for $d < w_0$ where d is the particle diameter and $w_0$ the beam diameter then the plane wave case is a good approximation. The distortion of the correlation function (§1.332) due to the non-uniform intensity has been discussed (Ross 1989) and corrective formulae are given. It was shown that distortion is greater for low scattering angles and depends upon the optical alignment of the system.

In summary the scattering matrix is a mathematical description of the way a particular size and shape of particle scatters radiation to its surroundings. It is usually written as follows:-

$$\begin{pmatrix} E_{i\perp} \\ E_{i\parallel} \end{pmatrix} \begin{pmatrix} S_1 & S_4 \\ S_3 & S_2 \end{pmatrix} = \begin{pmatrix} E_{s\perp} \\ E_{s\parallel} \end{pmatrix} \qquad (1.12)$$

Where the $E_i$'s represent the parallel and perpendicular components of the incident light amplitude, the $E_s$'s the scattered amplitudes and the S's describe the interaction of the light with the scattering medium.

### 1.22 Light scattering theories

The following sections describe exact and approximated theories of light scattering. There are many texts on the subject, much of the equations represented here follow Van der Hulst 1957.

#### 1.221 Mie theory

The theory of scattering of electromagnetic radiation from spheres has been available from the beginning of the century. One of its major contributors after whom the theory is now known, Gustav Mie, formulated the theory for spherical particles of known refractive index and size (Mie 1908). It allows calculation of the scattering matrix elements described in §1.21, equation 1.12 and values for the various coefficients that can be used

to model for example extinction measurements.

The theory can be used to a certain extent for non-spherical particles as an approximation but often, particularly for large particles, a calculation will take rather a long time ( a recursive formula is traditionally used). New developments in the mathematical theory of scattering(Gousbet and Grehan 1988) have brought about more concise expressions but often physical rather than computational approximations are an easier approach for more time economical formulae and these are treated separately below.

The place of such theory in DLS is in part of the data processing beyond the correlation calculations §1.33 to convert intensity weighted distributions into more interpretable mass,area or number distributions. Since in general particles of different properties have different light scattering patterns then details of size, shape and optical properties of components in the distribution should ideally be known. Evidently this is often not the case and care should be taken in interpreting the results from an over generalised theory. Commercial instruments are set up to be most general whereas in the application to process stream analysis in certain cases more specific data is available before measurement and indeed it is these systems which are of most interest here.

The theory is derived by solving Maxwell equations, which describe the propagation of EM radiation, using boundary conditions imposed by a sphere of refractive index $n_s$ and radius r present in a medium of refractive index $n_m$. The refractive index of the sphere can be complex, the real part describing the ratio of the speed of light in a vacuum to that in the particle and the imaginary part relating to a degree of absorption of energy by the particle. To make the theory simpler only a real medium refractive index is considered. The theory can be followed in a number of references. (See eg. Van der Hulst 1957).

The results are a pair of amplitude functions $a_n$ and $b_n$ from which all scattering information can be obtained. These amplitudes are oscillatory in form and this results in the oscillatory scattering diagrams shown in figs 1.7 a-b. These graphs were plotted using a modified version a computer program (Bohren and Huffman 1983) They show the variation of light intensity scattered from a sphere at a particular scattering angle. The incident light is vertically polarised with a wavelength of n mimicking HeNe laser light.

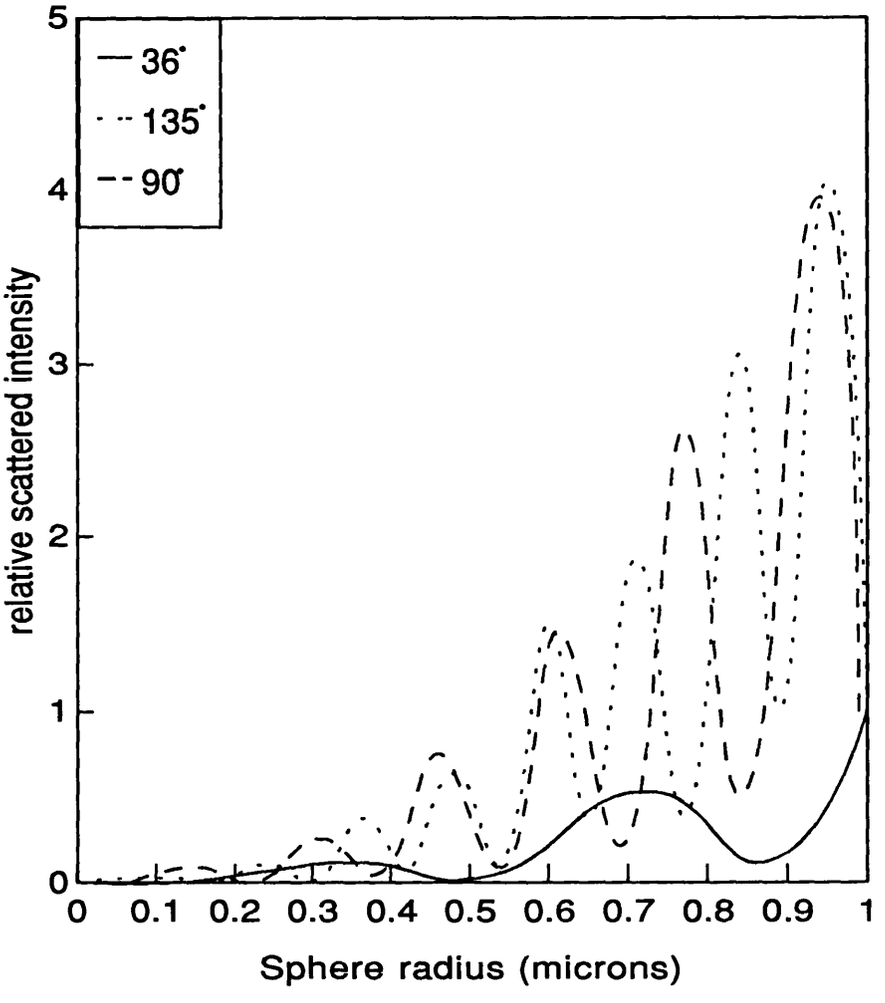


Fig 1.7a: Chart showing relative amount of light scattered from different sized particles at three angles using Mie theory. The scattered intensity between curves is not relative, the angular dependence of scattered light is shown in fig 1.7b.

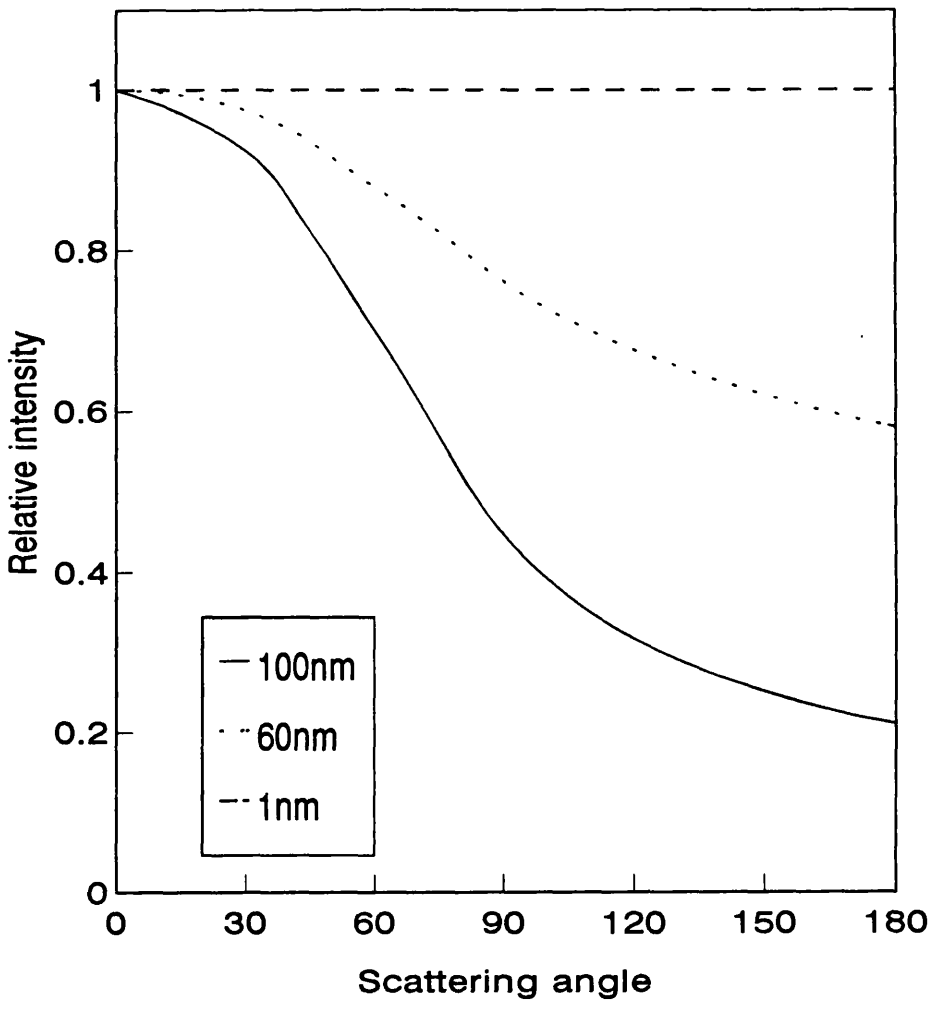


Fig 1.7b: Graph of relative amount of scattered intensity as a function of angle for three particle sizes using Mie theory. The curves are normalised to the forward direction. The wavelength of radiation is 633nm and the realative refractive index 1.13.

Usually plots use the size parameter $\alpha$ (see equation 1.11a, §1.1143) instead of radius to be completely general. This clouds the issue when discussing particle sizes and so the radius is used in the diagram here.

The main features apparent on these diagrams are:
i) Much more light is scattered by large particles than by small ones.
ii) There is a general oscillatory pattern of intensity as a function of angle as well as intensity as a function of radius.
iii) Larger particles scatter much more light in the forward direction.

### 1.222 Approximations and extensions to Mie theory

#### 1.2221 Rayleigh scattering

As mentioned in the previous section more is often gained by making approximations from a physical rather than a computational viewpoint. A simple approximation is to assume the radii of the particles to be small compared with the wavelength of the incident radiation ($\approx 0.5\mu m$) such that the electric field is nearly constant across the particle at any moment.

In fact the mathematical restriction on the particle properties are that the product of the size parameter and the modulus of the relative refractive index be much less than unity. Physically this implies that the diameter must be small or the particle should not differ in density from the medium greatly and not be a good absorber. For biological scatterers this covers a wide range of interest and so can be a useful approximation.

The resulting expression for the scattered intensity of incident unpolarised light is:

$$I_s = \frac{8\pi^4 r^6}{\lambda^4 r^2}\left|\frac{m^2-1}{m^2+2}\right|(1+\cos^2(\theta))\, I_i \qquad (1.13a)$$

This is a summation of vertically and horizontally polarised light so for laser light (usually vertically polarised) the scattered intensity is:

$$I_v = \frac{8\pi^4 r^6}{\lambda^4 r^2}\left|\frac{m^2-1}{m^2+2}\right| I_i \qquad (1.13b)$$

Here the two key features of Rayleigh scatterers are apparent.

$$I_v \propto \frac{1}{\lambda^4} \qquad (1.13c)$$

$$I_v \propto r^6 = volume\ squared$$

These are true only if the relative refractive index m is weakly dependent on the wavelength and the particle is non-absorbing as all light is assumed to be scattered and none absorbed.

It is important when considering approximations to consider their range of validity. The usual rule of thumb for the Rayleigh theory is that the radius should not exceed one twentieth of the wavelength of the incident light. For a HeNe laser this corresponds to particle a radius of about 30nm. More explicitly, for a 1% error with respect to Mie theory $\alpha|m| < 0.2$ and for 10% error $\alpha|m| < 0.5$. However it has been shown that due to a fortuitous cancellation of errors there is a second range of validity for relatively high size parameter (see Van der Hulst 1957)

### 1.2222 Rayleigh Gans theory

An extension to the Rayleigh theory to cope with larger sizes of particle is provided by the Rayleigh Gans approximation. The assumption here is that a particle can be divided into many small volumes each then considered as Rayleigh scatterers and the far field pattern is the resultant of the individual scattered fields from all such volumes. The downfall of the theory is that each of the volumes must individually scatter light which must reach the detection point without further interaction. This is evidently not the case for volumes inside the particle.

The mathematical conditions are $2Kr(m - 1) << 1$ where r is the radius, K is the scattering vector and m the relative refractive index of the particle to the medium. As an example, with a wavelength of n at a scattering angle of 90° and with a relative refractive index of 1.1, the approximation works out to be the particle radius, $r << 350nm$.

The scattered intensity is calculated as:-

$$I_s = \frac{4\pi^2 V^2}{\lambda^4 r^2} (m-1)^2 P(\theta) \qquad (1.14)$$

$P(\Theta)$ is a form factor for the particle and depends on shape so Rayleigh Gans theory is not only a spherical particle approximation. The form factor is calculated by:-

$$P(\theta) = \frac{1}{V^2} \left| \int e^{i\delta} dV \right|^2 \qquad (1.15)$$

where $\delta$ is the phase difference of light scattered from a volume element dV with reference to a common point. This describes the theory as the interference of light from all points in the particle.

A plot of the Mie theory and Rayleigh-Gans theory is shown in fig. 1.8. This shows agreement to within 10% over the range 0 - 1μm (for a relative refractive index of 1.03).

There is no second range of validity as with the Rayleigh case and the limitation is $m < 1.2$ and a up to a few hundred nanometres. The theory holds better for smaller scattering angles as here the phase differences of the individual volumes are smaller and less susceptible to error under the mathematical assumption.

### 1.2223 Geometrical optics

In the case of very large particles the approximation can be made that the incoming light is constructed of a numbers of rays. A ray is a channel of light energy small in width compared with the size of the particle but large compared with the wavelength of the light. The resulting scattered light can then be calculated by ray-tracing techniques

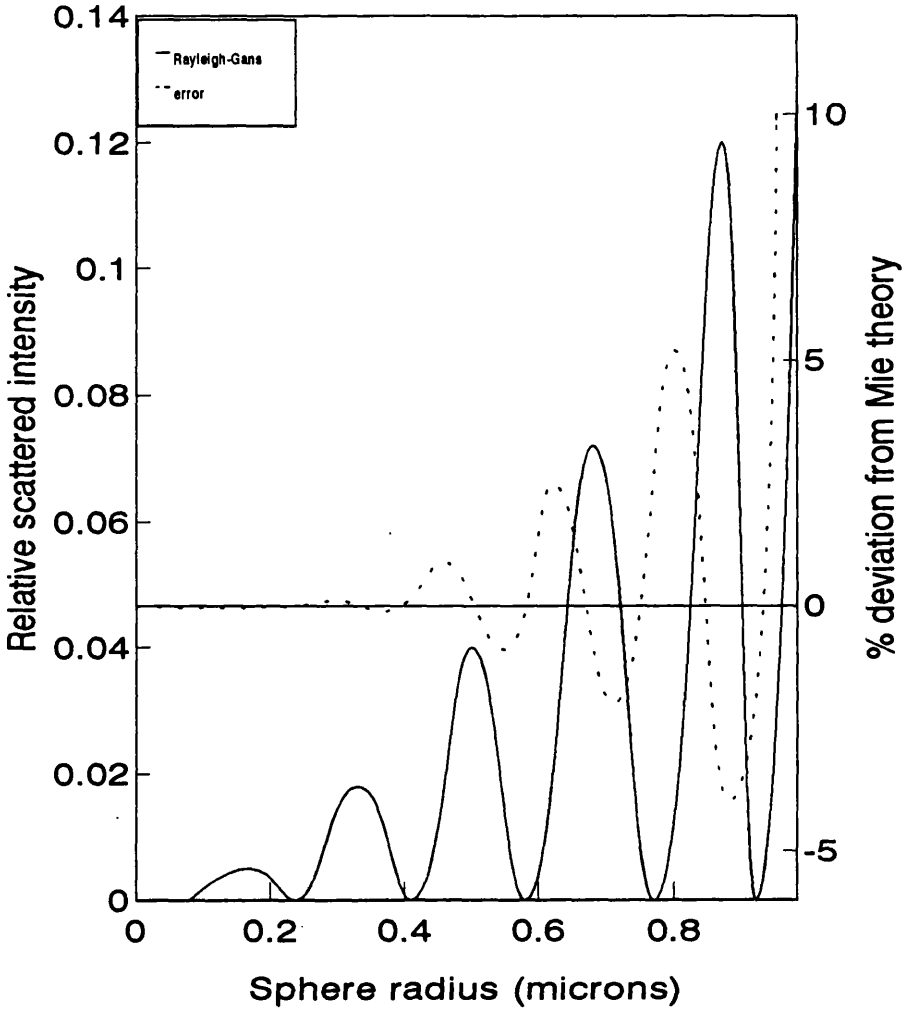


Fig 1.8: A plot of scattered intensity as a function of radius for the Rayleigh-Gans approximation. The percentage error with respect to Mie theory is also shown. The illuminating wavelength is 633nm and the relative refractive index is 1.03. The theory with these parameters is accurate (for spherical scatterers) to within 1% for radii up to about 0.6 microns.

considering the reflection and refraction of rays at the particle interface and phase shifts in traversing the particle using classical optics.

The resulting expression for the intensity (for perpendicularly polarised incident light scattered from a spherical particle) is :-

$$I=\frac{1}{k^2r^2}\left|\sum ka|\epsilon_1|D^{\frac{1}{2}}e^{i\sigma_1}\right|^2 \qquad (1.16)$$

where $\varepsilon_1$ is a term describing the ratio of incident to finally transmitted light energy for a particular ray.

$$D=\frac{\sin(\tau)\cos(\tau)}{\sin(\theta)\left|\frac{d\theta}{d\tau}\right|} \qquad (1.17)$$

$\theta$ and $\tau$ are angles shown in fig. 1.9. $\sigma_1$ is a term describing the phase shift of a particular ray and passing through the sphere. This theory is not of great use for DLS as its valid particle size range is at the upper limits of the DLS analysis size range but is included here for completeness. The ray optics approximation is sometimes used in other particle sizing instruments such as the time of transit method where a beam is scanned across a particle at known speed and the reflected pulse length taken to measure the particle size.

The approximation of rays mentioned in the first paragraph imposes a limit on the lower particle size that would be valid in this case. A rough guide to the limit of this approximation is that the lowest diameter that should be used is about 5 times the wavelength. For HeNe laser light this works out at approximately 3μm.

### 1.2224 Other approximations

Fig 1.10 gives a plot of m-$\alpha$ space showing schematically the regions of validity of the major theories.(m = relative refractive index, $\alpha$ = size parameter). It is noticeable that they are all crowded around the edges of the diagram corresponding to the fact that the limits of the theories are a combination of $\alpha$ small or large and $|m - 1| << 1$ or $m \rightarrow \infty$. Scattering in the middle region is difficult to classify as it is variable depending upon the size of $2\alpha(m - 1)$, without clearly defined boundaries.

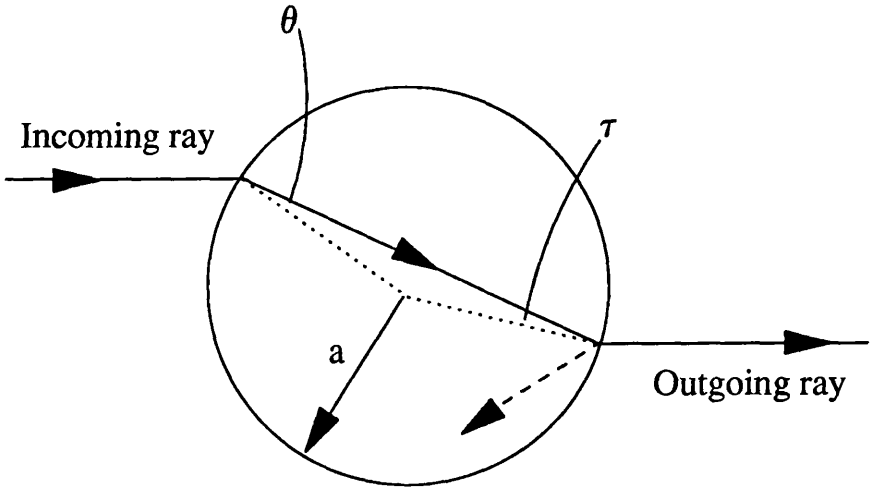


Fig 1.9: Diagram showing ray passing through a sphere indicating the angles in equation 1.17 for the geometrical optics approximation.

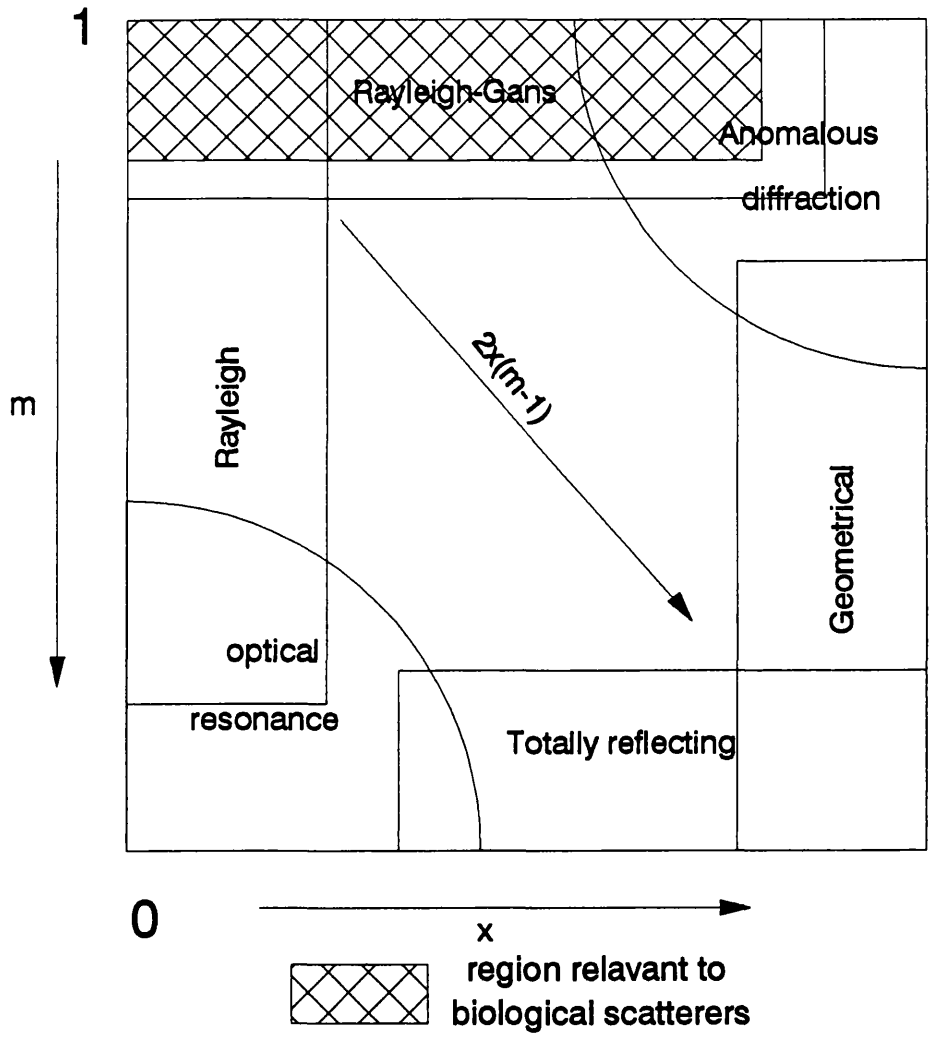


Fig 1.10:
Schematic plot of the range of validity of various approximations. The relative refractive index is plotted from on the left of the chart and the size parameter along the bottom. The region most relevant to biological scatterers ie. low refractive index and wide size range, is represented as the shaded section. This covers the Rayleigh, Rayleigh-Gans and Anomalous diffraction theories.

Regions on this diagram not yet described are anomalous diffraction, optical resonance and totally reflecting spheres. The latter two are not valid in the biological context as they apply most readily to metal particles. The approximate region appropriate to biological scatterers is shown in the shaded box. Anomalous diffraction deserves a mention as although it is not relevant in DLS, other sizing methods for larger particles make use of it and it can be used as a correction factor in optical density concentration calculations.

Anomalous diffraction is an extension of the geometrical theory where at small m, the light in the forward direction can be considered as an addition of diffracted and transmitted light. Due to m being small the transmitted light is undeviated. Evidently this theory only holds for a range of angles about the forward direction. The formal limitations are:-

$$|m - 1| \rightarrow 0$$
$$\alpha >> 1 \qquad (1.18)$$

the resulting light being an interference of diffracted and transmitted radiation gives an undulating plot of the scattering efficiency against $\alpha$. It is plotted as such as the theory only describes light scattered in the forward direction. An equation has been derived for the scattering efficiency of spherical particles in this approximation. ( Van der Hulst 1957) :-

$$Q_{sca}=2-\left(\frac{4}{\rho}\right)\sin(\rho)+\left(\frac{4}{\rho^2}\right)(1-\cos(\rho)) \qquad (1.19)$$

**1.223 Non spherical scatterers**

The emphasis on the preceding sections has been on spherical scatterers due to the relative ease of their mathematical analysis. However a great deal of biological scatterers are not spherical so the effect on the theories of this condition must be considered.

Exact solutions for ellipsoids, cylinders and spheres with or without varying refractive indices within the body of the particle have been calculated. In the Rayleigh-Gans approximation solutions exist for ellipsoids,cylinders,cubes,thin disks, chains of spheres

and random gaussian coils.

Evidence for the shape of a scatterer may be obtained by microscopy or indeed by light scattering measurements. A method for doing this is the so called dissymmetry measurement. This is a simple intensity measure at two complementary angles and can characterise the shape of the scattering particles fig. 1.11 .

An important measure of particle size of non_spherical scatterers is the radius of gyration. This is defined as :-

$$R_g^2 = \frac{1}{V}\int_V (r_m - r)^2 dr \qquad (1.20)$$

r m = centre of mass of particle

r = position of volume element dv

Which can be interpreted as a mean square average of the radius over the volume of the particle. It has been shown that the form factor describing the angular distribution of relative light intensity may be written :-

$$P(\theta)_{\theta \to 0} = 1 - \left(\frac{k^2 R_G^2}{3}\right) \qquad (1.21)$$

where k is the scattering angle. This means that a measure of size independent of shape can be made.

Also worth noting is the work where the scattered light is calculated by assuming some roughness function of the particle surface represented by an angle distribution function (Schuerman 1980). In principle any shape of particle may be represented. So far only particles with Gaussian slope distribution have been calculated, This theory is only valid in the geometrical optics regime as it considers rays reflected by the particle. Also it is strictly for absorbing particles. The use of other matrix elements in the scattering matrix (§1.21) where changes in the polarisation of the scattered light are detected and used to indicate departures from sphericity has been described (Barber and Hill 1980).

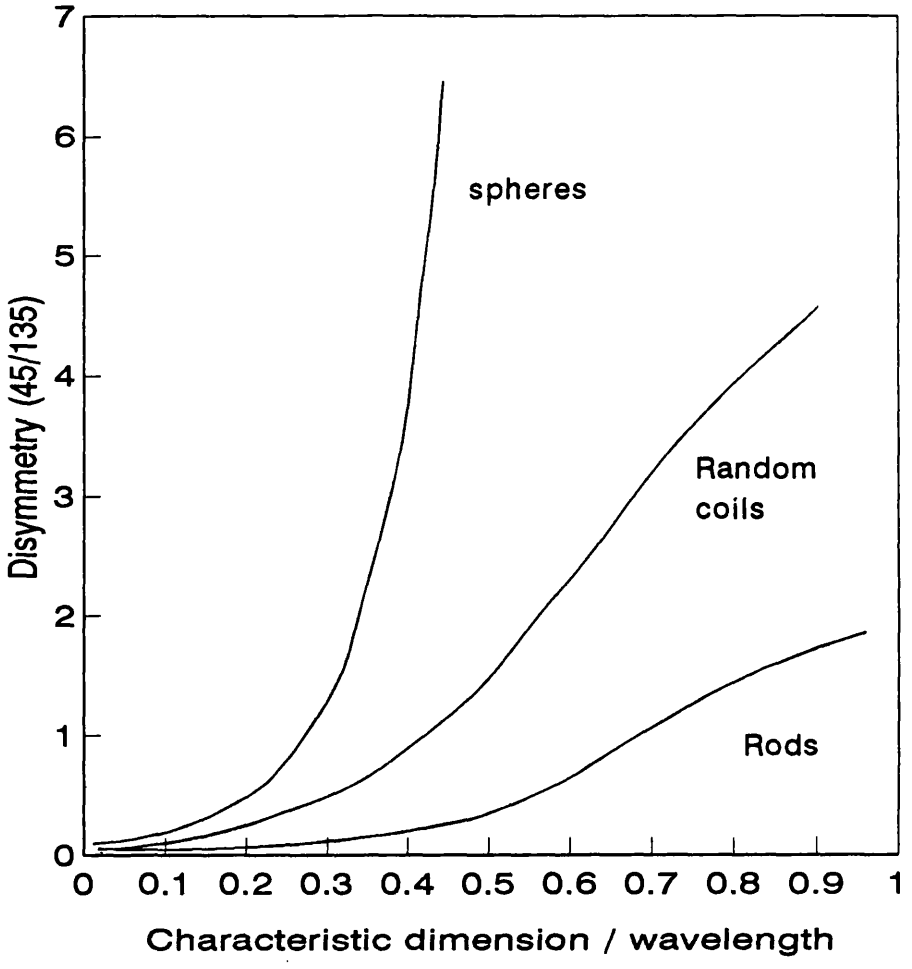


Fig 1.11: Plot of disymmetry ratio measured as the ratio of scattered intensity at 45° to that at 135°. If such a plot is constructed by either measurements made at various wavelengths or particle size for the same type of particle then an test of the shape may be made. Subsequently an appropriate scattering theory may be applied.

A promising method in this particular area is described (Schiffer 1990) who describes a numerical method to describe light scattering by irregular particles of arbitrary material. The method works well for irregularities in the particles smaller than the wavelength of the incident radiation with the added condition that the size parameter must be less than about 7 (see equation 1.11a).

When a collection of particles of irregular shape scatter light the effect is that of averaging the scattered light field over all particle orientations. This is because the particles will be undergoing rapid translation and rotation during any scattering experiment so that several orientations of the particle will be represented to the incoming light. Also with a large number of scatterers random orientations will be taken by the various particles so that the detected field is a summation over a large number of scatterers in different attitudes. The effect on the angular distribution of the scattered light is a smoothing process so that some distinctive features for a particular orientation of an irregular scatterer will become not so apparent. Particularly the polarisation of the scattered field will be different to that predicted for a preferred orientation and related to this fact is a measurement of the depolarisation factor for a particular particle which can give information on particle shape.

Although spherical particle calculations are useful they are usually only going to approximate the system of interest. Extensions to non-sphericity must be considered in any application.

For mathematically intractible problems and for verifying theories experiments may be arried out experiments at microwave wavelengths on scaled up models of particles. Being theoretically the same in terms of scattering properties measurements can be made on particles of any shape, size and refractive index required at visible scales. This allows shapes to be constructed to mimic particles for which theory is not yet developed. Care must be taken in translating the results to optical scatterers as absorbtion and other wavelength dependent properties are not modelled.

## 1.3 Dynamic Light Scattering

The signal processing aspect of DLS owes its foundation to the work of Hanbury Brown and Twiss (1956) and their experiments measuring stellar diameters using an analogue correlation technique. The application of correlation to light scattering measurements was studied in the late 1960's and early 1970's (Cummins and Pike 1974). Lasers were in the early stages of development as was digital electronics and it was several years before the cost of DLS became low enough for commercial instruments to become available. Throughout the 1970's DLS was applied to many systems particularly submicron particles which had previously been inaccessible in such a quick and unobtrusive manner. Biological systems seem to be the most popular subjects to study and these are reviewed in this section. The early 1970's and 1980's work seems mostly to concern improvements in the data analysis techniques and up to the present new methods of data analysis are being introduced. These are covered in §1.4. Many texts now cover the theory of dynamic light scattering (eg. Chu 1974,1991, Berne and Pecora 1976) and the following description is a brief overview from these.

A schematic of the dynamic light scattering experiment is shown in figure 1.12.

### 1.31 Correlation theory for dynamic light scattering

The incident laser light wave impinging on a suspension of scatterers can be described by the following equation:

$$E=E_0\exp(2\pi ft-\frac{2\pi x}{\lambda}) \qquad (1.22)$$

f is the frequency of the illuminating radiation,$\lambda$ is the wavelength and x is the distance into the sample. The scattered light field is a superposition of electric fields radiated from all charges in the scattering volume, the resultant field is therefore dependent on the positions of these charges. Particles or molecules in suspension are continually translating, rotating and vibrating due to thermal interactions and this leads to a change in the total scattered field as a function of time. Implicit in these fluctuations is information about the positions and orientations of the molecules and this information may be obtained from the

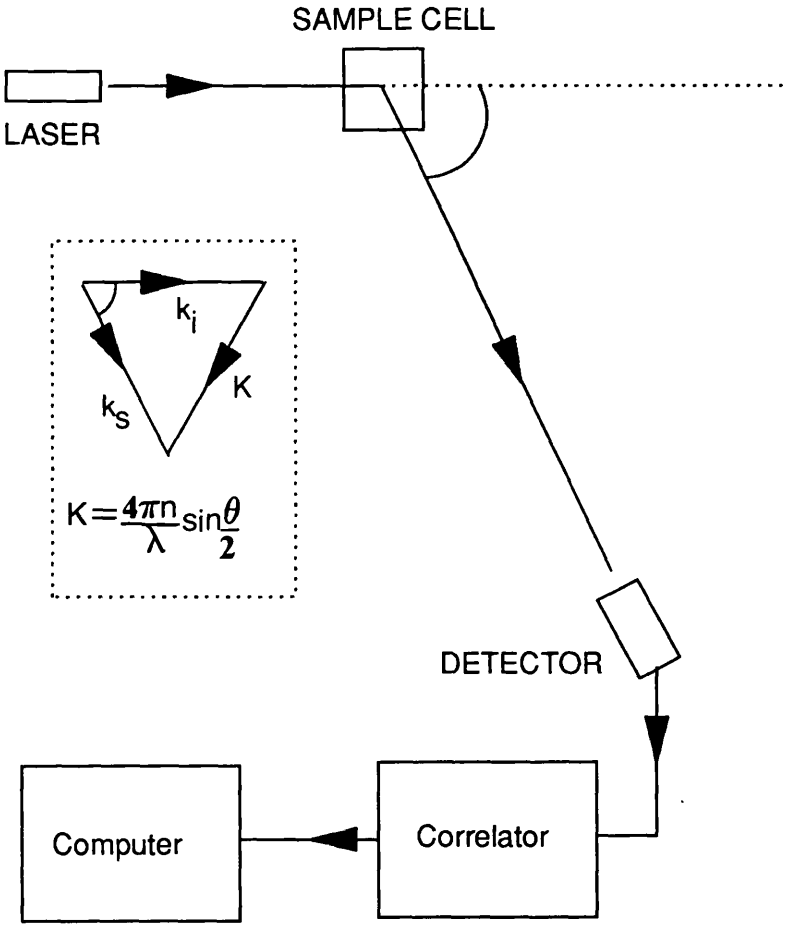


Fig 1.12:

Schematic of light scattering experiment with a detail of the scattering vector which appears in the equations describing the correlation function.

scattered light. The fact that thermal motion is erratic leads to random variation of the intensity fluctuations at the detector. However the rate at which it randomly fluctuates is dependent upon the rate of motion of the particles.

### 1.311 The form of the scattered light

If the light scattered from individual particles in the measurement volume is considered the amplitude at the detector can be written:-

$$E(t) \propto \sum_{i=1}^{N} a_i(t) \exp(-\phi_i(t)) \qquad (1.23)$$
$$\text{where } \phi_i(t) = \underline{k}.\underline{r}_i(t)$$

ie. a sum over N particles scattering from positions $r_i$ at time t. $\phi$ is the instantaneous phase relative to a fixed point at the detector due to the position of particle i at time t. Here it is assumed that:

a) The illumination is uniform across the measurement volume.
b) The light is spatially and temporally coherent across the volume.
c) Single scattering of light by particles occurs.

$a_i(t)$ is the scattering amplitude of particle i and is in general a function of the experimental set-up and particle size and shape as well as time. If the particles can be assumed to scatter the radiation identically and $a_i(t)$ can be considered as a scattering volume "occupation indicator". ie:-

$a_i(t) = 1$ if scatterer is in the volume
$a_i(t) = 0$ if not.

From the above expression the intensity of the scattered radiation can be calculated as:-

$$I(t) = E^*(t)\ E(t) \qquad (1.24)$$

### 1.312 Autocorrelation function estimators

The aim in order to analyse the light field at the detector is to describe its interaction with the system. The incident light field can be considered weak and so the system will respond linearly to it (see §1.21). It is necessary next to introduce time dependent correlation functions which describe the degree to which two dynamical properties are correlated over a period of time. If a statistically stationary system is considered where the light intensity at the detector maintains an average value over long timescales but fluctuates rapidly on relatively small time scales then the average and autocorrelation are described by the following equations:

$$\langle E(t)\rangle = \frac{1}{T}\int_0^T E(t)\,dT \qquad (1.25a)$$

$$\langle E(t)E^*(t+\tau)\rangle = \frac{1}{T}\int_0^T E(t)E^*(t+\tau)\,dT \qquad (1.25b)$$

Here T is the measurement time and $\tau$ the delay time. The angle brackets denote average values. In any experiment the intensity can only be sampled at discrete times so these integrals must be replaced by the estimators:

$$\langle E(t)\rangle = \frac{1}{N}\sum_1^N E(nt) \qquad (1.25c)$$

$$\langle E(t)E^*(t+\tau)\rangle = \frac{1}{N}\sum_1^N E(t)E^*(t+n\tau) \qquad (1.25d)$$

It can be shown that for the stationary system:

$$\langle E(0)E^*(0)\rangle \neq \langle E(0)E^*(T)\rangle, \text{ for large } T. \qquad (1.25e)$$

That is that the signal at long time scales is uncorrelated with that on the short time scale. The degree to which the data is correlated is determined by the fall over the first part of the correlation function. In many applications and in particular the light scattering experiments of diffusing systems the correlation function takes on the form of a decaying exponential. This is not always the case. Examples of other correlation functions exist eg. for swimming organisms (Boon 1983). Figure 1.12a shows a typical autocorrelation

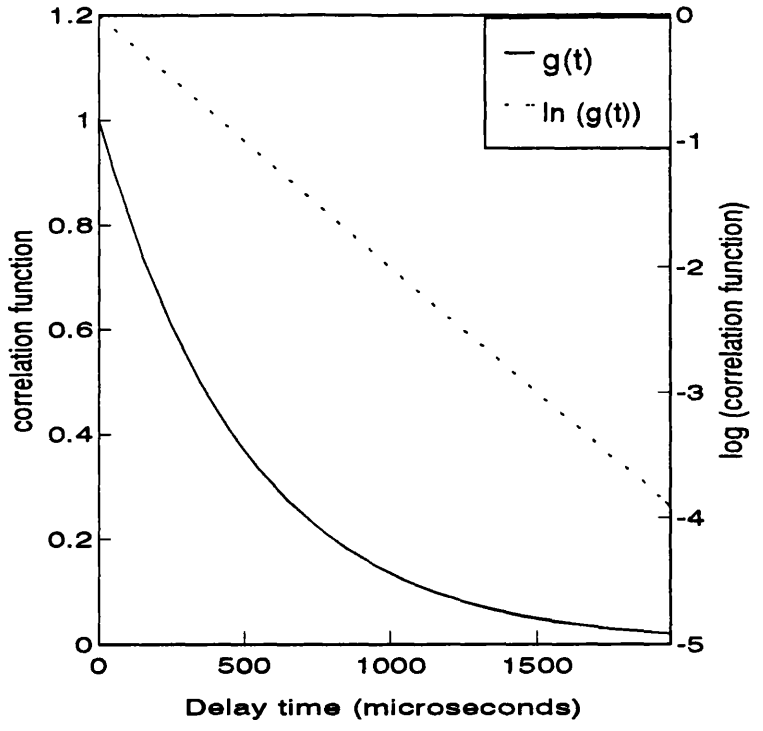


Fig 1.12: First order autocorrelation function according to equation 1.23a. The plot corresponds to data expected for an monodisperse suspension of 80nm diameter diffusing spheres at 25°C.

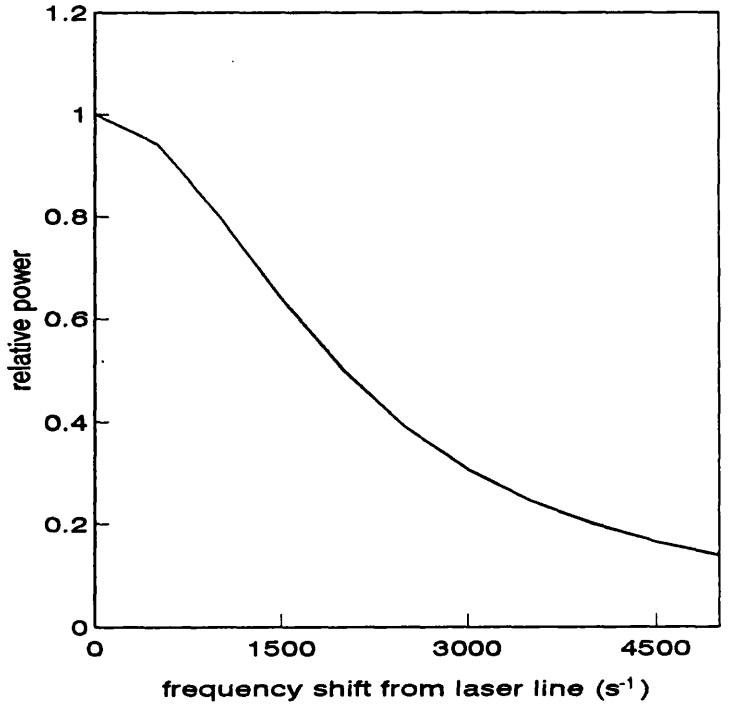


Fig 1.13: Spectrum of scattered light scattered from a monodisperse suspension of diffusing spheres of 80nm diameter at 25°C. The spectrum of the original laser line has a width of about 12 s-1 compared to the 2000 s-1 width at half maximum shown in the scattered light.

function for a diffusing system of non-interactive particles. In this case the relaxation time which is a measure of the degree of self correlation is given by the time it takes the function to decay to 1/e its original value.

$$\langle E(t)E^*(t+\tau)\rangle = I^{(1)}(\tau) = \exp(-2DK^2\tau) \qquad (1.26a)$$
$$\Gamma = DK^2 \qquad (1.26b)$$

The relaxation time is $1/\Gamma$, K is the scattering vector (see figure 1.12) and D is the diffusion coefficient.

When measuring diffusing particles of different size in suspension the correlation function becomes more complex than a single exponential decay. Each size or diffusion coefficient will contribute an exponential decay to the function therefore resulting in a multi-exponentially decaying series. The extraction of the original size or decay constant distribution,$G(\Gamma)$, from this autocorrelation function is discussed in §1.4.

### 1.32 PCS versus classical interferometry

Instead of time-domain analysis as presented here it is also possible to process to optical signal in terms of the frequency broadening that has occurred on scattering from the sample. In order to do this a Fabry-Perot interferometer is used to scan across the optical frequencies and determine the spectral distribution of the scattered light. For a monodisperse system the spectrum can be described by:

$$G(\omega) = \frac{1}{\pi} \frac{DK^2}{(\omega - \omega_L)^2 + [DK^2]^2} \qquad (1.27)$$

This Lorentzian spectrum is plotted in fig 1.13. The half width at half maximum can be measured to give $\varpi = DK^2$.

In fact DLS and interferometry are complementary techniques as they have different ranges of application. PCS is good for decay constants of the order of tens of nanoseconds up to tens of seconds. The interferometric technique is good for the shorter time scales ie. where the frequency broadening is larger. This is in the 1MHz region and up which corresponds to microseconds down to picoseconds and beyond.

A comparisonof the two techniques has been presented. (Vaughan 1974).

### 1.33 Averaging schemes

For non-interacting particles small compared to the illuminating wavelength the mean intensity of the light scattered by N macromolecules of molecular weight $M_w$ is $NM_w^2$It follows that:

$$G(\Gamma_i) = \frac{N_i M_i^2}{\sum_i N_i M_i^2} \qquad (1.28)$$

Using the relation between the diffusion coefficient,D, and the autocorrelation decay constant $\Gamma$ the diffusion coefficient intensity average follows:

$$\overline{D} = \frac{\overline{\Gamma}}{K^2} \qquad \Gamma_i = D_i K^2$$

$$\overline{D} = \frac{\sum_i N_i M_i^2 D_i}{\sum_i N_i M_i^2} \qquad (1.29)$$

An effective spherical radius is calculated by the Stokes-Einstein equation as shown here:

$$R_H = \frac{k_B T}{6\pi\eta\overline{D}} \qquad (1.30)$$

$\eta$ = *suspension viscosity*
$k_B$ = *Boltzmanns constant*
$T$ = *temperature*

Other averages frequently encountered in light scattering data analysis are the mass and number averages. These are calculated as follows:

$$\overline{D}_M = \frac{\sum_i N_i M_i D_i}{\sum_i N_i M_i} \qquad (1.31a)$$

$$\overline{D}_N = \frac{\sum_i N_i D_i}{\sum_i N_i} \qquad (1.31b)$$

All the above equations is for the approximation where the size of the particles small

compared with the wavelength of the scattered light. However often this is not the case and the expressions have to be generalised. This amounts to replacing the $M^2$ term in the first expression by a scattering factor. The form of this factor is shown for different ranges of particle size in §1.2. A discussion of average values and their comparison with other types of analysis has been carried out with experimental verification (Finsey and Jaeger 1990).

The raw data being a light intensity measurement is best interpreted in terms of the intensity averages. Sometimes it is useful to convert to the other terms but for the general cases this will mean making assumptions about the particles shape. This is also true when converting from diffusion coefficient to size where commonly the approximation of spherical particles is assumed.

### 1.34 Limitations of dynamic light scattering for particles in suspension

The theories described from the literature in the previous sections have used certain approximations to allow simplifications to be made. The requirement for a large amount of scatterers in the measurement volume to produce the required statistics for the above analysis is termed the Gaussian approximation and is described below. Other constraints imposed on systems are that particle interactions are negligible and that single scattering occurs. The effects and reality of such limitations are discussed along with the problem of polydispersity which is of major concern in this and many applications.

#### 1.341 Gaussian approximation.

So far the theory presented has been based on the amplitude or first order correlation functions. The detected signal is proportional to the intensity of the scattered radiation so that in processing the data the detected signal must be converted from an intensity correlation function into the amplitude correlation function. The Gaussian approximation holds for very large occupation numbers in the measurement volume and states that:

$$I^{(2)}(\tau) = 1 + |I^{(1)}(\tau)|^2 \qquad (1.32)$$

The first and second order correlation functions are denoted by the superscript in brackets.

For systems with small occupation numbers corrections must be applied to the above equation. In most biological systems however this will not be necessary.

### 1.342 Non-interacting particles

In order to measure reliably particle size current instruments performing a DLS measurement specify that the suspension or solution under analysis contains non-interacting scatterers. This simplifies the theoretical treatment to that described in §1.31 as positions of separate scatterers are not correlated over time and only individual particle motions are relevant.. When interactions no longer become negligible it has been shown (Pusey 1978) that the autocorrelation function consists of two distinct features in the case of monomodal dispersions. Firstly a fast decay which can be considered as caused by diffusion of the particle in the short term unhindered by its neighbours and secondly a slower decaying tail interpreted as hindered diffusion due to interactions with neighbouring particles. This can give information about the sample, particularly interparticle potentials. Examples of this and other applications have been discussed (Pusey 1979).

The degree of interaction between particles will depend upon both the type of particle and the suspending fluid. Ideally particles will be uncharged but practically all biological particles possess some sort of charge distribution. This might be neutralised by altering the pH of the system but a more easy and practicable solution is to increase the interparticle separation by diluting. This is also required because of the multiple scattering effect discussed in the next section.

### 1.343 Single and multiple scattering.

The equations described in §1.31 are approximate in the theoretical limit of very low concentration ie. single particle scattering is assumed. In practice this is a difficult aim to achieve and unless the multiply scattered and singly scattered light can be separated then the theory must be modified. This is discussed in the next section. A study of the effects of concentration on the results for a monodisperse system have been carried out (Van de Meeren 1988) and the conclusions were that oversizing of the particles occurred and an increase in the apparent polydispersity measured. The important criterion was not the

concentration itself but the mean separation of the particles (independent of size) which must be of the order of 15 microns or more to avoid distortion of the results due to multiple scattering. This results in a critical particle concentration that varies with particle size. A plot in the size area of interest is given in figure 1.14.

The alternative to maintaining the concentration in the desired region is to extend theories to cope with multiple scattering systems or to suppress the multiple scattering experimentally. The former case has been treated by many authors (eg. Dhont 1983) and recently the theory and practice of diffuse wave spectroscopy has been developed (Horne 1990). Commercial instruments exploiting this theory are available. However the application of such instruments may be limited in that they provide an average size but no estimate of distribution width and will not cope for more detailed systems. However the measurement correlates well with that obtained by dynamic light scattering in a dilute suspension of the same sample. The suppression of multiple scattering by a cross correlation technique has been described (Phillies et al 1981) and tested successfully, however the experimental set up becomes quite complicated and alignment crucial.

### 1.3431 Optical densities of concentrated suspensions.

Recently (Konak et al 1991) demonstration of the separation of the coherent and transmitted laser intensities in concentrated suspension of latex spheres has been presented. This amounts to separating contributions from direct unaltered light and scattered light at the detector. Their use of the Mandel-Rice formula allowed quantification of the dependence of the total intensity on pathlength (and consequently concentration) and the coherent part of the total intensity which is the unscattered contribution. The coherent part was shown to obey the Beer-Lambert law over the complete range of concentrations whereas the transmitted light departed from this at the higher concentrations. The size of the particles used in this study were 94nm and were in the Rayleigh limit. The extension of this to larger particles may cause problems as they tend to forward scatter to a greater extent. It is expected that the separation of coherent and incoherent (ie. that part due to multiple interactions) parts would become more difficult as for larger particles the parts will arrive at the detector closer together in time and hence need to be more resolved. However if this technique could be applied to concentrated complex mixtures it may

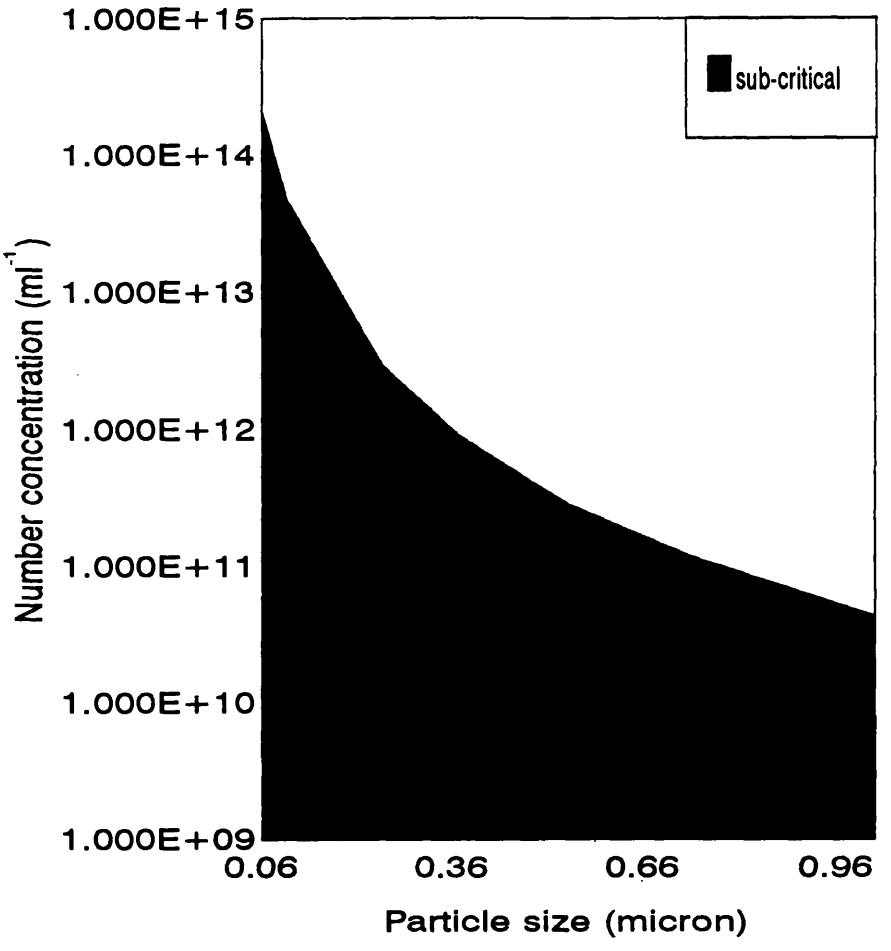


Fig 1.14: Plot to show the critical concentration at which DLS measurements are reportedly affected by multiple scattering processes. The shaded area indicated particles within the singly scattering approximation. (Van de Meeren 1988).

simplify the experimental measurement of concentrated suspensions.

The sensitivity of optical density measurements could then be enhanced at higher concentrations as the extrapolation of optical density against path length (concentration) shown in fig. 1.15 indicates a continuing linear trend rather than turn-over at higher concentration. For a mixture of particle size, in order to work out a concentration from the optical density, the scattering properties of the components of the mixture are required. This was covered in §1.1142 . However the use of the above method would greatly simplify and extend the application of this theory which is only applicable in the single scattering approximation.

This separation of multiple and single scattering was also carried out at an angle of 90 degrees and a proposed method for correcting for multiple scattering events in dynamic light scattering suggested.

A more direct method of separating the two components is being used in imaging applications in diffuse media. An ultrashort pulse of laser light (femtoseconds) is passed through the sample and the detector gated so as to only accept light in the first few picoseconds of receiving the transmitted pulse. This separates the directly transmitted light (ballistic contribution) from the multiply scattered (diffuse) contribution. This is currently being applied to imaging early tumours in breast cancer screening and object detection in dense fog or cloud (Alfano et al 1992). However currently very expensive components are required to implement such a system and could not be justified in the present application until such costs come down.

This method would be applicable only to optical density measurement and not DLS as the time scale of correlation is longer than the pulse and a correlation function could not be formed.

### 1.344 Polydispersity

Polydispersity is most obvious in suspension properties as a range of size of particles present. However the variation of any physical property of the particles measured will

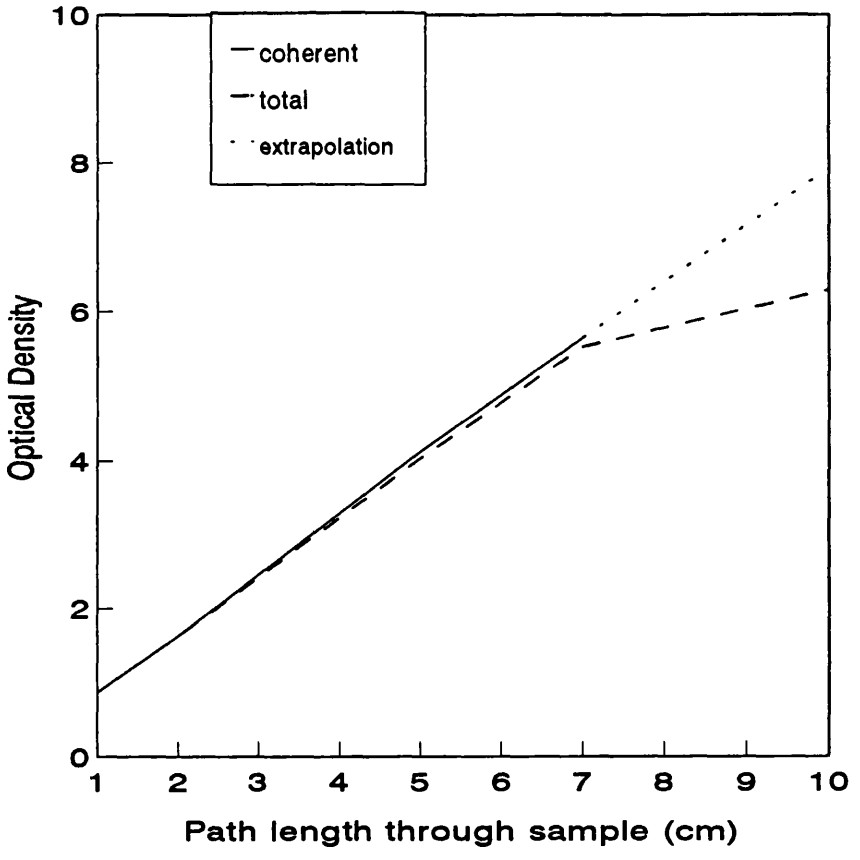


Fig 1.15: Variation of the direct (coherent) and total scattered (incoherent + coherent) contributions to the optical density signal of 94nm latex spheres.. An extrapolation suggests the extention of linearity of the coherent contribution to higher optical densities (Konak et al 1991).

amount to a change in the resulting size distribution of a DLS measurement. One advantage DLS has over other optical methods is that the measurement of size is based on a property that is independent of the optical properties of the particle and as such the accuracy of the size is not directly affected due to this fact. However attributing the amount of scattered light to a particular particle size will of course be directly sensitive to the optical properties. The variation of scattered light with particle properties was discussed in §1.2. In effect there are two sides to the polydispersity problem in DLS. The first is the usual interpretation where the data that constitutes the measurement has to be inverted to produce an intensity distribution. This distribution is subject to experimental errors for the most part and this inversion procedure forms a major part of this thesis. The second side to the problem is taking the intensity distribution and converting it into a realistic number or mass distribution and as such is open to theoretical approximation errors. This procedure implies knowledge of the particles present ie. their size,shape or refractive index. This knowledge is not always known and is more often approximated. On the whole biological particles have quite low refractive indices as they constitute a large amount of water. However there are several light absorbent and optically active parts of biological molecules that may contribute to the polydispersity problem.

In the present application the elements of primary concern are any substances in the broth which could cause interference. The yeast and virus-like particles themselves do not absorb a large amount in the red. However in working back to a knowledge of concentration of yeast and VLP in solution the refractive indices of each will be necessary unless a calibration is made.

### 1.41 Ill conditioned problems

The nature of the problem considered here (ie. the retrieval of the decay constant distribution in equation 1.35) is widely encountered. It is a subset of ill-conditioned problems, a subject which has generated an extensive literature (see eg. McWhirter and Pike 1978). The term ill-conditioned refers to the fact that there exists, in general, an infinite number of solutions ie. size distributions that will fit the noisy data that has been collected. The size distribution chosen by the fitting procedure is therefore program dependent. The same data set can produce different size distributions from different analysis methods. Several methods are discussed in §1.43.

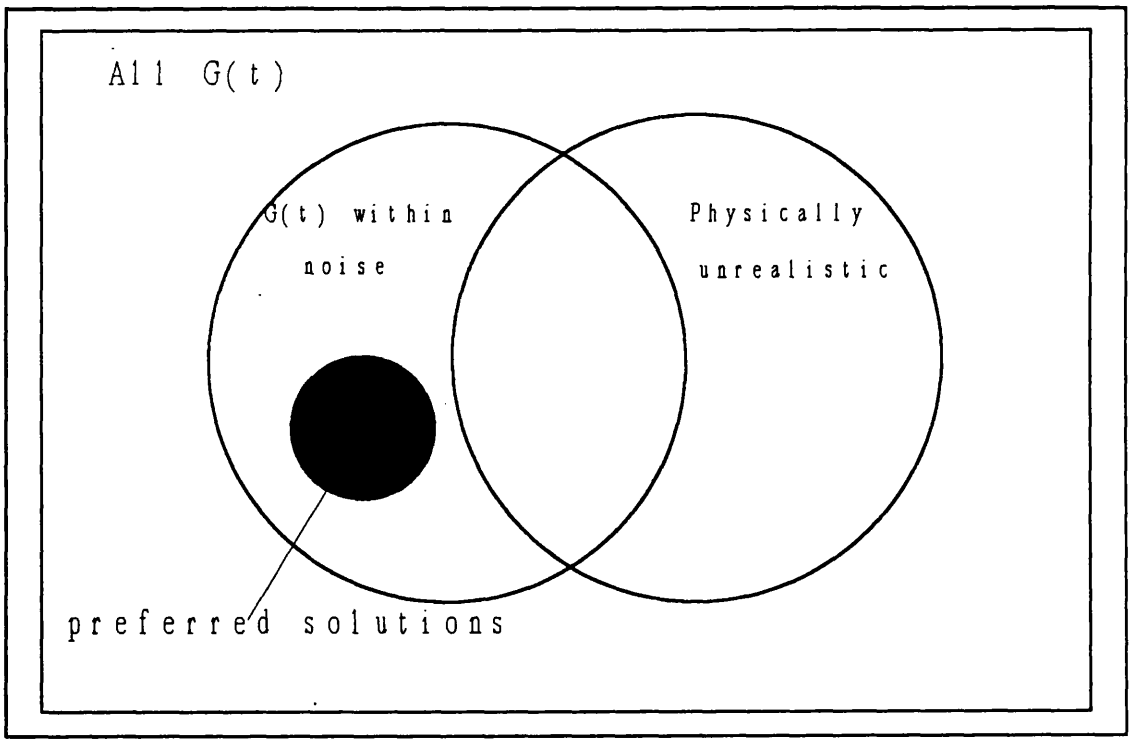


Fig. 1.16 Schematic of solution to ill- conditioned problems

### 1.42 Accuracy and errors

In order to improve the solution given by the computer, better quality ie. less noisy, data is desirable. In effect this reduces the size of the left hand circle in fig. 1.16. The signal to noise ratio of the data stream is improved as $\sqrt{N}$ where N is the number of samples taken. In principle, the best data will be taken with longer experimental times. There is

a trade-off against time available for measurement in an on-line analysis environment. Also care must be taken to avoid systematic effects such as dust and temperature drift over longer experiments.

**Systematic errors** can be avoided only by careful system alignment and sample preparation. The sort of conditions to be avoided to prevent unwanted intensity fluctuations at the detector are listed below.

a) Fluctuation in laser intensity: Drifts in laser frequency or intensity can occur due to temperature effects. A stabilisation circuit is necessary to reduce such fluctuations.

b) Reflections - wrong angle, local oscillation : Misalignment of the detector or small amounts of unscattered light entering the detector can lead to errors in the measured diffusion constant. Theoretically it is possible to compensate for this but often the error will go undetected as the data collected can still be good.

c) Dust and bubbles: Scattering from such contaminants can ruin the measurement in the worst case and at best reduce the accuracy. Ensuring a minimum of both dust and bubbles in the sample is essential

.

**1.421 Considerations on required data accuracy.**

This section is included to appraise the theoretical aspects of detecting small changes in the size distribution by the dynamic light scattering technique. Where guideline figures are available, the viability of the method for use in a particular application can be assessed. The procedure will be as follows:

1. Work out the change in correlation function due to a change in a particular form of size distribution.

2. Calculate the approximate noise level of the experiment. (The difficulty of doing this is highlighted in §1.434.)

3. Calculate the minimum detectable change in the correlogram.

4. Calculate the corresponding minimum detectable change in the size distribution.

The form of size distribution chosen is a double delta function to ease analysis and comprehension. It should give guidelines for a real distribution. The correlation function for such a distribution is shown by the following equation.

$$A\exp(-2\Gamma_1\tau) + (1-A)\exp(-2(\Gamma_1+\Delta\Gamma)) \qquad (1.33)$$

A is the fraction of the size distribution due to the decay constant $\Gamma_1$.
The change in this function with respect to A, integrated over all correlation delay time, $\tau$ and divided by the number of correlator channels is:

$$\delta = \frac{1}{N_{ch}}\int_0^\infty \exp(-2\Gamma\tau) - \exp(-2(\Gamma+\Delta\Gamma)\tau)\, d\tau \qquad (1.34a)$$

$$\rightarrow \quad \delta = \frac{1}{2\Gamma} - \frac{1}{2(\Gamma+\Delta\Gamma)} \qquad (1.34b)$$

A plot of the fractional change in correlator channels is shown in figure 1.16. This plot shows that an average change in the correlogram for a lower decay constant of about 1000 $s^{-1}$ and a separation of about 1500 s-1 is about 1%. This means that for a change in the distribution (ie. a shift in peak heights) of 0.1% to be theoretically detectable in this situation, the noise on the correlogram must be smaller than 0.1% per channel.

The noise due to finite experimental time has the straight forward formula given in section §1.42. For a 10 second experiment and for decay constants in the 1000 $s^{-1}$ region, this works out to be in the hundredths of percent range. Noise due to the presence of dust, misalignment of the optical system, and other system dependent errors is difficult to quantify. Evidently it will be necessary to keep them below 0.1% to detect a change in the size distribution in this situation.

It is important to remember that the change is given as an average change per channel. Some channels, particularly in the first part of the correlogram will change much more

than the average so that higher noise levels can be tolerated.

The data being treated here corresponds to the intensity distribution rather than to mass or volume distribution. Since in the approximation of small particles the intensity scattered is proportional to the square of the volume of the scatterers (§1.222) a 0.1% change in intensity requires roughly a 0.05% change in the volume from one peak to the other.

0.05% change in volume of large particles obviously corresponds to a smaller number concentration than 0.05% change in volume of smaller particles. In the present example the sizes considered corresponding to the decay constants chosen are about 30nm and 80nm. A change in volume of 80nm particles compared to a similar change in volume of 30nm particles corresponds to a number concentration change ratio of about 20. Hence twenty times the amount of smaller particles added and one of the larger particles removed would correspond to an equal change in intensity from each peak.

**1.43 Software analysis methods**

$$g(\tau) = \int_0^\infty G(\Gamma) \exp(-\Gamma\tau)\, d\Gamma \qquad (1.35)$$

The difficulty of inverting the Laplace transform equation above, to extract the size or decay constant distribution G(Γ) has been mentioned in §1.41. The problem has been addressed in many ways, usually with the emphasis on a minimum of *a priori* information. Reviews covering many of the methods with experimental results have been discussed ( Chu et al 1983, Stock and Ray 1985).

The methods fall into two main categories:-

i) Assumed size distribution shape
ii) Model-free algorithms

The methods are linear or non-linear least squares methods, with only one or two exceptions except those in §1.434 which use alternative statistical bases for solution convergence estimation.

### 1.431 Assumed size distribution shapes

#### 1.4311 Cumulants method

This method is useful for monodisperse size distributions. Starting from the correlation function weighted by the distribution function G(Γ). This defines the "average" correlation function or average exp(-Γτ).

$$\langle \exp(-\Gamma\tau) \rangle_{ave} = \int_0^\infty \exp(-\Gamma\tau)\, G(\Gamma)\, d\Gamma \qquad (1.36a)$$

It has been shown (Koppel 1972) that the moment generating function is equivalent to this average correlation function and since the function can be written in the form of a polynomial, the measured g(τ) can be least-squares fitted to this.

$$M(-\tau;\Gamma) \equiv \langle \exp(-\Gamma\tau) \rangle_{ave} \qquad (1.36b)$$

For a single exponential correlation function which is the case of pure monodispersity the polynomial coefficients turn out to be zero.

$$K(-\tau;\Gamma) = \sum_{m=1}^{\infty} K_m(\Gamma)\, \frac{-\tau^m}{m!} \qquad (1.36c)$$

$$\text{where} \quad K_m(\Gamma) = \left[\frac{d^m}{d(-\tau)^m}\right] K(-\tau;\Gamma)\Big|_{-\tau=0} \qquad (1.36d)$$

Non-linear coefficients appear non-zero for polydisperse systems.
Specifically:-

$$
\begin{aligned}
K_1 &= \bar{\Gamma} \ , \ \textit{average diffusion coefficient} \\
\frac{K_2}{K_1^{\,2}} &= \textit{relative width of distribution} \\
\frac{K_3}{K_1^{\,3}} &= \textit{skewness measure} \\
\frac{K_4}{K_1^{\,4}} &= \textit{kurtosis}
\end{aligned}
\qquad (1.37)
$$

Experimentally the equations take the form shown below. The parameters of the least squares fit are thus $c_o^{(m)}$ and the $K_{m(m)}$'s.
Each data point should be weighted by estimates of the average square deviation.

### 1.4312 Analytical expressions for distribution fitting.

The most straightforward method of calculating a size distribution is to assume totally the form of the distribution or autocorrelation function and decide the parameters by means of linear or non-linear least squares or maximum likelihood methods. Common functions used to simulate decay constant distributions are Pearson,Gamma and Shulz distributions (Chu et al 1979, Dhadwal 1991). Single or double exponential decays or the William-Watts distribution have been used to model the autocorrelation function (Patterson 1983). Such expressions are also useful for construction of size distributions in simulation exercises to test other data analysis methods.

### 1.432 Model free algorithms

### 1.4321 Eigenfunction expansion.

It has been shown that the Laplace inversion integral can be written in terms of eigenfunctions as shown below.

$$\lambda_\omega \phi_\omega(\tau) = \int_0^\infty \exp(-\Gamma\tau)\,\phi_\omega(\Gamma)\,d\Gamma \qquad (1.38a)$$

Expanding $g^{(1)}(\tau)$ and $G(\Gamma)$ in terms of these eigenfunctions:-

$$g^{(1)}(\tau) = \int_{-\infty}^{+\infty} b_\omega \phi_\omega(\tau)\,d\omega \qquad (1.38b)$$

$$G(\Gamma) = \int_{-\infty}^{+\infty} a_\omega \phi_\omega(\Gamma)\,d\omega \qquad (1.38c)$$

So that the first order correlation function can be written :-

$$g^{(1)}(\tau) = \int_{-\infty}^{+\infty} a_\omega \lambda_\omega \phi_\omega(\tau)\,d\omega \qquad (1.38d)$$

Then the $b_\omega$ in equation (1.38b) follows:-

$$b_\omega = a_\omega \lambda_\omega \rightarrow a_\omega = \frac{b_\omega}{\lambda_\omega} \qquad (1.38e)$$

It can be seen that by using a fitting procedure to find $b_\omega$ and $\lambda_\omega$ that $G(\Gamma)$ can be exactly reconstructed with this information. The problem lies with the form of the $\lambda_\omega$ which fall off close to zero as w increases. So for the higher terms any slight inaccuracy in the estimation of $b_\omega$ will be amplified and the reconstruction of $G(\Gamma)$ incorrect. The slight inaccuracies occur due to noise in the data. To overcome this a finite limit is put on the number of terms used to reconstruct $G(\Gamma)$ in the eigenvalue series.

The detail of the theory can be followed (Ostrowsky et al 1984) to produce a least squares fit described by equation 1.38f.

$$\sum_{i=1}^{\infty}\left((g(\tau_i)-\sum_{n=1}^{N}a_n\exp(-\Gamma_n\tau_i)\right)^2$$

$$a_n=\frac{\pi}{\omega_{max}}\bar{G}(\log\Gamma_n) \qquad (1.38f)$$

$$\Gamma_{n+1}=\Gamma_1\exp\left(\frac{n\pi}{\omega_{max}}\right)$$

The full function G(logΓ) can then be reconstructed through an interpolation formula or by shifting the sample points slightly and repeating until the entire range of Γ has been covered.

### 1.4322 **Histogram method**

This method relies on making an approximation of the autocorrelation function as a series of histogram steps covering a range of Gamma. This technique has been implemented with linearly and logarithmically spaced histogram steps (Fletcher and Ramsay 1983) the latter technique using the principle of the exponential sampling theorem described in section 2.1. In this case the histograms are shifted and overlapping sections are averaged to produce the final distribution. This amounts to a smoothing of the gamma distribution representation.

The approximation of the autocorrelation function is shown below. The integral over Γ is substituted by a summation and the remaining part of the integral can then be analytically evaluated for each step. In this way the whole range of Γ is covered rather than sampling at individual values of Γ.

$$g(\tau) = \sum_{j=1}^{N} G(\Gamma_j)\int_a^b \exp(-\Gamma_j\,\tau)\,d\Gamma$$

$$where\ a = \Gamma_j-\frac{\Gamma_j}{2},\ b =\Gamma_j+\frac{\Gamma_j}{2} \qquad (1.39)$$

$$or\ \ b-a = \frac{\Gamma_{j+1}}{\Gamma_j} = \exp\left(\frac{\pi}{\omega_{max}}\right)$$

The set of decay constants can then be found by least squares fitting of equation x to the data by a suitable algorithm. Again singular value decomposition is a popular method due

to its stability in the presence of noisy data.

### 1.4323 Sub-distribution method

A method where the final decay constant distribution is represented by a sum over several sub-distributions has been described (Cha and Min 1981). Examples for the form of these distributions used are Laguerre or Hermite polynomials. The data are then fitted to the equation:

$$g(\tau) = \left( \int_0^{\infty} \sum_{n=0}^{N_{max}} C_n G_n(\Gamma) \exp(-\Gamma\tau)\, d\Gamma \right)^2 \qquad (1.40)$$

where all the subdistribution parameters are linked. These parameters are then adjusted to satisfy the least squares criterion. The advantage of such a distribution is that the resulting distribution is smooth over the range of decay constants.

### 1.4324 Non-negatively constrained least squares. (NNLS)

In many applications physically realistic solutions can only be positive. This is the case here, as a negative decay constant is meaningless. The algorithm for a non-negatively constrained least squares analysis has been described (Lawson and Hanson 1974). Introducing positivity constraints into the algorithm constitutes a-priori information but does not imply any particular distribution shape. Again the problem is evaluated as a least squares one but the coefficients $G(\Gamma)$ are forced positive. The fitting routine fits to multiple exponentials as in §2.1 and the resulting values correspond to the areas of the histogram steps. The histogram steps are non-linearly spaced to an extent determined by the detectable difference between sequential exponential decays. This is important as the algorithm will throw away non-independent decays and apart from wasting processing time this can effect the final solution by producing spurious peaks. The steps are spaced as follows (Grabowski and Morrison 1983)

$$\Gamma_i = \frac{1}{(ai+b)^2} \qquad (1.41)$$

### 1.4325 S-exponential sum method

The correlation function, approximated by a sum of many exponential decays but constrained by a so called residual polynomial, has been described by (Cantor and Evans 1970) and has been applied to photon correlation (Nash and King 1982). A residual polynomial is defined as:

$$P(u) = 2\sum_{L=0}^{N} P_L u^L$$
$$\text{where } P_L = w_L[C(L\tau) - b(L\tau)] \qquad (1.42)$$
$$\text{and } u_i^L = \exp(-\Gamma_i L\tau)$$

and the conditions imposed for r exponentials are:

$$P(u_i) = 0 \quad i = 1, r \qquad (1.42a)$$
$$P(u) \geq 0$$

This method is very similar to the non-negatively constrained algorithm described in section 2.6 and is similarly guaranteed to converge to satisfy the above conditions. The difference lies in the adjustment of the exponential amplitudes to approach the solution.

### 1.4326 Regularised inversion/Constrained regularisation

There are several applications of this particular method of analysis applied to correlation function profile analysis (Provencher 1981, Dhadwal 1989), but the procedure is quite general. In describing the technique it is convenient to put equation 1.35 into operator formalism so that the data, b, can be expressed as:

$$\underline{b}=\underline{K}\,\underline{G}+\underline{r}$$

$b$ = *data vector*
$K$ = *Laplace kernel matrix*
$G$ = *Exact solution vector*
$r$ = *noise vector*

(1.43)

The noise term is of course indeterminate. Instead of the filtering techniques used in other methods regularisation seeks a solution to the equation.

$$F(\hat{G}) = \|\underline{b}-\underline{K}\,\hat{\underline{G}}\|^2 + \alpha\|\underline{C}\,\hat{\underline{G}}\|^2 \qquad (1.43a)$$

The latter term in the expression contains a-priori information about the solution. Alpha varies from 0 to 1. Evidently a value of zero will correspond to a direct inversion of the equation with no regularisation. Conversely alpha = 1 completely suppresses the noise but will oversmooth the solution. The desired solution corresponds to a particular value of alpha and the procedure is to solve equation x for different values of alpha and choose the best one with some convergence criterion ie. the relative difference in the least squares evaluation is less than a particular value after a certain number of iterations (Dhadwal 1989). Alternatively (Provencher 1982) calculate a probability factor to determine the value of smoothing parameter that predicts a solution that should be a balance between random artifacts appearing in the distribution and oversmoothing.

### 1.434 Other methods

#### 1.4341 Maximum entropy method (MEM)

A full assessment of this method of analysis, which is not yet fully developed, and its application to photon correlation data has been given (Chu 1991). The premis behind the technique is that it regularises the solution based on objective information contained in the data and not on a user introduced regularisation. However, estimates of the errors and how they vary across the data are required. Early work (Livesey et al 1986) implied that highly resolved complex spectra could be reconstructed using this method but in the actual application data was manually vetted to reject unlikely points. More recently the MEM using a Bayesian estimate (see Chu 1991) rather than least squares criterion for the

regularisation parameter has been described. It was shown to be a better method for resolving multimodal distributions than the constrained regularisation described in §1.4326. It is expected that further improvements in this area should be forthcoming.

### 1.4342 Fourier Inversion

Conversion of the Laplace transform into a Fourier transform problem by means of transforming co-ordinates and using the Fourier convolution theorem has been proposed (Gardner et al 1959) and modified (Provencher 1976) to cope with noisy data. The co-ordinate transforms required are:

$$\begin{aligned} \Gamma &\rightarrow e^{-z}-\beta \\ \tau &\rightarrow e^{-x} \end{aligned} \qquad (1.44)$$

Beta is a convergence parameter which can be adjusted to alter the spectral peak separation. The Fourier transform to be solved for which standard algorithms are available can be written:

$$g(z) = \frac{1}{2\pi}\int_{-\infty}^{\infty}\overline{g}(\mu)\exp(-i\mu z)\,d\mu \qquad (1.44a)$$

$$\overline{g}(\mu) = F(e^{x})$$

The body of the integral first must be evaluated from the data which involves a numerical integration. Also the Fourier transform algorithm involves a window function to avoid spurious components due to sharp cut-off points at the extremes of the integrand.

### 1.4343 Linear programming

In common with many of the analysis methods the linear programming method (Zimmerman et al 1984) uses a sum over several exponentials to estimate the correlation function (see equation 1.45a). The major difference between this and other methods is that it does not use the least squares criterion for establishing the best-fit solution. Instead the sum of absolute values of the residuals are minimised. The problem is formulated by defining each residual as the difference of two positive integers and similarly for the

baseline value. The problem can then be expressed as a linear programming exercise which is to minimise:

$$Z=\sum_{i=1}^{M}|\epsilon_i| \qquad (1.45)$$

subject to the constraints:

$$\sum_{j=1}^{N} x_j \exp(-\Gamma_j \tau_i) + B + \epsilon_i = g^{(2)}(\tau_i) \quad for\ i=1 \rightarrow M. \qquad (1.45a)$$

To solve this system the authors used a Simplex algorithm.

The spacing of the exponentials as in other methods must be determined by some method. In this case an initial quite wide logarithmically spaced set is used and on analysis of the residuals to check for systematic error this density is increased if necessary to improve the statistics. The goodness of fit conditions depend upon the number of sequences of consecutive residuals of the same sign. If this number is too great for the number of data points present then more exponentials are added until the statistics are satisfied.

### 1.434 Choosing methods for on-line analysis

A discussion of the relevant software analysis methods to apply to on-line monitoring and control is necessary here. While a large amount of effort over the past decade has been spent to extract the maximum amount of information possible from the ill-posed data set, the methods used are not always straightforward to implement in an autonomous manner which is required for hands-off operations in an automatic control or monitoring situation. Also in the present application there is additional information available to the algorithms. This reduces some of the advantages programs might have over others and brings them closer together in terms of their use in monitoring and control. In this situation it is advantageous to choose those easiest to implement without compromising the resulting distribution. In this comparative discussion of the techniques used the following points need to be considered:

1. Algorithm speed and storage requirements.

2. Amount of user information required to find the best solution.

3. Past experience of performance of methods in similar situations as the present application ie. peaky and mult imodal distributions.

4. The performance of the algorithms in the presence of noisy data.

Each point will be considered in turn:

**1. Algorithm speed and storage requirements.**

Algorithm speed and storage space are of prime importance when the result is sought in the shortest possible time and particularly when the data processing step is the longest part of the experimental set-up (see §1.02). Very high speed processor chips are now available but at a relatively high cost. Cheap computer power is however on the increase and it can be assumed that within the next few years processing power/cost will increase dramatically. Thus the choice of algorithm suitability due to speed is not of overriding importance as development of the technique will go hand in hand with an increase in computer advancement and consequently a reduction in algorithm execution time.

Currently it is sensible in a monitoring and control application to choose methods without large amounts of re-iterative convergence tests. Many methods seem to produce several solutions for the same data set with different starting information and choose the best result based on a goodness-of-fit criterion. However cheaper parallel processing hardware which perform many calculations simultaneously will reduce the time for such methods.

Storage space again is not of overriding concern as the cost of memory is dropping along with all solid-state equipment and computers now come equipped with more memory than most techniques described in this section will ever require in this application. It does become an issue however where large amounts of storage and retrieval affect the analysis time.

**2. Amount of user information required.**

This is one of the most important issues for an autonomous monitoring and control situation. Many of the methods described require a user to input values at the beginning or during processing to start or continue the algorithm. The main concern is mid-process information which must be based on user interaction with the program. This is not effective for use in monitoring and control as the human element has not been removed from the control loop. Methods should be chosen which perform well with no user interaction.

**3. Past experience of method performance.**

Performance in conditions prescribed by the system of interest is necessary in considering algorithm choice. The system of primary concern is one broad peak with a narrow spike at a defined size to simulate the presence of particle of defined size next to a broad distribution of particles (ie. virus-like particles in yeast homogenate. See §1.2). There are some programs notably constrained regularisation which might oversmooth the solution. Alternatively in this case a different regularising matrix could be sought to allow for a "spiky" solution. This would probably be subject to instability in the presence of noise which often causes over-oscillatory solutions.

The analysis methods that are of interest are those where it is easy and theoretically sensible to include a-priori information into the starting matrices. This information may be the noise level in the data if this can be experimentally assessed (see §1.42), the range of sizes to be covered (this is easy to include in all cases) or a weighting of the parameters in the algorithm so as to bias the result towards a desired direction. Weighting of the data points themselves is a different issue. It has been shown that it is advantageous to weight the points inversely as the square of the standard deviation of the data points.

In least squares methods it is quite straightforward to weight certain columns of the matrix to bias the solution to certain areas of size or decay constant. The range of size analysed is also simple to include. Since it is generally found that the range of $\Gamma$ can significantly affect the solution reached this is important starting information to include.

**4. Robustness to noise.**

In the software analysis assessment, chapter 5, noise is simulated by adding or subtracting a random number of counts to each data channel to a predetermined level. This simulates photon-counting noise. Noise due to dust and flare (see §1.42) will depend upon the sample cleanliness and system alignment. In real experiments there is no way to determine the contribution to the noise from each source. Dust is unquantifiable and thus cannot be simulated, flare can be minimised by careful alignment but its actual contribution is unknown (Madani and Kaler 1991). Chapter 7 on internodal light scattering offers a possible eradication of such noise contributions to the correlogram by holding large dust particles out of the beam. This and other applications are discussed.

Thus the performance of analysis methods in the presence of simulated noise is only an indication of their robustness and not an absolute measure of suitability. A table of the methods described in § 1.43 is shown on the next page.

**Comments on the considered algorithms.**

Brief comments on each of the analysis techniques that have been described in this section are now given referring to authors' past experience with consideration to the four points mentioned above in their applicability to on-line analysis.

Non-negatively constrained least squares (§1.4324)

guaranteed convergence after a predetermined number of interactions.

positivity of solution.

short processing time.

Histogram method (§1.4322)

Easy to implement.

robust to noise.

fast.

well reported in literature.

Exponential sampling (§1.4321)

Takes account of noise in the solution by sound theoretical methods.

Maximum entropy method (§1.4341)

complex program and theory.

relatively long run time.

requires knowledge of data errors.

Regularised inversion (§1.4326)

possible oversmoothing.

long run time.

Linear programming (§1.4343)

Implications of sensitivities to noise.

Sub-distribution method (§1.4323)

Poor performance in the presence of noise.

S-exponential sum (§1.4325)

Seems very similar to NNLS

Fourier inversion (§1.4342)

Sensitive to noise.

These comments are the basis for initially choosing methods to code for the purpose of on-line analysis.

## 2.0 Equipment design and construction

In this chapter an introduction to the design considerations necessary for a light scattering instrument for dynamic light scattering is given followed by a description of the design and construction of a miniaturised device designed for use in a process monitoring environment.

The construction of a dynamic light scattering instrument is common to many light scattering devices for measuring the properties of a small sample volume. Various miniaturised laser light scattering instruments appear in the literature (eg. Chu et al 1988, Chow et al 1988) and a comprehensive review has been made (Chu 1991). A light source (frequently a laser) is focused into a small volume in the sample cell. A detector is placed at the desired scattering angle to collect light around a narrow range of angles. This range is determined by the lens assembly design and is discussed in § 2.3. The detector gives an output in either analogue or digital form to be interpreted by the post-detection processing equipment as described below. A schematic of the experimental set-up is shown in figure 1.12 §1.3.

### 2.01 Lasers and their properties

Laser light can produce high power at a defined wavelength in such a way that it can be focused down to a small spot to produce high intensities in a small sample volume. This is particularly needed for the detection of small particles whose scattering efficiency is very small. Lasers are available in a large range of wavelength and power outputs. Shorter wavelengths may be desirable because of the higher scattering efficiencies of smaller particles in this region.

An essential criteria for the light source in a DLS instrument is stability of intensity over the experimental time scale. This can be threatened by thermal drift or power supply fluctuations on timescales anywhere between microseconds and tens of seconds. This can affect the baseline measurement or produce spurious "internal correlations" which would produce artifacts in the result. The absence of such internal correlations is important ie. the light signal from the laser should produce a flat autocorrelation function rather than

the exponential decay shown in §1.31. For some years bench scale laser light sources with highly stabilised power supplies and intensity stabilisation circuits have been used for DLS and have met the above requirements.

The other important property of laser radiation is its coherence. Coherence a measure of how well the phase of the light wave is maintained either across or along the beam. The former is termed spatial coherence and the latter temporal coherence. Spatial and temporal coherence is important in DLS as it is the basis behind which, the light scattered from individual particles in the sample, interferes. Lasers display very good coherence properties due to their defined wavelength and small source dimensions. Non-laser radiation can be used for DLS when the geometry of the beam is arranged so as to maximise the lesser coherent properties. However laser radiation allows for easier design and higher power illumination.

**2.02 Detectors**

Photon correlation generally operates on a very weakly scattered signal. This is partly due to the requirement of dilute samples (§1.34) and partly due to the processing requirements. A very sensitive detector is therefore required and the most widely used is the photomultiplier tube. The device amplifies the signal from single photons hitting the sensitive area to produce either an amplified pulse to indicate detection of an individual photon or an integrated voltage proportional to the instantaneous intensity. These two methods of detection are discussed in §2.1 and the former is shown to be most desirable both due to the inherent 'digital' nature of the scattered light and that of the processing electronics.

The detector should be chosen so as to maximise detection at the required wavelength or wavelengths. A wide variety is available but the use of a laser source simplifies selection as operation at a narrow band of wavelengths only need be considered.

Stabilised voltage supplies again are necessary as fluctuations will cause concurrent variations in the gain of the detector which will be interpreted by the post-detection electronics as an intensity fluctuation.

### 2.021 Coherence area

An important design consideration for detector geometry is the coherence area of the scattered light signal. This can be considered as the area over which the signal from extremal points in the source will still interfere, to contribute to the intensity fluctuation signal. Non-interferent contributions merely increase the noise in the detection process; hence good design of the detector geometry is essential to effect a good signal to noise ratio. This is similar in concept to the spatial coherence of the laser source but this time the source may be considered as the scattering sample. The scattering mechanism produces an incoherent source and equations for calculating the coherence area for a two or three dimensional source have been derived (Lastovka 1967, Dhadwal and Chu 1989). The detector can be designed around such equations to maximise efficiency.

## 2.1 Signal processing

The first stage of post-detection processing consists of forming the correlation function by means of multiplication of the sampled signal by itself at a range of delay times and summing these values over time. This process is simple mathematically but can lead to an enormous amount of calculations and hence processing time. The correlation function can be represented mathematically as below:

$$G^{(2)}(\tau) = \frac{1}{M}\sum_{i=1}^{M} n(t)\,n(t+\tau_i) \qquad (2.1)$$

Where n is the number of photon counts in a sampling interval. The theoretical aspects of the correlation function have been covered in §1.312. The samples may be taken either by a digital or analogue detection process. In general nowadays all photon correlation instruments use digital detection. A comparison of the two sampling schemes has benn discussed by (Oliver 1977) with the conclusion is that photon counting techniques are preferable to the analogue scheme as the latter gives rise to unwanted correlations between samples.

The second stage in the processing is inverting the correlation function to obtain a decay constant distribution. This was discussed in detail in §1.4.

To cover an extensive decay time range most correlators now have non-linearly spaced channels. This is also implemented for a similar reason to the exponential sampling scheme described in §1.4321. That is, the information inherent in the data may be extracted to the level of the noise with appropriate spacing. The non-linear spacing while allowing a wide range of decay constants to be covered will also compromise resolution. Equation 2.2 shows spacing of the sample times with the fundamental sample time,$\tau$ and a dilation factor $\delta$, which normally takes on any real value between 1 abd 4. Prior knowledge of the distribution range can be pivotal in successful inversion of the data. It has been shown (Pike et al 1983) that if the range is known the channel spacing, or dilation factor, should be reduced according to the ratio of the upper and lower limits of the range. This then increases the resolution of the result. It was shown that the resolution is only on the ratio and not on the individual limits of the range.

$$\tau, \delta\tau, \delta^2\tau, \delta^3\tau, \ldots . \qquad (2.2)$$

For fast correlation hardware correlators are generally used. These are quite costly. However developments in hardware correlators described in the next section make them very attractive for on-line measurements. The alternative is to compute the correlation in a microcomputer. This will also be required for subsequent processing and user interaction and so incurs no extra cost. These options are discussed in the following sections. Initially however a discussion on clipping and scaling is included to demonstrate data reduction of the incoming signal to simplify or speed up subsequent calculations.

## 2.11 **Clipping and Scaling**

The clipped photocount signal is defined as:-

$$\begin{aligned} n_{i_c} &= 0 \ for \ n_i \leq K \\ &= 1 \ for \ n_i > K \end{aligned} \qquad (2.3)$$

where n is the number of photon counts for a sampling interval and K is the clipping level. Using this in the correlation estimator (equation 2.1) we have:-

$$G_c(j\tau) = \frac{1}{N}\sum_{1}^{N} n_{c_i} n_{(i+j)} \qquad (2.4a)$$

It can be seen that less complex calculations will be necessary as each correlation channel j will either require $n_{i+j}$ or zero to be added to it rather than needing a multiplication for each channel. The above method is termed single clipped correlation. Similarly a double clipped correlation function can be defined where both terms in the product are clipped:

$$G_{dc}(j\tau) = \frac{1}{N}\sum_{i=1}^{N} n_{c_i} n_{c_{i+j}} \qquad (2.4b)$$

Here the appropriate correlation channel needs to be incremented or left as it is depending on the value $n_{ci}$ exceeding the clipping level, K.

It has been shown that the single and double clipped correlation functions (Pike 1976) are undistorted provided a random clipping level is applied. The application of a random clipping level is termed "scaling" (although this term was originally used to describe a method of random clipping level selection in hardware (Oliver 1974)). In some digital correlators the term scaling also refers to the division of the input pulses to the correlator by a fixed amount to allow higher photon counts per sample time to be used. In this text the former definition is used.

The random clipping level $K_i$ for the ith time interval assumes integer values between 0

$$\begin{aligned} n_{sc_i} &= 1 \ for \ n_i > K_i \\ &= 0 \ for \ n_i \leq K_i \end{aligned} \qquad (2.4c)$$

and $K_{max}$ with equal probability. So the scaled and clipped value of $n_i$ is :-

The value of $K_{max}$ must be chosen so that $n_i$ has negligible probability of exceeding it. (Adrian 1982). Here it was also shown that under conditions of low signal and high background light levels (eg. flare from a window in a photon correlation experiment) so

called "self-scaling" can occur and this can be preferable to scaled correlation.

The above discussion of distortion in correlation functions in the clipped and scaled limit applies only to gaussian signals sec. Clipped correlation if non-gaussian signals leads to distortions (Pike 1976).

For low light levels an alternative processing method has been discussed by several authors (Lopez and Rebolledo 1982, Moreno et al 1988) where instead of photon counting as the signal arrives, the time interval between successive photons is measured and this statistically contains the same information as the correlation function. It was demonstrated as a successful alternative to photon correlation where the photon count is much less than 1 per sample time.

## 2.12 Dedicated correlators

Hardwired programmable correlators are the most common choice for a commercial DLS system. They offer a fair amount of flexibility and a minimum sample time dependent only on hardware design rather than software which may be unpredictable. Particularly useful is the inclusion of monitor channels which estimate the autocorrelation function at large delay times to give an accurate measure of the baseline of the correlogram. This measure and the calculated baseline from the correlator channels gives an in-range measurement for the experiment as if the autocorrelation function (see §1.312) has not decayed fully the complete size range has not been recovered.

Since the recent activity in DLS research many authors have published enhanced hardware methods of correlation and correlator interfaces. These usually come in the form of a microcomputer card or interfaced system. An upgraded commercial instrument by adding a transputer array to transfer data, perform calculations and control the conventional hardwired correlator has been described (Brugé et al 1988). The system is designed so as to improve data quality by data selection techniques programmed into the transputer. This is interfaced to a computer which is used almost solely as a display device. In this way on-line data can be displayed and the user can interact with the program to alter its course during execution. Digital signal processing chips programmed have been used to

specifically perform correlation calculations (Correia and Santos 1989). The dedicated instruction set and high throughput allow real time visualisation of correlograms. As before the processing task is taken away from the microcomputer which then becomes a display, storage and user interface.

Other systems have been described allowing greater flexibility in the experiment such as a microprocessor unit where raw data may be stored and processed repeatedly with time-slicing techniques to get the best from the data (Fuchs et al 1988) . Normally raw data is lost in conventional correlators.

### 2.13 Computer correlation

Correlators, where the bulk of the correlation takes place in the memory of a microcomputer may be termed software correlators. Careful timing considerations are necessary for the input-output transfer of data to be processed. Often hardware systems to perform data queuing are necessary to buffer the input and prevent loss of data.

These systems are at a disadvantage compared to hardware dedicated systems however computer power, as highlighted in §1.434 is on the increase and memory costs are dropping. Software correlation is a cost effective simplification of a DLS system.

A computer based photon correlator has been constructed (Nouillez and Boon 1986) and the problems of data queuing mentioned above are discussed. The difficulty of very short sample times is a particular problem for software systems where the determining factor is the input-output link speed. Table 2.1. compares fastest sample times obtainable on the referenced systems. In many applications such short sample times are not necessary and software correlators become a viable choice.

| | min sample time | speed |
|---|---|---|
| software system | 5uS | 2MHz |
| microprocessor unit | 500nS | 16MHz |
| DSP unit | 100nS | 40Mhz |
| hardwired correlator | 50nS | 20MHz |

Table 2.1: Comparison of some correlators in the literature.

Performing correlation calculations in software requires large amounts of calculations to be performed. The number of calculations will be $NC^2$ where N is the number of data and C the number of correlator channels. For a 64 channel correlogram, a sample time of 50μs and an experimental data collection time of 10s this requires about 300,000 calculations. Fast processing is required to reduce the calculation time of the correlogram.

## 2.2 Miniaturisation

The problem with optical systems can be their sensitivity to vibration or shock due to stringent alignment requirements, particularly where large distances exist between the components of the system. The advent of miniaturised optical sources, detectors and passive components allows the design of a close packed unit which is more robust to misalignment and can be more easily protected against unwanted external substances eg. dust or moisture.

### 2.21 Semiconductor lasers

More recently solid state laser diodes have become available with the advantages of being cheap, small and robust. These have been tested for internal correlations (Brown et al 1986) and have been deemed suitable for DLS use.

Commercial DLS instruments operate in the 5-100mW range and usually in the green or red part of the spectrum. Currently diode lasers are only available at substantial powers in the red and infra-red regions although recent research has developed a much shorter wavelength variety but at lower power. The signal to noise considerations must be borne in mind when arguing for shorter wavelength lasers. As has been highlighted (Phillies 1990) moving to shorter wavelengths where generally lasers are more expensive does not always improve the signal to noise of the experiment any better than using a higher power laser of a longer wavelength.

### 2.22 Photodiodes

The solid state equivalent of the photomultiplier tube is the avalanche photodiode. This

detects single photon events and, when cooled to temperatures close to zero °C, currently available models rival the performance of the more costly photomultiplier tubes. (Brown et al 1987). Both types of detector are designed to be sensitive to a certain part of the spectrum. The longer wavelength models are at the moment easier to fabricate however as in the case of the diode lasers work is underway to enhance performance of the photodiodes at shorter wavelengths. Similar requirements for the absence of internal correlations are required for this part of the light scattering set-up and work has been carried out to verify this for the photodiodes (Brown and Grant 1987). More recently modules which carry out the cooling and stringent voltage stabilisation requirements for these devices have been commercialised making the use of such detectors easier and more applicable to a robust miniaturised implementation. These modules require only low voltage inputs and output a digital signal compatible with computer hardware (RCA electro-optics VA Canada).

### 2.23 Passive optical components

Almost all components are now available in miniaturised form. Millimetre scale lenses and the ubiquitous fibre optic cables are of most interest in the DLS application. In many optical applications large lenses are required to maximise light capture and throughput. However when a collimated or focused laser is used the beam can be controlled more easily and large lenses are not necessary. Fibre optics can be used to carry the signal from one point to another without interference or alignment difficulties.

### 2.24 Computers

Due to increased demand and application computers have advanced rapidly in the past decade and much more is yet promised. The result is that huge amounts of processing power are now available at reasonable cost. Their application to DLS is discussed in §2.1. The major element of size in computers comes with their interfaces to the outside world ie. monitors, keyboards, printers and their associated electronics however portable computers with expansion card slots for specialised instrument cards and protection against hostile environments are now available. This may be advantageous if a portable measurement system is required.

## 2.25 DLS system for on-line analysis

The following section describes a dynamic light scattering device which has been designed and constructed but not yet commissioned successfully due to a failure in the detection system. The device is destined to be integrated with sample preparation equipment (see chapter 8).

### Equipment construction

The light scattering unit is designed to comprise the laser, and laser focusing and scattered light detection optics in one head to ensure a steady alignment which should be unaffected by vibration. A brass block has been machined to accept a $1cm^2$ cuvette and holes for incident and scattered light have been drilled. The semi-conductor laser is fixed onto the same block. Brass was used because of its good thermal conductivity, so as to ensure rapid heat transfer away from the laser.

The brass block has holes drilled at 90° and 0° for the beam to pass through so that 90° scattering can be detected and optical density measurements may be carried out in the same unit. The block is mounted onto a brass plate and the whole unit is encased in a stainless steel case for splash-proof protection and light fastness. Power cables and the fibre-optic light guide enter through the walls of the box. Ultimately a rechargeable battery source would be ideal to minimise the cables and it would fit into the base of the box. A diagram of the head is shown in figure 2.1

### The light source

The light source selected was a 780nm Sharp semiconductor laser (LT024MD, Access Pacific, UK) which gives an optical power output of 20mW at 780nm. The laser is driven via an output stabilising integrated circuit (Sharp IRC02A, Access Pacific, UK) requiring voltage inputs of ∓5V @ 100mA. Powers greater than 20mW are available but have increasingly higher heat losses, which must be conducted away. the unit is designed using a laser collimator module (model A, Access Pacific, Bedford, UK) see fig 2.2, so that

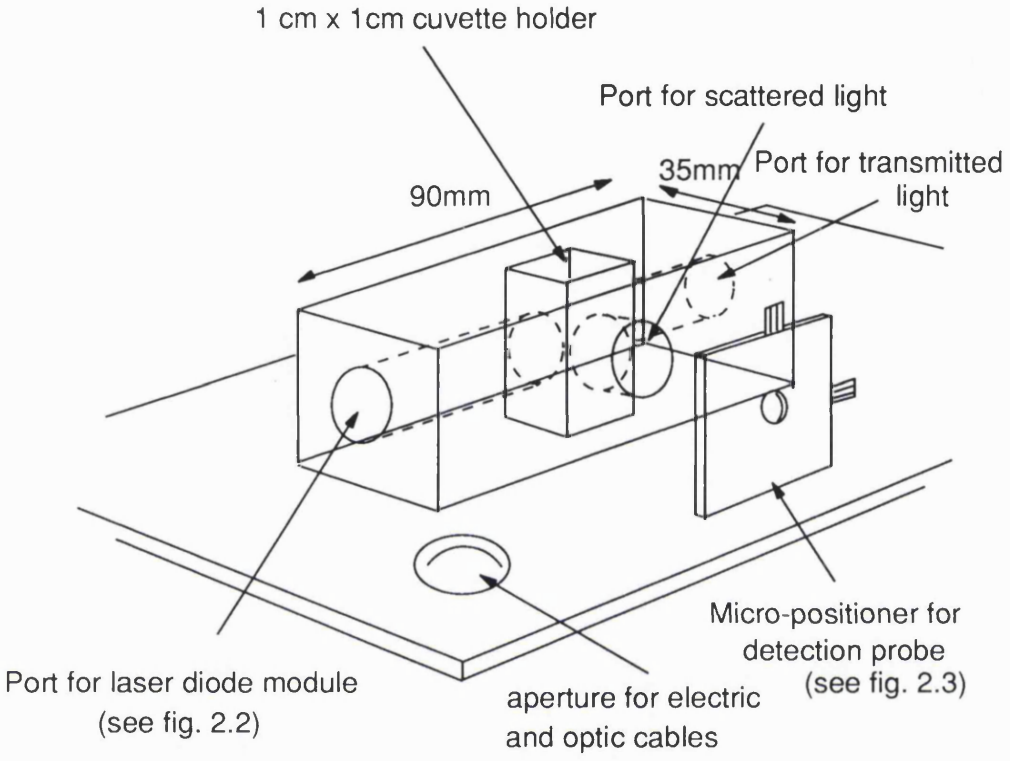


Fig 2.1:
Sketch of optical head mounted on a brass plate. The plate forms a lid for the box containing the laser drive electronics and ultimately a rechargeable battery. There is also a cover to provide protection from liquids and dust.

should the need arise, lasers may be interchanged easily. The focusing optics consist of a 12.5mm focal length lens with pre-collimating optics (Access Pacific) to produce a beam approximately 25μm x 40μm at the beam waist focus.

**Sample cell**

A three windowed fluorescence cell (Hellma, UK) was used to minimise unwanted light scatter from internal reflections. The cell has a volume of 750μl and is of the flow through variety to allow continuous sample replacement.

**Detection optics**

The design of the detection optics has followed similar studies in the literature (Dhadwal and Chu 1989) where gradient index rod (GRIN) lenses were used with optical fibres to construct compact probes for DLS collection optics. GRIN lenses are 1 - 3 mm in diameter and several millimetres long. A fibre-optic connector has been modified in order to accept such a lens and launch the collected light down a fibre to the detector (see figure 2.3a) The lens used is a 0.25 pitch 1.8mm diameter lens (optimised for 830nm operation which is the closest available to the desired 780nm value. The connector is a FSMA standard plug (FL3405 Leetech, London, UK) modified to accept a narrow pitch screw-fitted GRIN lens holder constructed in-house from aluminium rod. This allows fine adjustment of the fibre to lens distance in the probe (see figure 2.3b). The fibre used was a 50μm core multi-mode fibre (FL3401-1500 Leetech, London, UK) of 10 metres length for remote operation, terminated with a FSMA plug for connection into the detection unit.

The probe is currently mounted in a micro-adjustor (Melles-Griot, Aldershot, UK) to allow fine x-y-z movement.

**Detector**

The detector used is a photon counting module recently introduced to the market (RCA SPCM-100). The module requires only low voltage inputs (+12V and ∓5V) and accepts a FSMA fibre connector for the optical input and converts the photodetections into

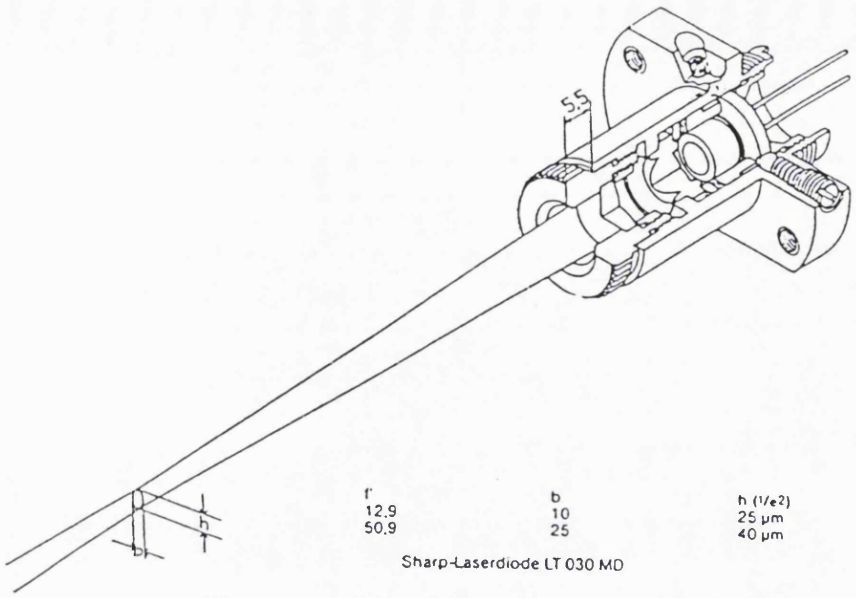


Fig 2.2: Diagram of laser diode module which accepts a wide range of semiconductor lasers of different power and wavelength.

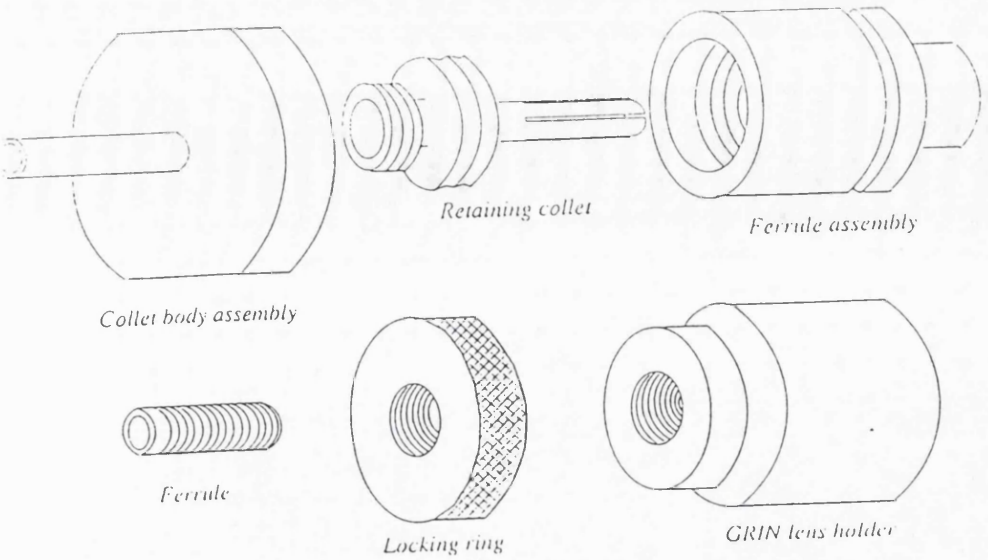


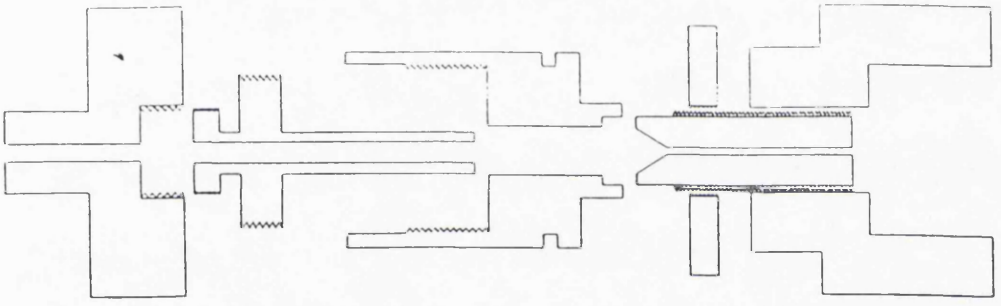

Fig 2.3a: Drawing of modified fibre-optic probe to accomodate the GRIN lens for launching scattered light into the fibre.

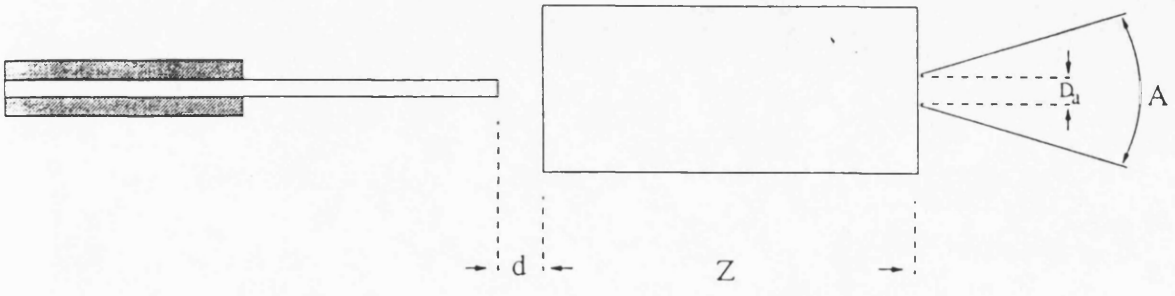


Fig 2.3b: Sketch of GRIN lens and fibre-optic cable showing acceptance angle, A and effective aperture $D_a$

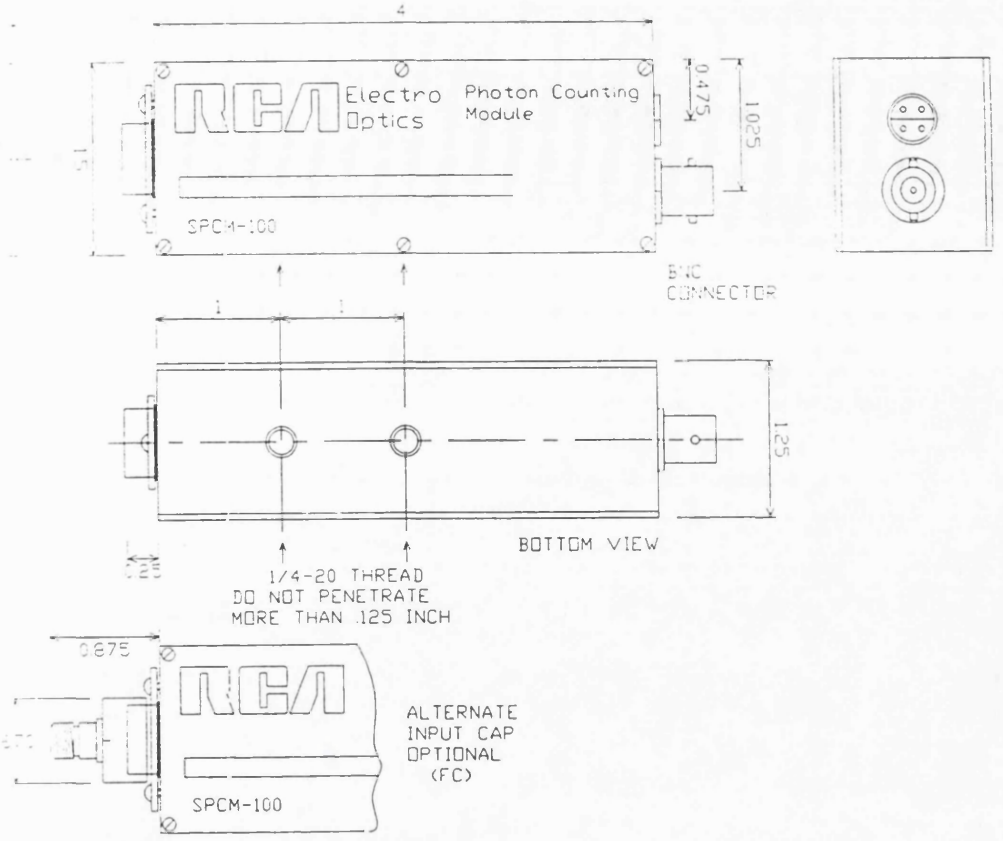


Fig 2.4: Diagram of RCA photon counting module with dimensions. The plan shows the 3 connections - power supplies, electronic output, and optical input.

computer-compatible (TTL) pulses at the output. Internally an avalanche photodiode (see eg. Brown et al 1986), which is cooled to reduce thermal noise, sensitive over the range 400nm - 900nm is housed. The maximum count rate that the modules can cope with is 1 X $10^6$ counts per second which is adequate for a photon counting experiment where typically 50 x $10^3$ counts per second are detected. Dimensions of the module are shown on fig 2.4.
The electrical pulses are now available for either computer correlation as described in §2.13 or to be input to a hardwired correlator (§2.12).

**Correlator**

The correlator comprises an Acorn Archimedes computer (Acorn, UK) with an interface card custom designed (Institute of Biotechnology, Cambridge, UK) to consist of a first-in-first-out (FIFO) memory of size 16Kbytes so that data queueing may be performed by the software. For a 10μs sampletime,the smallest likely to be encountered in this application, this size memory will fill up in about 160μs. Thus the memory needs to be cleared frequently during data collection where experimental times are of the order of seconds.

Data is read from the correlator card into the computer memory and then a machine code routine has been written to perform the correlation calculations described in §1.3. Processing time varies according to the sample-time chosen, however for 10 second experiments processing time for a 64 point correlation function is between 30 - 90s.

**Power supplies**

The power supply requirements for the full system are a +5V (1.5A), -5V (0.02A) and +12V (0.05A). These are provided by benchtop power supplies currently but for operation in a pilot plant environment battery power is more desirable. High amp-hour rechargeable batteries are available (see eg. Radio Spares (RS) components catalogue 1992).

## Chapter 3: Materials and methods

### 3.1 Homogenate preparation

Blocks of baker's yeast Saccharomyces cerevisiae
(The Distillers Company, Surrey, U.K.) were suspended in 100mM phosphate buffer, pH 6.5 to give a final cell concentration of 600kg packed wt cell $m^{-3}$. The suspension was disrupted at 4 °C, using a high pressure homogenizer (Lab. 60, APV, Crawley, Sussex, U.K.) at 500 bar with the equivalent of 5 discrete passes. The resulting cell homogenate was adjusted using 2 M NaOH to pH 7.4 to produce unclarified homogenate.

Clarified homogenate was prepared by a high-g spin in an Europa 24M MSE centrifuge (MSE, Crawley,Sussex) 20,000g for spin times between 15 - 95 mins or in a benchtop microfuge (Denley, UK) at 15000rpm for 15mins.
Dilution is described in the appropriate chapters.

### 3.2 Virus-like particle preparation

method 1:
1) Grow yeast culture in suitable selective media until cell density is >2 x $10^7$/ml.
2) Harvest cells by centrifugation at 3000rpm for 30 minutes (Sorvall H600A rotor). Resuspend cells in 20ml of distilled water.
3) Transfer cells to 50ml Falcon tubes (approx. 4 x $10^{11}$ cells/tube) and collect cells by centrifuging in a bench centrifuge at 200g for 5 minutes, discard supernatant.
4) Resuspend cells with distilled water and re-centrifuge as before.
5) Repeat cell washing procedure once more with distilled water and then twice with TEN buffer (10mMTris, 2mMEDTA, 140mMNaCl, pH7.4).
6) From this stage all procedures are performed at 4 degrees C using pre-chilled buffers.
7) To each tube add 4 mls TEN buffer containing the protease inhibitors aprotonin, antipain, chymostatin, leupeptin and pepstatin each at 1.25µg/ml. Resuspend cells.

8) 5 mls acid washed glass beads (40 mesh) are added to each tube.
9) The tubes are vortexed for 10, 30 second periods interspersed with 30 second periods of cooling on ice.
10) The suspension is centrifuged at 2000g for 5 minutes. Remove and retain the supernatant.
11) 4 mls fresh TEN buffer (containing the above protease inhibitors) is added to the cell pellet and the vortexing and centrifugation is repeated as above.
12) 3 mls fresh TEN buffer (containing the above protease inhibitors) is added to the cell pellet and the vortexing and centrifugation is repeated as above.
13) The supernatants are pooled and centrifuged at 13,000g (Sorvall Hb4 rotor, 9000rpm) for 20 minutes.
14) The resultant supernatant is centrifuged at 100,000g (Beckman SW40 rotor 30,000rpm for 1 hr or SW28 for 1.5 hr at 28,000rpm).
15) The resultant pellet is resuspended with 1ml TEN (containing the above protease inhibitors) per litre original culture using a Dounce homogeniser.
16) Centrifuge the suspension at 13,000g (Sorvall Hb4 rotor at 9,000rpm) for 20 minutes.
17) Using sucrose dissolved in TEN buffer prepare 5-20% linear sucrose density gradients of 30 mls on top of a 2ml cushion of 60% sucrose in a Beckman SW28 rotor tube.
18) Load each gradient with up to 2mls of the supernatant (from stage 16) and centrifuge at 53,000g (25,000rpm Beckman SW28 rotor) for 6 hours.
19) Following centrifugation the Ty-VLPs are located at the interface between the sucrose gradient and the cushion and are collected using a Pasteur pipette.
20) The sucrose is removed from this crude particle preparation by dialysis against TEN buffer for 36 hours.
(British Biotechnology Ltd)

method 2:
Ty-VLPs were purified from crude homogenate by differential centrifugation (the miniprep process) followed by gel filtration on Sephacryl S-1000 superfine:

The starting material for the miniprep process is crude homogenate, obtained by disruption

of 90g dw $L^{-1}$ cell suspension in the LD30 homogeniser (5 passes, at 7250 psi). Ty-VLPs were purified as follows:

1) Homogenate (20mls) was centrifuged (9000g, for 20 minutes at 4 degrees C. to remove the cell debris.

2) Supernatant (8mls) was then spun in an ultracentrifuge (190,000g, for 180 minutes at 4 degrees C.) to pellet the Ty-VLPs onto a 60% sucrose cushion (1ml thick); the supernatant (7mls) which contained the majority of the soluble protein was discarded. The VLP enriched pellet (2mls) was resuspended in chilled $PO_4$ buffer (4mls, 100mM pH 7.4).

3) The resuspended pellet (4 of the 6mls) was layered onto a 35% sucrose cushion (6mls) and recentrifuged (190,000g, for 360 minutes at 4 degrees C.). the Ty-VLPs passed through the 35% sucrose and were pelleted onto a second 60% sucrose cushion (1ml). The pellet (2ml) was collected and applied to the gel filtration column:

### 3.21 Gel filtration

Gel filtration was carried out on a Sephacryl S-1000 column (void volume = 9.5mls, total volume = 21.9mls). Miniprep material (100ul) was loaded to the column, and eluted with TEN buffer (10mM Tris, 1mM EDTA, 150mM NaCl, pH 7.8) at a flow rate of 0.5ml $min^{-1}$. The peak containing Ty-VLPs (5ml) was collected.

### 3.22 Protein assay

(after Ehresmann et al 1973)

Measurement of absorbance at two wavelengths (234.5nm and 228.5nm) using a Phillips PU800 spectrophotometer was performed. The protein concentration is then calculated as the difference of the two absorbance values multiplied by 0.328. This gives the concentration in mg/ml.

### 3.3 Malvern system 4700c

The Malvern System 4700c consists of a variable angle spectrometer with laser illumination coupled with a computing correlator processor. It is a modular laser light scattering system for DLS and total intensity measurements of submicron particle size

(0.001 - 3μm), molecular weight and diffusion coefficients.

The spectrometer consists of a goniometer with a large diameter precision turntable, which can be controlled manually (PCS 100SM) or by computer, with stepping motor driven automatic operation (PCS 100SM). It has wide spaced angular contact bearing and gives accurate measurement at angle from 8 - 150 degrees. the resolution is 0.01 degrees and the arm wobble $<10^{-5}$rad.

The system can be used with a variety of types of laser. For this project it was operated using a 30mW Helium-Neon (HeNe) laser (Model Spectra-Physics 124b).

The index matching cell assembly (PCS4) is combined with a pump and filter system (RR98). The cell assembly is temperature controlled and there is a refractive index matching bath with collet mounting for accurate centralisation of the sample cell. The refractive index matching fluid in the vat surrounding the sample cell is recirculated and refiltered to help achieve flare-free measurements. Accurate temperature control of index matching fluid in the bath allows experiments to be carried out above or below ambient temperatures.

The optics and detector system uses integrated coaxial optics, a photomultiplier tube, an amplifier and a discriminator unit. There are interchangeable filters, a reflex viewing system and turret selection of aperture from 25μm to 500μm diameters.

The signal processor is a Malvern Multi-8 Type 7032 computing correlator with variable time expansion. It has 8 x N (256 level) multibit processing and sample times are 50ns to 1s. The correlator operating system software (7032-OS) provides full manual control of system parameters, automatic experiment sequencing, entry of experimental data, particle size analysis, storage and recall of correlograms, cumulants analysis and displays results in both graphic and tabular form.

### 3.4 Computer software

Non-commercial data analysis software was implemented in the C programming language

for portability across systems. The C compiler used was Zortech C++ developers edition (Zortech Ltd, London, UK) for IBM compatible machines (286/386sx machines 1MB RAM 40MB hard disk, 1.44MB 3.5" floppy drive, VGA display) and Acorn C compiler (Acornsoft, UK) for the Acorn Archimedes computer (4MB RAM 20MB hard disk, 800K 3.5" floppy drive).

## Chapter 4: Characterisation of yeast homogenate.

The purpose of this chapter is to pave the way for the modelling and algorithm testing in the following chapter. A general knowledge of the type of size distribution to be expected is necessary before embarking on simulation experiments. Also an inspection of the absorbance spectrum of homogenate suspensions may give useful information for optical analytical methods.

### 4.1 Wavelength scans of yeast homogenate.

The homogenate used in this set of experiments was an original preparation of 600 g/l in phosphate buffer. The homogenisation conditions were 5 passes at 500 bar and the homogenate held between 4 - 10 °C throughout. The original preparation was diluted to bring the optical density of the suspension into the linear region of the spectrophotometer throughout the scan ie < 0.5 Abs at 600nm. In the case of unclarified homogenate this required a several hundred-fold dilution with de-ionised water. The clarified samples were produced by diluting crude homogenate 1:1 with de-ionised water before spinning at 15000 rmp for 15 minutes in a bench-top microfuge (Denley, UK) and then pipetting 0.25ml into 3ml de-ionised water. The pre-dilution before spinning allowed a sufficient quantity of supernatant above the sediment to be drawn off.

The spectrophotometers used were Perkin-Elmer Lambda II and a Philips PU800 models. A scan speed of 120nm/min was used to cover the range from 190-800nm with a bandwidth of 0.1nm and smoothing over 2nm. Quartz cuvettes were used for transmission at the UV wavelengths.

VLP homogenate was also scanned over the same regions. The preparation method for this is given in chapter 3. Since the preparation is more dilute this was directly spun and then 0.25mls extracted into 3mls as above.

The aim of the wavelength scan was to identify any characteristic absorption regions in the spectrum that might be used to enhance photon correlation measurements. For example a region of absorption by the homogenate could be exploited by operating at this

wavelength where the product could possibly be a comparably efficient scatterer.

### 4.11 Wavelength scans of whole yeast and yeast homogenate

Figure 4.1 shows the variation of the OD of whole yeast, crude yeast homogenate and clarified yeast homogenate prepared by the above method over the wavelength range 800nm to 300nm. Figure 4.2 expands the scale over the range 350nm to 500nm for the clarified homogenate.

Whole yeast, as expected, shows a nearly constant value over the entire range of wavelengths. Their relatively large size (3 - 8μm) places them into the Mie region (§1.2). In this region one might expect undulations in the extinction signal due to for example anomalous diffraction effects (§1.2224, eq 1.20). In practice the optical design of the system may not allow these affects to be detected as they depend upon detection at only a very narrow range of forward angles so that only the true extinction signal reaches the detector and forward scattered light does not. Also, as the positions of the maxima and minima depend upon the particle size, the polydispersity of the sample can smooth out the undulating signal. This result shows that concentrations based on OD measurements can be carried out anywhere in this range of wavelengths (in practice 600nm is commonly used) providing other media components do not have a strong extinction band at the chosen wavelength.

The signal for crude yeast homogenate shows a different spectrum to that of whole yeast. The lower range of wavelengths show an increasing value of OD starting gradually at about 750nm. This increase can be attributed to the addition of smaller particles to the suspension. These smaller particles scatter light at shorter wavelengths preferentially (§1.2221) thus the turbidity increases towards smaller values of wavelength. The relationship for a monodisperse suspension for a turbidity spectrum can be described by (Schchegolev and Klenin):

$$f(\lambda) = A\lambda^{-n} \qquad (4.1)$$

Here n is called the waveexponent. For very small particles this tends to a value of 4 which is equivalent to the Rayleigh scattering region (see §1.2221 ). With a distribution

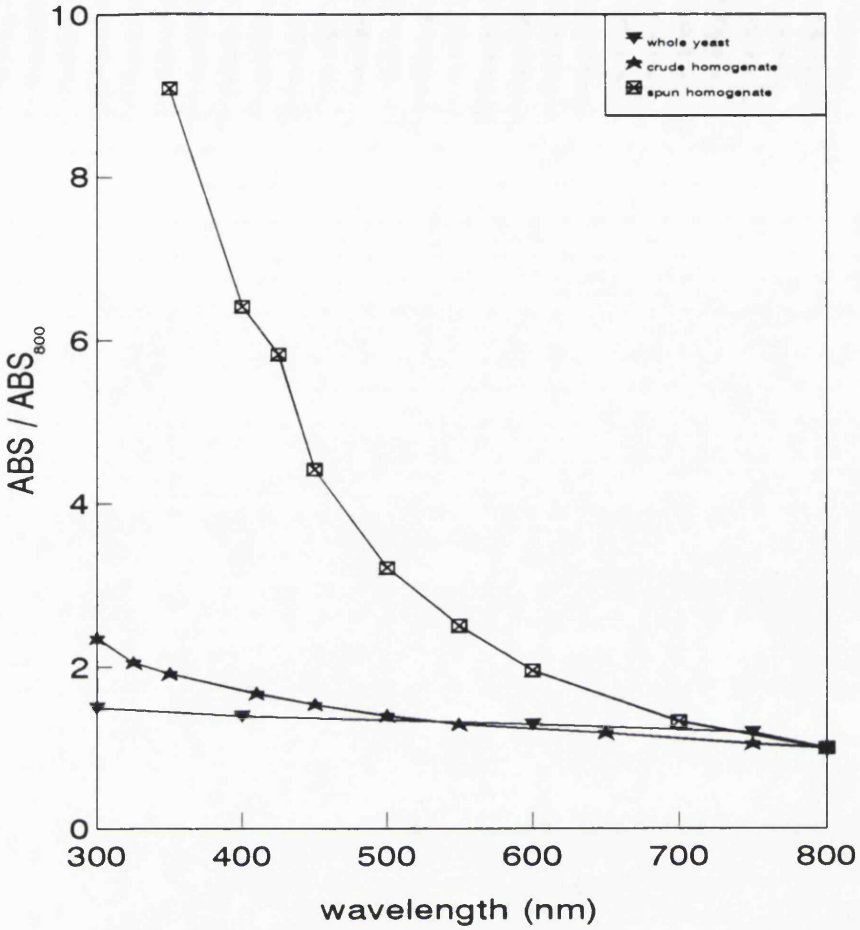


fig 4.1: Chart showing wavelength scans of whole yeast and clarified and unclarified yeast homogenate. The plots are relative to the absorbance of the suspensions at 800nm. The absorbances of the three suspensions at 800nm are 0.112, 0.670 and 0.124 for whole yeast, unclarified and clarified yeast homogenate suspensions respectively. The icreasing absorbance at the shorter wavelengths for homogenised suspensions is due to the presence of the smaller particles. A shoulder is observed in the clarified homogenate curve which is shown in expanded scale in fig 4.2.

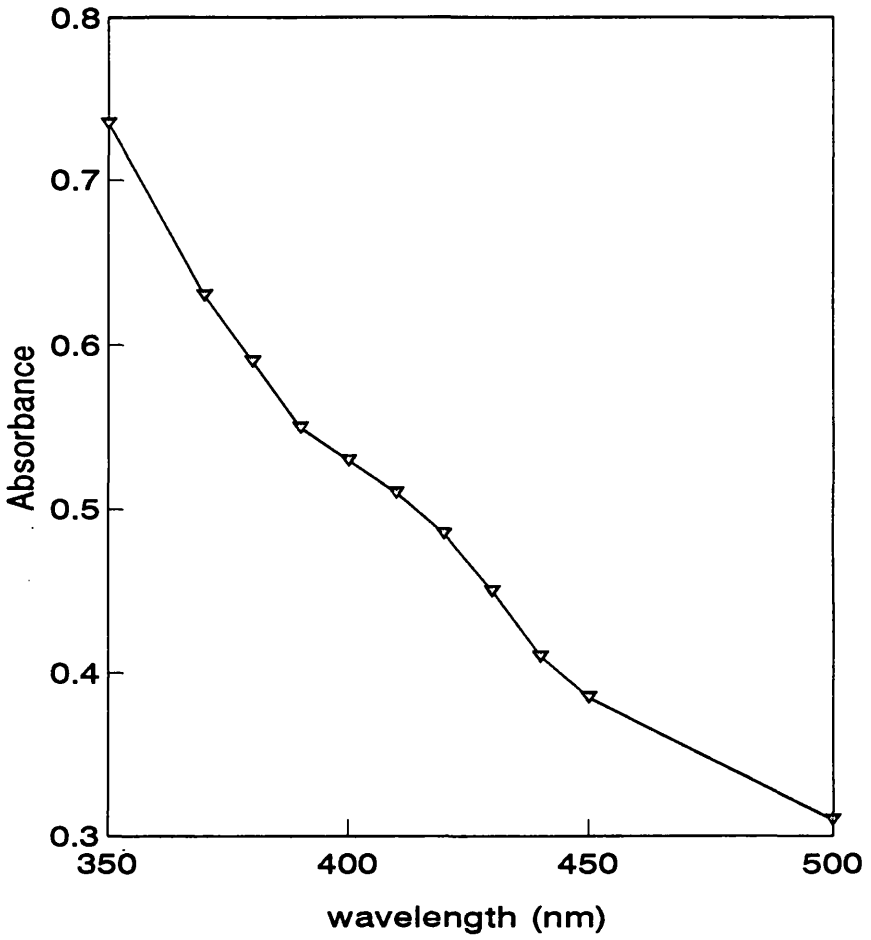


Fig 4.2: Expanded region of wavelength scan of clarified yeast homogenate showing the increase in absorbance in the 400nm region. This may be explained as either a particle size effect or a particularly absorbant species in this region. If it is a particle size effect then this would indicate a bimodal distribution of homogenate due to the variation of extinction efficiency with particle size (see text)..

of particle size this formula expands to a sum over different values of n of equation 4.1. A similar model has been used (Bertero et al 1988) as a method of particle sizing where the turbidity spectrum is fitted to such an equation.

Clarified yeast homogenate shows a similar trend to that of the crude homogenate except that the increase is far more significant. There is also an anomalous region where the increase of turbidity drops and then increases again in the region of 400nm. This is shown in detail in figure 4.2 where the derivative spectrum of the homogenate is shown over the anomalous region. The explanation of this phenomenon is possibly due to the nature of the particle size distribution of the homogenate. Although many of the larger species have been removed in the centrifugation step a number will remain. The large particle sizes tend to show a decrease at shorter wavelength over a particular range. This can be shown by latex samples as displayed in figure 4.3. The small sizes have increasing OD towards shorter wavelength but the trace for 0.48μm drops after peaking at 420nm. A particular mixture of particles in this region and those in the smaller size region could lead to a levelling-out of the turbidity scan before then resuming an upward gradient. This particular shape would be created with a small number of large particles mixed with a relatively large number of smaller particles which is just that expected in yeast homogenate.

An alternative explanation is that cytochromes absorb strongly at 420nm which may briefly increase the optical density in this region to produce the shoulder in the spectrum.

The conclusion to the aim of these investigations are that in yeast suspensions there may be an advantage to be gained by moving to shorter wavelengths for optical scattering where the smaller particles will scatter more effectively particularly if the size difference between small and large species is large. In whole yeast for example shorter wavelengths should enhance small component detection within the media.

In the homogenised suspension however the large fraction of smaller disrupted species may negate the advantage as they will also scatter correspondingly increasing amounts of light.

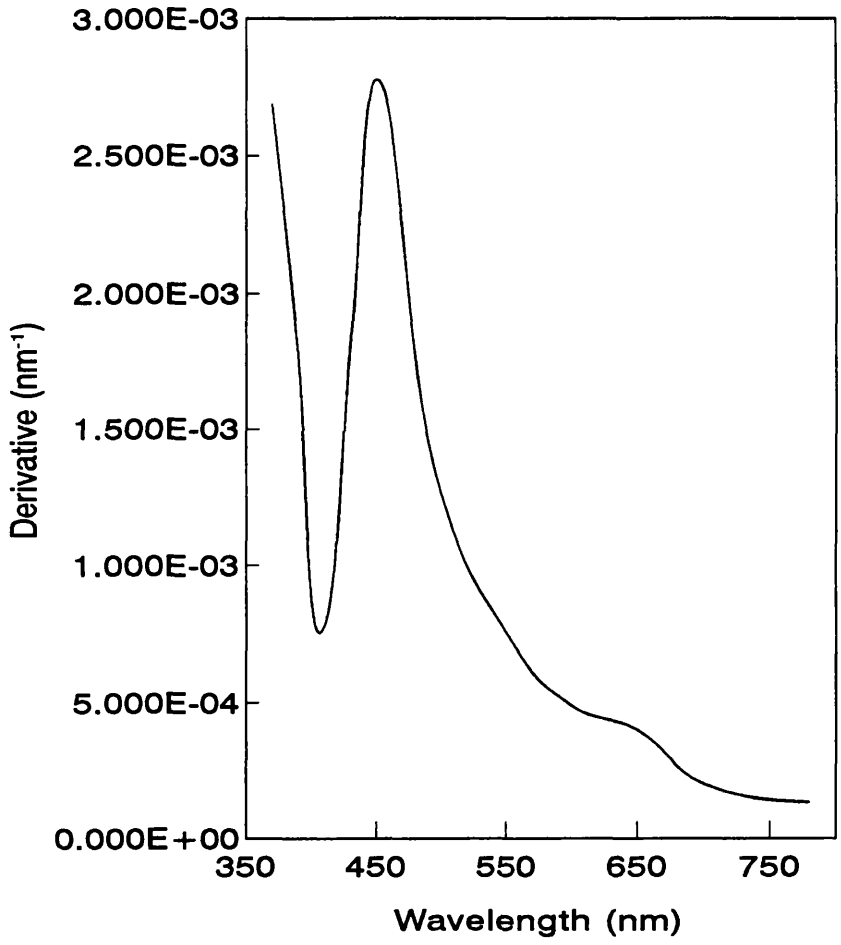


Fig 4.3: Chart showing the derivative spectrum of clarified yeast homogenate. The shoulder region of the absorbance spectrum gives rise to the peak in the derivative plot. The possibility of using this phenomenon as the basis of a spectrophotometric assay for materials in homogenate is discussed in §4.12. Two wavelengths may be selected where equal derivative values exist and in principal subtraction will lead to zero for homogenate alone but a finite value proportional to any additional material present.

### 4.12 Spectrophotometric difference assay in clarified homogenate

Consideration can be given to an assay in clarified homogenate using the anomalous feature in figure 4.1. Considering the derivative spectrum (figure 4.2), at several points the function is triple-valued. Taking two such points and subtracting the result is zero. However if an extra component is present eg. product particle, then subtraction will lead to a finite value proportional to the amount of the component present. The procedure can be assessed as follows:

If the turbidity spectrum of the clarified yeast homogenate is denoted $Y(\lambda)$ and that due to the product as $P(\lambda)$ the derivative spectra will be $dY/d\lambda$ and $dP/d\lambda$. For the mixture of yeast and product we have:

$$S(\lambda) = Y(\lambda) + P(\lambda) \qquad (4.2a)$$

$$\frac{dS}{d\lambda} = \frac{dY}{d\lambda} + \frac{dP}{d\lambda} \qquad (4.2b)$$

If $dY/d\lambda$ is equal at two particular wavelengths then a subtraction will yield

$$\left[\frac{dY}{d\lambda}_{\lambda_1} - \frac{dY}{d\lambda}_{\lambda_2}\right] + \left[\frac{dP}{d\lambda}_{\lambda_1} - \frac{dP}{d\lambda}_{\lambda_2}\right] \qquad (4.3)$$

The first term in brackets is the zero term and the second term will be non-zero and proportional to the amount of product. Providing the $P(\lambda)$ signal is large enough compared to $Y(\lambda)$ to within the sensitivity of the instrument (in this case 0.001 OD) and $dP/d\lambda$ varies significantly over the critical region this technique may be used to measure a product in yeast homogenate.

As a demonstration of the latter conditions the derivative spectra of 150nm latex is shown in figure 4.4. This can be fitted well to equation 4.1 §4.11 by a non-linear least-squares analysis to give the parameters $nA = 7.79 \times 10^8\ nm^{-1}$ and $n+1 = 4.57$. This demonstrates

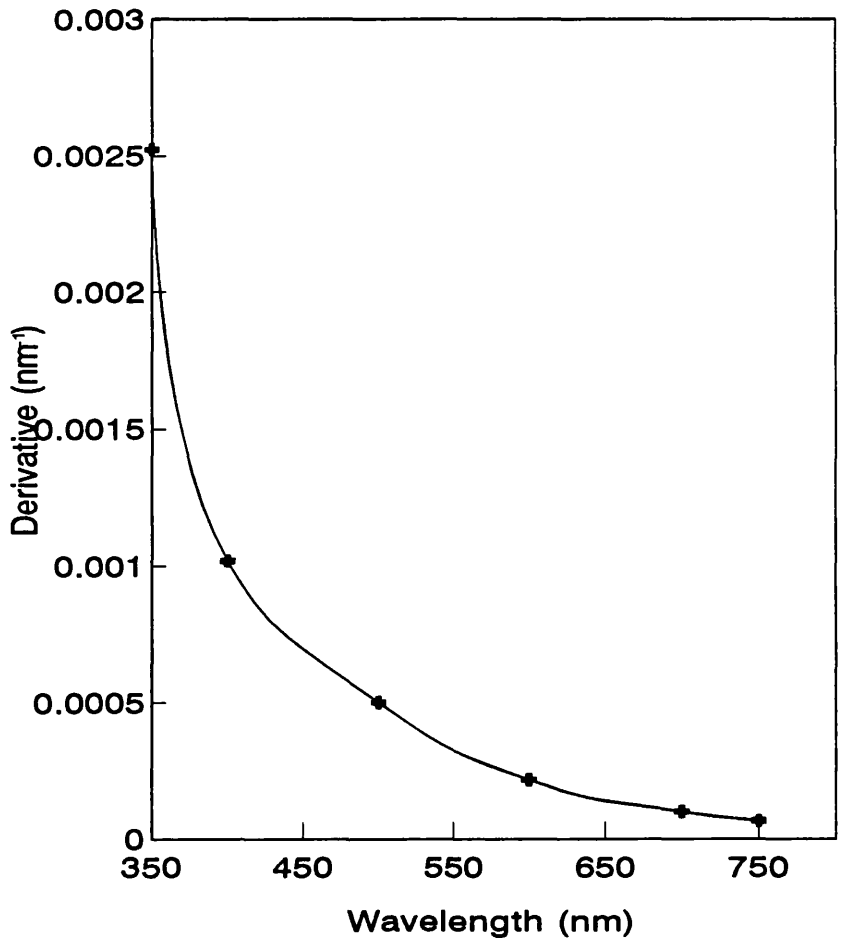


Fig 4.4: Plot of derivative spectrum of 150nm latex spheres at approximately 0.005% v/v (≈ 5 mg/ml) concentration. This gives rise to a difference of 7.67 x $10^{-4}$ $nm^{-1}$ over the 400nm - 550nm region. Concentrations to less than 0.1 of this value will still be within the range of the instrument, however in order to measure the particles in homogenate dilution is necessary. The extent of dilution and the concentration of product to be measured before dilution must be considered.

that the particle size is within the limits of the theory and describes analytically the spectrum shown in figure 4.4 ($P(\lambda) = 7.79 \times 10^8 \lambda^{-4.57}$). Choosing eg. wavelengths at 400nm and 550nm the difference term in equation 4.3 will be $7.67 \times 10^{-4}$ $nm^{-1}$. The concentration of 150nm latex required to be within the sensitivity of the spectrophotometer is approximately 0.0005 % by volume. In a real situation when the sample is diluted before the measurement the final concentration may be too low for detection; what is important is the initial concentration of homogenate which will determine the dilution factor. Hence the sample should be diluted as little as possible while keeping the OD in the linear region.

The final graph to discuss in this section is the wavelength scan of clarified VLP homogenate, shown in fig. 4.5. Similar features appear in the spectrum and using the technique above an estimate of VLP present can be made. The value is 0.002% as a fraction of the total volume present., assuming the same scattering efficiency as 80nm latex spheres. In practice latex is much more refractive than biological material. Since the refractive index of the VLP's is not known the exact concentration cannot be quantified. Estimates of VLP concentration from assays on total protein and fractions of that protein from gel filtration estimate 5mg/ml total protein 2-3mg/ml of which is VLP. (Milburn, private communication). If 0.002% volume concentration assuming latex scatterers actually corresponds to 0.15 mg/ml (2 mg/ml diluted 0.25:3.25) or about 0.015% volume. Thus VLP's appear to be 7.5 times less efficient in scattering than latex beads.

An estimate of concentration based on this method will only useful if the derivative spectra for the yeast homogenate are consistent for a particular preparation method or even better over a wide range of methods. The evidence here suggests consistency over several different centrifuge conditions - but further work is required to determine the reproducibility of such scans.

### 4.13 Wavelength scan of aged yeast homogenate

An interesting result is shown in figure 4.6. The sample is aged yeast homogenate which has been left at 4 °C for approximately 24hrs. The region at 400nm now forms a plateau from 400 - 410nm and can be seen to be constant across this range in the expanded scale.

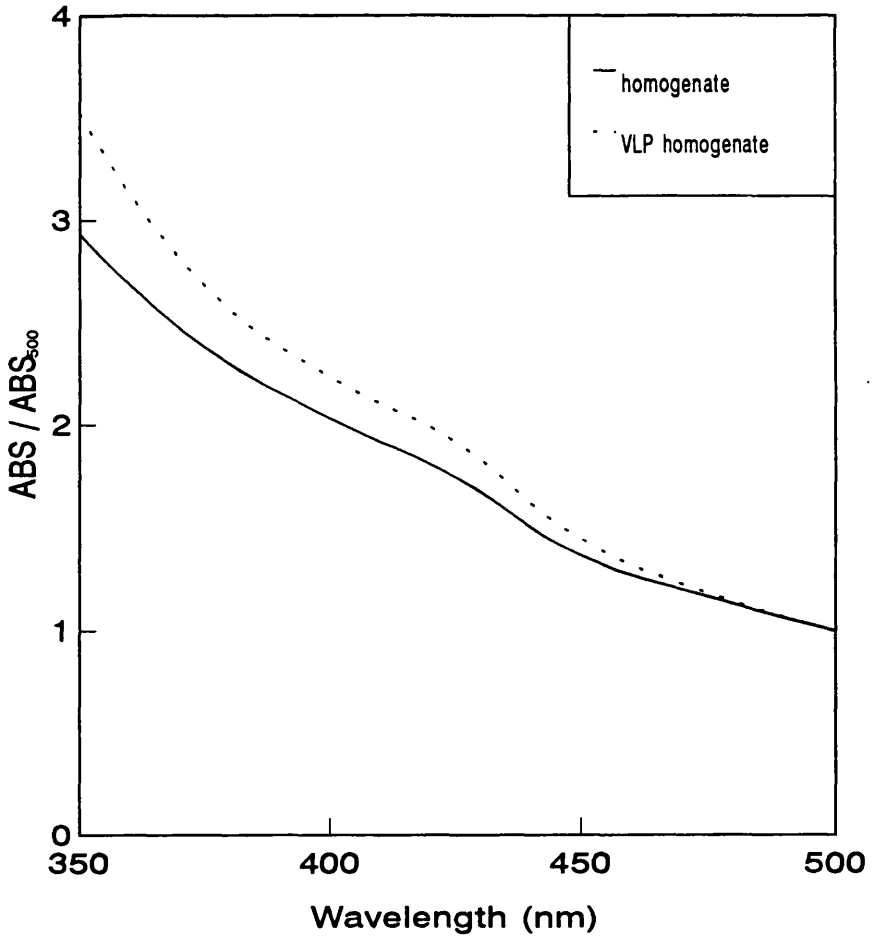


Fig 4.5: Chart to show the difference between VLP homogenate and homogenate without VLP's present across the wavelength range 350nm - 500nm. The traces relate to different concentrations of suspensions so they are normalised at 500nm. There is a distinct difference between the two traces at lower wavelengths where the VLP's contribute to the small particle scattering contribution to the absorbance. Derivative values at 406nm and 500nm are equal for the lower trace (see fig 4.4) and for the upper trace differ by $1.05 \times 10^{-3}$ $nm^{-1}$. If the same scattering efficiency as an 80nm latex is assumed for the VLP's this gives VLP a concentration of approximately 0.002%. Since VLP's are far less refractile than latex their concentration will be significantly greater (see text).

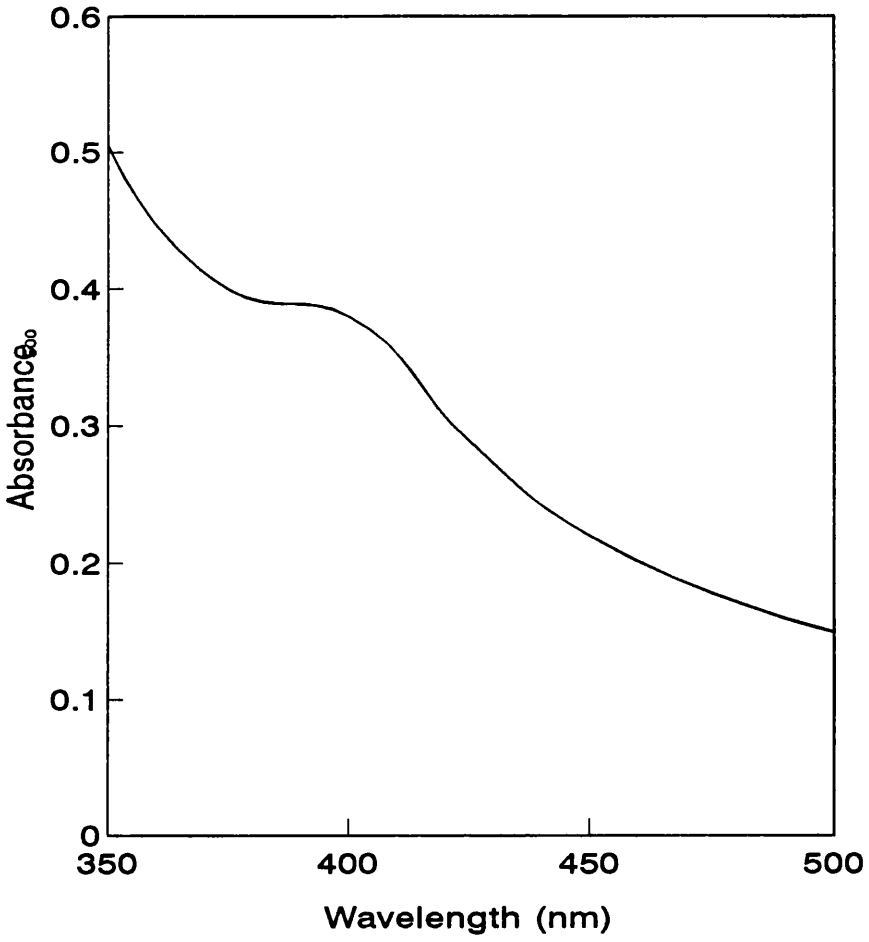


Fig 4.6: Chart showing a wavelength scan of aged yeast homogenate. The shoulder apparent in fig 4.1 has developed into a plateau region. This may be explained by a change in the size distribution by either agglomeration or denaturation. However it is curious that the plateau does not turn downwards but stays flat before resuming a positive gradient again.

This can partly be explained by size effects. Flocculation of the suspension has probably occurred in aging and even after the preparative spin a larger fraction of the suspension is made up of larger species. This would put more weight on the descending component of the spectrum at shorter wavelengths. An alternative explanation is that protease attack has modified the size distribution to produce a similar effect. It is curious in either case that the plateau should be flat and not reduce in value before increasing again as might be expected if the mechanism above is responsible for the effect. The third possibility is the cytochromes absorbance mentioned earlier, in conjunction with a size distribution change may produce such an effect.

### 4.2 Dynamic light scattering analysis of yeast homogenate

Dynamic light scattering was carried out on clarified yeast homogenate. The commercial software of the Malvern 4700 was used which involves a lengthy analysis to optimise the fit by varying the starting conditions such as range and resolution. Ten 10s experiments were collated on each run and those with merit and in-range figures within 1 standard deviation of the data set in the run were selected for analysis. The merit figure is the ratio of the initial point in the correlogram to the baseline value and is a measure of the signal to noise ratio of the experiment. The in-range figure compares the far-point baseline estimate with the last few correlator channels. This checks that the correlation function has decayed close to the baseline and hence the full range of particle size has been covered.

An aperture of 100μm was selected and the sample time was automatically selected by the computer. The fundamental sample time ranged between 10 - 50μS and the dilation of the correlator was 4. (see §2.1)

Three figures are shown for different levels of clarification. All were subjected to a 20,000g spin in an Europa 24M, MSE centrifuge (MSE, Crawley, Sussex, UK). At intervals of 15, 75 and 155 minutes samples were taken from the centrifuge.

The most obvious feature of all three graphs is the bimodal distribution of size. This complements the theory from the wavelength scans that the distribution was suspected to be bimodal.

In fig 4.6a the lowest particle size registered is about 100nm, in figure 4.6b, 75nm and in figure 3 60nm. The overall distribution average falls from 4.6a-4.6b but not from 4.6b-c. It would seem that the larger particle size seems to broaden and even shift to a higher size with longer centrifuge times. This may be due to agglomeration after removal from the centrifuge or possibly numerical instability in the computer algorithm. As was mentioned in §1.4 there will be difficulty in obtaining accurate data with the larger particle sizes and this may be a manifestation of this fact. Two figures (4.6a and 4.6b) show an apparently complementary shifting of intensity between peaks ie. a drop in the lower peak gives rise to an increas in the other peak. This would suggest that the ill-conditioned nature of the analysis procedure leads to a number of distributions all fitting the data ie. the peak to peak variation is indistinguishable in the data.

An interesting point concerned with convergence of the program to a suitable solution is shown in figure 4.7. The chi squared fit value is plotted against experimental time for 15 calculations. There seems to be a trend towards poorer fits with longer experimental times, the inverse of the expected trend. Longer experimental times should lead to better data (§1.4) and thus a better convergence to the model. What might be affecting the measurement is the presence of dust or perhaps large agglomerates infrequently entering the beam but distorting the result by affecting the baseline value of the correlogram.

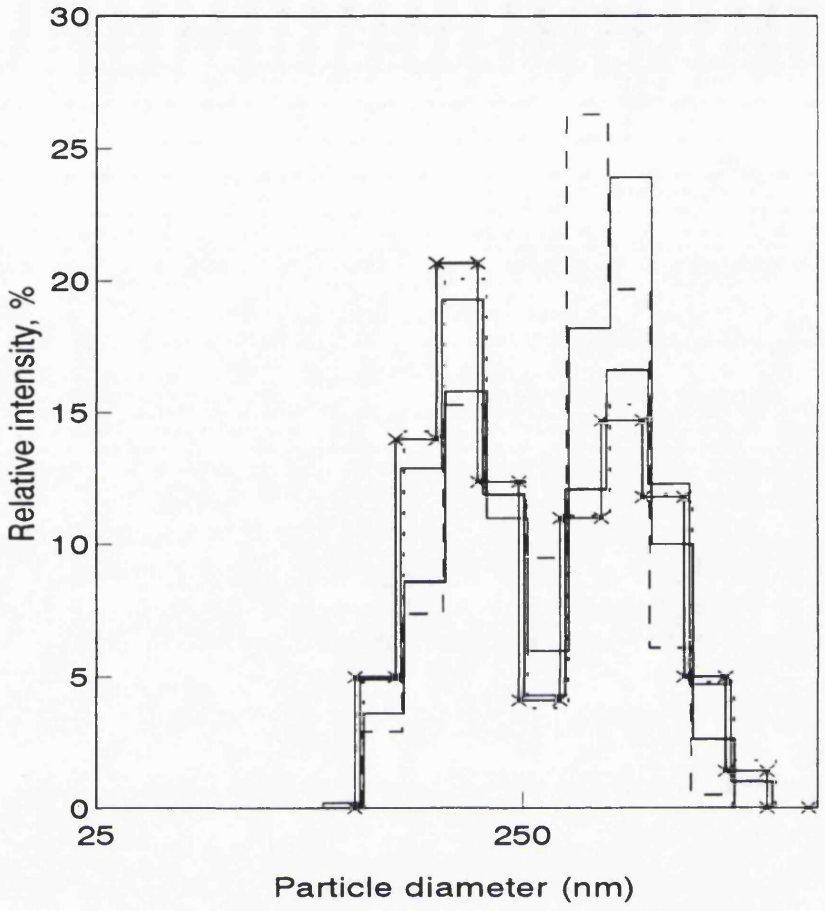


Fig 4.6a: Size distribution of clarified yeast homogenate by DLS using Malvern software. The centrifugation conditions were 15 minutes at 20000g. A bimodal distribution is apparent peaking at 200nm and 400nm. An overlay of 5 results is shown to demonstrata the variation encountered. It is noticeable that increases in the upper peak are linked to decreases in the lower peak. This is very likely the ill-conditioned nature of the problem leading to several solutions to the same sample.

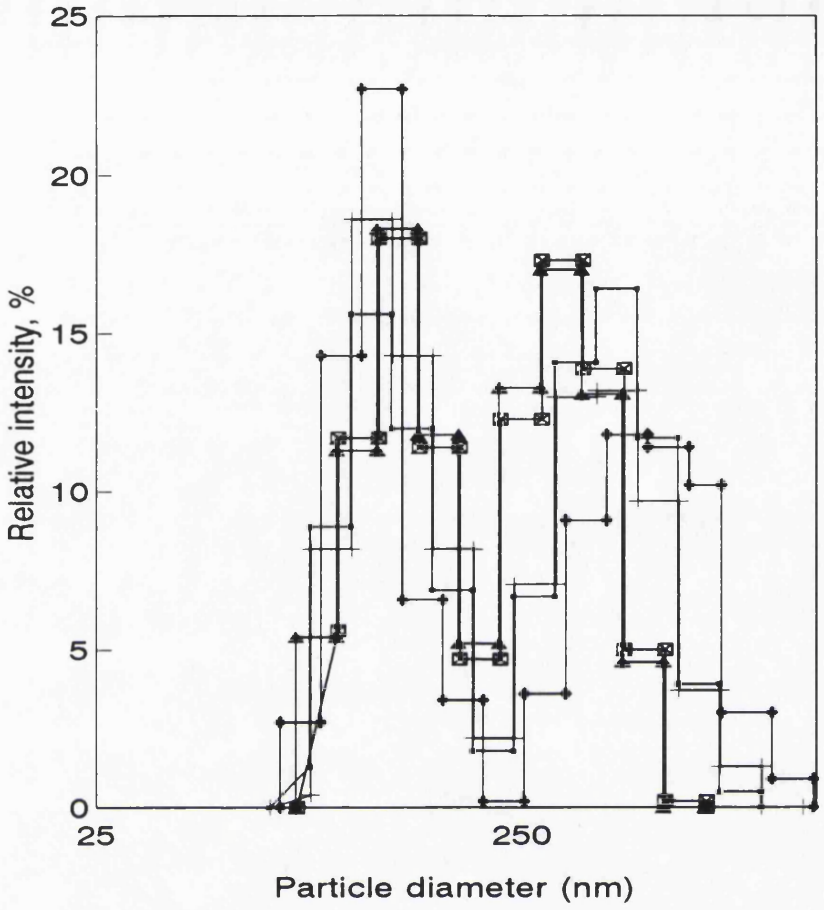


Fig 4.6b: Size distribution of clarified yeast homogenate by DLS using Malvern software. The centrifugation conditions were 75 minutes at 20000g. Again a bimodal distribution is apparent. A lower minimum particle diameter is measured, 75nm compared to 100nm in fig 4.6a. A similar trend of peak complementarity is noticed as in fig 4.6a.

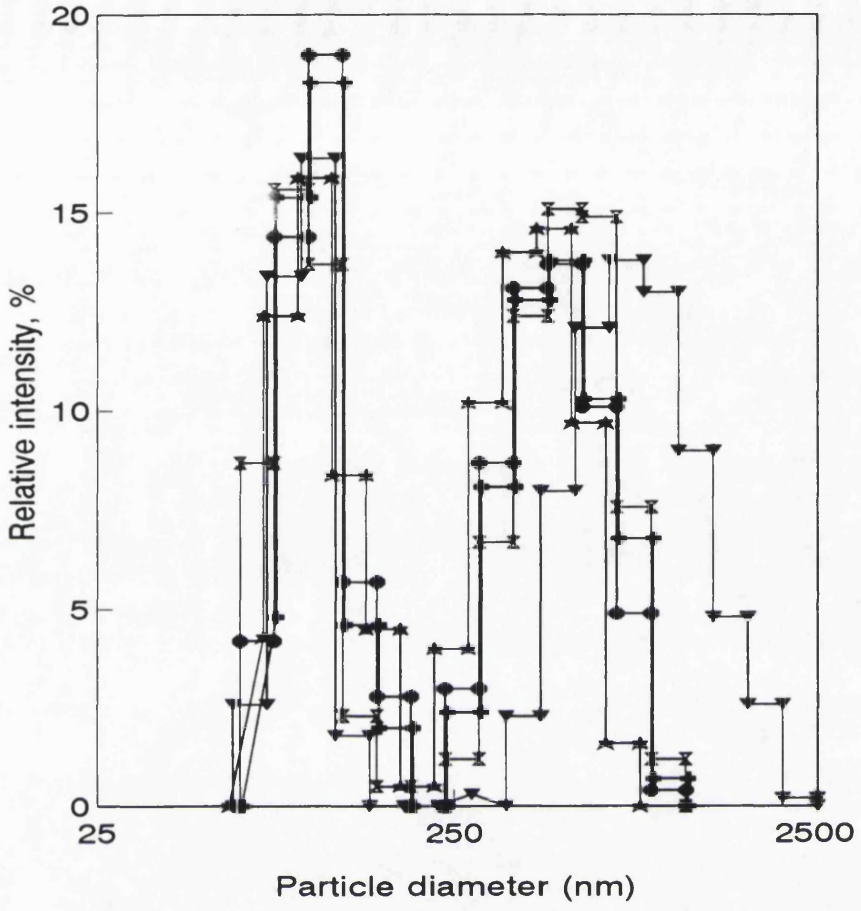


Fig 4.6c: Size distributions of clarified yeast homogenate by DLS using Malvern software. The centrifuge conditions were 155 minutes at 20,000g. In these examples the size distributions seem to be more stable except in one case where a significant shift in the upper peak is observed. The minimum particle diameter measured in this case is about 60nm but broadening of the upper peak occurs.

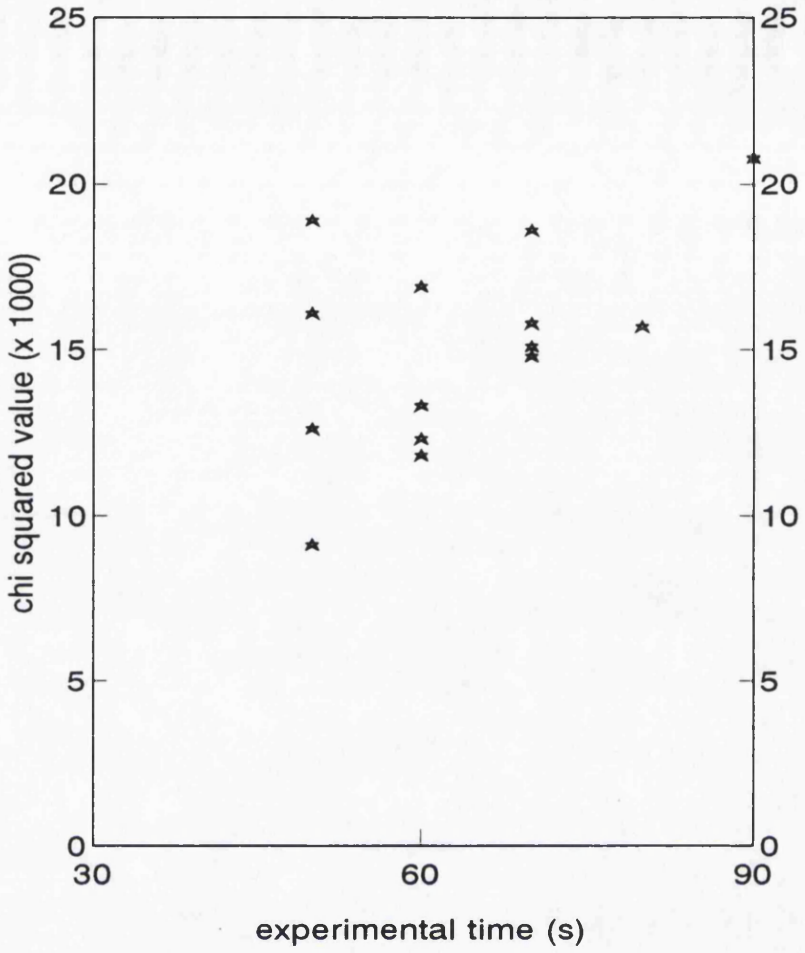


Fig 4.7: Chart showing an apparently positive correlation between experimental time and chi-sqared fit value for the Malvern 4700 analyser. This is an unexpected trend as an increased data collection time should produce less noisy data and allow a closer fit in the analysis. The apparent reduction in fit quality might be explained by dust or other contaminants in the samples unpredictably affecting the data at each run and affecting longer runs the most.

## Chapter 5: Computer simulations and analysis

### 5.1 Computer simulation of size distributions

In order to test the numerical algorithms written to invert the data collected from a dynamic light scattering experiment, a simulation of the decay constant distribution expected is required. Convolving the distribution by means of equation 1.35 §1.43 to produce data of the sort expected from experiments allows assessment of the algorithm in controlled conditions. The type of functions to simulate a DLS decay constant distributions commonly chosen by authors in the past are Schultz, Pearson, Gaussian and rectangular distributions (Stock and Ray 1985).

The true distribution of cell disintegrates is not known, however work (Agerkvist and Enfors, 1990) has shown DLS on E. Coli that a bimodal distribution is created in three different forms of disruption. Work on yeast by (Keshavarz-Moore et al 1987), by the electrical sensing zone method also shows a bimodal distribution, and the research described in chapter 4 on characterisation of yeast homogenate by optical methods gives two further pieces of evidence to point to a bimodal distribution of homogenate by means of DLS and a wavelength scan. It is assumed then, that the size distribution of homogenate is bimodal. The actual form of the peaks in most cases is symmetrical on a logarithmic axis. When transferring from size to diffusion coefficient, the raw measurement, a transform of 1/R is required (see §1.2). Since the size distribution is defined over a relatively narrow size range a symmetrical distribution in diffusion coefficient as well as size distribution results. Hence a Gaussian distribution may be used to simulate the decay constant distribution in this situation.
The decay constant distribution is evaluated at 64 points corresponding to the 64 channels to be evaluated for the correlation function.

### 5.2 Simulation of correlograms

To simulate the DLS data the Laplace integral equation (eq 1.35 §1.41) can be evaluated by numerical means having substituted a function for the decay constant. The integral

needs to be normalised in such a way that the area under the decay constant distribution function is unity. Subsequently a background value must be multiplied by each channel which represents the total intensity scattered by the sample. The coherence factor $\beta$ is also multiplied to the function to simulate the real situation where light is collected from more than one coherence area of the sample (see §2.021).

The results from clarified homogenate suspensions suggest that the distribution will be bimodal with one peak in the region of 200nm and the other in the region of 450nm both with similar widths (full width at half maximum, fwhm) of about 200nm. For the longer centrifugation times the lower peak reduces in width and size to about 125nm with a width of 80nm. The upper peak falls at about 350 - 400nm with a width of 200-300nm. All sizes quoted here are equivalent spherical diameters.

The experiments to produce the above results were carried out at 90° and at a temperature of 18.1°C. The decay constants corresponding to the size regions quoted above are shown in the following table.

| $R_H$ (nm) | $D_H$ (nm) | $\Gamma(S^{-1})$ |
|---|---|---|
| 225 | 450 | 328 |
| 200 | 400 | 370 |
| 175 | 350 | 420 |
| 100 | 200 | 740 |
| 62.5 | 125 | 1183 |

Table 5.1: Decay constants, radius and diameter equivalents.

The test size distributions chosen are based around these decay constants as typical size distributions that will be encountered. Added to the list is a simulation of homogenate plus a product particle at low size to simulate the presence of virus-like particles in clarified yeast homogenate. Table 5.2 shows the chosen size distributions from which correlogram data is simulated. The first column shows the minimum and maximum decay constant, the second column the sample time, the following columns show the mean and standard deviation of peaks present in the decay constant distribution. The standard deviation is

approximated by taking half the fwhm value of the peaks in the preliminary results above and converting to the equivalent decay constant range.

| $\Gamma_{min}/\Gamma_{max}$ | $\tau$ | $\Gamma$ d | $\sigma_\Gamma$ $\sigma_d$ |
|---|---|---|---|
| 200/800 | 100us | 500 (300nm) | 100 (60nm) |
| 0/2000 | 200us | 370 (400nm) | 115 (125nm) |
| | | 1184 (125nm) | 380 (40nm) |
| 0/2000 | 100us | 370 (400nm) | 115 (125nm) |
| | | 1184 (125nm) | 380 (40nm) |
| | | 1850 (80nm) | 75 (3nm) |

Table 5.2: Simulated size distribution details

### 5.3 Initial assessment of performance of algorithms

Each data analysis method has been tested with the simulated unimodal distribution and bimodal distribution described in the table. No additional noise was added so the only noise effects present in the data are those to round-off or truncation in the computer. The performance of each method is shown in figures 5.1 through 5.9. The test for goodness of fit is the $\chi^2$ criterion which is shown here:

$$\chi^2 = \frac{1}{N_p} \sum_{i=1}^{ndata} ((data(i) - fit(i))^2$$

where $N_p$ is the number of parameters and i represents the ith data or fit point.

### 5.31 Histogram method

Figure 5.1a shows two results for the histogram method. One is an unweighted fit with 7 histograms and the other a weighted fit with 40 histograms. Both display very good $\chi^2$ values. The fit with less histograms follows the true line more closely and has a slightly lower $\chi^2$ value of 0.007. Attempting to perform an unweighted fit with more than 7 histograms in this situation leads to an unstable solution with many negative amplitudes. This reflects the resolution limit achievable from the method. The range of $\Gamma$ covered in

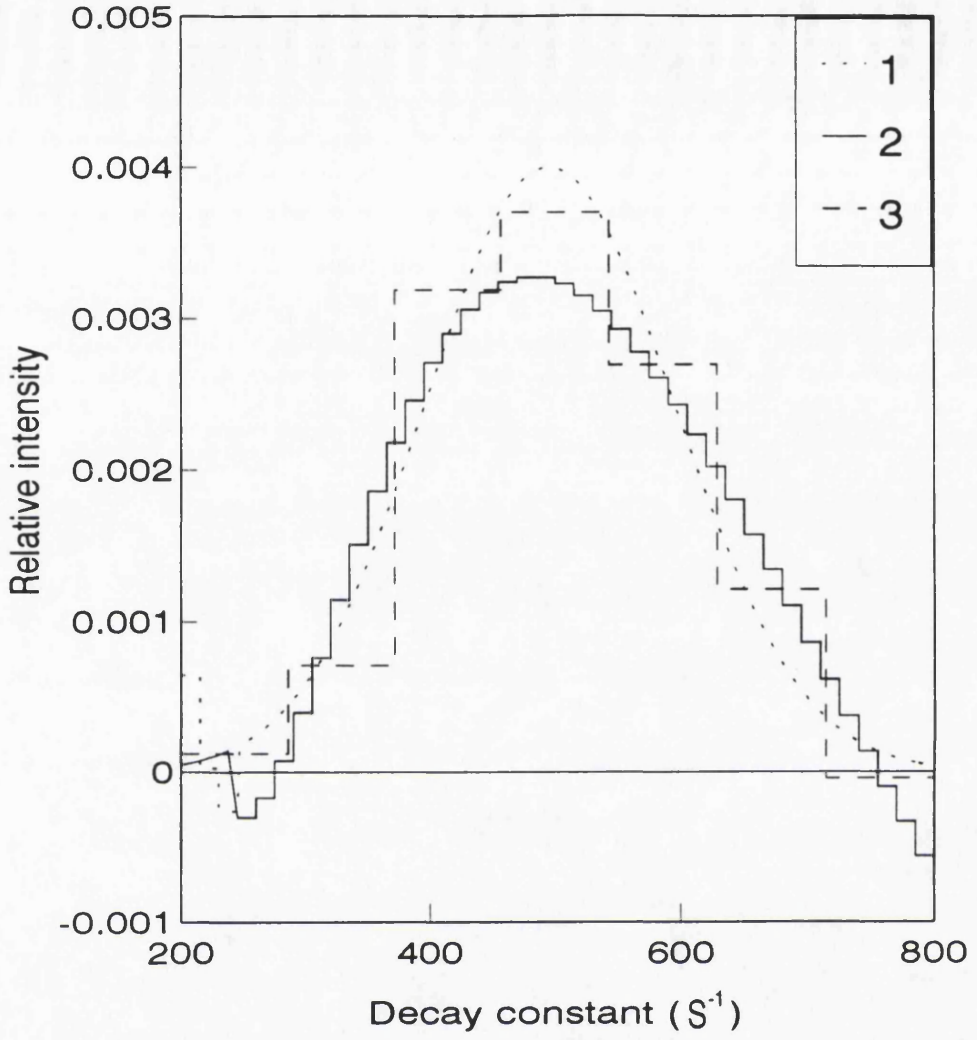


Fig 5.1a: Performance of weighted and unweighted histogram fits to a monomodal distribution. Histogram 2 is a 7 parameter unweighted fit with a $x^2$ value of 0.007. Histogram 3 shows that 40 or more parameters may be fitted with a weighted fit although some negative portions are present at the edges. This results in a low $x^2$ value of $2e^{-6}$.

this example is 600 $s^{-1}$. The weighting procedure improves the performance in this situation by stabilising the solution across the range. The very good $\chi^2$ value is an effect from the negative portions of the graph at the outskirts which is an over-fitting effect. Figure 5.1b shows the same method applied to a bimodal distribution. Again a very good fit is achieved. The resolution (histogram spacing) in this case is lower (2000/15 (133 $s^{-1}$) compared to 600/7 (85 $s^{-1}$)). This is most likely due to the more complex distribution to be fitted.

### 5.32 Trapezoidal method

Figures 5.2a and 5.2b show the performance of the trapezoidal method to a unimodal and bimodal distribution respectively. In both cases poor fits result. The method seems to under-estimate the distribution for most of the range and there is evidence of a spurious extra peak forming at about 1,600 S-1 in the bimodal fit. Both fits have very large $\chi 2$ values indicating the poor reconstruction of the original distribution.

### 5.33 Exponential sampling method

Figures 5.3a and 5.3b show results for reconstruction of unimodal and bimodal distributions by the exponential sampling method. The graphs are shown as vertical bars as this method estimates exponentially sampled points on the graph rather than an integrated area as most of the other methods. Good results are shown in both cases but the bimodal fit tends to over and under-estimate across the range. Care must be taken when interpreting the $\chi 2$ values from this method as it is easy to have a very low $\chi 2$ value but a highly oscillatory fit to the distribution. This generally occurs when the interleaving process is used as described in §1.4321 rather than increasing $w_{max}$, the decay constant distribution sampling frequency (See §1.4321). Also low values of $w_{max}$ rather than producing reasonable but under-resolved fits to the data actually produce very poor fits oscillatory in nature and with negative values. This is the same as the effect when wmax is too high as over-sampling occurs.

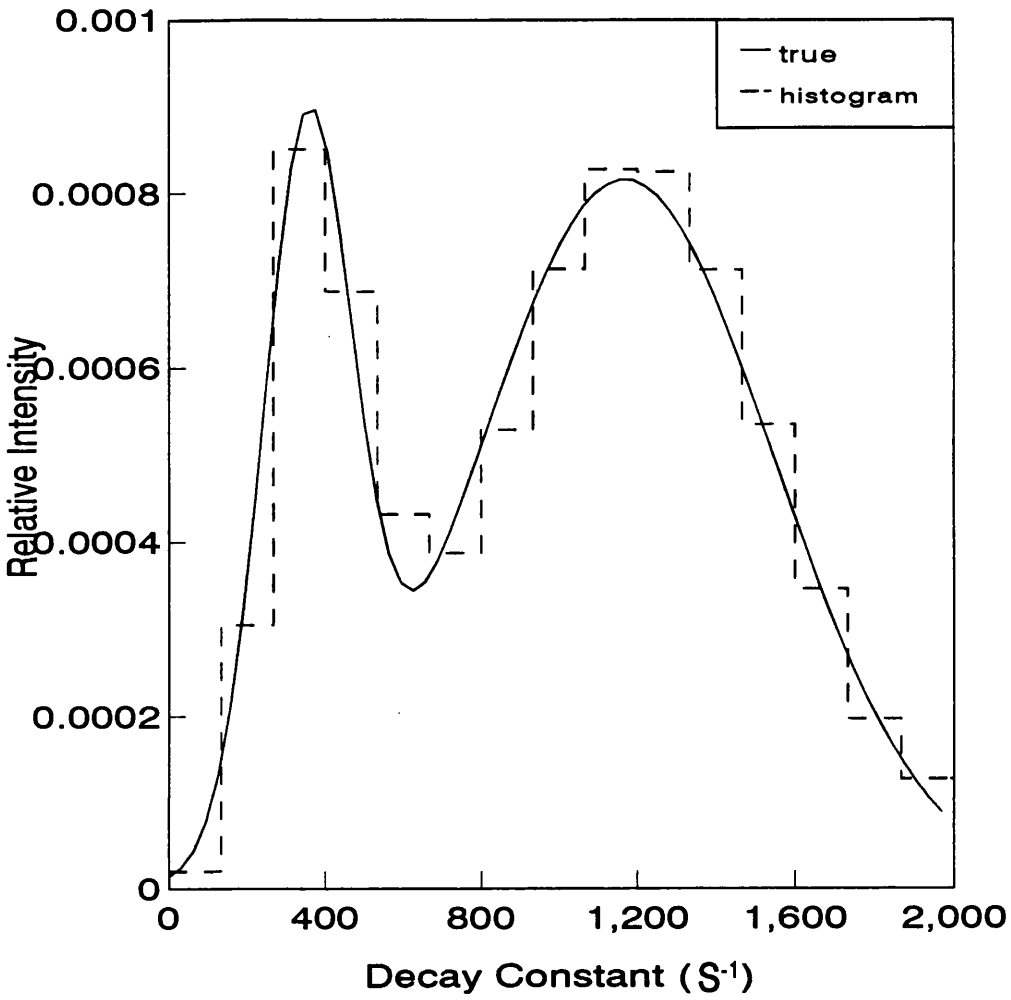


Fig 5.1b: Performance of the histogram method to reconstruct a bimodal distribution. 15 parameters are used in the range 0 to 2000 $S^{-1}$. A very good fit is achieved with a $x^2$ of 0.000221.

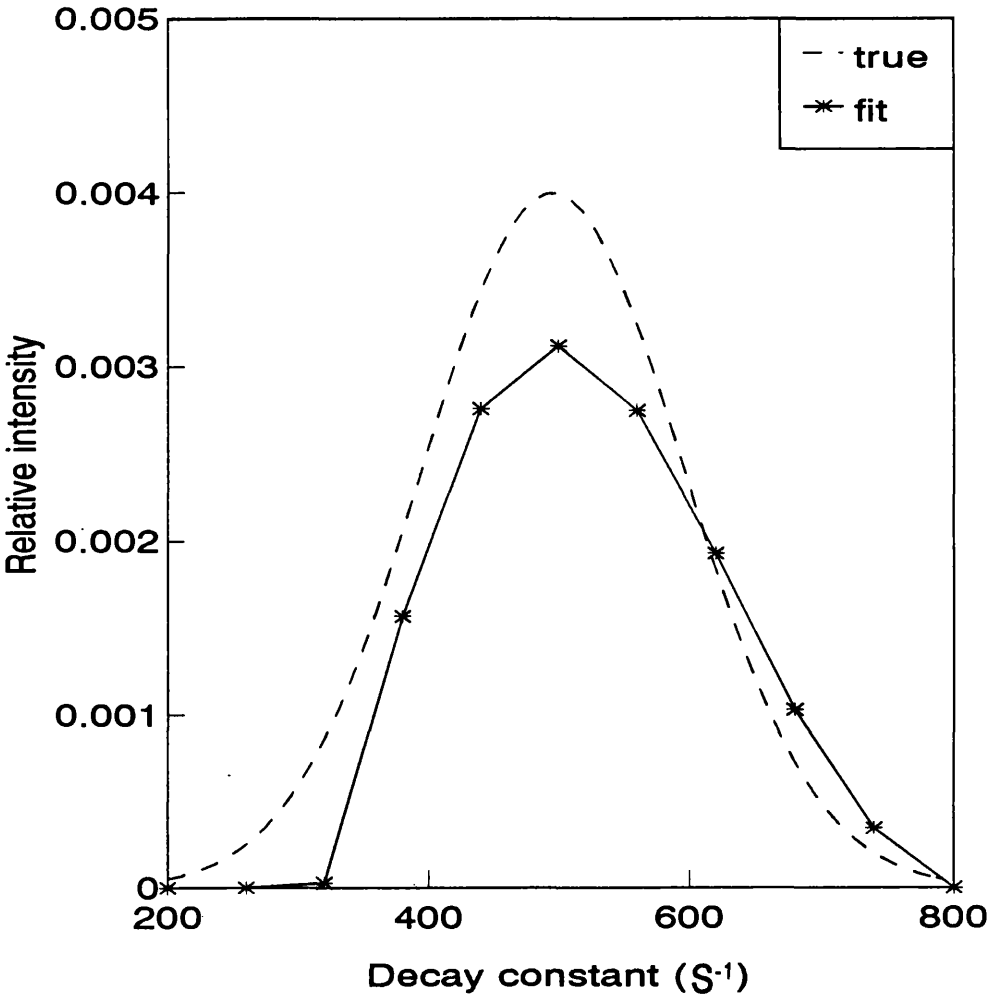


Fig 5.2a: Trapezoidal fit to monomodal distribution. 11 parameters are used in the range 200 to 800 S-1. A very large $x^2$ value is returned indicating the under-estimation at the lower end of the range.

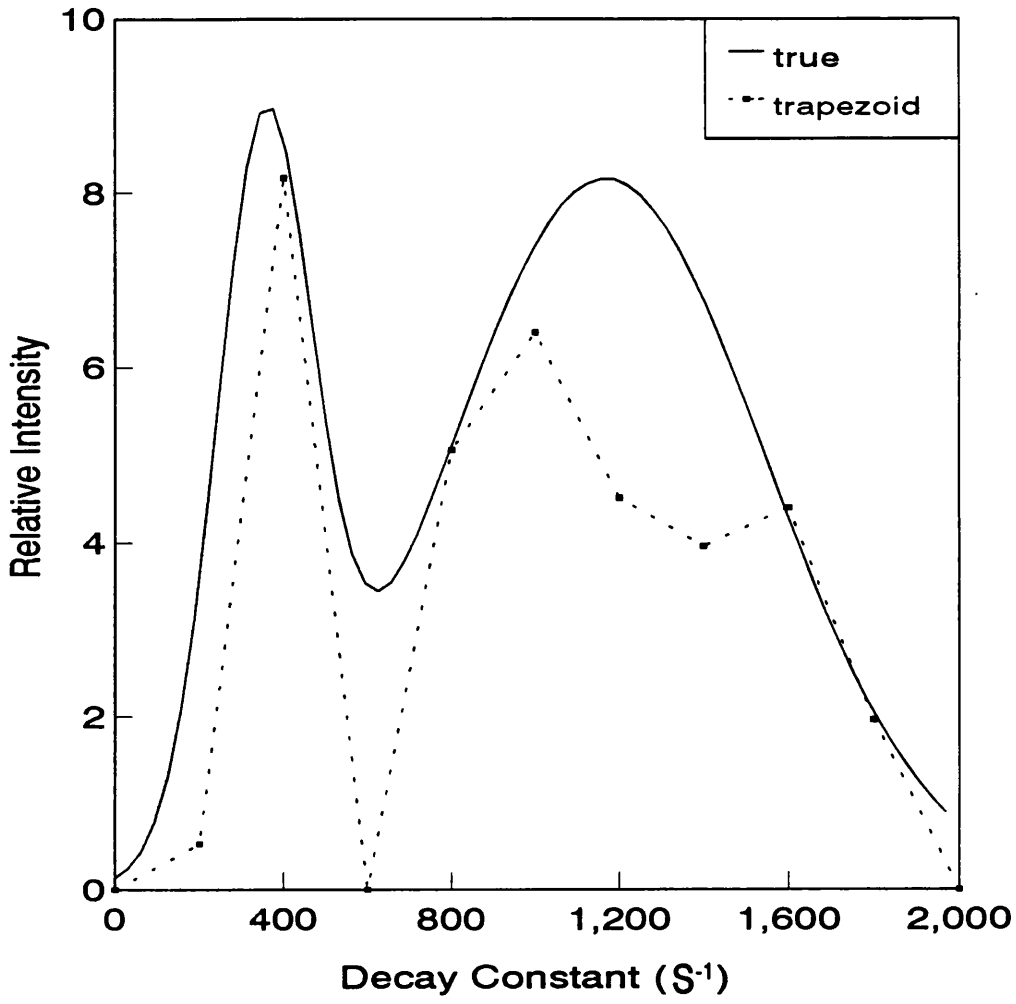


Fig 5.2b: Performance of trapezoidal fit to a bimodal distrbution. A poor fit with under-estimation across the range occurs resulting in a high $x^2$ value. The range of analysis is 0 to 2000 $S^{-1}$ with 10 parameters.

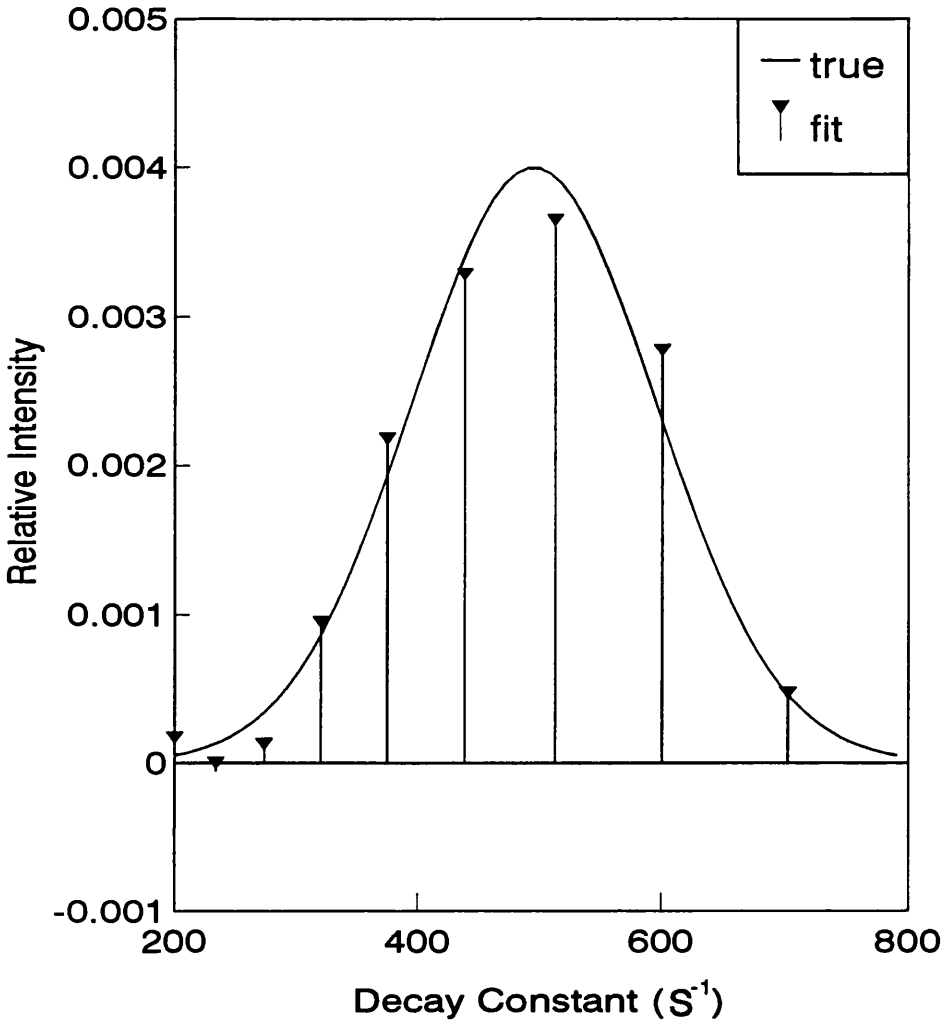


Fig 5.3a: Performance of the exponential sampling method to fit a monomodal distribution. The range is 200 to 800 $S^{-1}$ and $w_{max}$ is 20. It is preferable to choose a higher $w_{max}$ to increase resolution than a lower one and interleave several fits as the latter leads to instability in the solution. $x^2$ for this fit is 0.00139.

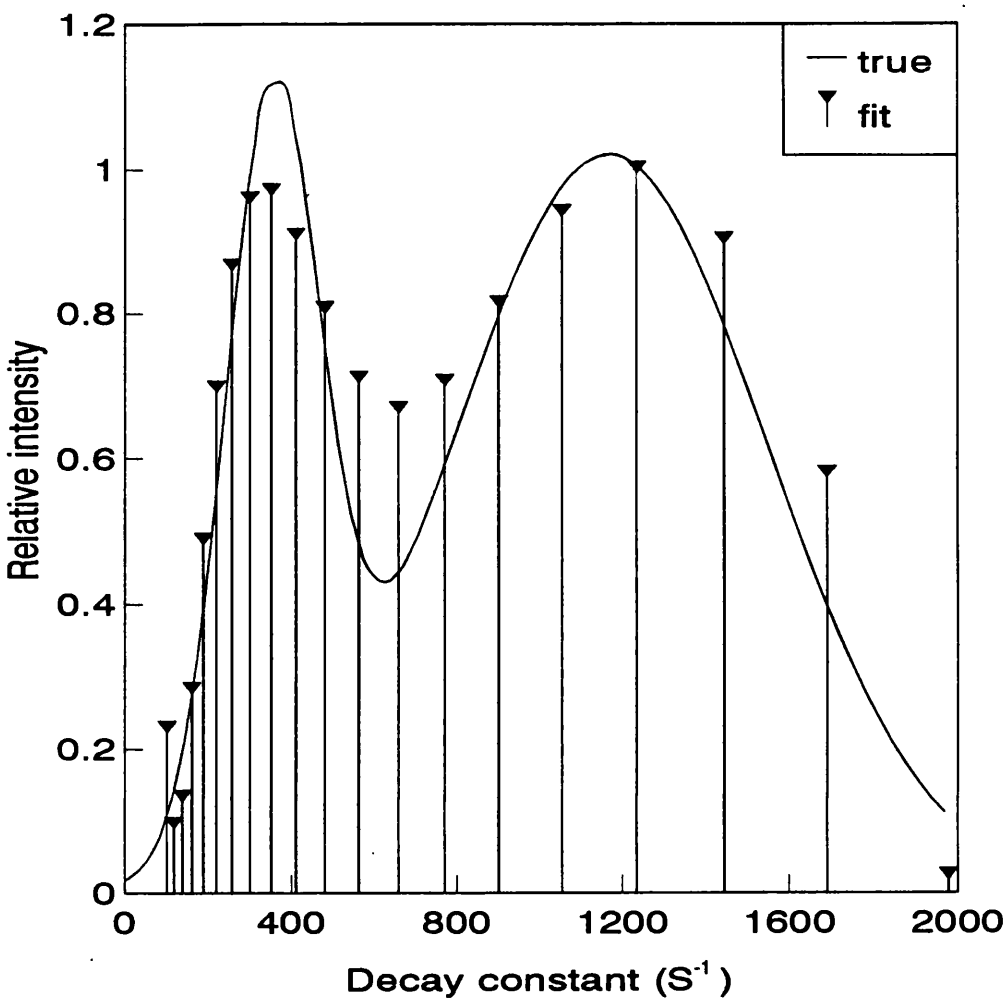


Fig 5.3b: Performance of the exponential sampling algortihm to reconstruct a bimodal distribution. A $x^2$ value of 0.013 is returned and a reasonable fit is recorded visually. The fit shows under and over-estimation throughout the graph. The analysis range is 100 to 2000 $s^{-1}$ and $w_{max}$ is 20.

### 5.34 Exponentially spaced histogram method

Figures 5.4a and 5.4b show fits to the unimodal and bimodal distributions using the exponential histogram method. As in the normal histogram method good fits are achieved in both cases. There is however an upturn at low $\Gamma$ in the case of the bimodal fit and the lower peak does seem to be slightly shifted to higher $\Gamma$. This upturn is also apparent in the exponential sampling reconstruction in figure 5.9. The range for the bimodal fit starts at 100 $s^{-1}$ and covers up to 2000 $s^{-1}$. $w_{max}$ is 20 corresponding to 19 histogram steps in this graph and 7 steps in the unimodal plot whose range spans 200 to 1000 $s^{-1}$.

### 5.35 Non-negatively constrained least squares method

Figures 5.5a and 5.5b demonstrate the results achievable from the NNLS analysis routine. The unimodal fit performs quite well visually but has a high $\chi^2$ value due to the over-estimation at high $\Gamma$. The fit to a bimodal distribution is very poor. Most of the 10 parameters are zero and the remaining ones do not make up the area although a bimodal distribution does result.

### 5.36 Regularised iterative method

Figure 5.6a shows the performance of the regularised iterative procedure for data inversion. Fits are shown for different values of the smoothing parameter $\alpha$. Without smoothing the peak occurs in the correct location of 500 $s^{-1}$ but is underestimated due to the area taken up by the spurious peak at the right-hand edge of the chart. A large value of $\alpha$ leads to over-smoothing which removes the upper peak but shifts the correct peak down and broadens the distribution. A smaller value makes little difference. In this situation it would seem that truncation at 800 $s^{-1}$ and renormalisation would produce a better fit. However in order to converge properly the full analysis range of 200 to 1300 $s^{-1}$ is required. The performance of this method to a bimodal distribution is very poor (fig.5.6b). The resulting distribution is bimodal but the upper peak is over-estimated and appears at the edge of the diagram independent of the analysis range.

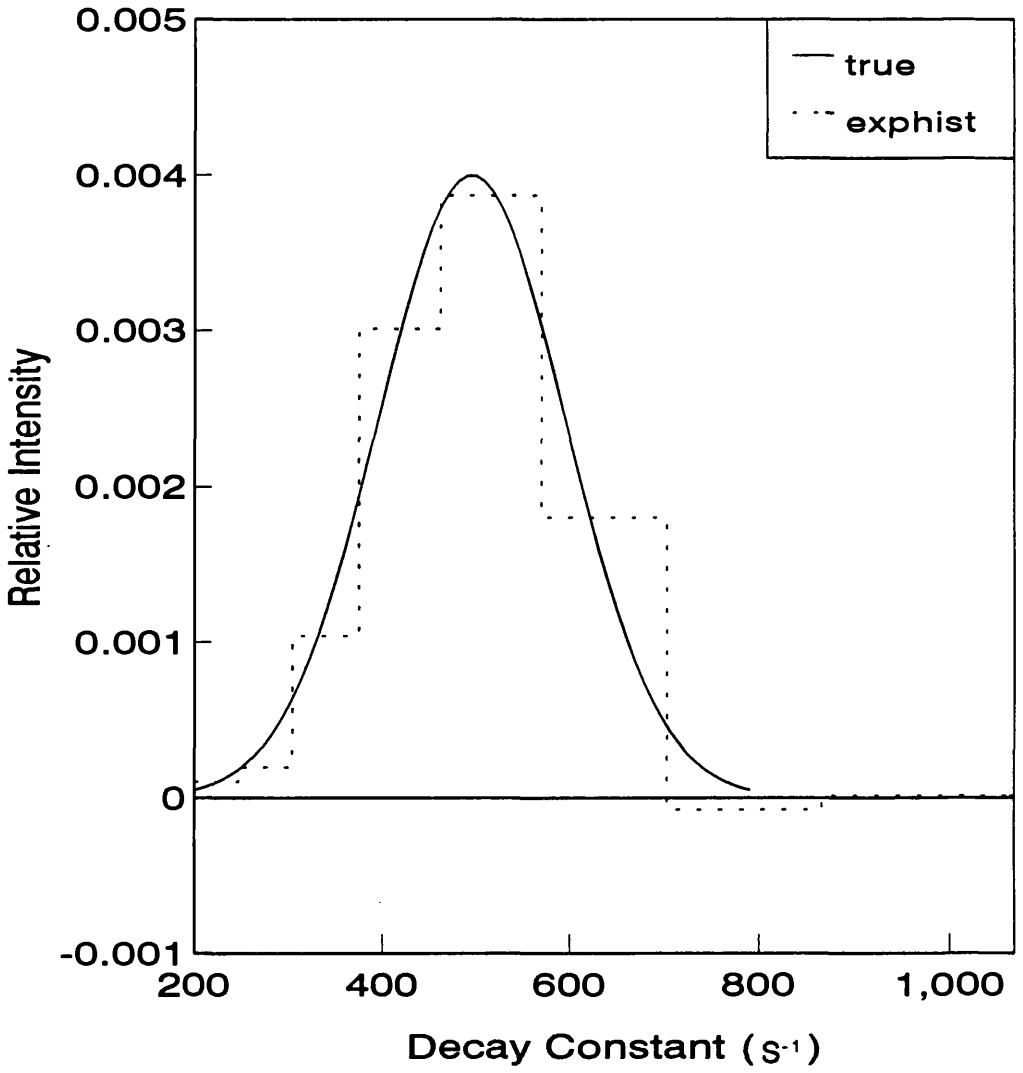


Fig 5.4a: Performance of the exponetially spaced histogram method to a monomodal distribution. The range covered is 200 to 1000 $S^{-1}$ with a $w_{max}$ of 15. A very close fit to the true distribution is acheived with a $x^2$ value of 0.0069.

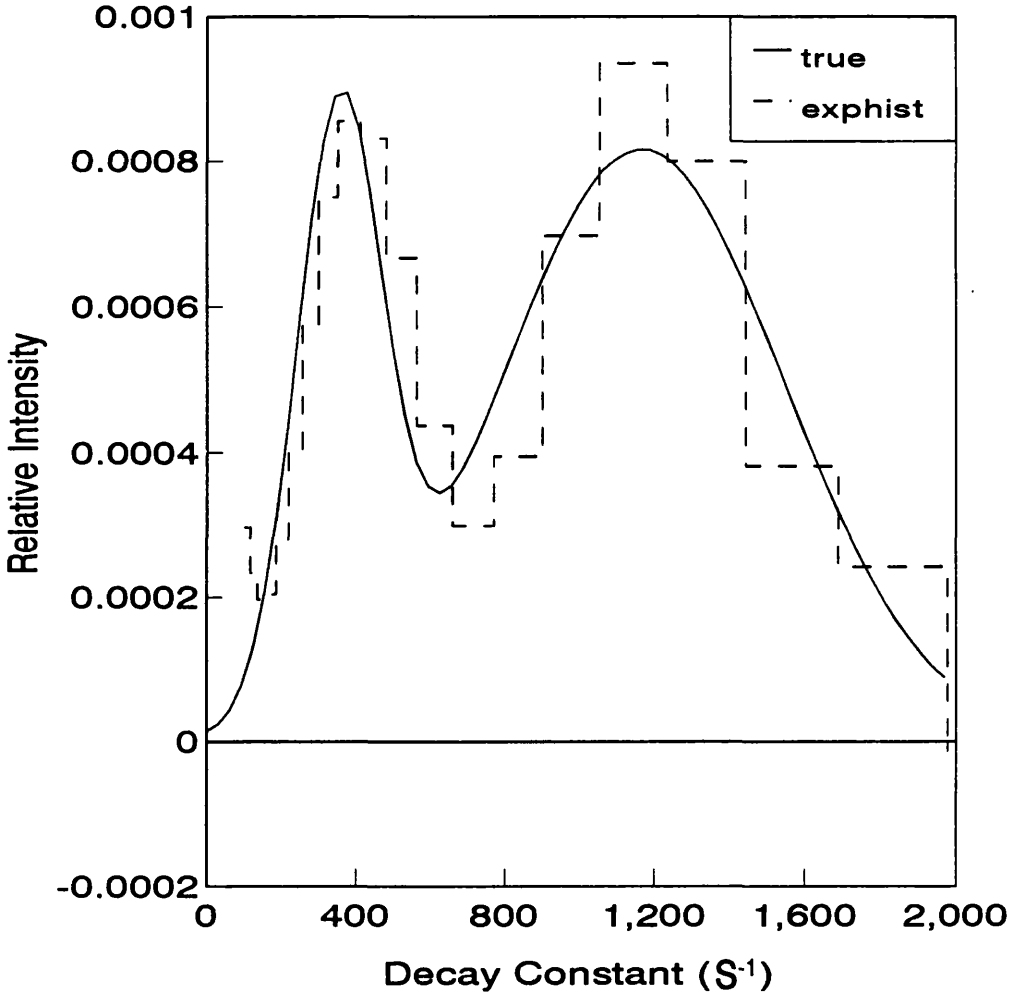


Fig 5.4b: Performance of the exponentially spaced histogram method to reconstruct a bimodal distribution. The range of analysis is 100 to 2000$S^{-1}$ and a $x^2$ fit of 0.217 x $10^{-3}$ is achieved.

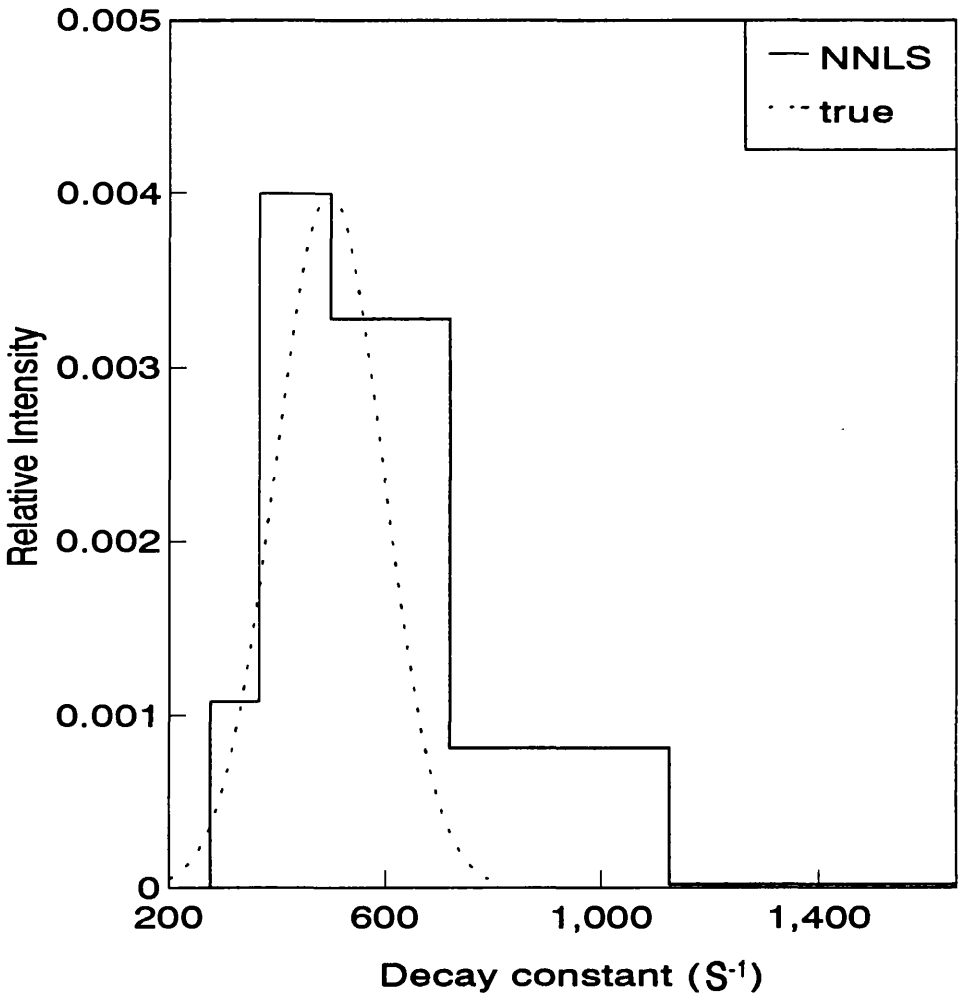


Fig 5.5a: Performance of non-negatively constrained least squares analysis method to a monomodal distribution. The range covered is 250 to 1500 $S^{-1}$ with 6 quadratically spaced histograms as described in the text. A reasonable fit is achieved but overestimation at higher decay constant values occurs. This results in a high $x^2$ value.

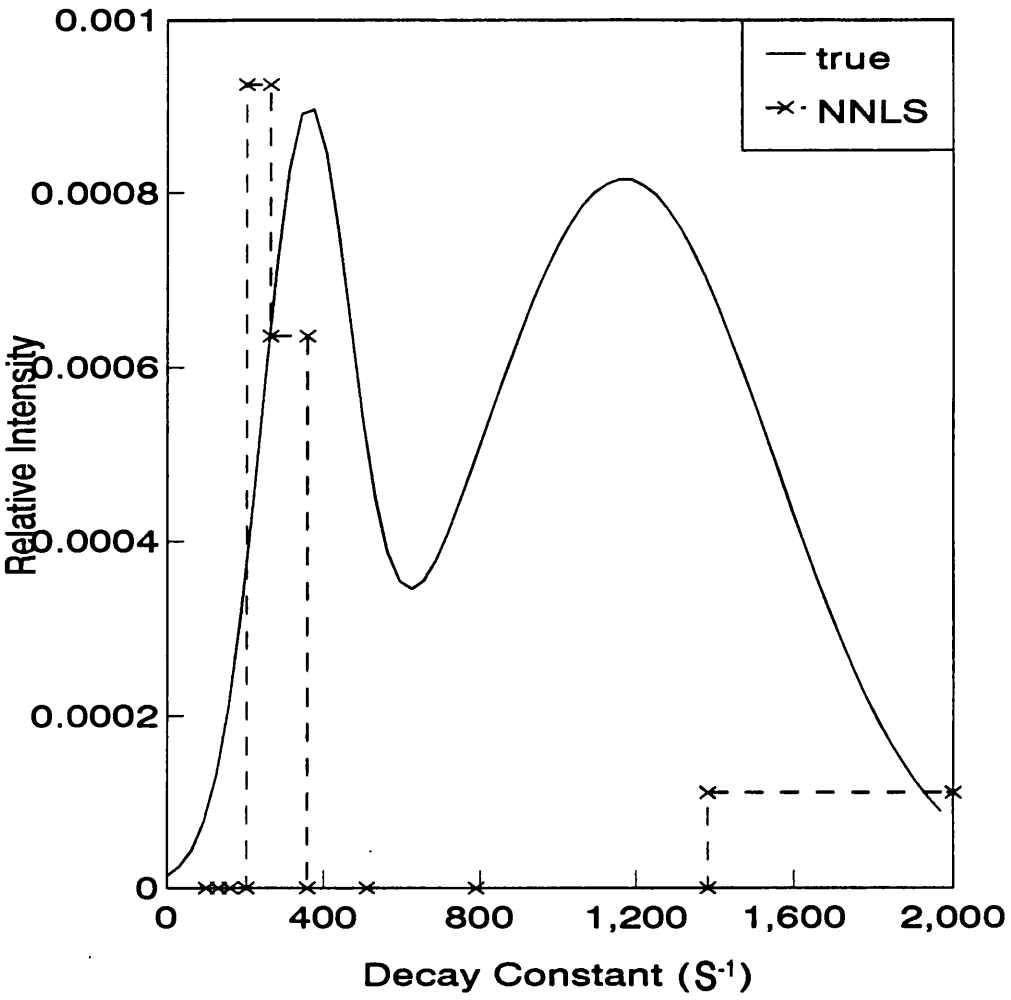


Fig 5.5b: Performance of the non-negatively constrained least squares analysis to a bimodal distribution. 10 parameters in the range 100 to 2000$s^{-1}$ are fitted. Most of the parameters converge to zero leaving a poor fit although a bimodal distribution is recorded.

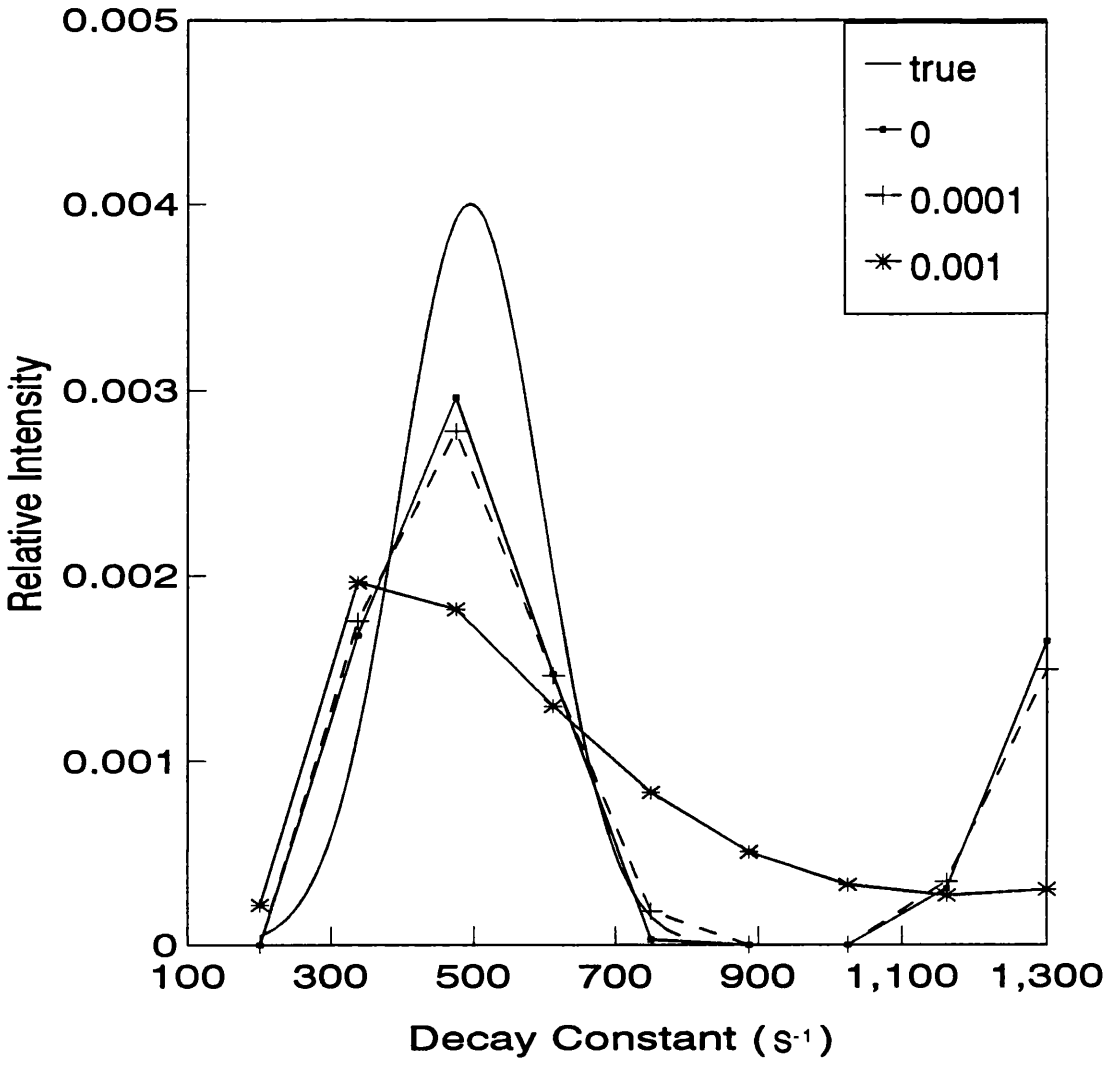


Fig 5.6a: Performance of regularised iterative algorithm to a monomodal distribution. Three fits are shown each for a different value of smoothing parameter alpha. A relatively large value oversmooths the solution whereas smaller values lead to a spurious peak at the high end of the graph. In all cases the distribution is underestimated. More iterations may improve the solution but a better approach may be to truncate the graph between the two peaks and renormalise the distribution.

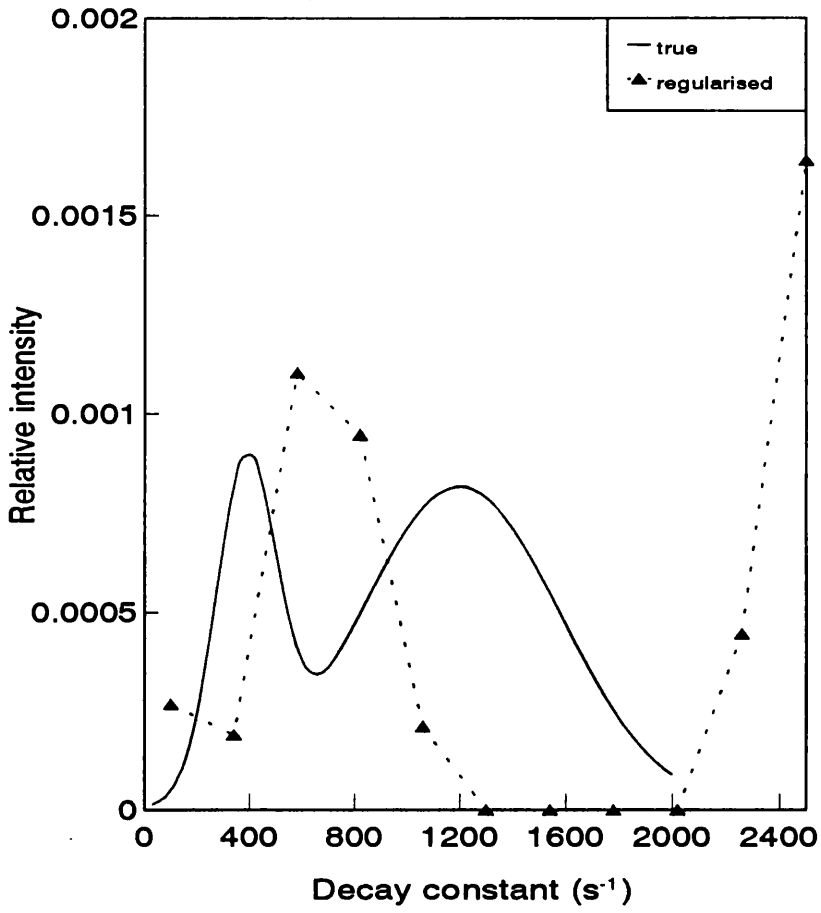


Fig 5.6b: Performance of the regularised iterative procedure to reconstruct a bimodal distribution. The plot shows a large peak at high decay constant and the lower peak falls approximately at the average of the two, thus poor resolution is achieved. The upper peak is a feature of this technique but in this situation it is larger than in the case of unimodal distributions.

## 5.4 Performance of algorithms in noisy conditions

In the initial assessment it appears that the trapezoidal constructions and the NNLS algorithm,since they do not produce good fits in the absence of noise, will not perform well in noisy conditions. They will not be considered further. The following section tests the algorithms in the presence of varying amounts of random noise added as percentage of the baseline value to each correlogram channel. The percentage noise quoted is the standard deviation of noise value over the correlogram. Noise samples are created using the Box transform method (Numerical Recipies).

### 5.41 Exponential sampling

Figs. 5.7a and b show the performance of the exponential sampling method in inverting a bimodal distribution with 0.04% noise and 0.09% noise added. The chief features are that $w_{max}$ is reduced slightly and that the range covered needs to be increased for convergence of the algorithm. Again values of $w_{max}$ up to close to the convergence produce over oscillatory results.

### 5.42 Exponentially spaced histogram

The exponentially spaced histogram method in the presence of 0.04% and 0.09% is shown on fig.5.8a. It demonstrates that for low values of $\Gamma$, close fitting is achieved to the distribution whereas, whatever the upper range, negative portions always occur at the last amplitude. The consequence is the incorrect estimation of the last peak.

### 5.43 Histogram method

Fig. 5.8b shows the performance histogram method to three levels of noise on the data, 0.04%, 0.09% and 0.4%. It is notable that this is the only method that was able to cope with larger noise levels than 0.1%. Detail of the algorithm is given later in this section but in its operation manipulation of the singular values of the singular value decomposition

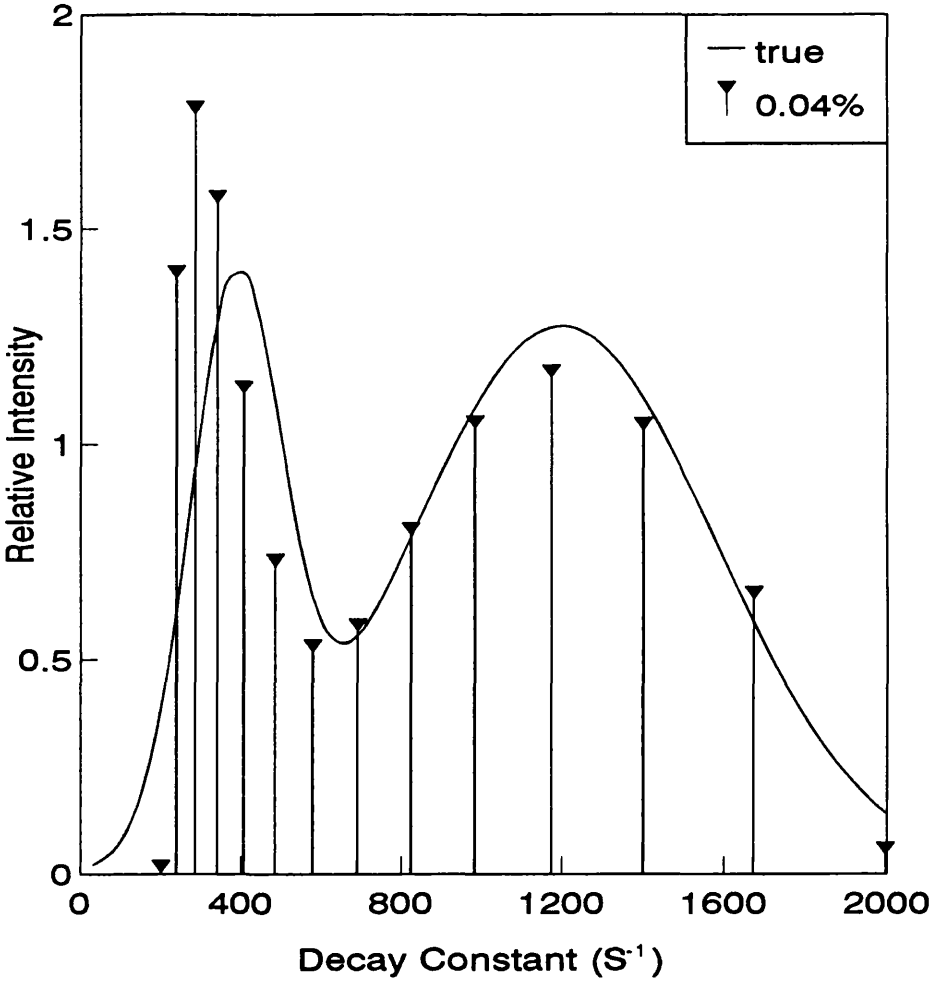


Fig 5.7a: Performance of exponential sampling method in the presence of 0.04% noise in the data. The decay constant range is 200 to 2200 $S^{-1}$ and $w_{max}$ is 17.75. The upper peak is fitted well but the lower isunder-estimated in position and over-estimated in magnitude. For convergence in this case the range had to be changed from the noise-free situation where the range covered 100 to 2000 $S^{-1}$.

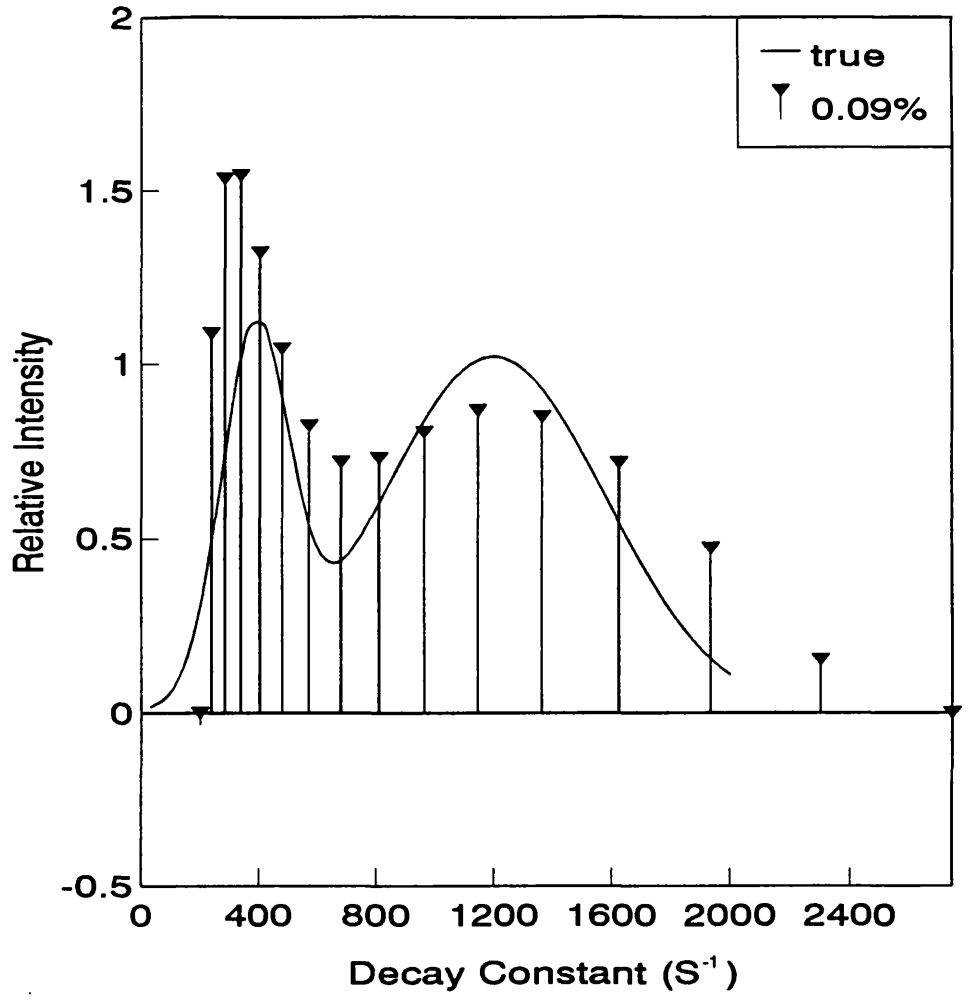


Fig 5.7b: Performance of the exponential sampling method in the presence of 0.09% noise. Over-estimation occurs at the lower peak and the upper peak is broadened. The range used for this analysis was 200 to 3000 $S^{-1}$ indicative of the broader range needed for more noisy data. $w_{max}$ is 18.

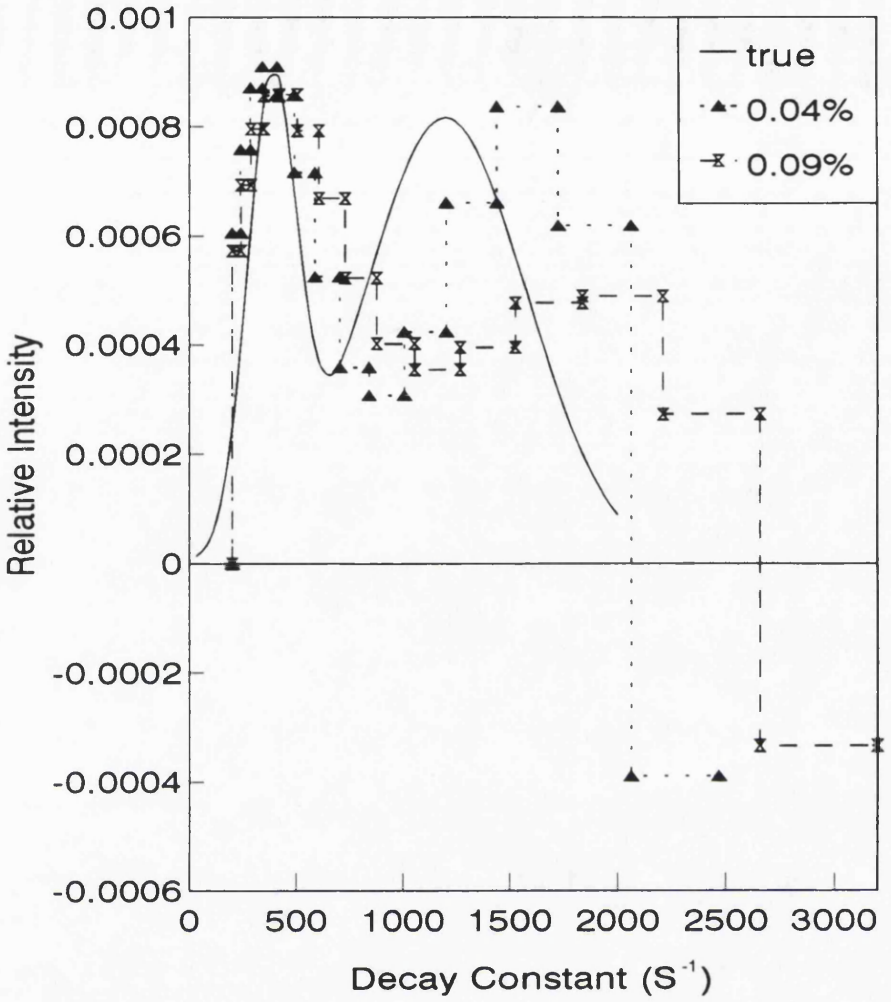


Fig 5.8a: Performance of the exponentially spaced histogram method in the inversion of a bimodal distribution from noisy data. Two noise levels are shown 0.04% and 0.09%. The upper decay constant is misrepresented in both cases. It is interesting to note that this is converse to the exponential sampling result where the lower decay constant was more in error. The range in both analyses was 200 to 3000 $s^{-1}$ and $w_m$ was 18.

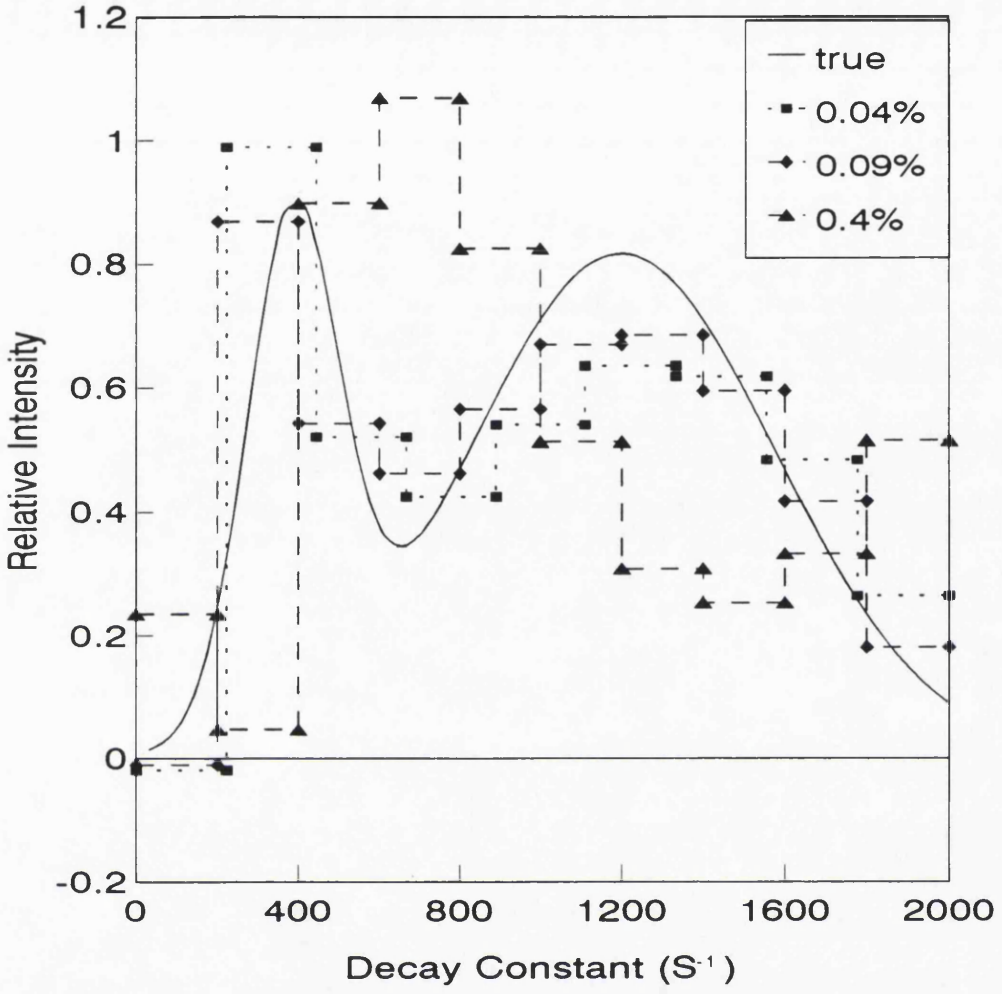


Fig 5.8b: Performance of histogram method in the inversion of noisy data. Three noise levels are shown. The lowest producing the closest fit to the original distribution though under-estimating the upper peak. The result from data with 0.09% noise added over-estimates the lower peak and under-estimates the upper peak. The result for the highest data noise level loses resolution altogether and produces a peak close to the mean of the distribution.

(SVD) amounts to a noise filtering process which the other methods approach in a different manner. The fits for the lower two noise levels, give reasonable reconstructions of the decay constant distribution and for the higher noise level, instead of producing meaningless results , the resolution is lost and an average of the distribution is returned.

### 5.44 Regularised inversion

The regularised inversion procedure was able to resolve a bimodal as was demonstrated in §5.36. Reports in the literature (Dhadwal 1989) do not suggest this, so it is suspected that the algorithm coded here directly from equations in the literature has been compromised in some way. The reason that it is being considered further is partly because it is expected that the algorithm can perform more adequately and also in the considerations of parallel processing the equations are very suitable for translating into a parallel format. This is described further in §5.3.

Figs 5.9a and b show the results of the regularised iterative procedure in the presence of 0.04% and 0.09% noise respectively. In the case of 0.04% noise, the solution is underestimated as before and a spurious peak appears at high $\Gamma$ on the edge of the chart. Increasing the value of the smoothing parameter from zero flattens the upper peak but shifts the lower peak to a lower decay constant. The higher noise level data (fig.5.9b) produces a more distinct spurious peak at higher $\Gamma$. This is reverted to the usual artifact at the edge of the chart with the application of smoothing and a better estimate of the distribution is achieved.

### 5.5 Discussion

The performance of the exponential sampling method and the histogram method appear to work well in the presence of noise up to ≈0.1% standard deviation. The histogram method will converge at higher noise levels, however the resulting distribution losses resolution. The range of $\Gamma$ that is required for the exponential sampling method increases as the noise on the data increases however the histogram method is able to operate at the same decay constant limits, for different noise values. Regularised inversion suppresses

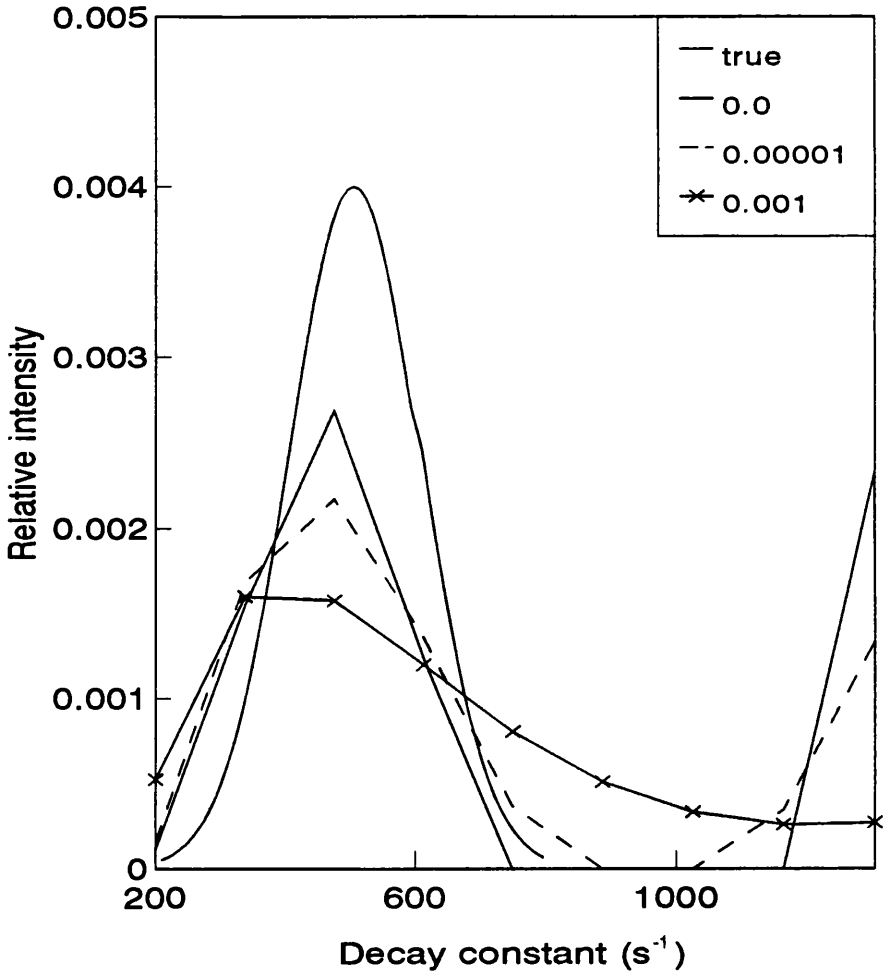


Fig 5.9a: Performance of the regularised iterative algorithm with 0.04% noise added to the data for a monomodal distribution and for different values of regularising parameter. It can be seen that the regularising parameter removes the peak at higher decay constant but that the resulting solution is oversmoothed and begins to shift towards lower decay constant.

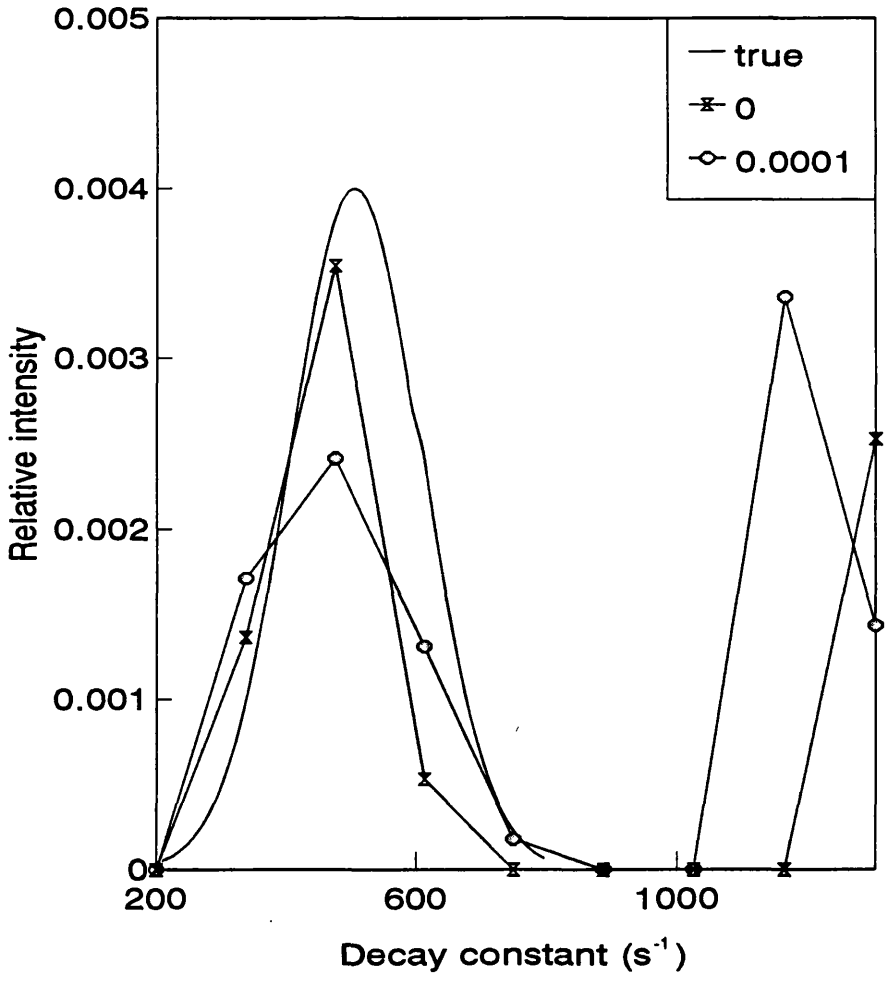


Fig 5.9b: Performance of the regularised iterative algorithm with 0.09% noise added to the data. The unsmoothed result produces a bimodal distribution whereas a smoothing parameter of 0.0001 returns the result to the typical peak at the edge of the graph observed in the noise-free plots. In both cases the distribution is under-estimated. The range used was 200 to 1500 $s^{-1}$.

noise effectively but oversmooths the solution and is only effective as coded here, on unimodal distributions.

### 5.6 Implementation of the histogram method

The histogram method follows the theory described in §1.4322. The resulting decay constant distribution is calculated using singular value decomposition (SVD) as suggested by most authors who implement linear least square fits of this sort. A feature of SVD analysis is its ability to filter out elements of the data which contribute to the instability of the solution. Knowledge of the level of noise in the data is ideally required in order to chose a threshold value for the program to use to effectively remove some data from contributing to the solution. A clear description of the technique is given in (Numerical recipes) from where the algorithm was taken.

The version of the histogram method used in these experiments is based on a method (Kulkarni 1991) for image restoration signal processing where a neural network approach to reducing the weights in a SVD system using a-priori knowledge about the data statistics is described. A much simpler implementation is adapted here where the weights in the single value decomposition are changed in turn to bring the solution closer to a realistic distribution. The steps are as follows:

1) Enter $G_{max}$ and $G_{min}$ and number of histograms to fit.

2) Perform SVD analysis (least squares fit) - the result is an erratic distribution of positive and negative values.

3) Increase the value of the smallest weight by a step value and check the change to the distribution.

4) If all histograms are positive, exit.

5) If present weight has reached maximum effective limit move to the initially next smallest weight and return to step 3.

The usefulness of this technique is that it fits to the level of the noise in the data without needing to know the noise levels before hand. The algorithm speed depends on the number of histograms chosen.

In the neural network application a critical weight had to be arrived at and all weights below this value were adjusted simultaneously until the data satisfied a particular criterion. This method was applied to this application first but it was realised that autonomous choice of the critical weight by the program in the different noise conditions would be difficult. A more robust method, if inelegant, is to start at the lowest weight and work up as described in the algorithm.

### 5.7 Implementation of the regularised iterative algorithm in parallel processing

It is noticed that the form of equations for the regularised iterative procedure lend themselves to a parallel calculation architecture (Dhadwal et al). The published results suggest better performance than was found here and speeding up of processing of this technique,which requires tens of thousands, and sometimes over 100,000 iterations to converge would be desirable. Fig.5.9c shows the schematic of a regularised iterative parallel architecture.

### 5.8 Considerations for product monitoring

The simulation experiments so far have indicated that for rapid data analysis where noise in the data is relatively high, even with the inclusion of a-priori information such as range of decay constants and positivity, the solutions are seen to be rather erratic. An alternative approach is presented here, where the difference in correlogram due to homogenate plus a product are subtracted. The difference in this case will provide a measure of the amount of product present. The noise on the correlogram will be the problem in distinguishing between curves and due to the subtraction process will be larger than the correlogram noise by a factor of $\sqrt{2}$ . However there is no instability due to algorithm performance. The key consideration is the stability of the homogenate correlogram for different conditions so that in the situation where the measurement is to be applied, the appropriate baseline is subtracted.

Figs. 5.10 and 5.11 assess the difference method with the homogenate decay constant distribution curves used previously in this chapter. Fig 5.10 shows the amount of light

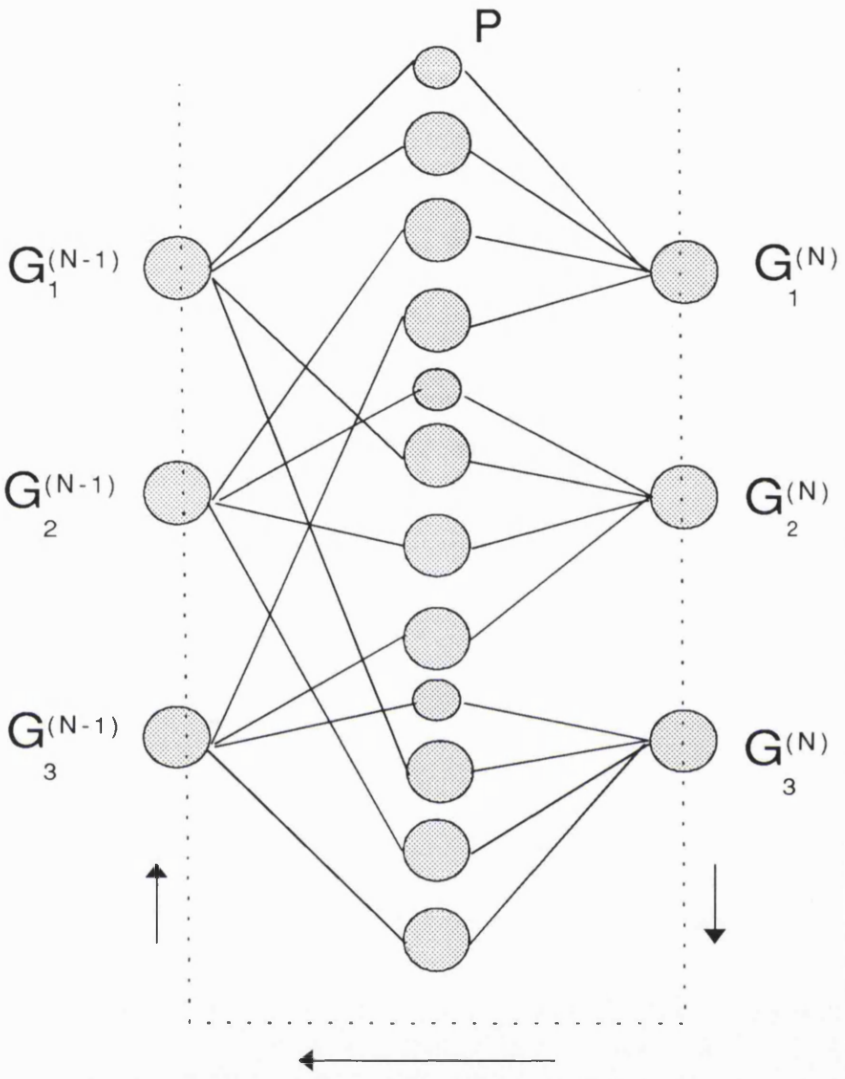


Fig 5.10: Schematic of parallel implementation of regularised iterative algorithm. This represents the formula $G^{(N)} = G^{(1)} + P\ G^{(N-1)}$ which is at the heart of the algorithm. The smoothing parameteris contained in P along with the model for the correlation function to be fitted to.

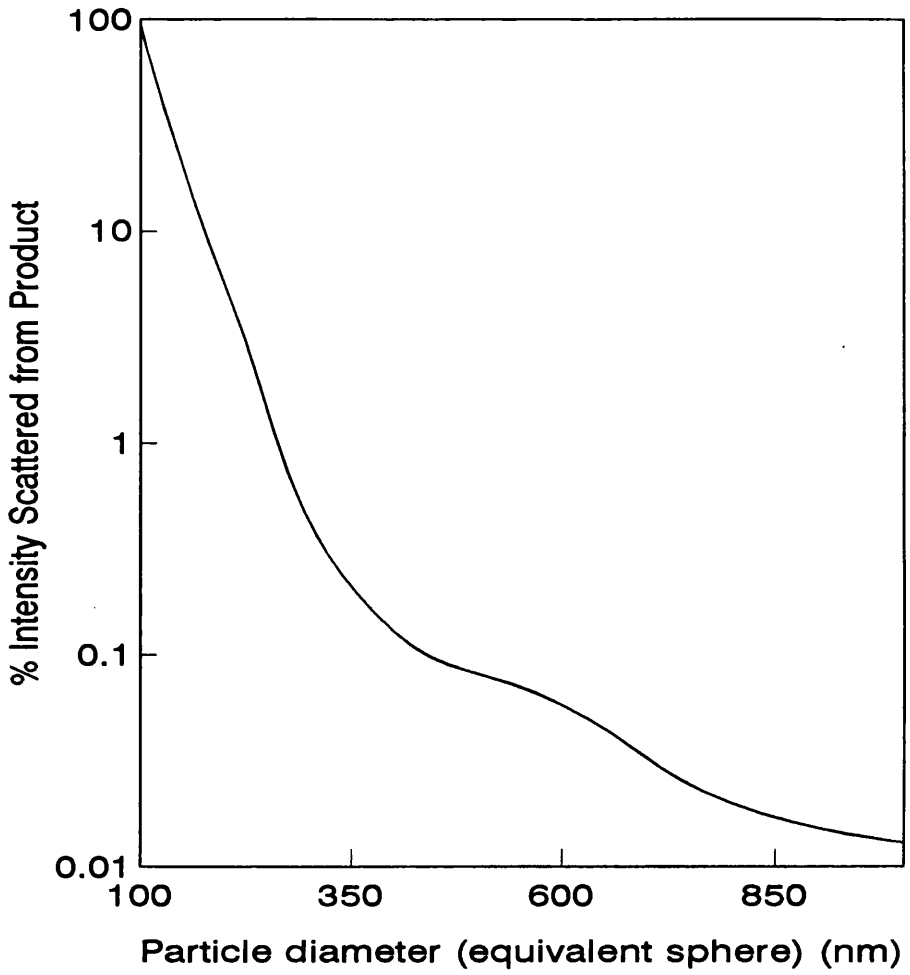


Fig 5.10: Chart constructed from a simulated size distribution to demostrate the percentage of intensity scattered from the product to be detected. This is plotted as a function of the maximum particle size present in the distribution so gives an idea of the improvement gained by removing the larger particles from the suspension. The base distribution has a maximum particle size of 500nm and a 10% volume fraction of product. The intensities are calculated assuming Rayleigh-Gans scattering (§1.2222).

scattered form an 80nm particle in the presence of homogenate and the improvement made by removing the largest particles from the suspension. In order to obtain 1% scattering from the product, particles down to 200nm should be removed. Fig. 5.11 demonstrates the difference method for a wide range of percentage light scattered from the product. The characteristic curves indicate that the maximum sensitivity is found in the first half of the function. A change of about 0.15 is achieved for the pure product at the maximum point.

The heavy bias in this method to a particular type of size distribution of homogenate indicates that other information on the process conditions will be necessary before carrying out the correct size distribution is assumed.

### 5.9 Summary

In summary, this chapter has reviewed some potential programs suitable for fast processing of noisy data and presented an algorithm developed from another application whereby autonomous operation maybe carried out on data where noise levels are previously unknown but available. Consideration has been given to the extension of a method of data inversion to parallel architecture to increase the speed of the operation.

In order to reliably detect product particle in homogenate the more direct approach of subtraction technique described in §5.8 may have advantages.

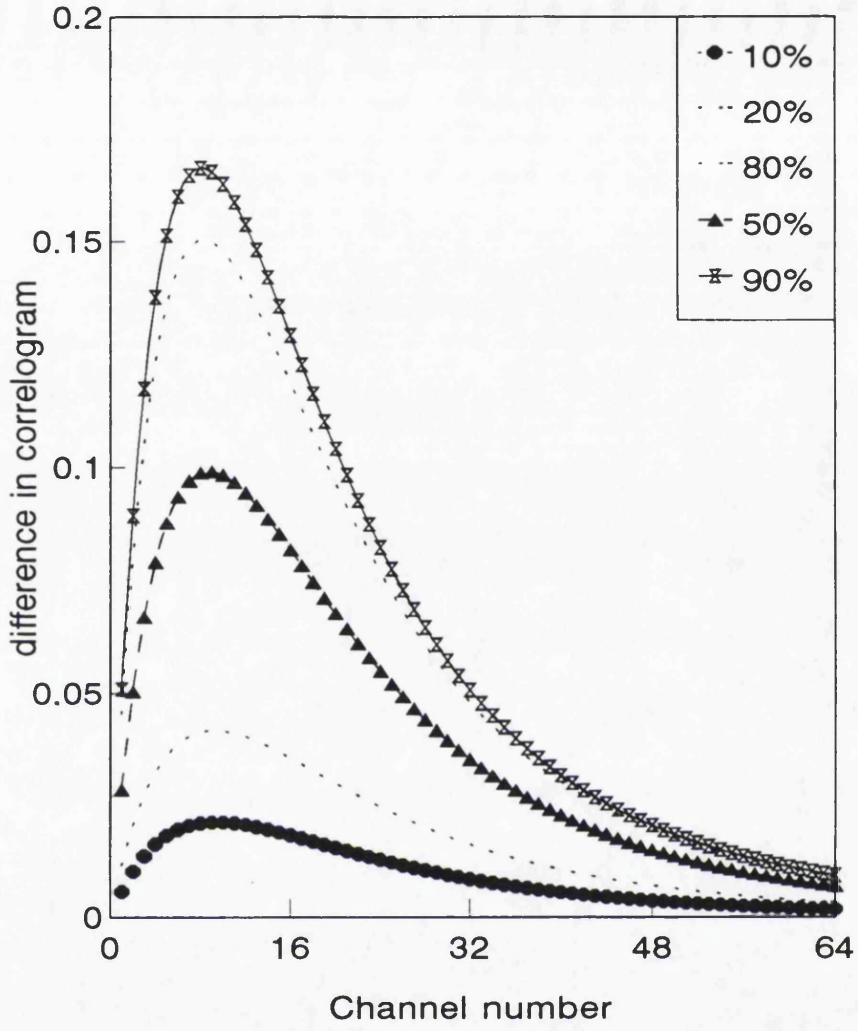


Fig 5.11: Plot of the difference between a correlogram due to a distribution of homogenate and one due to a product particle of 80nm diameter in homogenate. The percentages in the legend represent the percentage of light scattered from the product. This plot suggests that a difference of 2 x $10^{-3}$ in the correlogram results per percent change in scattering from product.

## Chapter 6 : Analysis of light scattering from experimental data.

### 6.1 Analysis of virus-like particles by dynamic light scattering

| Intensity mean (nm) | width (nm) | Number mean (nm) | width (nm) |
|---|---|---|---|
| 83.3 | 34.1 | 49.5 | 11.9 |
| 85.3 | 35.4 | 47.7 | 11.6 |
| 82.3 | 29.6 | 49.6 | 12.3 |
| 83.2 | 36.1 | 48.8 | 11.3 |
| 80.3 | 29.2 | 50.4 | 12 |
| 85.8 | 32.9 | 49.9 | 12.4 |
| 85.5 | 34.3 | 49.3 | 12.2 |
| 80.9 | 29.0 | 49.9 | 12.2 |
| 80.5 | 31.1 | 50.1 | 11.7 |
| 84.2 | 32 | 49.1 | 12.1 |

Table 6.1: DLS measurement of virus-like particle diameter showing intensity and number averages for 10 measurements. This preparation of VLP's was prepared by method 1 described in chapter 3. Experimental conditions were:- angle 90°, temperature 19.9 °C and aperture 100μm.

The results in the above table show that the virus-like particle preparation by method 1 gives a particle size distribution with intensity mean of 83.1nm ± 4nm and a width of 32.3 ± 6nm. Hence the choice of an 85nm latex for the simulation experiments to replace virus-like particles. The above experiments were carried out using the Malvern 4700 software.

## 6.2 Latex standards.

The Malvern 4700 autosizer is described in chapter 3. All the following experiments in this section were carried out at a temperature of 24.7 °C and a scattering angle of 90°. The aperture was 100μm unless stated otherwise. Latex standards (IDC latex spheres, Polymer Laboratories, Portland OR and Polysciences Inc, Warrington PA) of diameters 39nm, 85nm, 480nm and 1030nm were used to cover most of the range of application for the instrument. Sample times of 15μS, 30μS, 150μS and 300μS respectively were set in the correlator to analyse the latex suspensions. The shorter sample times were used to analyse the smaller particles. The latex spheres were supplied in two approximated concentrations. The 39nm and 85nm were 10% by volume and the 480nm and 1030nm were 2.5% by volume. These were diluted for analysis several hundred-fold until the scattered intensity displayed single scattering. This can be approximated by observing the surrounding region of the laser beam to detect significant diffusion of light due to multiple scattering from this region or, alternatively, the concentration of the sample may be increased and a measurement of the scattered light made for each concentration. If a change in concentration gives rise to a proportionate change in scattered light then the sample concentration will be within the single scattering region. In this set of experiments the former of the techniques was used. The average scattered light intensity measured as photon counts per second was $50 \times 10^3$ $s^{-1}$ for the 39nm, $80 \times 10^3$ $s^{-1}$ for the 85nm, $15 \times 10^3$ $s^{-1}$ for the 480nm and $30 \times 10^3$ $s^{-1}$ for the 1030nm particles.

Experiments were carried out for three different total experiment times of 10s, 30s and 60s. Statistical analysis was performed to assess the variation of the correlogram and distributions calculated by using the cumulants method (§1.4311) and the histogram method (§1.4322 and §5.6) of data analysis. The histogram method has been assessed as the most suitable in the present application (chapter 5) and the cumulants method can be used as a quick alternative for monomodal distributions or in the case of multi-modals as a precursor to assess the range of an unknown sample to then choose range limits for a more detailed analysis such as the histogram method.

## 6.21 The cumulants method.

Table 6.2 shows results of analyses of latex spheres by the cumulants method. It appears that the size returned is dependent upon the experiment length presumably as a result of the different noise level on the data. A longer experiment duration may improve photon

| | Ave | sd | width | sd | d | d |
|---|---|---|---|---|---|---|
| 10 second experiment time | | | | | | |
| 39nm | 4208.0 | 172.8 | 0.054 | 0.045 | 36.1 | |
| 85nm | 2043.6 | 67.2 | 0.062 | 0.058 | 74.4 | |
| 480nm | 367.9 | 34.7 | 0.24 | 0.15 | 413.4 | |
| 1030nm | 207.5 | 14.4 | 0.27 | 0.063 | 734.7 | |
| 30 second experiment time | | | | | | |
| 39nm | 4333.5 | 113.3 | 0.045 | 0.034 | 35.1 | |
| 85nm | 2019.0 | 40.3 | 0.051 | 0.032 | 75.3 | |
| 480nm | 337.1 | 16.7 | 0.087 | 0.063 | 451.2 | |
| 1030nm | 169.2 | 10.9 | 0.15 | 0.12 | 898.9 | |

Table 6.2: Cumulants method analysis data.

counting noise but any long-term fluctuations due to, for example, the presence of small amounts of large contaminants, bias the result to produce a larger polydispersity than the true value. The data in the table shows a large standard deviation on the distribution width suggesting that this is indeed the case. However in all cases the size is underestimated. The Malvern software attempts to overcome the dust problem by taking several short duration measurements and accepting or rejecting correlograms dependent upon a quality criterion such as the merit or in-range measures (described in §4.2) being within a certain range. In this application it is desirable to perform as shorter measurement as possible to enable on-line reaction to a system.

### 6.22 Histogram method applied to latex sphere data.

Figures 6.1a-b show the performance of the histogram method described in chapter 5 in inverting latex sphere light scattering data. The results for 1030nm, 480nm, 85nm and 39nm were averages of 690nm, 370nm, 68nm and 37nm respectively. However the peak intensities are at 1215nm, 670nm, 70nm and 37nm respectively. The reason for the large discrepancy between the quoted values and those measured in this set of experiments is the noise on the data due to the short experimental period (10s). The method appears to overestimate the lower section of the distributions.

### 6.23 Performance of the histogram method to homogenate and latex mixtures

The chart in figure 6.2 shows a typical performance of the histogram method to latex and homogenate suspensions. The homogenate in this case is spun at 20000g for 2 hours.. The approximate volume percent of homogenate is indicated by means of scattered intensities of the individual components before mixing. The data used in this case was collected using the multiple sample-time facility in the Malvern 4700 correlator to cover a wider range of particle size. An explanation of this is given in §2.1 Also longer experimental times were required in order for the program to converge. The general feature of a decrease in one peak and an increase in the other follows the sample well but the position of the lower peak seems to be erratic.

## 6.3 The difference method

### 6.31 The difference method with homogenate and latex mixtures

In figure 6.3a the difference method described in chapter 5 is shown in response to different mixtures of homogenate and latex spheres. The volume ratios are calculated approximately according to the intensity proportional to volume squared relationship. The graph shows that in principle the addition of latex may be detected in the presence of 90% by volume of homogenate, the sensitivity increasing when less homogenate is present. The homogenate in this example again is spun at 20000g for 2 hours. In comparison to the

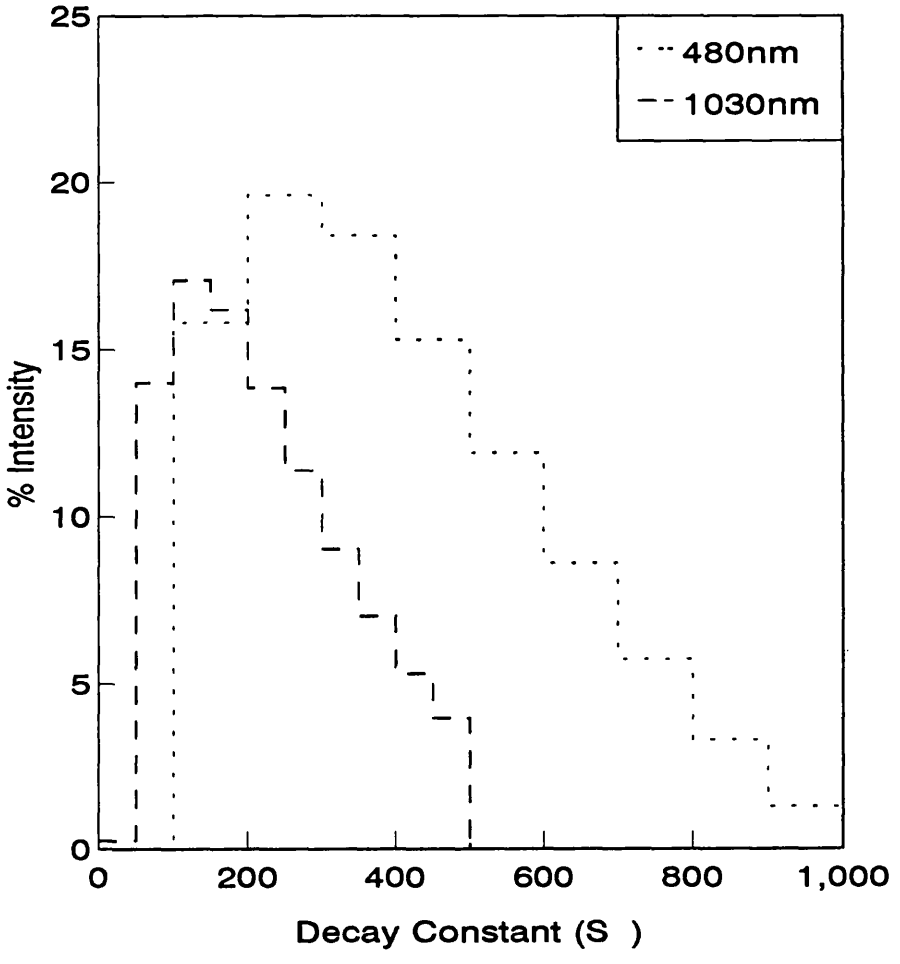


Fig 6.1a: Inversion of latex sphere correlogram data for 480 and 1030nm standards. The data collection time was 10s. The resulting average diameters calculated from the average decay constant are 690nm and 370nm. The underestimation can be explained by the noise on the data.

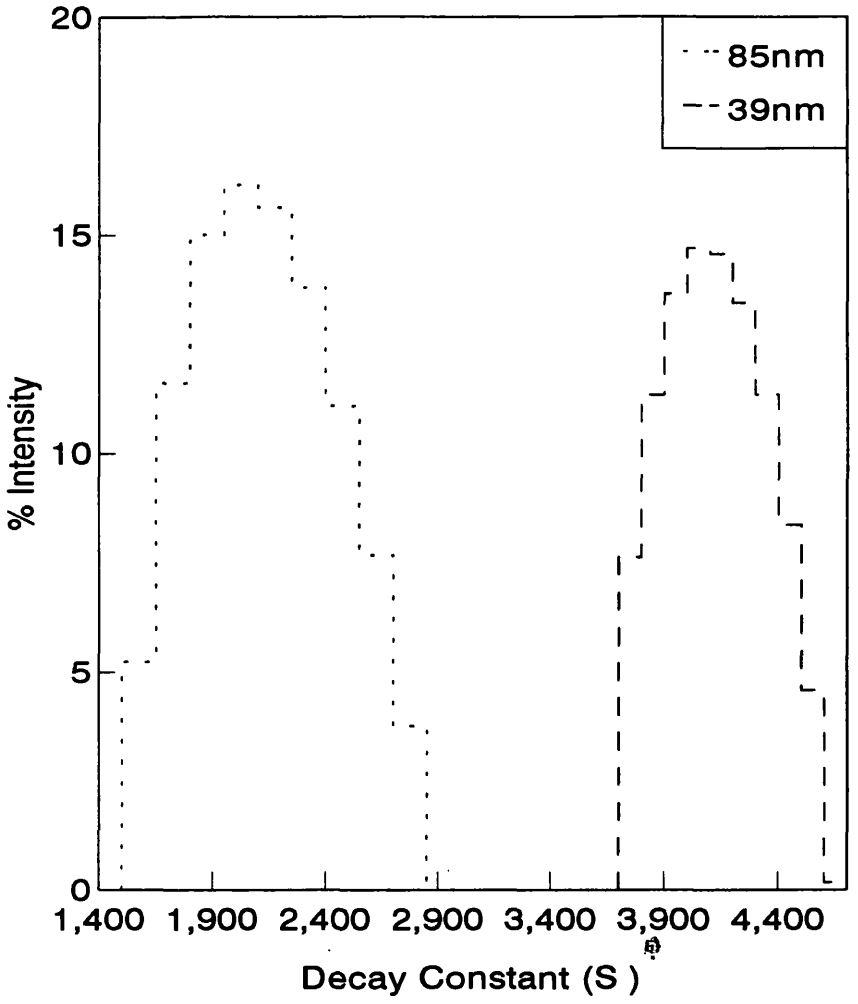


Fig 6.1b: Inversion of 39nm and 85nm latex standard correlogram data. The data collection time was 10s. The average diameters are calculated from the average diffusion coefficients as 36.9nm and 68.1nm. As in fig 6.1a, there is a discrepancy in the size of the standards and the measured distribution. The deviation in this case however is lower. The photon counting noise (see §1.4) on the correlograms will be lower due to the smaller diameters and consequently larger number of total samples of the scattered light taken. This could explain the closer estimates to the diameters.

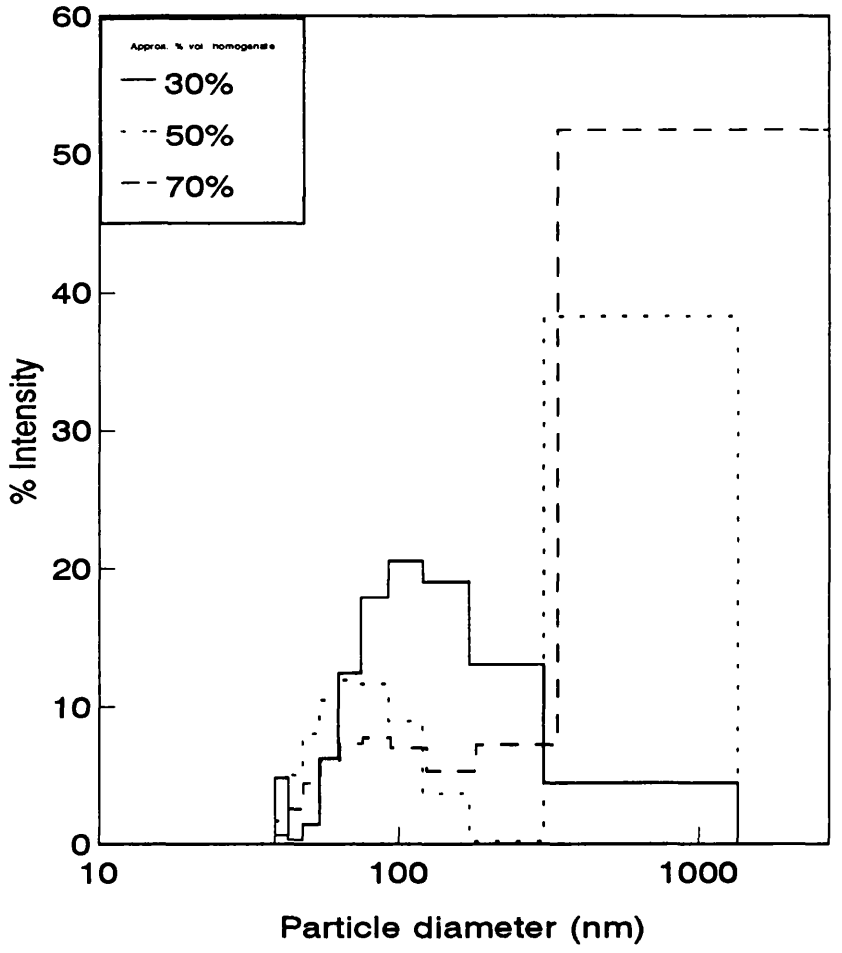


Fig 6.2: Graph showing inversions using the histogram method of correlogram data from mixtures of 85nm latex spheres and clarified homogenate. The essential features of a growing peak at lower size and diminishing peak at the upper size range is recorded, however the position of the lower peak is erratic. The volume percent of homogenate in the mixture is approximated by the scattered intensities of the components before mixing and using the relation: intensity $\approx$ volume$^2$.

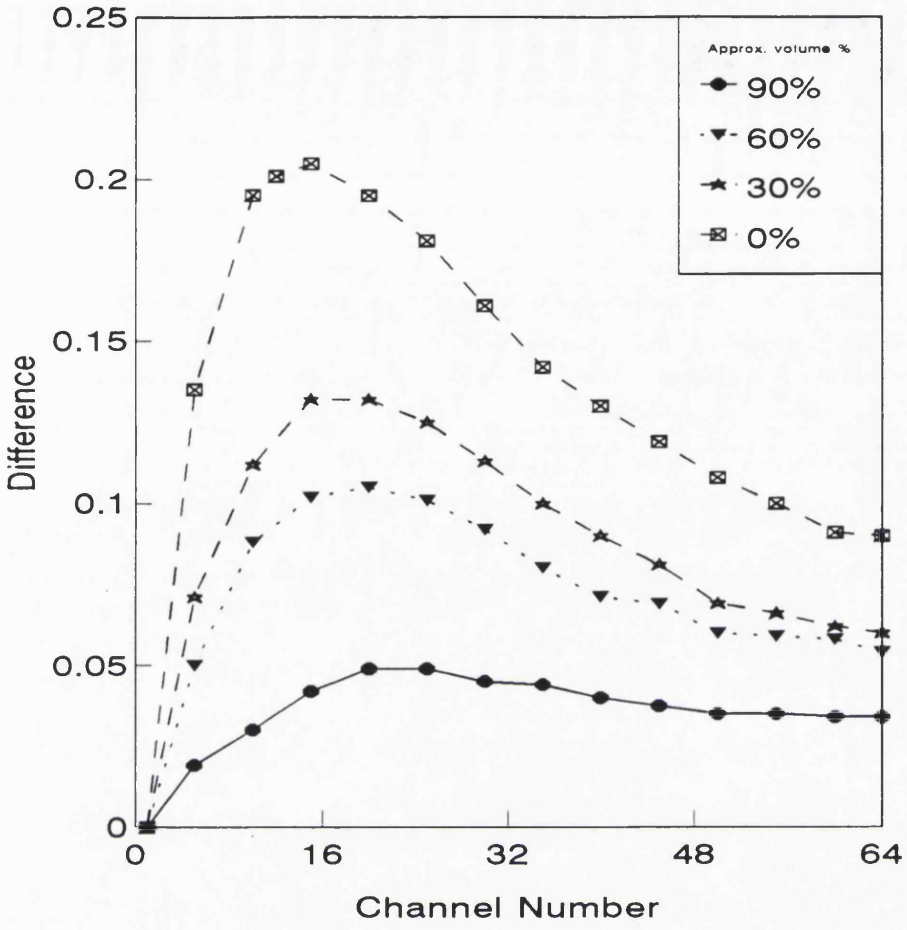


Fig 6.3a: Graph to show the difference between homogenate and mixtures of homogenate and latex correlograms. The different percentage volumes are approximated by recording the fraction of the scattered light from the separate components (85nm latex and spun homogenate) and taking the square root (intensity ≈ (volume)$^2$) to give the amount of homogenate present in the suspension. The trace for latex alone appears at the top with maximum difference and as more homgenate is added the difference approaches the baseline.

simulated curves in Chapter 5, fig. 5.11, these have higher tails at the high channel numbers and their main peak is at a higher channel number. The reason for this is that the real particles are more polydisperse than represented in the simulation. The curves otherwise are very representative of the real situation.

The addition of latex below the 10% level incurred problems due to overlapping so that indistinguishable curves resulted. However it would be possible to infer that the latex is present to less than 10% by volume when the plot is in the overlap region.

### 6.32 Difference method for clarified homogenate and VLP mixtures

Figure 6.3b shows the VLP and homogenate mixtures for clarified homogenate. The amount of VLP present before mixing was estimated by means of the assay described in chapter 3. The VLP was collected from gel column fractions also detailed in chapter 3. The percentages quoted are wet weight homogenate to VLP fractions. The chart for clarified homogenate shows that the technique is sensitive only at very low levels of homogenate addition. More than 5% leads to erratic and overlapping plots so that concentrations up to this level only may be estimated by this method. The higher sensitivity of latex in the same method is due to its greater scattering efficiency derived from its greater refractive index. At the 5% level the correlogram difference is about 0.02. The latex curves for similar levels shows a 0.18 difference in correlogram at maximum. This suggests that the VLP's scatter 6 times less efficiently than the latex, a similar result to that in chapter 4 where the ratio was estimated at 7.5 times.

### 6.33 Difference method for unclarified homogenate and VLP mixtures.

Figure 6.3c shows VLP and unclarified homogenate mixtures with weight percent calculated as in §6.32. In this case the technique is apparently extended to greater concentrations of homogenate. This is due to the relative size of the VLP and unclarified homogenate. The amount of material close to the VLP size has been reduced and the larger particles have a greater difference in correlogram value over the graph. (This is discussed theoretically in §1.421. This suggests that should the situation arise where the VLP makes up the larger portion of the mixture then the VLP may be measured to a

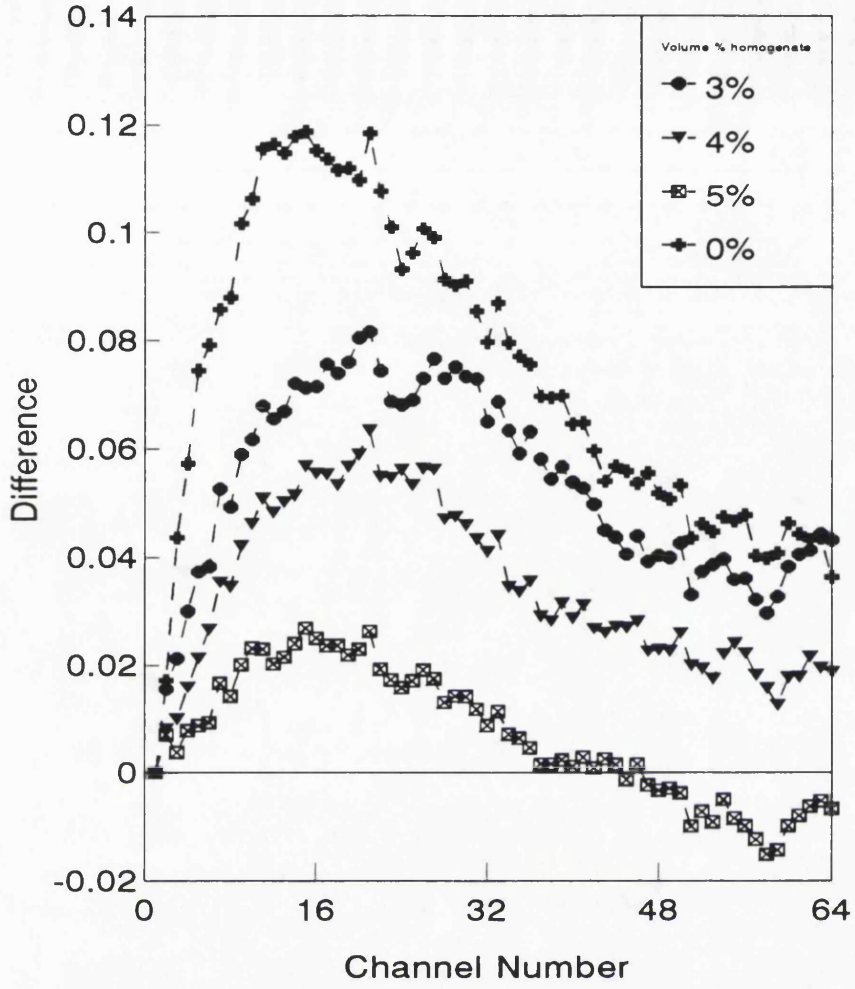


Fig 6.3b: Graph showing the difference method applied to the different mixtures of VLP and clarified homogenate suspensions. The graph shows that approximately 95% or more VLP is required for the technique to detect the product in the homogenate. Curve matching techniques may then be used to estimate the percentage VLP to homogenate. The deviation of the curves from those simulated in chapter 5 suggests a more polydisperse product.

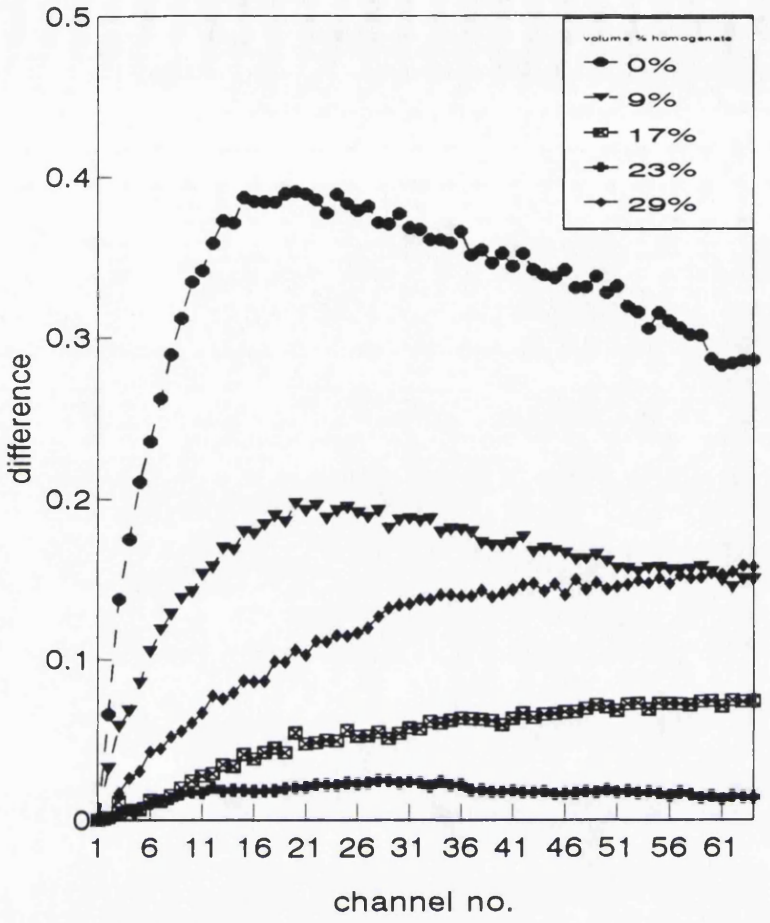


Fig 6.3c: Graph showing difference method applied to VLP and unclarified homogenate suspensions. The chart seems to indicate a greater range of applicability than in clarified homogenate (fig 1.3b). This is due to the large size difference between the homogenate and VLP's. In practice a large increase in number of VLP's produced per cell in fermentation would be required for this distribution to occur. These curves appear to be smoother than the unclarified results due to the change of scale of the y-axis.

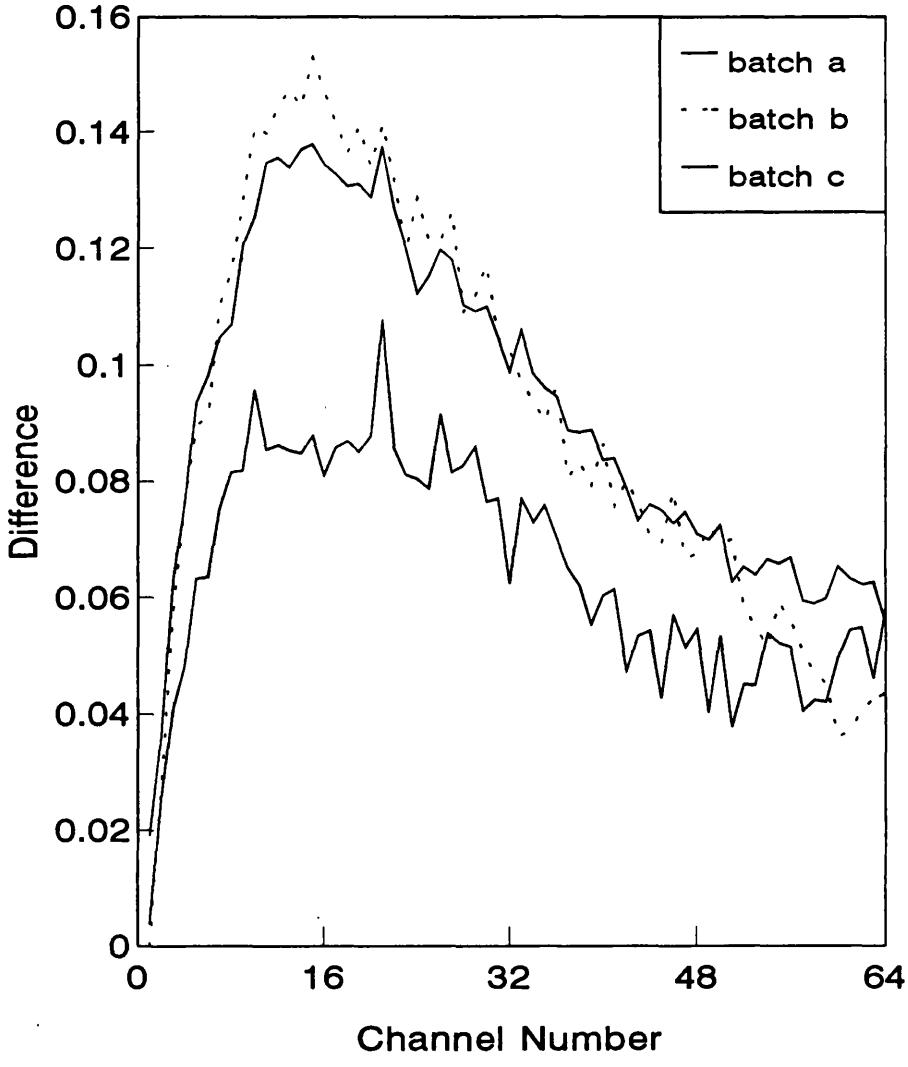


Fig 6.4: Graph showing the difference method applied to three different batches of VLP elutions. The baseline is singly scattering clarified homogenate. This shows that the technique can be susceptible to large batch to batch variation - two traces lie close together while the third falls below the others across the range by up to 40%. The two curves that lie close together were measurements from the same column run whereas the other was measured on a separate occasion.

greater sensitivity than in the case of clarified homogenate and VLP mixtures. In practice it is hard to envisage such a case. Currently the debris at the start of the downstream process chain forms about 90% of the volume of the VLP and debris particle mixture (Milburn 1992). This places a curve well on the x-axis. Removal of the gross contaminants then reduces the concentration but the clarified graph (figure 6.3b) must then be used.

### 6.4 Run to run variation of correlograms

Given the variation of the distributions calculated by the Malvern software (chapter 4) and the other analysis method in this chapter it is sensible to assess the variation in correlogram values in different conditions to indicate the best method for collecting the data. To this end 50 runs each of different diameter latex beads (39nm,85nm,220nm,480nm, and 1030nm) were carried out at run times of 10s, 30s and 60s. The results are plotted in figures 6.5a-e. The plots shown are fractional standard deviation in each channel ie. the standard deviation divided by the mean at each channel. This is calculated for the second order correlation function (§2.1) which is the data presented to the analysis methods.

The features in the figures to note are:

1. An increasing variation with channel number.
2. An increasing variation with particle size.
3. Occasional large variation in the first few channels.
4. A decreasing variation with run length *except* for the largest particles.

These standard deviations should not be interpreted as random noise on the data which is a much lower percentage but rather an indication of the run to run measure of systematic variations. This will give an indication of the applicability of the methods discussed in this chapter.

The larger variations for the higher channel numbers is due to their susceptibility to large unwanted particulates in the sample. The correlogram should decay to a steady baseline which can however be distorted due to these large particles passing through the beam for

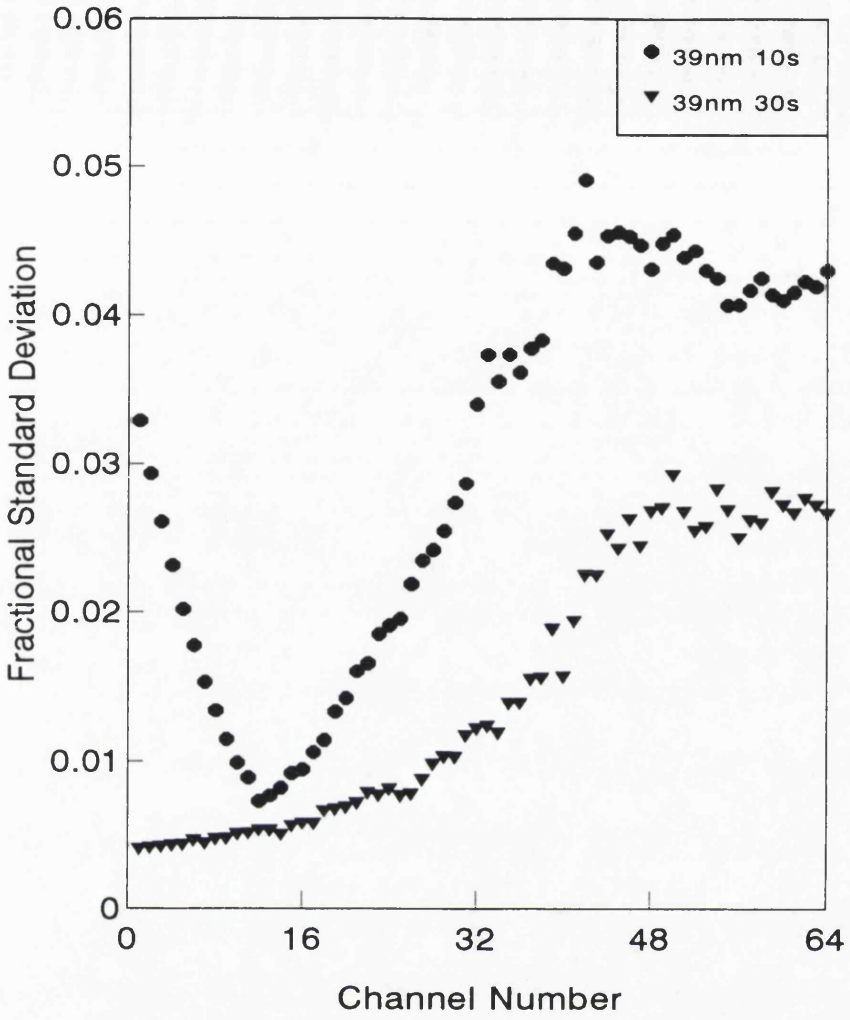


Fig 6.5a: Graph plotting the fractional standard deviation across the channels for 39nm latex sphere data. The data set consists of 50 correlograms. The general trend which exists for all particle sizes is larger variation at higher channel number. This is most likely due to the presence of unwanted dust or other contaminating material which tends to affect the baseline value ie. higher channels. The upturn at the lower end for the 10s experiments is more difficult to explain. It suggests a change in the alignment during the 50 runs.

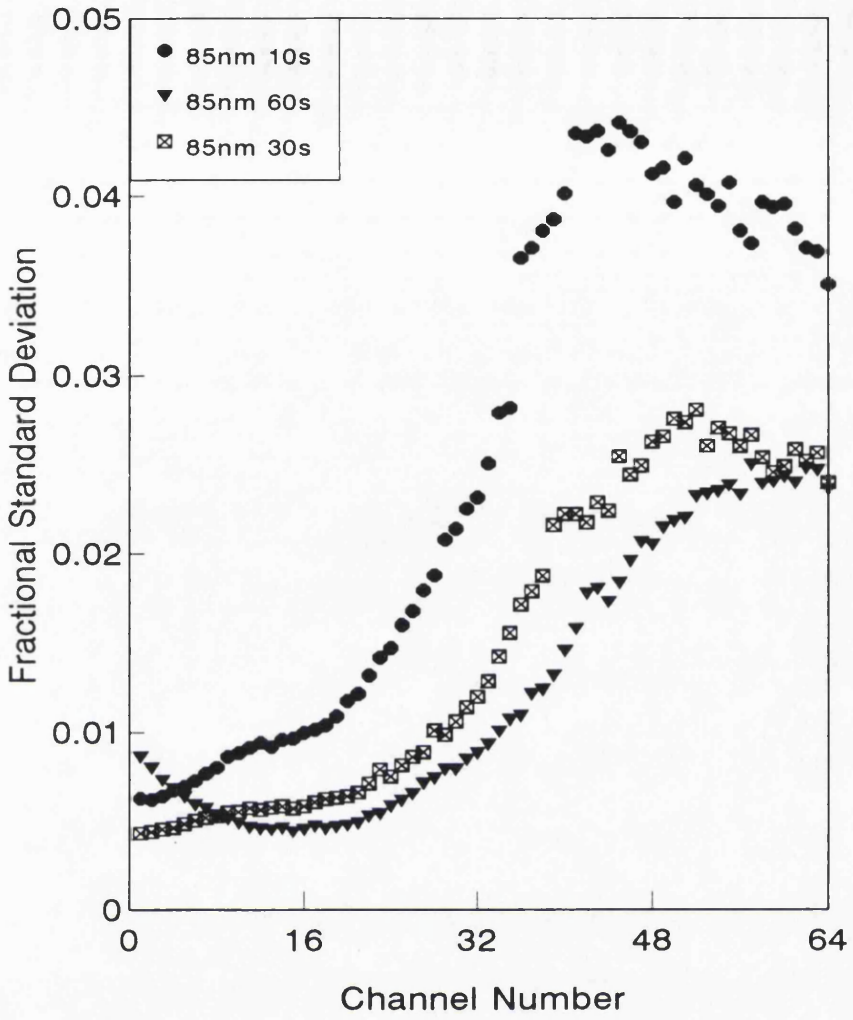


Fig 6.5b: Chart plotting the fractional standard deviation of correlogram channels for 85nm particles and for different experimental times. It is notable that longer experimental times lead to lower standard deviations. The low upturn feature is again present as in fig 6.5a but to a lower degree. Again this may be due to a disturbed alignment for a number of the set of runs. Generally the level of deviations is the same as the 39nm data.

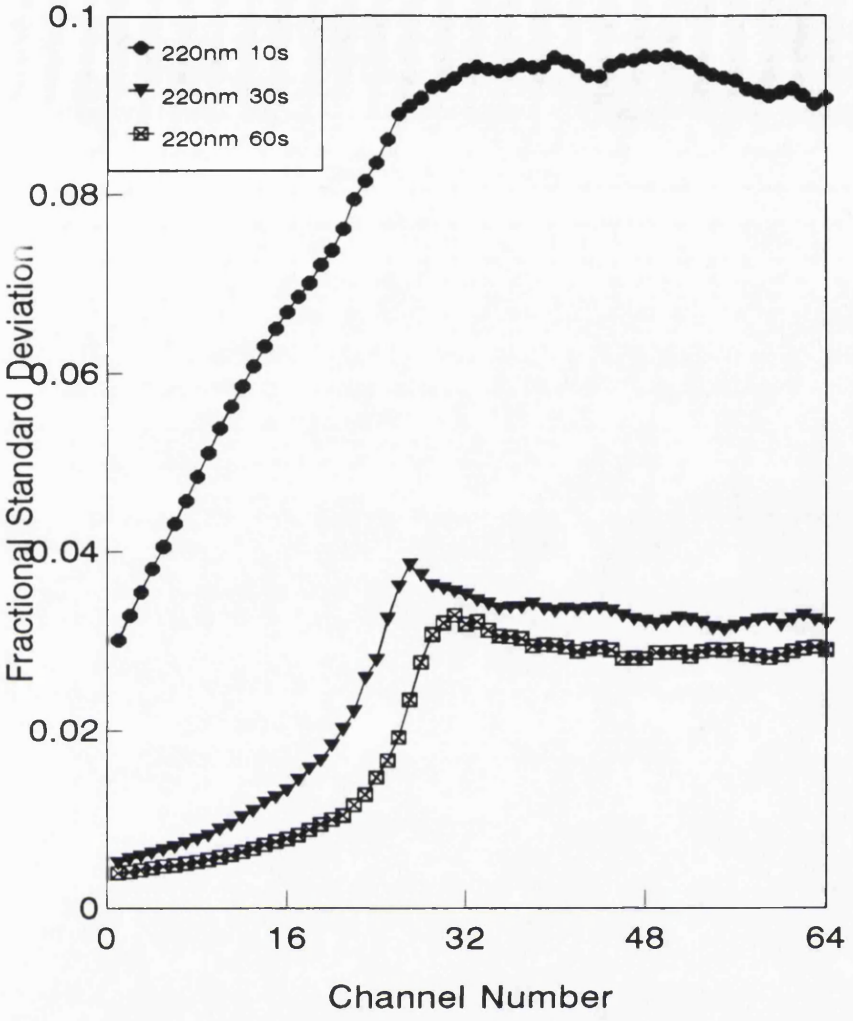


Fig 6.5c: Chart plotting the fractional standard deviation across correlogram channels for 220nm latex spheres. The general feature of lower variance for longer experimental time is continued and for the 30s and 60s data the deviation level is comparable to that in figs 6.5a-b. The 10s data shows a particularly high deviation, a trend which continues through to the higher particle sizes. Also to be noted is the earlier levelling-out of the deviations at about channel 30 rather than channel 50. This is due to the sample time chosen.

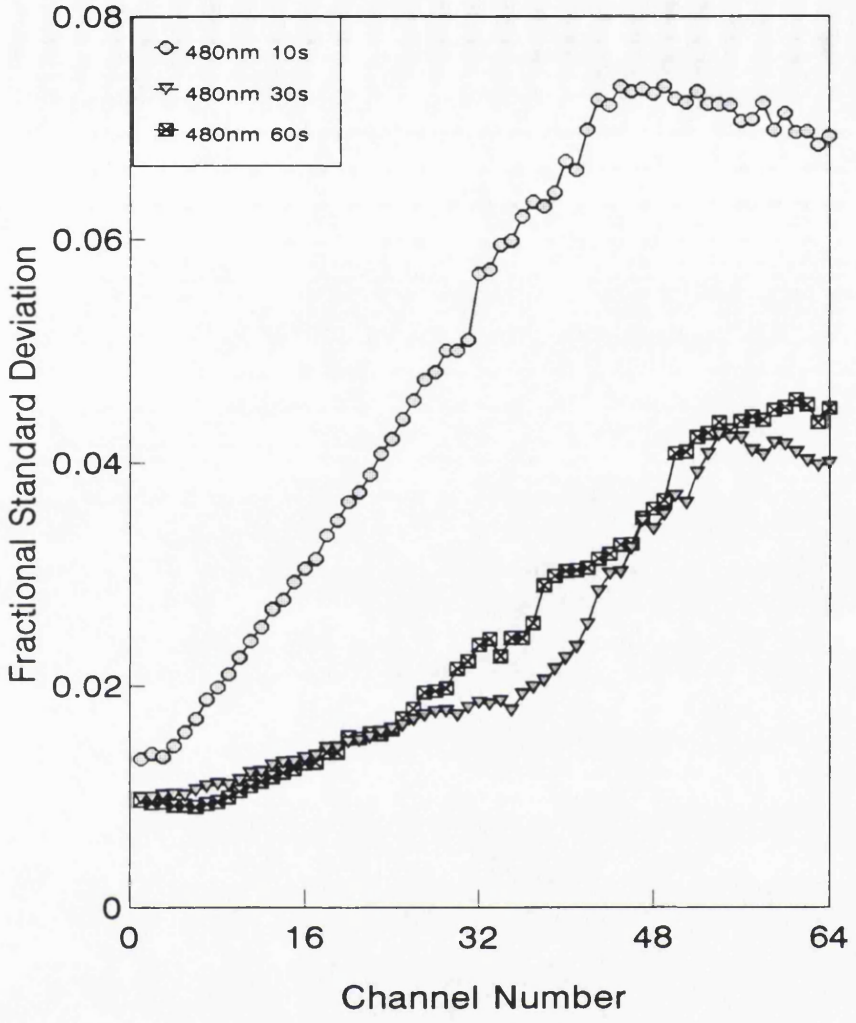


Fig 6.5d: Chart showing fractional standard deviation across the correlogram channels for 480nm latex particles at different experimental times. The deviations are generally higher than the previous charts (figs 6.5a-c) for lower particle diameters. Again the 10s data is significantly higher than the 30s or 60s data.

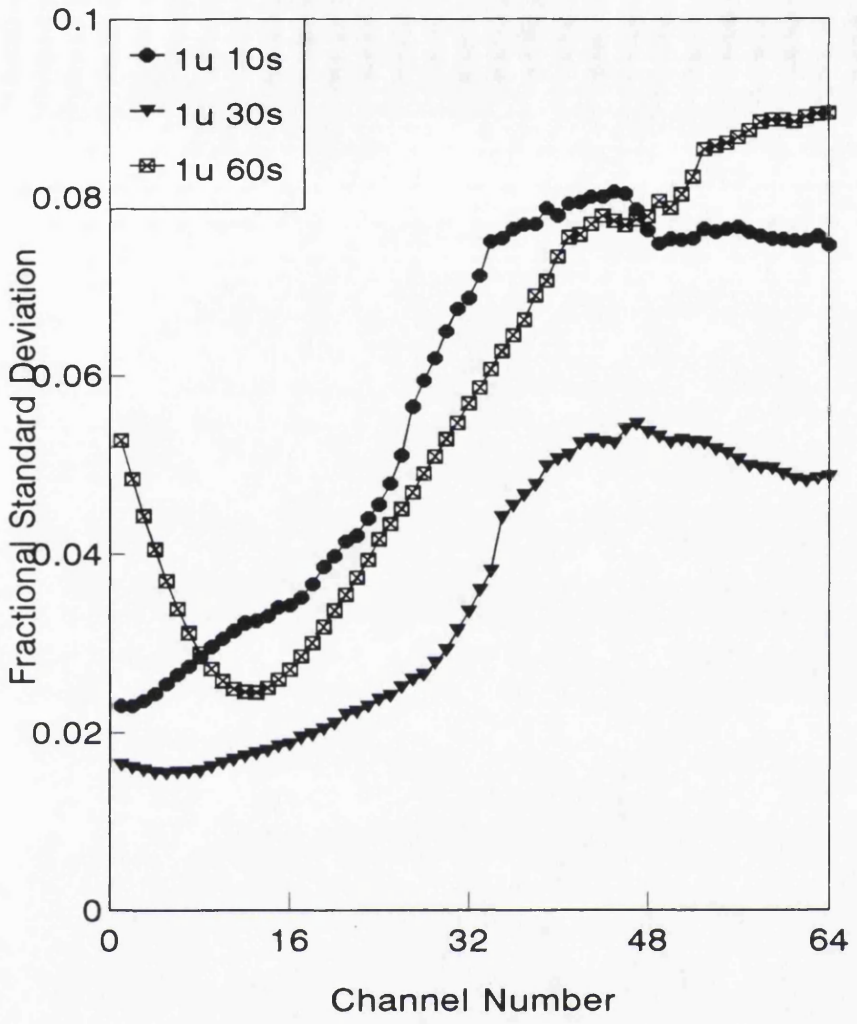


Fig 6.5e: Chart plotting fractional standard deviation in correlogram across the channels. The general trend to higher deviation continues but in this case the 60s data points show a larger deviation across the chart than the 30s data which is the converse of the trend in the other charts, (figs 6.5a-d). Again there is an upturn for one of the data sets at low channel number. This is explained previously as system misalignment some of the correlograms in the data set.

a short period of the data collection.

The feature at low channel number is either due to alignment or size distribution change for several of the correlograms in the sample of 50. Effects due to flare from the cuvette or small amounts of light reflected from other parts of the instrument into the detector alter the correlation function (the theory presented in §1.3 would need to be modified to allow for such a direct scattered contribution which introduces a "light-beating" term on mixing at the detector see eg. Ford 1983) could lead to variation more distinct at lower channel numbers than high ones.

The decreasing standard deviations with run time is expected as of data collected over long times should be more stable and any fluctuations due to unwanted scattering tend to be averaged-out over the duration. However for large particles the converse is true - long run-times produce larger deviations. This is probably due to the size range of the particles to be measured being closer to the contaminant (dust etc.) sizes and the correlator then being more susceptible to change at lower channel numbers.

In general the larger particles give rise to larger variations. The number of samples collected in a fixed length experiment decreases with increasing particle size as the sample time must be larger to measure the correlation function adequately. Hence each channel is calculated from less samples in the case of the larger particles and the increased chance of spurious data from unwanted scattering causing variation in the correlogram.

### 6.5 Conclusion

In summary a method for the rapid analysis of light scattering data has been presented which, requires the range of particles to be measured to be input. The method works well for relatively noisy data collected from experiments on suspensions of latex spheres. Better results are obtained for smaller diameter particles. For broader size distributions the technique can pick out bimodal distributions and shows the correct trends for mixtures of latex sphere and clarified yeast homogenate mixtures, however the relative contribution to the scattered intensity across particle size may not reliably be measured for such short experimental times.

A technique where the difference between correlogram data for a product particle and the homogenate similar to that from which the product is released is described. It is demonstrated with the use of homogenate laced with latex spheres and shows thatcurves may be constructed as a measure of relative concentration of the two components. This technique is then applied to virus-like particles where such particles are mixed in known quantity into the homogenate and measured. It is shown that similar curves may be built up and there is potential for a relative measure of concentration for VLP's where they constitute more than 95% of the mixture. Large batch to batch variations can result either due to actual variations in product quality (due to eg. agglomeration) or the variance of correlogram channels. The largest such variations are shown to be due to the presence of larger particles and removal of these would improve batch to batch results. The sensitivity however is concerned with the proximity of the lower size debris particles to the product. Removal of these clearly will improve sensitivity. The technique then becomes one of quality control where deviation by a percentage from a standard curve would indicate intolerance.

## Chapter 7: Internodal light scattering

The work presented in this chapter is a joint project across two PhD programmes: this thesis and a thesis on ultrasonic manipulation of particles (G.B.Davies, in preparation). This section will start with a brief description of the application of ultrasonic standing waves to create bands of alternately concentrated and unconcentrated regions in a particulate suspension. Then the concept of performing light scattering analysis within such bands will be described and its application to analysis in the biological dispersions discussed. Results with latex suspension and yeast homogenate are presented in the final section.

### 7.1 Ultrasonic separation of biological particles

Ultrasonic standing waves cause migration of the fine particles in suspension to the nodes of the sound field which are spaced at half-wavelength distances. The mechanisms behind this phenomena have been the subject of research since their initial observation by Kundt (Kundt and Lehmann 1874).

The driving force for migration is the radiation pressure exerted on the particle, other forces arising from particle sound wave interaction become of importance only when the particles are concentrated at the nodes, acting to stabilise the bands of particles. The radiation pressure on a spherical particle in a plane stationary wave is described in equation 7.1.

$$P_r = 4\pi a^3 \kappa E F \sin(2\kappa x) \qquad 7.1$$

where kappa is the phase constant; E, the mean energy density of the standing wave; a, the particle radius; x, the time averaged position of the particle from the node; and F, a correction factor that accounts for the compressibility of the particle and the different impedances of the particle and the fluid.

$$F = \frac{\Lambda+2(\Lambda-1)/3}{1+2\Lambda} - \frac{1}{3\Lambda\sigma^2} \qquad 7.2$$

where

$$\Lambda = \frac{\rho_1}{\rho_0} \ , \ \sigma = \frac{c_1}{c_0} \qquad 7.3$$

rho is the density and c is the sound velocity ; subscripts 0 and 1 refer to the fluid and particle properties respectively.

The point of interest is the very strong dependence on the radiation pressure on the particle radius (P is proportional to the radius cubed) which means the radiation pressure falls off rapidly with falling particle size. This can be exploited to fractionate particles of different radii. The radiation pressure displays only a relatively weak dependence on the particle density and the particle compressibility.

By controlling the intensity of the sound field produced, any particles over a chosen radius can be immobilised at the nodal plane of the stationary wave, leaving the smaller particles free in the inter-nodal spaces.

### 7.2 Light scattering from internodal regions

The dimensions of the internodal space are in the order of several hundred microns. The value is dependent upon the driving frequency of the ultrasonic transducer. Laser beam waists in the dynamic light scattering analyses are of the order of 10's to 100's of micron. It is conceivable then that a laser bean may be passed between the nodal planes in the suspension to impinge on whatever is present between the nodes. Figure 7.1 shows this schematically with particles above a certain size threshold being held away from the laser beam while smaller particles are left for analysis by the laser beam.

### 7.21 Application to bioprocess analysis

Previous chapters in this thesis have concentrated on the analysis of light scattering data for the monitoring of products in downstream processing. Many of the problems arise due to the presence of large particulate material in the sample. The larger particles, by having

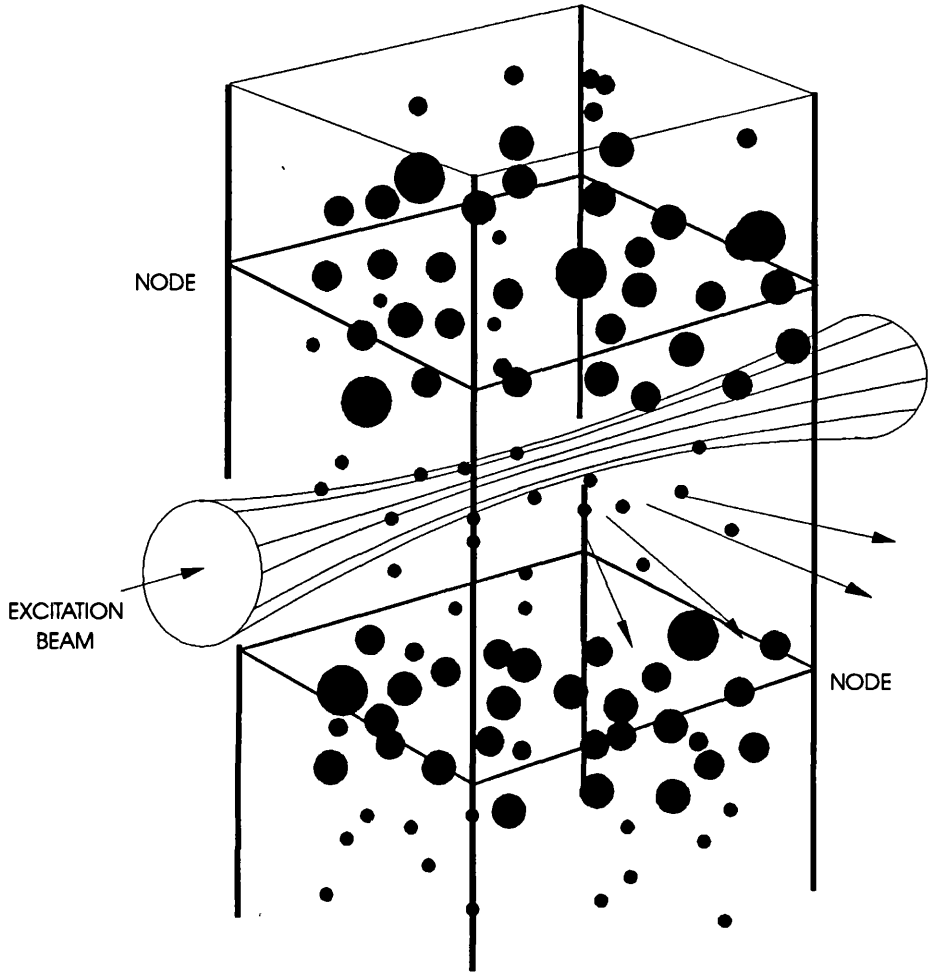


Fig 7.1: Schematic of light scattering from internodal regions in an ultrasonically separated suspension. The distance between nodes for a 1MHz frequency sound wave is 750μm and the laser beam is focused to a waist of approximately 100μm.

Larger particles are held away from the laser beam at the nodes whereas the smaller particles are left for analysis.

a much greater scattering efficiency (§1.2) either hide the particles of interest or bias the result in an unpredictable fashion eg. dust particles randomly passing through the beam.

Also it was shown in Chapter 6 that the presence of the larger particles leads to a higher variance in the correlogram - the first processing stage in the dynamic light scattering analysis.

The ability to remove such effects by using the ultrasonic banding technique and analysis between the bands would be a great advantage in both bioprocess analysis and other areas. An additional advantage for online analysis systems is that sample preparation may be performed rapidly and in-situ.

The experiments presented in this chapter show that steps towards such a device have been made. The analysis technique has been termed internodal light scattering (ILS).

### 7.22 Design of the ultrasonic cell

The detailed design and construction of ultrasonic separation/manipulation equipment is discussed elsewhere (Davies, in preparation). The key parameters in the design for this application are minimum particle size affected, concentration of suspensions able to banded and volume of sample to be analysed. These principles affect the choice of transducer, resonant frequency and power input. Also to be considered are the dimensions affecting the focusing of the laser beam through the internodal space, and subsequent interaction of the scattered light with the concentration of the particles at the nodal planes.

The cell constructed uses a 1MHz transducer (Morgan Matroc Ltd) glued securely to a dural waveguide which screws directly into a custom built cuvette holder designed to fit into the Malvern 4700 analyser (chapter 3). The transducer is driven by an Audley Scientific Stabilised Frequency Signal Generator and Dual Ultrasonic Amplifier. A diagram of the apparatus is shown in figure 7.1a

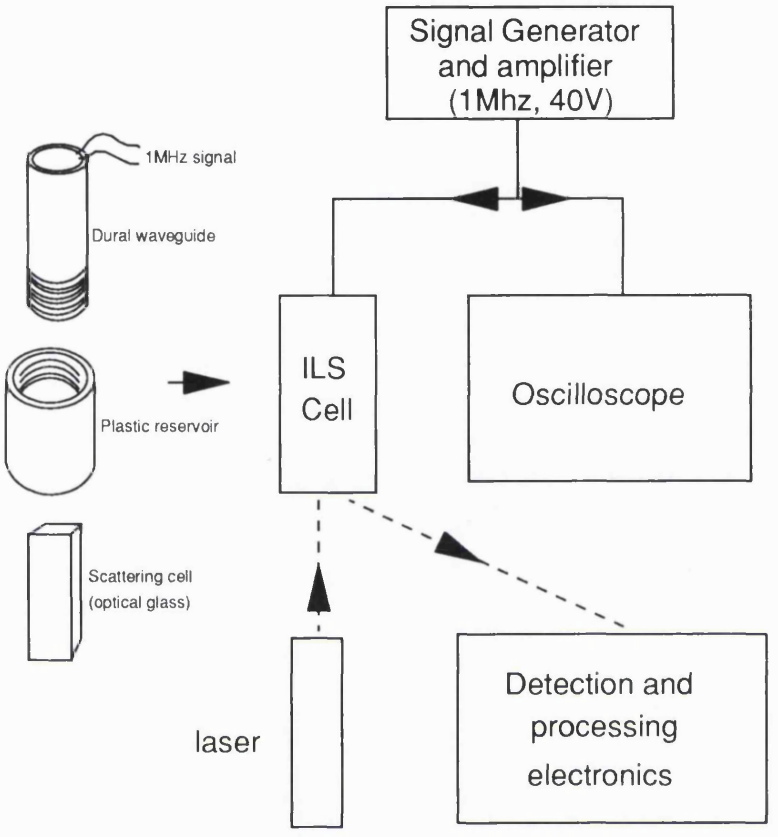


Fig 7.1a:

Diagram of ultrasonic cell construction and schematic of experimental set-up. A full reservoir which is sealed to the scattering cell is required to transmit the ultrasound to the sample to be analysed. A 1Mhz signal is used here but other frequencies are available. Higher frequencies reduce the risk of bubble creation due to cavitation in the sample but give less space between nodes in which to pass the laser beam.

## 7.3 Internodal light scattering on latex mixtures

### 7.31 39nm and 4000nm latex

The plot in figure 7.2 shows the results of a unimodal (Cumulants §1.4311) analysis on a mixture of 39 and 4000 nm latex suspension. This clearly shows the ILS analysis picking out the unbanded smaller particle size in the mixture. Included in the figure is a trace of a normal analysis of 39nm particles alone. This shows a slightly narrower distribution. Presumably in the ILS analysis stray light scattered from the concentration of the larger particles at the nodal planes is entering the detector and distorting the measurement. However, the distortion is only slight.

### 7.32 2um and 39nm latex

Figure 7.3 shows 2μm and 39nm particles in the ILS cell. Plots here are shown of analysis between bands and on a band in the ultrasonic cell. The between the bands signal shows a clear peak at 39nm indicating complete removal of the 2000nm particles from the analysis area. The result from the analysis on the band indicates a measurement of 18500nm, about 9 times their actual size. This must be due to concentration or the acoustic field hindering diffusion, as multiple scattered light when interpreted in a DLS experiment will give rise to a lower than expected particle size.

### 7.33 15um and 85nm latex

The plot in figure 7.4 shows the trace for a 15um and 85nm latex mixture shows a bimodal distribution in both normal analysis mode and ILS mode. However, in the case of the ILS analysis, the peak at 85nm increases dramatically, indicating a substantial proportion of the 15um particles have shifted. The remaining signal in the region 200nm - 1200nm must be due to other contaminants in the sample. This peak correlates with the upper peak in figure 7.4 which is described in the next paragraph. It would seem that such sizes are below the critical size for banding for this equipment.

### 7.34 1.4um and 85nm latex

## 7.3 Internodal light scattering on latex mixtures

### 7.31 39nm and 4000nm latex

The plot in figure 7.2 shows the results of a unimodal (Cumulants §1.4311) analysis on a mixture of 39 and 4000 nm latex suspension. This clearly shows the ILS analysis picking out the unbanded smaller particle size in the mixture. Included in the figure is a trace of a normal analysis of 39nm particles alone. This shows a slightly narrower distribution. Presumably in the ILS analysis stray light scattered from the concentration of the larger particles at the nodal planes is entering the detector and distorting the measurement. However, the distortion is only slight.

### 7.32 2um and 39nm latex

Figure 7.3 shows 2μm and 39nm particles in the ILS cell. Plots here are shown of analysis between bands and on a band in the ultrasonic cell. The between the bands signal shows a clear peak at 39nm indicating complete removal of the 2000nm particles from the analysis area. The result from the analysis on the band indicates a measurement of 18500nm, about 9 times their actual size. This must be due to concentration or the acoustic field hindering diffusion, as multiple scattered light when interpreted in a DLS experiment will give rise to a lower than expected particle size.

### 7.33 15um and 85nm latex

The plot in figure 7.4 shows the trace for a 15um and 85nm latex mixture shows a bimodal distribution in both normal analysis mode and ILS mode. However, in the case of the ILS analysis, the peak at 85nm increases dramatically, indicating a substantial proportion of the 15um particles have shifted. The remaining signal in the region 200nm - 1200nm must be due to other contaminants in the sample. This peak correlates with the upper peak in figure 7.4 which is described in the next paragraph. It would seem that such sizes are below the critical size for banding for this equipment.

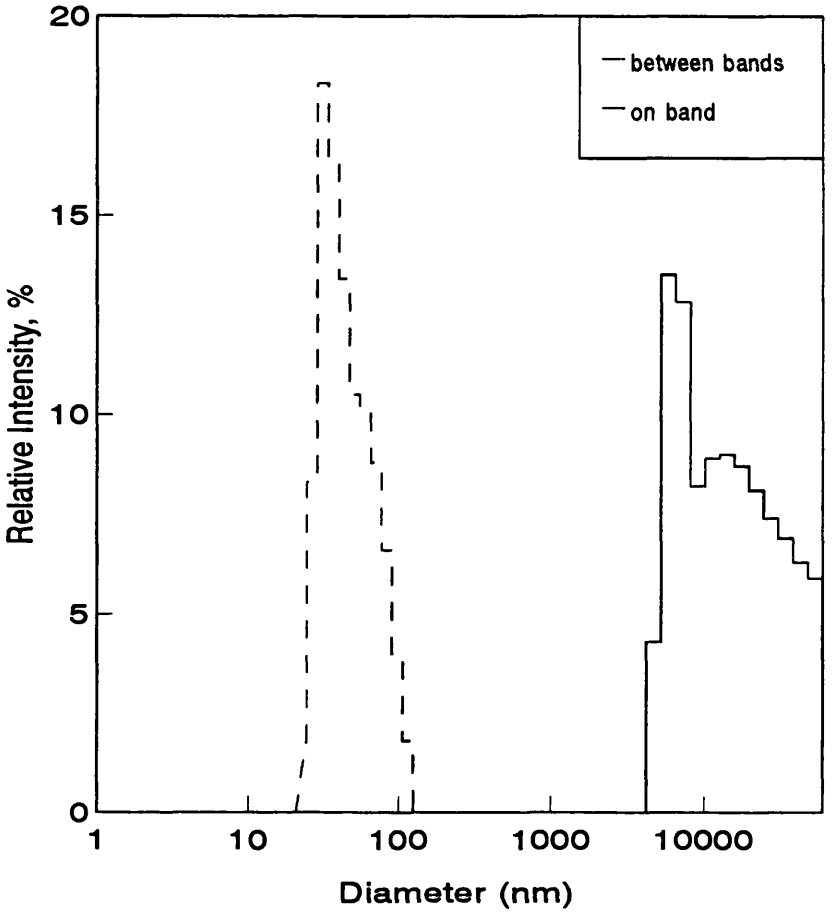


Fig 7.3: Internodal and nodal analyses of a mixture of 2000nm and 39nm latex spheres. Between the nodes the suspension is evidently clear of 2000nm particles and a distribution mean of 49.3nm is measured. The deviation from the expected size of 39nm is again most likely due to scattering from the larger particles at the nodal planes (see fig 7.2). A measurement with the laser beam adjusted to intentionally scatter from the nodal region is also shown. This gives a diameter of 18500nm for the distribution mean. This is indicative of the high concentration present in the bands as multiple scattering in a DLS analysis usually gives rise to an underestimate of particle size. Diffusion is being hindered either due to the ultrasonic forces or to interparticle interaction such as charge repulsion. Such hinderance will give rise to a larger effective diameter.

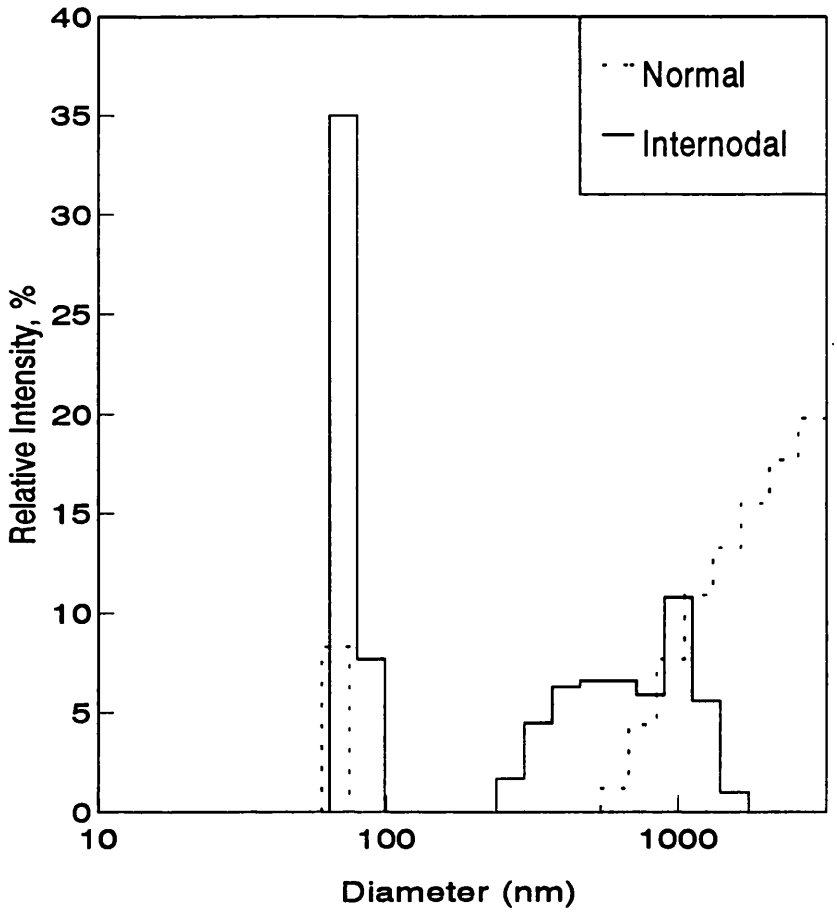


Fig 7.4: Internodal analyis (solid line) and normal DLS analysis of a mixture of 85nm and a small quantity of 15000nm latex spheres. The internodal result shows a greatly increased contribution in the 80nm region demonstrating removal of a substantial fraction of the larger particles. However a broad peak at around 1000nm is apparent. This is due to other contaminants in the sample. The difficulty of moving such particles in the current experimental set-up is demonstrated in the next figure (fig 7.5).

### 7.34 1.4um and 85nm latex

This plot demonstrates the size limit of this ultrasonic cell for moving particles. The distribution was unchanged from the previous analysis indicating that no change took place in the sample. This result does not define the limit for the technique, only of this particular cell, because redesign using, eg. two transducers instead of one will extend the range to lower particle sizes.

### 7.4 ILS analysis of yeast homogenate

Unclarified yeast homogenate, prepared as described in chapter 3, diluted approximately 10:1 was placed in the ILS analyser to monitor the improvement that could be gained in yeast based product analysis. Several runs were performed but it was found in practice that it was very difficult to produce consistent results or to keep the bands stable as easily as with the latex suspensions. This is probably because power levels need to be higher due to the reduced density of the particles ( see equation 7.3).

When held stable long enough to perform several analyses a result of 636 ±215nm and a polydispersity of 0.438 ±0.051 were returned. The suspension without ultrasound was 1003 ±328.2nm with a polydispersity of 0.535 ±0.186. The scattered light level from the normal and internodal samples was 129.9 ±14.4K Counts $s^{-1}$ and 79.8 ±14.5K Counts $s^{-1}$ respectively indicating that material contributing to over a third the scattered intensity had been shifted to the nodal plane.

### 7.5 Summary

A novel technique for in-situ sample preparation and analysis by light scattering has been presented. The method has been demonstrated successfully with latex particle mixtures to remove particles ≈ 1.4$\mu$m and above away from the laser beam and allow analysis of inter-nodal components. The performance of the method for biological material was promising although the stability of the sound field in this set-up appears to be a problem. Other configurations for ultrasonic manipulation of biological particles have produced more consistent results (Davies and Titchener-Hooker 1991) where the additional design consideration of the light scattering geometry need not be considered.

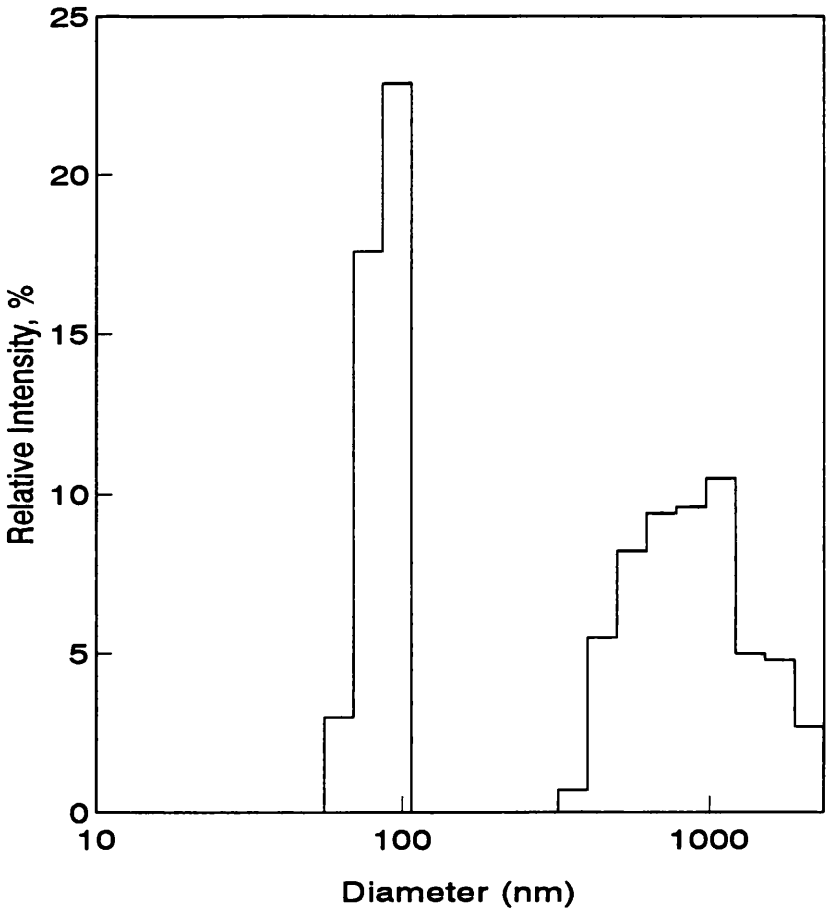


Fig 7.5: Chart to show internodal analysis of a suspension of 1.4 micron and 85nm latex spheres. The original distribution (not shown) is very similar and shows that, for this experimental set-up, the banding limit for latex spheres is about 1.4 microns. It will be possible to extend banding to lower particle sizes by appropriate modification to the design of the ultrasonic cell.

## Chapter 8: Future directions

### 8.1 Optical measurement of virus-like particles

For rapid on-line detection and quantification of virus-like particles in yeast homogenate to become reality for more than just the far end of the process chain, development of some of the methods discussed in this thesis should pave the way. Three methods of detecting particulates in a homogenate suspension have been discussed - a spectrophotometric assay, a particle size distribution analysis, and difference method against a known background.

The spectrophotometric assay (Chapter 4) has not been well characterised in terms of its application over a range of conditions and this will be necessary.

The size distribution method in an on-line environment fails in detection of small amounts of product due to the excessive noise on the signal. Improvement of signal to noise ratio in by eg. addition of analyte to initiate a chemical or physical change will be necessary in this case.

The difference method (Chapter 6) shows application to contaminant detection for fairly pure preparations. Extension of this further upstream by rapid sample preparation will be useful.

The use of antigens to virus-like particles has recently become a prospect and use of their binding reactions in terms of either aggregation or fluorescence labelling would be a great benefit.

As improvements in the growth and processing of the virus-like particles are made then by this means the methods presented here may find further application eg. further upstream.

## 8.2 Analysis of size distributions on-line

A software method has been developed for fast size distribution measurement with relatively high noise levels (Chapter 5). The extension,refinement and fuller testing of this method is required to produce more accurate results.

The description of a parallel processing architecture for a more standard processing technique with noise suppression has been indicated (Chapter 5). Implementation of this should effect a rapid and robust process analysis.

## 8.3 Internodal light scattering

The application of internodal light scattering (chapter 7) to biological systems needs to be investigated. Particularly the design of the ultrasonic geometry to effect more efficient separation and provide a possible means of small component measurement in turbid solutions.

The integration of the on-line dynamic light scattering system (chapter 2) into an ILS instrument could be a useful analysis tool for bioprocess systems.

The application of ILS to laboratory measurements where dust contaminants in samples could easily be held away from the laser beam thus improving data collection with the absence of noise from such contaminants.

It may be worth investigating whether the change in size distribution by ILS analysis with an increase in ultrasonic power between consecutive measurements could be useful to fractionate size distributions for analysis.

**Bibliography**

ABBEY.K.M SHOOK.J. CHU.B.,Correlation function profile analysis in laser light scattering III: A hybrid photon correlation spectrometer. in The application of laser light scattering to the study of biological motion. Earnshaw.J.C. Steer.M.W. Plenum. pp77-88. (1983).

ACKERSON.B.J., Application of the method of cumulants for interacting Brownian particle systems, in Photon correlation spectroscopy and velocimetry. Ed. Cummins. Pike. Plenum. pp440-443. (1976).

ACKERSON.B.J., Correlations for interacting Brownian particles I,,J Chem Phys 64 (1) Jan (1976)

ACKERSON.B.J., Correlations for interacting Brownian particles II,J Chem Phys 69 (2) Jul (1978)

ADRIAN.R.J, Statistical stability of clipped photon correlations in the self scaling limit. in Photon correlation techniques in fluid mechanics.d. Schulz-Dubois.E.O. pp242-255 (1983)

AGERKVIST.I. ENFORS-SO, Characterization of E. Coli cell disintegrates from a bead mill and high pressure homogenisers, Biotech. Bioeng. 36 pp1083-1089 (1990)

AMAL.R. et al, Structure and kinetics of aggregating colloidal haematite. Coll Surf 46 pp1-19 (1990)

AUWERTER.H. HORN.D.J. Colloid Interface Sci. 25. pp399-409 (1985).

BARBER.P.W. HILL.S.C. Effects of particle nonsphericity on light scattering. Optical Particle Sizing, proceedings 1988 Eds Grehan, Gousbet. Wiley

BARTHOLDI.M. SALZMAN.G.C. HILBERT.R.D. KERKER. Differential light scattering photometer for rapid analysis of single particles in flow. Appl. Opt. 19 (10) pp1575-1581 (1980)

BELL.D.J. HOARE.M. DUNNILL.P. The formation of protein precipitates and their centrifugal recovery. Adv. in Biochem. Eng/Biotech 26 Ed A. Fietcher

BENEDEK.G.B. Biological and medical applications of light scattering spectroscopy. in Photon correlation and light beating spectroscopy. Eds. Cummins. Pike. Plenum. pp241-245 (1976).

BERNE.B.J. Dynamics of charged macromolecules in solution. in Photon correlation and light beating spectroscopy. Eds. Cummins. Pike. Plenum. pp344-385 (1976).

BERTERO.M. BOCCACCI.P. DE MOL.C. PIKE.E.R. Extraction of polydispersity information in photon correlation, spectroscopy, Optical Particle Sizing:Theory and Practice.

BERTERO.M. DE MOL.C. PIKE.E.R. Particle sizing by inversion of extinction data.Optical Particle Sizing:Theory and Practice

BERTERO.M. PIKE.E.R. On the extraction of information from photon correlation spectroscopy.in Photon correlation techniques in fluid mechanics. Ed. Schulz-Dubois.E.O. pp298-302 (1983).

BERTERO.M. et al. Light scattering polydispersity analysis of molecular diffusion by Laplace transform inversion in weighted spaces. J. Chem. Phys. 82 (3) pp1551-1554 Feb (1985).

BERTOLOTTI.M. Multiple Scattering. in Photon correlation spectroscopy and velocimetry. Eds. Cummins. Pike. Plenum (1976).

BERTOLOTTI.M. Photon statistics. in Photon correlation and light beating spectroscopy. Eds. Cummins. Pike. Plenum pp41-74 (1974).

BICKEL.W.S. DAVIDSON.J.F. HUFFMAN.D.R. KILKSON. Application of polarization effects in light scattering: A new biophysical tool. Proc. Nat. Acad. Sci. 73 (2) pp486-490 (1976).

BICKEL.W.S. STAFFORD.M.E. Biological particles as irregularly shaped scatterers. in Light scattering by irregularly shaped particles. Schuerman. Plenum. pp299-305. (1980).

BICKEL.W.S. et al. Application of polarisation effects in light scattering: a new biophysical tool. Proc. Nat. Acad. Sci. 73 (2) pp486-490 (1976).

BOHREN. C.F. HUFFMAN D.R. Absorption and scattering of light by small particles. Wiley. New York (1983)

BONNERJEA.J. OH.S. HOARE.M. DUNNILL.P. Protein purification: The right step at the right time. Biotechnol. 4 pp954-958 Nov (1986).

BOON.J.P. Motility and small-scale hydrodynamics. in The application of laser light scattering to the study of biological motion. Ed. Earnshaw J.C. Steer.M.W. Plenum. pp562-607. (1983).

BOPP.S. TROPEA.C. ZHAN.L. The use of graded index fibres in fibre-optic laser doppler anemometry probes. Rev. Sci. Instrum. 60 (10) pp3195-3200 Oct (1989).

BOTT.S.E.Autocorrelation in photon correlation spectroscopy. Laboratory Practice 38 (4).

BOTT.S.E. Enhanced resolution particle size distribution by multiple angle photon correlation spectroscopy. in Ed. Wiley.L.J. and Sons. Particle Size Analysis. (1988).

BOTT.S.E. Submicrometer particle sizing by photon correlation spectroscopy: Use of multiple angle detection in ACS Symposium - Particle size distribution assessment and characterisation.

BOULAUD-D MADELAINE-G,Optical methods in submicronic aerosol measurement,,Optical Particle Sizing, proceedings 1988 Eds Grehan, Gousbet. Wiley

BOXMAN.A. et al. Deconvolution of light scattering patterns by observing intensity fluctuations. Appl. Opt. 30 (33) 20 Nov (1991).

BRIANZI.P. FRONTINI.M. On the regularised inversion of the Laplace transform,,Inverse Problems 7 pp335-368 (1991).

BROWN.D.J. FELTON.P.G. Direct measurement of concentration and size for particles of different shapes using laser light diffraction. Chem. Eng. Res. Des. 63 pp125-132 (1985).

BROWN.R.G.W. Dynamic light scattering using monomode optical fibres. Submitted to Appl. Opt. (1987).

BROWN.R.G.W. Laser fibre optics in biotechnology. Tibtech. 3 (8) pp200-203 (1985).

BROWN.R.G.W. Miniature components for photon correlation laser anemometry. 3rd Int. Symp. on Laser Anemometry Dec. 1987 ASME Winter annual meeting.

BROWN.R.G.W. On-line analysis of proteins using optical techniques. in Separations for biotechnology. Eds. Verrall.M.J. Hudson SCI Ellis M.

BROWN.R.G.W. GRANT.R.S. Photon statistical properties of visible laser diodes. Rev. Sci. Instrum. 58 (6) pp928-931 June (1987).

BROWN.R.G.W. JACKSON.A.P. Monomode fibre components for dynamic light scattering. J. Phys. E.: Sci. Instrum. 20 pp1503-1507 (1987).

BROWN.R.G.W. et al. Characterisation of silicon avalanche photodiodes for photon correlation measurements 2: Active quenching. Appl. Opt. 26 (12) pp2383-2389 (1987).

BROWN.R.G.W. et al. Characterisation of silicon avalanche photodiodes for photon correlation measurements 1: Passive quenching. Appl. Opt. 25 (22) pp4122-4126 (1986).

BRUGE.F. SAN BIAGIO.P.L. FORNILI.S.L. New photon correlator design based on transputer array concurrency. Rev. Sci. Instrum. 60 (11) November (1989).

BRUGE.F. et al. Transputer based upgrading of a laser photon correlator. Rev. Sci. Instrum. 60 (2) pp 222-225 Feb (1989).

BULLOUGH.R.K. et al. Quantum intensity-intensity correlation statistics of radiation from coherently and incoherently driven systems. in Coherence, cooperation and fluctuations. Ed. Haake.F. et al. Cambridge University Press. pp115-131 (1986).

BYRNE.P.O. et al. An optical probe for the enumeration of bacteria in liquid media. J. Phys. E. : (Sci Instrum) 22 pp146-150 (1989).

BRITISH BIOTECHNOLOGY LIMITED. Summary of information on hybrid Ty-virus like particle technology. British Biotechnology internal publication.

CANTRELL.C.D. N-fold photoelectric counting statistics of Gaussian light. Phys. Rev. A 1 (3) pp672-685 March (1970).

CARR.J.G. ATKINSON.T. CLARKE.D.J. Laser light scattering applied to biotechnology. In Applied Biotechnology, Proc. Biotech 86 (World Biotech Report, On-Line Conferences) Vol 1 D15.

CARR.R.J.G. et al. Determination of protein size in chromatography column eluants by on-line photon correlation spectroscopy. Anal. Biochem. 175 pp492-499 (1988).

CHA.C.Y. MIN.K.W. Photon correlation spectroscopy of polymer solutions. J. Polym. Sci. Polym. Phys. 21 pp807-820 (1983).

CHEN.S.H. TARTAGLIA.P. PUSEY.P.N. Light scattering from independent particles - Nongaussian correction to the clipped intensity correlation function. J. Phys. A: Math., Nucl., Gen., 6 pp490-495 (1972).

CHINSOO.L. LIM.H. New device for continuously monitoring the optical density of concentrated microbial cultures. Biotech. Bioeng. XXII pp639-642 (1980).

CHOW.K.M. et al. On-line photon correlation spectroscopy using fibre-optic probes. J. Phys. E: Sci. Instrum. 21 pp1186-1190 (1988).

CHU.B. Correlation function profile analysis in laser light scattering. in The application of laser light scattering to the study of biological motion. Earnshaw.J.C. Steer.M.W. Plenum. pp53-76. (1983).

CHU.B. DINAPOLI.A. Extraction of distributions of decay times in photon correlation of polydisperse macromolecular solutions. In Measurement of suspended particles by Quasielastic light sacttering Ed. Dahneke B.E. Wiley 1983 pp81-105.

CHU.B. GULARI.E. GULARI.E. Photon correlation measurements of colloidal size distributions II.Details of histogram approach and comparison of methods of data analysis. Physica Scripta 19 pp476-485 (1979).

CHU.B. RENLIANG.X. SULONG.N. Applications of prism cell light scattering spectrometer to particle sizing in polymer solutions. Part. Part. Sys. Charact. 6 pp34-38 (1989).

CHU.B. XU.R. DINAPOLI.A. Light scattering studies of a colloidal suspension of iron oxide particles. J. Coll. Int. Sci. 116 (1) pp182-195 (1983).

CLAES.P. et al. On-line molecular size detection for protein chromatography. American Lab. Feb (1990).

CLAES.P. et al . Applications of molecular size detection in column chromatography. Separations for Biotechnology Sci & Elsevier Applied Science (1990).

CLARKE.D.J. et al. Some approaches to downstream processing monitoring and the development of new separation techniques. Separations for Biotechnology Eds M.S. Verrall M.J. Hudson SCI Ellis H. (1987)

COAKLEY W.T. et al Cell manipulation in ultrasonic wave fields. J. Chem. Tech. Biotechnol. 44, pp44-62 1989

CORBIN.F. GREHAN.G. GOUESBET.G. MAHEU.B. Interaction between a sphere and a gaussian beam: computations on a micro-computer. Part. Part. Sys. Charact. 5. pp103-108 (1988).

CORNILLANT.J. High resolution submicron measurement with a laser particle size analyser. International Laboratory pp28-36 Sept (1987).

CORREIA.C. SANTOS.F.P. A new non-clipped correlator for photon count spectroscopy. Rev. Sci. Instrum. 60 (9) pp2973-2939 Sept (1989).

COVA.S. LONGONI.S. ADREONI.A. Towards picosecond resolution with single photon avalanche photodiodes. Rev. Sci. Instrum. 52 (3) pp408-412 (1981).

CUMMINS.H.Z. in Photon correlation and light beating spectroscopy. Eds. Cummins. Pike. Plenum. (1974).

CUMMINS.H.Z. Analysis of diffusion of biological materials by quasielastic light scattering. in The application of laser light scattering to the study of biological motion. Earnshaw.J.C. Steer.M.W. Plenum. pp171-208. (1983).

CUMMINS.H.Z. PUSEY.P.N. Dynamics of macromolecular motion. in Photon correlation spectroscopy and velocimetry. Eds. Cummins. Pike. Plenum. (1976).

CUMMINS.H.Z. SWINNEY.H.L. Light beating spectroscopy: Coherence and signal to noise considerations (source spectrum and statistics). in Progress in Optics Ed.Wolf.E. vol VIII (1970).

DANOVICH.G.R. SERDYVK.I.N. A solution of an inverse scattering problem: Approximation of polydisperse scattering data as a sum of many exponential curves. in Photon correlation techniques in fluid mechanics. Ed. Schulz-Dubois.E.O. pp315-321 (1983).

DAVIES G.B. Study of the application of ultrasonic standing waves to the segregation of fine biological particles from liquids. PhD thesis University College London 1992.

DAVIES G.B. TITCHENER-HOOKER N.J. Ultrasonic recovery of biological particles pre-print from IEEE Ultrasonics Symposium December 1991.

DEGIORGIO.V. Photon correlation techniques. in Photon correlation spectroscopy and velocimetry. Eds. Cummins. Pike.Plenum pp142-163 (1976).

DEGIORGIO.V. Physical principles of light scattering. in The application of laser light scattering to the study of biological motion. Earnshaw.J.C. Steer.M.W. Plenum. pp9-30 (1983).

DHADWAL.H.S. Regularised inversion of correlation functions in dynamic light scattering. Part. Part. Syst. Charact. 6 pp28-33 (1989).

DHADWAL.H.S. Regularised inversion of correlation functions in dynamic light scattering. Part. Sys. Char. 6 pp28-33 (1989).

DHADWAL.H.S. ANSARI.R.R. MEYER.W.V. A fiber-optic probe for particle sizing in concentrated suspensions. Rev. Sci. Instrum. 62 (12) Dec (1991).

DHADWAL.H.S. CHU.B. A fiber-optic light scattering spectrometer. Rev. Sci. Instrum. 60 (50 pp845-853 May (1989).

DHONT.J.K.G. Multiple Rayleigh-Gans-Debeye light scattering in colloidal systems. in Photon correlation techniques in fluid mechanics. Ed. Schulz-Dubois.E.O. pp384-392 (1983).

DINAPOLI.A. CHU.B. CHA.C. Molecular weight distributions of polyacrylamide by photon correlation spectroscopy. Macromolecules. 15 pp1174-1180 (1982).

DITTER.W. EISENLAUER.J. HORN.D. Laser optical method for dynamic flocculation testing in flowing dispersions.

DORSHOW.R.B. Photon counting dead time measurement in commercial laser light scattering instrumentation. Rev. Sci. Instrum. 61 (1) pp186-188 Jan (1990).

DRESCHER.S. HEIDENREICH.E. MULLER.G. Technologically relevant particle shape analysis. Part. Part. Sys. Charact. 7 pp30-35 (1990).

DREWEL.M. SCHATZEL.K. Laser light scattering and correlation techniques of colloidal suspensions. Z. Phys. B: Condensed matter 68 pp229-232 (1987).

DREXHAGE.M.G. MOGNIHAN.C.T. Infrared optical fibres. Scientific American Nov (1988).

DUBIN.S.B. LUNACEK.J.H. BENEDEK.G.B. Observations of the spectrum of light scattered by solutions of biological macromolecules. Proc. Nat. Acad. Sci. 57 pp1164-1171 (1967).

DUNNILL.P. Biochemical Engineering and Biotechnology. Chem. Eng. Res. Des. 65 pp211-217 May (1987).

DUNNILL.P. Biochemical engineering its origins and future. The Chemical Engineer pp42-44 Dec (1988).

DUNNILL.P. Biosafety in the large-scale isolation of intracellular microbial enzymes. Chem. Ind. p877-879 Nov (1982).

DUNNILL-P,Trends in downstream processing of proteins and enzymes,,Proc Biochem pp9-13 Oct 1983

DUNNILL.P. LILLY.M.D. Continuous enzyme isolation. Biotechnol. & Bioeng. Symp. 3 pp97-113 (1972).

DURST.F. Employment of light scattering information to lay out optical measuring systems for measurements of particle properties. in Optical Particle Sizing, proceedings Eds.Grehan. Gousbet. Wiley..(1988).

DYSON.R.D. ISENBERG.I. Analysis of exponential curves by a method of moments with special attention to sedimentation equilibrium and fluorescence decay. Biochemistry 10:17 pp3233-3241 (1971).

EHRESMANN.B. IMBULT.P. WEIL.J.H. Spectrophotometric determination of protein concentration in cell extracts containing tRNA's and rRNA's. Analytical Biochemistry. 54. pp454-463. (1973)

EISENLAUER.J. HORN.D. Influence of shear and salt on flocculation in laminar tube flow. in Solid Liquid separation Ed J. Gregory Ellis Horwood Pub (1984).

EMBURY.J. Absorption by small regular non-spherical particles in the Rayleigh region. in Light scattering by irregularly shaped particles. Schuerman. Plenum pp97-102 (1980).

FARADPOUR.F.A. Size analysis of micrometer sized suspensions by forward lobe light scattering in the anomalous regime. Particle Size Analysis 1988 John Wiley Ed Lloyd P.J.

FERRI.F. GIGLIO.M. PERINI.U. Inversion of light scattering data from fractals by the Chahine iterative algorithm . Appl. Opt. 28 (5) pp3074-3082 Aug (1989).

FIJNANT.H.M. Van RIJSWIJK. Laser intensity fluctuation in the heterodyne detection of scattered light. in Photon correlation spectroscopy and velocimetry. Eds. Cummins. Pike. Plenum. pp465-470 (1976).

FINE.S. et al. Laser irradiation of biological systems. IEEE Spect. April (1964).

FLETCHER.G.C. RAMSAY.D.J. Photon correlation spectroscopy of polydisperse samples. I. Histogram method with exponential sampling. Optica Acta 30 (8) pp1183-1196 (1983).

FORD.J.R. CHU.B. Correlation function profile analysis in laser light scattering III an iterative procedure. in Photon correlation techniques in fluid mechanics. Ed. Schulz-Dubois pp303-314 (1983).

FORD.T. RICKWOOD.D. Research and development of centrifugation techniques. Biotech. Lab. March (1989).

FUCHS.H.F. JORDE.C. GLATTER.O. Interactive data-acquisition and evaluation system for quasielastic light scattering. Rev. Sci. Instrum. 60 (5) pp854-857 May (1989).

FUJIME.S. TAKASAKI-OHSITA.M. MAEDA.T. Dynamic light scattering from semidilute suspensions of fd virus. Macromolecules 20 pp1292-1295 (1987).

GAFNI.A. MODLIN.R.L. BRAND.L. Analysis by fluorescence decay curves by means of the Laplace transformat transformation. Biophysical Journal 15: pp263-280 (1975).

GARDINER.S.A.M. et al. Process design for recombinant protein recovery from inclusion bodies. Proc. 4th. European Cng. on Biotechnology, Amsterdam, (1987) Vol.2 Eds. Neijssel.O.M. van der Meer.R.R. Luyben.K.

GLATTER.O. HOFER.M. Interpretation of elastic light scattering data III Determination of size distributions of polydisperse systems. J. Coll. Int. Sci. 122 (2) pp496-506 April (1988a).

GLATTER.O. HOFER.M. Interpretation of elastic light scattering data in real space II Non-spherical and inhomogeneous monodisperse systems. J. Coll. Int. Sci. 122 (2) pp484-495 April (1988b).

GLATTER.O. HOFER.M. Particle sizing of polydisperse systems by Mie scattering. Optical Particle Sizing. proceedings 1988c Eds Grehan, Gousbet. Wiley

GLATTER.O. HOFER.M. JORDE.C. EIGNER.W.D. Interpretation of elastic light scattering data in real space. J. Coll. Int. Sci. 105 (2) pp577-586 June (1985).

GLATTER.O. SIEBERER.J. SCHNABLEGGER.H. A comparative study on different scattering techniques and data evaluation methods for sizing of colloidal systems using light scattering. Part. Part. Syst. Charact. 8: pp274-281 (1991).

GOUSBET.G. MAHEU.B. GREHAN.G. Scattering of a gaussian beam by a sphere using a bromwich formulation case of arbitrary location. Part. Part. Sys. Charact. 5 pp1-8 (1988).

GOUSBET.G. GREHAN.G. Expressions to compute the coefficients g in the generalised Lorentz Mie theory using finite series. J. Opt. (Paris) 19 (1) pp35-48 (1988).

GREGORY.J. Laminar dispersion and the monitoring of flocculation processes. J. Coll. Int. Sci. 118 (2) pp397-409 (1987).

GREGORY.J. Turbidity fluctuations in flowing suspensions. J. Coll. Int. Sci. 105 (2) pp357-371 (1984).

GREGORY.J. NELSON.D.W. A new optical method for flocculation monitoring. Solid-Liquid separation Ed J. Gregory Ellis Horwood Pub (1984).

GREGORY.J. NELSON.W. Monitoring of aggregates in flowing suspensions. Coll. Surf. 18 pp175-188 (1986).

GRIFFIN.M.C.A. ANDERSON.M. Laser light scattering of the fractionation of casein micelles in skim milk by controlled pore glass chromatography. in The application of laser light scattering to the study of biological motion. Earnshaw. J.C. Steer.M.W. Plenum. (1983).

GRINVALD.A. STEINBERG.I.Z. On the analysis of fluorescence decay kinetics by the method of least-squares. Analyitical Biochemistry 59 pp583-598 (1974).

GULARI.E. GULARI.E. TSUNASHIMA.Y. CHU.B. Photon correlation spectroscopy of particle distributions. J. Chem. Phys. 70 (8) 15 Apr (1979).

HANBURY-BROWN.R. TWISS.R.Q. A test of a new type of interferometer on Sirius. Nature 178 Nov (1956).

HANBURY-BROWN.R. TWISS.R.Q. Correlation between photons in two coherent beams of light. Nature 177 Jan (1956).

HARDING.S.E. et al. Laser light scattering in biochemistry. Biochemical Society Transactions pp477-516 (1991).

HASPIDIS.K. KUMAR.K. SARTO.G.L. Submicron particle size analysis by dynamic light scattering. Int. Labmate Iss no. 0143-5140.

HAYASHI.S. Measurements of absolute concentration and size distribution of particles by laser small angle scattering. Optical Particle Sizing, proceedings 1988 Eds Grehan, Gousbet. Wiley.

HEMSLEY.D.J. et al. The use of calibration techniques for the development and application of optical particle sizing instruments. Optical Particle Sizing, proceedings 1988 Eds Grehan, Gousbet. Wiley.

HETHERINGTON.P.J. et al. Release of protein from baker's yeast (Saccharomyces cerevisiae) by disruption in an industrial homogeniser. Trans. Instn. Chem. Eng... 49. pp142-48. (1971)

HOARE.M. et al. Disruption of protein percipitates during shear in Couette flow and in pumps. Ind. Eng. Chem. Fundam. 21. pp402-406. (1982).

HOARE.M. DUNNILL.P. Processing with proteins - the immediate challenge. Chem. Eng. Sept (1986).

HOARE.M. DUNNILL.P. Protein processing - new prospects. Chem. Eng. Dec (1986).

HOLTZ.M. Light scattering from structured particles. in Photon correlation spectroscopy and velocimetry. Eds. Cummins. Pike. Plenum. (1976).

HUNT T.M. Particle counting by size - Which method is right? INPARTECH 88 2nd Int. conference. Imperial College London 13th-14th Sept. 1988.

HWANG.S.O. FELDBERG.R.S. Effect of inclusion body production on culture turbidity and cell dry weight in growing bacterial cultures. Biotechnol. Prog. 6 pp48-50 (1990).

JAKEMAN.E. The effect of heterodyne detection on the statisical accuracy of optical linewidth measurements. J. Phys. A: Gen. Phys. 5 L49-52 (1972).

JAKEMAN.E. PIKE.E.R. SWAIN.S. Statistical accuracy in the digital autocorrelation of photon counting fluctuations. J. Phys. A: Gen. Phys. 4 pp517-534 (1971).

JEPRAS.R.I. et al. Application of photon correlation spectroscopy as a technique for detecting culture contamination. Biotechnology and Bioengineering 38: pp929-940 (1991).

KERKER.M. Light scattering theory: A progress report. Optical Particle Sizing, proceedings 1988 Eds Grehan, Gousbet. Wiley.

KESHAVARZ-MOORE.E. et al. Reactor properties of a high speed bead mill for microbial cell rupture. Biotechnol. Bioeng. XXI pp745-774 (1979).

KILLINGER.R.T. ZERULL.R.H. Effects of particle shape to be considered for optical particle sizing. Optical Particle Sizing, proceedings 1988 Eds Grehan, Gousbet. Wiley.

KOCH.A.L. Turbidity measurements of bacterial cultures in some available commercial instruments. Anal. Biochem. 38 pp252-259 (1970).

KOGELNIK.H. LI.T. Laser beams and resonators. Appl. Opt. 5 (10) pp1150-1567 (1966).

KONAK.C.et al. Effect of multiple light scattering on transmitted and scattered light. Applied Optics 30:33, pp4865-4871 (1991).

KOPPEL.D.E. Analysis of macromolecular polydispersity in intensity correlation spectroscopy: The method of cumulants. J. Chem. Phys. 37 (11) pp4814-4820 Dec 1972.

KOPPEL.D.E. Study of escherichia coli ribosomes by intensity fluctuation spectroscopy of scattered laser light. Biochemistry 13 pp2712-2719 (1974).

KRAHN.W. LUCKAS.M. LUCAS.K. Determination of particle size distribution in fluids using photon correlation spectroscopy. Part. Part. Stst. Charact. 5 pp72-76 (1988).

KULA.M.R. Extraction processes. 8th Int. Biotech. Sym. Paris. (1988). Ed.Durand.S. Bobichon.L. Florent.J.

KULA.M.R. Trends and future prospects of aqueous two-phase extraction. Bioseparations. 1. pp181-189. (1990).

KULICKE.W.M. et al. Light scattering. in Progress in Polymer Science Vol 8 pp388-399 (1982).

KULKARNI.A.D. Solving ill-posed problems with artificial neural networks. Neural Networks 4:pp477-484, (1991).

KUNDT A. LEHMANN O. Ueber longitudinale Schwingungen und Klangfiguren in cylindrischen Flussigkeitssaulen. Annalen der Physik und Chemie 153 (9) pp1-12 1874.

LEE.Y.H. Pulsed light probe for cell density measurement. Biotech. Bioeng. XXIII pp1903-1906 (1981).

LESCHONSKI.K. On-line analysis, its potential and its problems. Part. Charact. 1 pp7-13 (1984).

LESKOVAR.P.R. et al. Photon counting system for subnanosecond fluorescence lifetime measurements.Rev.Sci.Instrum.47:9 pp1113-1121 (1976).

LETTIERI.T.R. HEMBREE.G.G. Dimensional calibration of the NBS 0.3um diameter particle sizing standard. J. Coll. Int. Sci. 127 (2) pp566-572 (1988).

LICINIO.P. DELAYE.M. Mutual and self diffusion in concentrated alpha-crystallin protein dispersions. A dynamic light scattering study. J. Phys. France 49 pp975-981 (1988).

LIGHTSTONE.A.W. MCINTYRE.R.J. Photon counting silicon avalanche photodiodes for photon correlation spectroscopy. R.C.A. publication (1988).

LIGHTSTONE.A.W. et al. Photon counting modules using RCA avalanche photodiodes. R.C.A. internal publication.

LIVESEY.A.K. LICINIO.P. DELAYE.M. Maximum entropy analysis of quasielastic light scattering from colloidal dispersions. J. Chem. Phys. 84 (9)pp5102-5107 (1986).

LOPEZ.R.J. REBOLLEDO.M.A. Spectral study of light with a very low intensity by means of the measurement of Laplace or Fourier transform of the time-interval probability. Optics Communications. 42:1 pp34-38. (1982).

LUONG.J.H.T. et al.Developments and applications of biosensors. Tibtech. 6 pp310-316 Dec (1988).

MADANI.H. KALER.E.W. Measurement of polydisperse colloidal suspensions with quasielastic light scattering. Part. Part. Syst. Charact. 8 pp259-266 (1991).

MAHEU.B. GREHAN.G. GOUESBET.G. Laser beam scattering by individual spherical particles: Numerical results and application to optical sizing. Optical Particle Sizing, proceedings 1988 Eds Grehan, Gousbet. Wiley.

MAHEU.B. GREHAN.G. GOUESBET.G. Laser beam scattering by individual spherical particles: numerical results and application to optical sizing. Part. Charact. 4 pp141-146 (1987).

MANNWEILER.K. TITCHENER-HOOKER.N.J. HOARE.M. Biochemical engineering improvements in the centrifugal recovery of biological particles. I.Chem.Eng.Symposium. Advances in biochemical engineering. Newcastle. pp105-117 (1989).

MCWHIRTER.J.G. PIKE.E.R. On the numerical inversion of the Laplace transform and similar Fredholm integral equations of the first kind. J. Phys. A: Maths. Gen. 11 (9) pp1729-1745 (1978).

MERKENS.H. SCARLETT.B. Standardisation and calibration of particle size measuring techniques. Inpartech. 88 2nd Int. Conf. Imperial College preprint.

MILKLANTZ.H. et al. The molecular weight distribution of Heparin determined with a HPLC LALLS coupling technique. J. L. Cromat. 9 (10) pp2073-2093 (1986).

MORENO.F. GONZALEZ.F. LOPEZ.R.J. LAVIN.A. Time-interval statistics through a Laplace transform method in quasi-elastic light scattering experiments for low intensity levels. Opt. Lett. 13 (6) pp637-639 (1988).

MOSQUEIRA.F.G. et al. Characteristics of mechanically disrupted bakers yeast in relation to its separation in industrial centrifuges. Biotech. Bioeng. XXIII pp335-343 (1981).

MROCZKA.J. Diversity of reading in water pollution measurements. J. Phys. E: Sci. Instrum. 21 pp952-954 (1988).

MUNRO.D. RANDLE.K.J. Photon correlation spectroscopy of polymer latices. in Photon correlation spectroscopy and velocimetry. Eds. Cummins. Pike. Plenum. (1976).

McWHIRTER. A well conditioned cubic b-spline model for processing laser anemometry data. Optica Acta 28 (11) pp1453-1475.

NAKAGAKI.M. HELLER.W. Effect of light scattering upon the refractive index of dispersed colloidal spheres. J. Appl. Phys. 27 (9) pp975-979 (1956).

NAQWI.A. DURST.F. Focusing of diode laser beams: a simple mathematical model. Appl. Opt. 29 (12) pp1780-1785 (1990).

NAQWI.A.A. DURST.F. Light scattering applied to LDA and PDA measurements. Part 1: Theory and numerical treatments. Part. Part. Syst. Charact. 8: pp245-258 (1991).

NASH.P.J. KING.T.A. Analysis of photon correlation spectral decay curves by the S-exponential sum method. J. Chem. Soc. Farad. Trans. 2 79 pp989-1009 (1983).

NEUMAN.R.D. JONES.M.A. ZHOU.N.F. Photon correlation spectroscopy applied to hydrometallurgical solvent extraction systems. Coll. Surf. 46 pp41-61 (1990).

NGAI.K.L. et al. Physical interpretations of various dynamic light scattering data their interconnections and relations to other relaxation data. J. Chem. Phys. 86 (9) pp4768-4778 May (1987).

NIKTARI.M. et al. The modelling and control of fractionation processes for enzyme and protein purification. Preprint.(1990).

NOULLEZ.A. BOON.J.P. Microprocessor based photon correlator. Rev. Sci.Instrum. 57 (10) pp2523-2528.

OLIVER.C..J. A comparison of current measurement with photon counting in the use of photomultiplier tubes. EMI publication (1977).

OLIVER.C.J. Correlation techniques. inPhoton correlation and light beating spectroscopy. Eds. Cummins. Pike. Plenum. pp151-224 (1974).

OLIVER.C.J. The extraction of spectral parameters in photon correlation spectroscopy. Adv. in Phys. 27 (3) pp387-435 (1978).

OSTROWSKY.N. Particle characterisation by photon correlation spectroscopy. in Particle Size Analysis (1988) Ed P.J. Lloyd John Wiley and Sons.

OSTROWSKY.N. SORNETTE.D. Data reduction in polydisperse diffusion studies. in Photon correlation techniques in fluid mechanics. Ed. Schulz-Dubois.E.O. pp286-297 (1983).

OSTROWSKY.N. SORNETTE.D. PARKER.P. PIKE.E.R. Exponential samplng method for light scattering polydispersity analysis. Opt. Acta. 28 (8) pp1059-1070 (1981).

PAPAMICHAEL.N. Improved economics of enzyme recovery by aqueous phase extraction by recycling of phase chemicals: a case study. Proc.4th Euorpean cong. on Biotechnol.(1987) Amsterdam.pp519-522.

PARKER.T. DALGLEISH.D.G. The use of light scattering and turbidity measurements to study the kinetics of extensively aggregating proteins: alpha-s Casein. Biopolymers 16 pp2533-2547 (1977).

PEARCE.W.A. Inference of scatterer size distribution from single scattering matrix data. in Light scattering by irregularly shaped particles. Schuerman. Plenum. pp307-318 (1980).

PETER.S. RIT.A. et al. Deconvolution procedures in laser light scattering instruments. Inpartech. 88 2nd Int. Conf. Imperial College preprint.

PHILLIES.G.D. Quasielastic light scattering. Analytical Chemistry. 60:20 pp1049A-1057A (1990).

PIKE.E.R. Introductory lecture. in Photon correlation and light beating spectroscopy. Eds. Cummins. Pike. Plenum. pp3-8 (1974).

PIKE.E.R. Photon correlation spectroscopy of classical and non-classical light fields and its debt to Glauber and Harvard. in Absorption and scattering of light by small particles. Bohren. Huffman. Wiley. pp9-30 (1983).

PIKE.E.R. The theory of light scattering. in Photon correlation and light beating spectroscopy. Eds. Cummins. Pike. Plenum. pp9-40 (1974).

PREIKSCHAT.E. New inline method to measure cell count and cell size in fermenters using a focussed laser beam. Proc. 4th European Congress on Biotechnology (1987) Vol 3 Elsevier Science.

PROVENCHER.S.W. A Fourier method for the analysis of exponential decay curves. Biophys. J. 16 pp27-41 (1976).

PROVENCHER.S.W. A general purpose constrained regularisation method for inverting photon correlation data. in Photon clrrelation techniques in fluid mechanics. Ed. Schulz- Dubois. pp322-328 (1983).

PROVENCHER.S.W. An eigenfunction expansion method for the analysis of exponential decay curves. J. Chem. Phys. 64 (7) pp2772-2777 April (1976).

PROVENCHER.S.W. HENDRIX.J. DE MAEYER.L. Direct determination of molecular weight distributions of polystyrene in cyclohexane with photon correlation spectroscopy. J. Chem. Phys. 69 (9) pp4273-4276 Nov (1978).

PROVENCHER.W. A constrained regularisation method for inverting data represented by a linear algebraic or integral equations. Comp. Phys. Comm. 27 pp213-227 (1982).

PUSEY.P.N. Intensity fluctuation spectroscopy of charged Brownian particles: The coherent scattering function. J. Phys. A: Maths. Gen. 11 (1) (1978).

PUSEY.P.N. Macromolecular diffusion. Photon correlation and light beating spectroscopy. Eds. Cummins. Pike. Plenum. pp387-428 (1974).

PUSEY.P.N. Statistical properties of scattered radiation. in Photon correlation spectroscopy and velocimetry. Eds. Cummins. Pike. Plenum. (1976).

PUSEY.P.N. The dynamics of interacting Browninan particles. in Photon correlatoin techniques in fluid mechanics. Ed. Schulz-Dubois.E.O. pp335-347 (1983).

PUSEY.P.N. The study of Brownian motion by intensity fluctuation spectroscopy. Phil. Trans. R. Soc. Lon. A 293 pp293-439 (1979).

PUSEY.P.N. SCHAEFER.D.W. KOPPEL.D.E. Single-interval statistics of light scattered by identical independent scatterers. J. Phys. A:Math. Nucl. Gen. 7 (4) pp530-540 (1974).

RANDLE.K.J. Statistical optics and its application to colloid science. Chem. Ind. 19 Jan. pp74-81 (1980).

RANSOHOFF.T.C. et al. Automation of biopharmaceutical processes. BioPharm. March (1990).

RARITY.J.G. RANDLE.K.J. The application of number fluctuation spectroscopy to aggregating systems and the measurement of rotational (anti-)correlation functions. in Photon correlation techniques in fluid mechanics. Ed. Schuls-Dubois.E.O. (1983).

RAYNER.D.M. McKINNON.A.E. SZABO.A.G. Confldence in fluoroscence lifetime determinations: a ratio correction for the photomultiplier time response variation with wavelength. Can. J. Chem. 54:pp3246-3259 (1976).

RAYNOR.D.M. McKINNON.A.E. SZABO.A.G. Correction of instrumental time response variation with wavelength in fluorescence lifetime determinations in the ultraviolet region. Rev. Sci. Instrum. 48:8 pp1050-1054 (1977).

ROSS.D.A. Laser measurement of Brownian movement with a focussed beam. Optics and laser technol. 21 (3) (1989).

ROSS.D.A. Optimal filtering applied to the inversion of the Laplace transform. Optical Particle Sizing, proceedings (1988) Eds. Grehan, Gousbet. Wiley.

ROSS.D.A. DHADWAL.H.S. DYOTT.R.B. The determination of the mean and standard deviation of the size distribution of a colloidal suspension of submicron particles using. J. Coll. Int. Sci. 64 (3) pp533-542 May (1978).

ROSS.D.A. NGUYEN.T.H. Spectral properties of the Regularized Inversion of the Laplace Transform. Part. Part. Syst. Charact. 7 pp80-86 (1990).

SATO.Y. ISHIKAWA.N. TAGAKI.T. High performance size exclusion chromatography and molar mass measurement by LALLS of recombinant yeast derived human hepatitus . J. Chromat. 507 pp25-31 (1990).

SCHAEFER.D.W. Applications of photon statistics and photon correlation. inLaser applications to optics and spectroscopy. Ed. Jacobs.S.F. et al. Addisson Wesley. pp245-280 (1975).

SCHATZEL.K. Rate correlation and data preprocessing with digital correlators and structurators. in Photon correlation techniques in fluid mechanics. Ed. Schulz-Dubois.E.O. pp226-241 (1983).

SCHATZEL.K. DREWEL.M. STIMAC.S. Photon correlation measurements at large lag times: improving statistical accuracy. J. of Modern Optics 35:4 pp711-718 (1988).

SCHIFFER.R. Perturbation approach for light scattering by an ensemble of irregular particles of arbitrary material. Appl. Opt. 29 (10) 1 April (1990).

SCHMITZ.K.S. YU.J.W. Lambda depression/overlay histogram analysis of poly(acrylate) as a function of added salt. Optical Particle Sizing, proceedings 1988 Eds Grehan, Gousbet. Wiley.

SCHRADER.H.W. EISERT.W.G. High resolution particle sizing using the combination of time of flight and light scattering measurements. Appl. Opt. 25 (23) pp4396-4401 (1986).

SCHUERMAN.D.W. *In*, Light scattering by irregularly shaped particles. Ed Scherman D.W. Plenum. press April (1980)

SCHULZ-DUBOIS.E.O. High resolution intensity interferometry by photon correlation. in Photon correlation techniques in fluid mechanics. Ed Schulz-Dubois.E.O. (1983).

SHOEMAKER.R.L. Nonlinear spectroscopy. in Laser applications to optics and spectroscopy. Ed. Jacobs.S.F. et al. Addisson Wesley. p453-504 (1975).

SINGHAM.S. BOHREN.E. Hybrid method in light scattering by an arbitrary particle. Appl. Opt. 28 (3) pp517-522.

SKILLING.J.BRYAN.R.K.Maximum entropy image reconstruction:General algorithm . Mon. Not. R. Astr. Soc. 211 pp111-124 (1984).

SMALL.E.W. ISENBERG.I. On moment index displacement J. CHEM. PHYS. 66:8 pp3347-3351 (1977).

STEER.M.W, Applications of laser light scattering to biological systems. in The application of laser light scattering to the study of biological motion. Earnshaw.J.C. Steer.M.W. Plenum. pp43-52 (1983).

STELZER.E. RUF.H. GRELL.E. Analysis and resolution of polydisperse systems. in Photon correlation techniques in fluid mechanics. Ed. Schulz-Dubois.E.O. (1983).

STOCK.R.S. RAY.W.H. Interpretation of photon correlation spectroscopy data: a comparison of analysis methods. J. of Polymer Science: Polymer Physics Ed. : 23, pp1393-1447, (1985).

STREIB.J. Particle size analysis using photon correlation spectroscopy. Chem. Ing. Tech. 60 (2) (1988).

STREIB.J. Particle size distributions from photon correlation spectroscopy(in German). Chem. Ing. Tech. 60 (2) pp138-139 (1988).

TAYLOR.G. et al. Size and density of protein inclusion bodies. Biotechnology 4 June pp553-557 (1986).

TAYLOR.T.W. ACKERSON.B.J. Double scattering in a structured system of particles. in The aplication of laser light scattering to the study of biological motion. Earnshaw.J.C. Steer.M.W. Plenum. pp254-24 (1983).

THOMAS.J.C. Fibre optic dynamic light scattering from concentrated dispersions. 2. Concentration dependence of the apparent diffusion coefficient for small spheres. American Chemical Society. 5. pp1350-1355. (1989).

TURNER.M. Downstream processing-hygiene or containment. Chem. Ind. pp876 Nov (1982).

TUZUN.U. FARADPOUR.F.A. Comparison of light scattering with other techniques for particle size measurement. Part. Charact. 2 pp104-112 (1985).

ULRICH.J. STEPANSKI.M. Use of the laser diffraction technique for particle size measurement at high suspension densities,Part. Part. Sys. Charact. 7 pp25-29 (1990).

VAN DER BERG.J.W.A. et al. Polyethelyneimine I: Fractionation; Mark Houwink relation. Journal of Royal Netherlands Chemical Society 92 (1) pp3-10 (1973).

VAUGHAN.J.M. Correlation compared with interferometry for laser scattering spectroscopy. in Photon correlation and light beating spectroscopy. Eds. Cummins. Pike. Plenum. pp429-456 (1974).

Van de MEEREN.P.P.A. Van de DEELEN.J. BAERT.L. Optimisation of quasi-elastic light scattering measurements. Particle Size Analysis 1988 Ed Lloyd P.J. John Wiley (1988).

VanVELUWEN.A. LEKKERKERKER.H.N.W. KRUIF. VRIJ. Influence of polydispersity on dynamic light scattering measurements on concentrated suspensions. J. Chem. Phys. 89 (5) pp2810-2815 (1988).

WALKER.C.T. Light scattering. in Laser applications to optics and spectroscopy. Ed. Jacobs.S.F. et al. Addisson Wesley. pp281-350 (1975).

WANG. Biotechnology - status and prospectives. Al. Ch. E. Monograph Series 18 (84) (1988).

WEDD.M.W. Introduction to sub-micron particle sizing by photon correlation spectroscopy.Malvern Instruments internal publication.

WEGER.E. KARASIKOR.N. Dual discipline technique to characterise both size and shape. Int. Labmate Iss no 0143 5140.

WEHNERT.G. et al. Fluorescence probe (in German). Chem. Ing. Tech. 62 (3) pp211-212 (1990).

WEICHERT.R. Determination of extinction efficiency and particle size distribution by photosedimentation using light of different wavelengths. Particle Size Analysis (1981) Ed N.G. Stanley-Wood T. Allen Wiley Heyden.

WEINER.B.B. THOMAS.J. Introduction to particle sizing by photon correlation spectroscopy. Brookhaven Instruments internal publication.

WYATT.P.J. JACKSON.C. WYATT.G.K. Absolute GPC determinations of molecular weights and sizes from light scattering. American Lab. May (1988).

ZERULL.R.H. KILLINGER.R.T. GIESE.R.H. Optical particle sizing and particle characterisation based on polarisation measurements,Optical Particle Sizing, proceedings 1988 Eds Grehan, Gousbet. Wiley.

ZIMM B.H. J. Chem. Phys. 16 pp1093-1099 (1948)

ZIMMERMAN.K. DELAYE.M. LICINIO.P. Analysis of multiexponential decay by a linear programming method: Application to light scattering spectroscopy. J. Chem. Phys. 82 (5) 1 March (1985).